AUBURN UNIVERSITY

SAMUEL GINN
COLLEGE OF ENGINEERING

Nano-conditioning of Expansive Soil Using Electrokinetics

by

Najibullah Zulfeqar, Ph.D. Student

Ali Khosravi, Ph.D., P.E.

Shiqiang (Nick) Zou, Ph.D.

Department of Civil and Environmental Engineering

Auburn University

October 2024

Highway Research Center

Harbert Engineering Center

Auburn University, Alabama 36849

TABLE OF CONTENTS

CHAPTER 1

1. Introduction

The "Black Belt" region of central and western Alabama, known for its dark, highly expansive soil with a high percentage of smectite clay minerals (ALDOT, 2021), faces significant geotechnical challenges (Figure 1.1). Expansive soils, commonly referred to as swelling soils, are characterized by their capacity to undergo significant volume changes in response to moisture variations (Jones Jr & Holtz, 1973; Gromko, 1974; Chen, 2012; Jones & Jefferson, 2012).

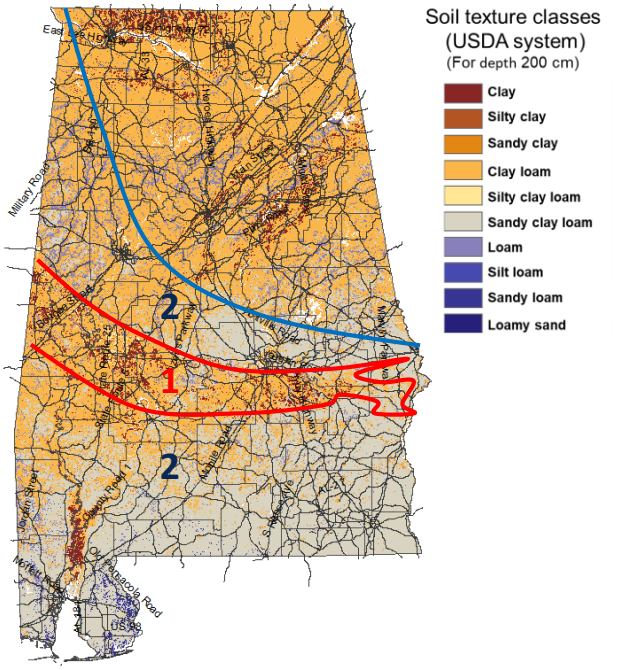

Figure 1.1: Map of Alabama soil type (from 0 to 2 m depth) (Ghorbani et al., 2024).

These changes in volume can exert considerable stress on buildings, roads, and other infrastructures, leading to cracked foundations (Jones & Jefferson, 2012; Dye, 2008; Walsh et al., 2009; Houston et al., 2011), failed retaining walls (Liu & Vanapalli, 2017), uneven road surfaces (Puppala et al., 2003; Xeidakis et al., 2004), and damaged pipelines (Gallage et al., 2012; Bouatia et al., 2020; Raj Singh et al., 2021). Expansive soils are estimated to cause more damage annually

to structures than earthquakes, floods, and hurricanes combined, highlighting their impact on construction and maintenance costs worldwide (Chen, 2012; Jones & Jefferson, 2012; Jones Jr & Holtz, 1973; Abdelhafez et al., 2022; Dunham-Friel & Carraro, 2011).

Current practice uses several solutions to mitigate the risks associated with expansive soils. Traditional methods primarily involve mechanical stabilization techniques, such as soil replacement with non-expansive materials (Houston et al., 2016; Puppala, 2021), installation of moisture barriers to regulate soil hydration levels (Jones & Jefferson, 2012; Steinberg, 2000), and the construction of heavily reinforced foundations designed to resist movements induced by soil volume changes (Chen, 2012; Houston et al., 2011; Madhyannapu & Puppala, 2014; Nelson et al., 2015). While effective to a degree, these approaches can be costly and environmentally detrimental. Also, they may not adequately address the differential movements caused by extreme moisture variations (Dunham-Friel & Carraro, 2011; Puppala, 2021; Puppala et al., 2003). Modern strategies present a more dynamic approach to managing expansive soils. Techniques such as the use of biotechnological innovations to alter soil properties without harming the ecosystem, chemical stabilization methods that treat soils with lime or cement (Basma & Tuncer, 1991; Buhler & Cerato, 2007; Kumar & Thyagaraj, 2020; Liu et al., 2019; Madhyannapu & Puppala, 2014; Nalbantoglu, 2006; Puppala et al., 2003; Salahudeen et al., 2014; Saride et al., 2013), use of polymer (Soğancı, 2015), and industrial waste implementation (Dunham-Friel & Carraro, 2011) are increasingly common. Additionally, the integration of smart technologies, including sensors that monitor soil conditions in real-time, offers the potential for proactive management of soil-related issues (Dye, 2008). These advanced technologies often come with high initial costs, maintenance challenges, and potential environmental degradation, particularly with chemical methods (Correia et al., 2016; Puppala, 2021). Both traditional and modern methods fall short in

offering a truly adaptive solution to the challenges posed by expansive soils, highlighting the need for further research into innovative and responsive technologies.

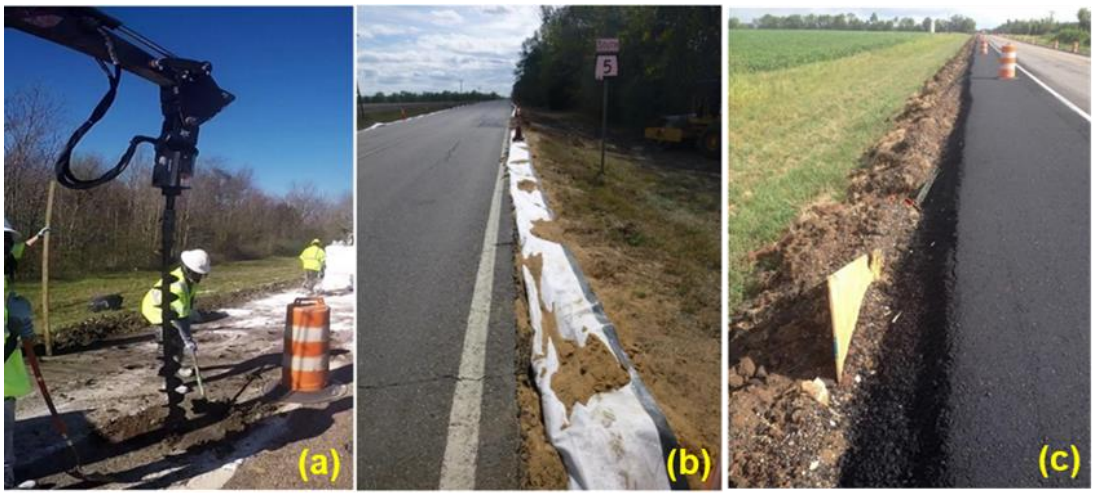

Figure 1.2: Current practice to improve road performance over expansive soil: **a)** Lime Column Installation, **b)** Vertical Barriers Construction, and **c)** Paved Shoulders After Paving (Photo from Kennedy 2019).

An alternative approach is the use of electrical injection of nanoparticles (NPs) to improve expansive soil's deformation behavior and strength characteristics. NPs show promise due to their high surface area, cation exchange capacity, and ability to modify soil properties by reducing moisture content, plasticity, and swell-shrink potential while improving strength and modifying physicochemical characteristics (Krishnan & Shukla, 2019; Ikeagwuani & Nwonu, 2019). However, the conventional delivery and mixing methods for NPs in soil matrix are costly, require excavation, affect only localized areas, and are impractical under existing structures without demolition. Therefore, there is a need to explore non-destructive, in-situ techniques for NPs delivery and distribution. Electrokinetics has recently emerged as an innovative technique for soil conditioning, utilizing an electric field applied to wet soil to cause the migration of charged

substances, facilitating their transport and distribution within the soil through three main mechanisms, i.e., electromigration, electroosmosis, and electrophoresis (Abdullah & Al-Abadi, 2010; Eykholt & Daniel, 1994; Gray & Mitchell, 1967). Electromigration involves the transport of ionic species towards the oppositely charged electrode. For example, positively charged cations migrate toward the cathode, while negatively charged anions towards the anode. Electroosmosis drives the movement of pore fluid within the soil matrix from the anode to the cathode, while electrophoresis enables the migration of charged colloidal particles, such as the clay particles suspended in the soil-water mixture.

This study plans to leverage electrokinetics to distribute nanomaterials within expansive soils, aiming to reduce their plasticity and swell potential, and improve strength. Our specific goals are to investigate the effects of various nanoparticles, including MgO and SiO_2, on reducing the plasticity index (PI), and to evaluate the resulting improvements in the strength and deformation behavior of the treated soils; and (2) assess the distribution and effectiveness of nanoparticle dispersal through electrokinetics within an electric field. To evaluate the effectiveness of these techniques in Alabama's native soils, we began by developing and conducting element-scale laboratory experiments to characterize the hydraulic and mechanical behavior of soils that have undergone nano-conditioning via conventional soil mixing. These experiments include soil index testing, unconfined compressive strength (UCS) measurements, and soil water retention curves (SWRC) analyses. Following these initial tests, we will conduct table-top electrokinetics experiments to evaluate how effectively electrokinetics can distribute nanoparticles within the soil matrix. The testing methods and procedures developed through this research will provide a comprehensive understanding of how nano-conditioning, facilitated by electrokinetics, enhances expansive soils' hydraulic and mechanical properties across different scales. This study will also

offer valuable insights into optimizing these techniques and implementing them effectively, considering key factors that influence their performance in real-world geotechnical applications.

1.1.Research Objectives

This research aims to develop a rapid and cost-effective nano-conditioning approach using electrokinetics to improve the mechanical characteristics and hydraulic properties of expansive soils. Our specific goals in this study are to:

1. Investigate the effect of MgO and SiO_2 nanoparticles (NPs) on expansive soil mechanical properties such as the plasticity index, unconfined compressive strength, and swell potential.
2. Evaluate the effect of NPs on the soil hydraulic properties, such as soil water retention curve (SWRC) and hydraulic conductivity.
3. Explore the effect of electrokinetics on the soil physicochemical properties such as plasticity index, soil vertical swell strain, unconfined compressive strength, pH, (electric conductivity) EC, and soil fabric and mineralogy.
4. Distribution of NPs in the soil in the presence of an electric field as a driving force.
5. Simulate the distribution of the MgO NPs in the soil using COMSOL Multiphysics software.

The results from this study would offer an innovative approach for the Alabama Department of Transportation (ALDOT) and similar organizations, addressing the limitations of conventional soil stabilization methods. By introducing a non-destructive in-situ soil stabilization technique, this research presents a novel solution to overcome the challenges faced by traditional soil stabilization methods, enabling more effective and efficient treatment methods of expansive soils in pavement and infrastructure projects.

1.2. Research Approach

The proposed study employed a three-phase approach to evaluate the effectiveness of nano-conditioning combined with electrokinetics as a method for stabilizing and strengthening expansive soils beneath roads and highways. In the first phase, element-scale nano-conditioning experiments were conducted, including Atterberg limits testing, unconfined compressive strength tests, and soil water retention curve (SWRC) analyses. These experiments characterized the effects of nano-conditioning on the hydro-mechanical properties of Alabama's expansive soils. The second phase of our study focuses on examining the electrokinetic effect alone on the expansive soil properties. Our specific goals are to investigate the impact of electrokinetics on reducing the plasticity index (PI), enhancing strength, and decreasing the swell potential of the soil. The third phase involved tabletop electrokinetics experiments to assess the performance of the electrokinetics effect in conjunction with nano-conditioning. In the fourth phase, the study used numerical simulations using COMSOL Multiphysics software to perform a parametric study to understand further key parameters affecting the performance of electrokinetics in distributing nanomaterials in expansive soils.

1.3. Report Organization

This report is organized into seven chapters that comprehensively address the issue of expansive soils and innovative approaches to stabilize them. Chapter 1 serves as an introduction to the topic. It includes the research objectives, approach, and an overview of the report organization. Chapter 2 provides a literature review on expansive soils, covering the associated problems, financial impacts, and identification methods. This chapter also focuses on soil stabilization techniques, specifically nanoparticle treatment and electrokinetic stabilization. It explains the mechanisms

involved in electrokinetic stabilization and discusses the materials and methodologies used in these innovative approaches. Chapter 3 is allocated for the materials and methodologies employed in this research. Chapter 4 presents the laboratory results and analysis from experimental investigations. Chapter 5 explores numerical modeling using COMSOL Multiphysics software to evaluate the nanoparticle distribution in soil using electrokinetics. Chapter 6 presents a preliminary techno-economic assessment of electrokinetic nano-conditioning application in real-world scenarios, identifying a 0.5-mile site for its application along the AL-5 highway in Alabama. Chapter 7 presents a summary of the report, outlines key conclusions, provides recommendations for further research, and discusses future research directions. Through this comprehensive study, incorporating a literature review, innovative stabilization techniques, experimental investigations, and numerical modeling, the research aims to contribute to the development of effective solutions for addressing the challenges posed by expansive soils.

CHAPTER 2
Literature Review

2.1. Introduction

Expansive soils, also known as shrink-swell soils, expand and contract significantly in volume with changes in moisture content. Due to the seasonal moisture fluctuation, they swell when they get wet and shrink when they get dry (Agarwal & Sachan, 2024; Barman & Dash, 2022). Seasonal changes in moisture levels lead to volume instability in the soil, causing stresses that can damage the superstructure, especially lightly loaded ones. This can manifest in various ways, such as building distortions, floor and pavement upheavals, fractures in slab on grade members, and damages to channel linings, reservoirs, irrigation systems, railways, canals, and underground water supply networks (Belchior et al., 2017; Ito & Azam, 2013; Khattab et al., 2007). Due to the cyclic swelling and shrinkage of soil throughout different seasons, structural damage can occur repeatedly, causing a huge amount of maintenance cost. For instance, as Ito and Azam (2013) highlighted, the maintenance costs of an 850 km long water supply network with a fracture rate of 0.27 breaks/km/year exceed $2 million annually. Research by Jones Jr and Holtz (1973) indicates that in a typical year, damage caused by expensive soil is more than twice the damage from floods, hurricanes, tornadoes, and earthquakes in the United States. The significant economic and structural implications of expansive soils highlight the importance of understanding the factors influencing their shrink-swell behavior.

2.2.Expansion and Contraction Mechanism in Expansive Soils

Clay particles in soil typically exhibit negative surface charges. These charges can originate from three primary sources: (1) isomorphous substitution in tetrahedral and octahedral sheets (e.g., Al^{3+}

replacing Si^{4+} in the tetrahedral sheet or Mg^{2+} replacing Al^{3+} in the octahedral sheet), (2) broken bonds around particle edges (occurring at the termination of silica-alumina units, exposing unsatisfied negative charges), and (3) replacement of the exposed hydroxyl hydrogen (also known as proton dissociation from surface hydroxyl groups) (Khorshidi & Lu, 2017; Mitchell and Soga 2005; Moore and Reynolds 1997; Grim 1968).

These negative charges are balanced by salt cations (such as sodium, calcium, magnesium, and potassium) dissolved in soil water and adsorbed onto clay surfaces as exchangeable cations. The cations in soil exist in different hydration stages. In completely dry soil, cations have very low hydration and are held close to clay surfaces by strong electrostatic forces. As water becomes available, it bonds with the cations through hydration (Nelson & Miller, 1997). The hydration process can be understood by considering three components of soil together: the mineral, the cations, and the associated water. Water is held in three regions around the cation, termed A, B, and C, collectively called water of hydration (Figure 2.1). Region A, the innermost layer, is the immobilization region where water is tightly held and immobile. Region B has less structure and is held less tightly by the ion. Region C contains water in its normal structure, polarized by a weak ionic field (Frank and Wen 1957).

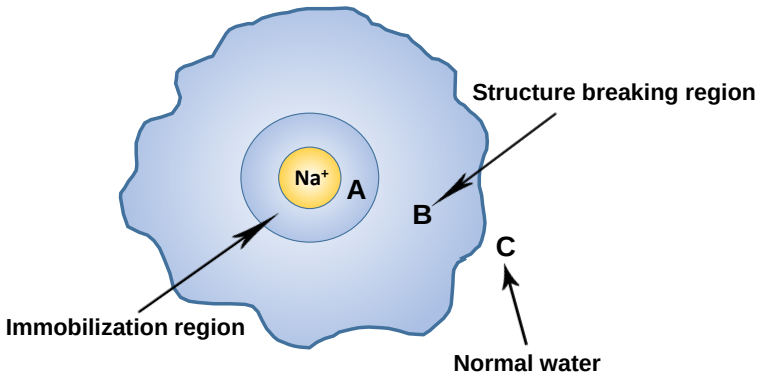

Figue 2.1: Ion water interaction (modified from Frank and Wen 1957).

As water is added to the soil, it's initially drawn into regions A and B due to the high energy of hydration. With more water addition, the hydration of region B is completed. Finally, when excess water is available, it fills region C. This progression demonstrates the gradual hydration of cations between clay particles, which can lead to particle separation and potential soil swelling (Nelson & Miller, 1997; Frank and Wen, 1957). When expansive soils absorb water, the clay minerals within the soil structure begin to swell. This swelling occurs through two main mechanisms: crystalline and osmotic swelling. Crystalline swelling occurs when water is introduced to dry soil, hydrating the cations adsorbed on clay surfaces. This process is energetically favorable and dominant at close particle spacings (<22 Å), as reported by Norrish (1954) for the swelling of montmorillonite. It corresponds to the initial hydration of regions A and B around the cations (Norrish, 1954; Slade et al., 1991). Osmotic swelling follows, becoming dominant at larger particle spacings (>35 Å). It's driven by the concentration gradient of cations between clay particles and the bulk soil solution. Osmotic forces draw water into interparticle spaces, diluting the higher cation concentration near clay surfaces. This process develops region C in the hydration model and forms most of the micelle fluid (Lambe, 1958). The transition between crystalline and osmotic swelling is gradual. During drying, the process reverses, with osmotic water removed first, then some crystalline water, causing soil shrinkage. This cyclic swelling and shrinking behavior names these soils "shrink-swell soils" and causes structural damage, as depicted in Figure 2.2 (Norrish, 1954; Slade et al., 1991).

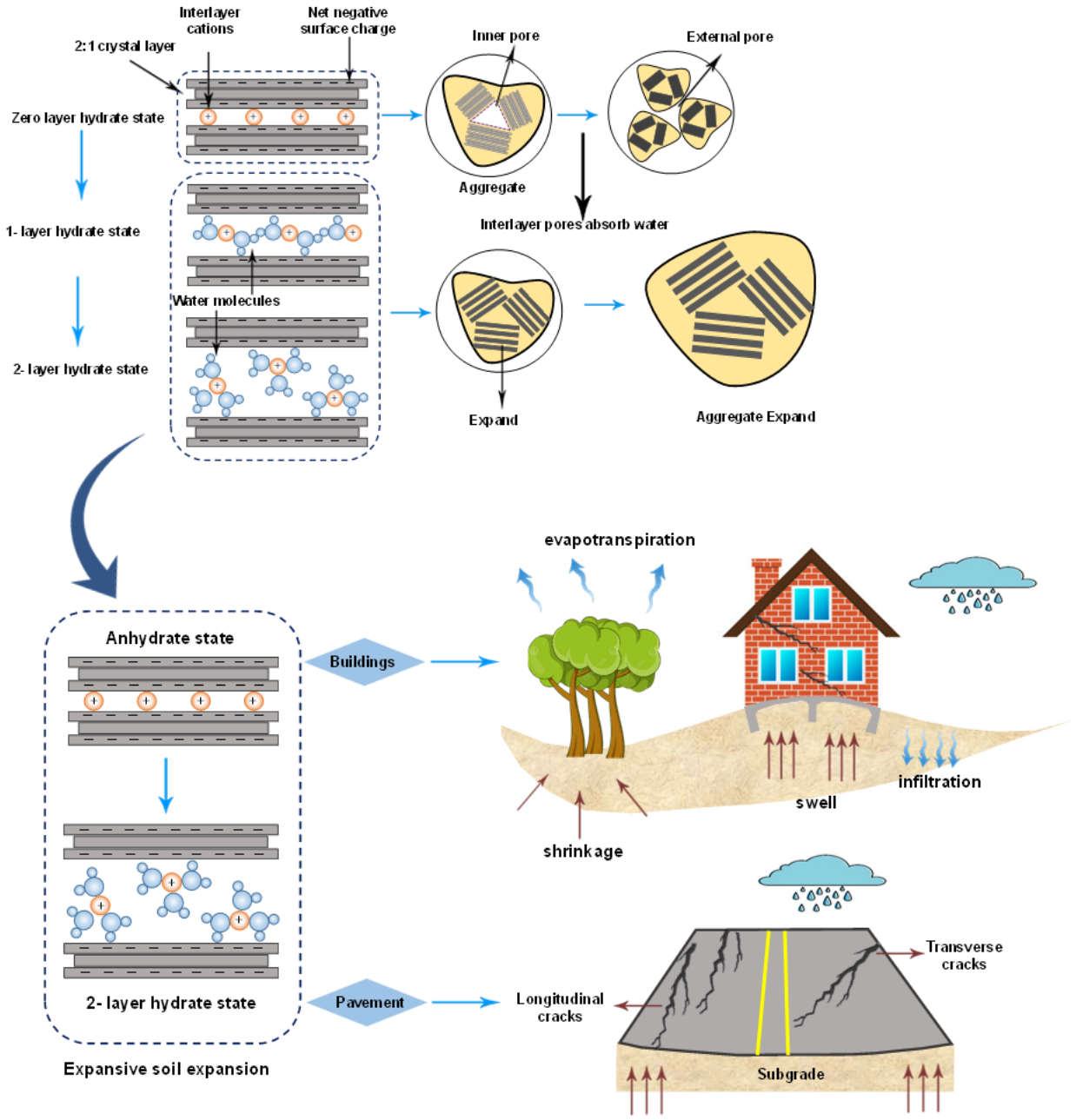

Figure 2.2: Expansion mechanism of expansive soil with its effect on the building and pavement.

The extent of swelling depends on several factors, at both micro and macroscale. The microscale factors include clay mineralogy and soil water chemistry. The swell potential of the expansive soil mass depends on the amount and type of clay minerals in the soil, their arrangement,

the specific surface area of clay particles, and the chemistry of the soil water (Nelson & Miller, 1997; Nelson et al., 2015). Clay minerals exhibit varying degrees of expansiveness, some groups being highly expansive, while others are considered non-expansive. The smectite group, which includes minerals like montmorillonite, is known for its high swell potential. On the other hand, the mica group, containing illite and vermiculite, can also be expansive, while the kaolinite group is generally considered non-expansive. Among the highly expansive clay minerals, montmorillonite stands out as a particularly troublesome mineral. Montmorillonite, a 2:1 clay mineral, exhibits a high swell potential due to its charge deficiency and weak Van der Waals forces between the two basal silica sheets. Water and exchangeable cations can quickly enter and separate the primary layers of montmorillonite (Barman & Dash, 2022; Nelson & Miller, 1997). Thus, when cleavage of the mineral occurs, the sheets will separate, and expansion takes place. Soil water chemistry is another important factor. Cations such as Na^{+}, Ca^{2+}, Mg^{2+}, and K^{+} are dissolved in water and adsorbed onto the clay surface as exchangeable cations to balance the clay surface charges as mentioned before. Due to the hydration of the cations and adsorptive forces by the clay, the swell potential increases, resulting in changes to the soil's diffuse double layer (DDL). For soils with the same mineralogy, those with Na^{+} cations have more swell potential than samples with Ca^{2+} or Mg^{2+}. On the other hand, the macroscale factors include moisture content, plasticity, and soil density (Nelson & Miller, 1997). As stated by Nelson et al. (2015) macroscale reflects the microscale nature of the soil.

2.3. Identification of Expansive Soil

The identification of expansive soils is a critical aspect of construction projects to prevent post-construction damage. Recognizing the presence of expansive soils in a project area allows engineers to implement preemptive mitigation measures, thereby reducing the risk of damage to

structures over time. Methods for determining the swell potential of expansive soils can generally be categorized into two groups. The first category focuses on evaluating the physical properties of soils, such as Atterberg limits, free swell, and potential volume change. These measurements provide valuable insights into the soil's behavior under varying moisture conditions. The second category involves analyzing soils' mineralogical and chemical properties, including clay content, cation exchange capacity, and specific surface area. These factors offer a deeper understanding of the soil's composition and its potential for expansion. While practicing geotechnical engineers typically rely on physical property measurements to identify expansive soils, it is essential not to overlook the importance of assessing mineralogical and chemical properties. This approach, more common among agricultural and geological practitioners, can provide a more comprehensive understanding of soil behavior and lead to more effective mitigation strategies (Nelson et al., 2015).

2.3.1. Methods Based on Physical Properties

Several physical methods are used to determine the expansive soil. One easy and direct approach to identifying the expansive soil is evaluating the soil's plasticity characteristics through the Atterberg limits, which provide the plasticity index and liquid limit (LL). Higher PI values generally indicate the presence of expansive minerals, as these minerals tend to exhibit higher plasticity, as shown in Figure 2.3. Seed et al. (1962) classified the degree of soil expansiveness based on PI values, noting that a PI < 10 indicates low expansion potential, while a PI >35 signifies high expansiveness; values in between indicate moderate to medium expansiveness. Peck et al. (1991) also suggested a correlation between PI and the potential for soil expansion. In the same way, Chen (2012) and Dakshanamurthy and Raman (1973) classified the degree of expansion based on the soil liquid limit as shown in Table 2.1. However, research by Zapata et al. (2006)

highlighted that PI alone is not always a definitive measure; the correlation improves significantly when combined with the percentage of soil passing the No. 200 sieve.

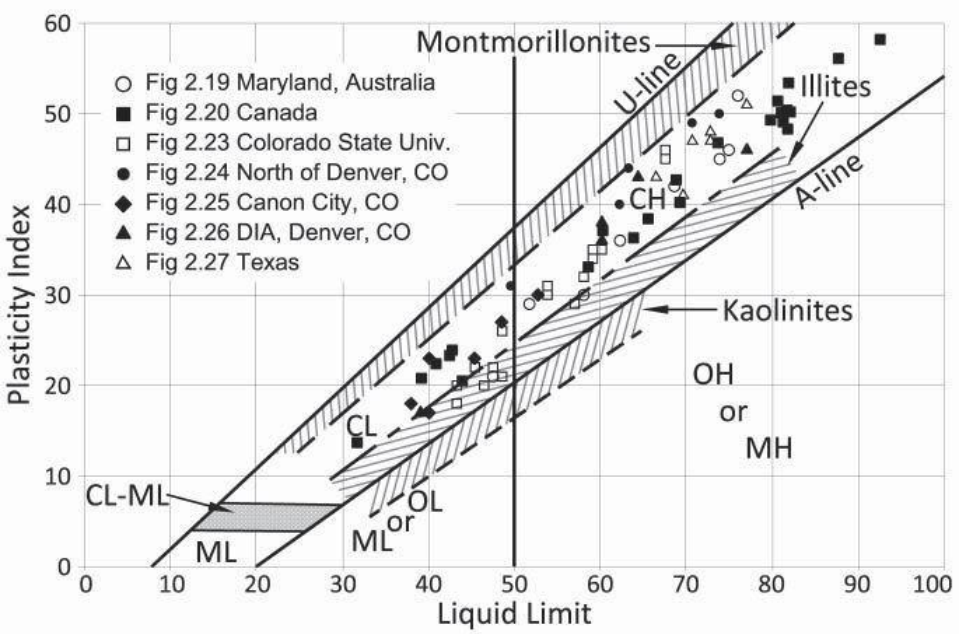

Figure 2.3: Plasticity characteristics of clay minerals ((Nelson et al., 2015)

Additionally, the soil's activity (A_c), defined as the ratio of PI to the percentage of clay-sized particles, is another critical parameter. Skempton (1953) classified soils based on activity, with active clays having the highest expansion potential. Active clays provide the most potential for expansion.

$$\text{Activity}\left(A_c\right) = \frac{\text{Plasticity Index}}{\%\ \text{by weight finer than}\ 2\mu\text{m}} \qquad (2-1)$$

$$\text{Inactive clays} \longrightarrow A_c < 0.75$$
$$\text{Normal clays} \longrightarrow 0.75 < A_c < 1.25$$
$$\text{Active clays} \longrightarrow A_c > 1.25$$

Table 2.1: Classifications for degree of expansion (swelling potential)

Degree of expansion	Seed et al. (1962)	Peck et al. (1991)	Chen (2012)	Daksanmurthy and Raman (1973)
Very high	PI > 35	>35	LL > 60	LL > 70
High	20 < PI ≤ 35	20–55	40 < LL ≤ 60	50 < LL ≤ 70
Medium	10 ≤ PI ≤ 20	0–15	30 ≤ LL ≤ 40	35 ≤ LL ≤ 50
Low	PI < 10	0–15	LL <30	20 ≤ LL ≤ 35

Another used method is the free swell test, which measures the volume change of soil when submerged in water. This test provides a direct indication of the soil's expansion potential. Soils such as sodium montmorillonite can exhibit free swell values ranging from 1,200 to 2,000 percent. The simplicity and ease of this test have made it a standard in various building codes, including those in China (Nelson et al., 2015). The Potential Volume Change (PVC) method, developed by Lambe (1960), uses a remolded soil sample in an oedometer to measure swell pressure. Although straightforward, the test's accuracy can vary depending on the stiffness of the proving ring, making it more suitable for identifying potential expansive behavior rather than providing precise design parameters.

The Expansion Index (EI) test, which originated in California in the late 1960s, offers a standardized method for assessing soil expansion. This test involves compacting a soil sample under controlled conditions and measuring its thickness change when saturated. The EI is calculated and used to classify soils based on their expansion potential. Recognized by several building codes, including the International Building Code, this method provides a reliable measure of soil expansiveness. Additional tests include the Coefficient of Linear Extensibility (COLE) test, which measures the linear strain of an undisturbed soil sample from moist to dry conditions, and the Standard Absorption Moisture Content (SAMC) test, which determines the equilibrium

moisture content of soil under standardized humidity conditions. Each of these methods offers unique insights into the expansive properties of soils, facilitating comprehensive identification and assessment (Nelson et al., 2015).

2.3.2. Mineralogical Methods

The identification of expansive clay minerals is a key method for classifying soil as potentially expansive. Techniques such as X-ray diffraction (XRD), differential thermal analysis (DTA), and electron microscopy are commonly employed for this purpose. X-ray diffraction (XRD) is particularly effective in identifying clay minerals like montmorillonite, illite, and kaolinite, each of which exhibits a unique XRD pattern characterized by distinct peaks and intensities. In addition to these techniques, chemical methods such as cation exchange capacity (CEC), specific surface area (SSA), and total potassium (TP) are also used to identify and classify clay minerals, providing further insight into the soil's expansive potential (Nelson et al., 2015).

2.4.Where are expansive soils found?

Expansive soils are prevalent across numerous global regions, notably in arid and semi-arid areas, and in locations where prolonged droughts are followed by wet conditions. Factors such as geology (parent material), climate, hydrology, geomorphology, and vegetation contribute to their distribution (Jones & Jefferson, 2012). Problems associated with expansive soil have been reported on six continents and more than 40 countries around the globe (Nelson et al., 2015). Expansive soil maps in North America have been developed by researchers using agricultural soil maps and soil reports (Ching & Fredlund, 1984; Hamilton, 1965; Hart, 1974; Krohn & JE, 1980; Olive et

al., 1989; Patrick & Snethen, 1976; Snethen et al., 1977; Snethen et al., 1975). Figure 2.4 shows the distribution of expansive soil throughout the United States of America.

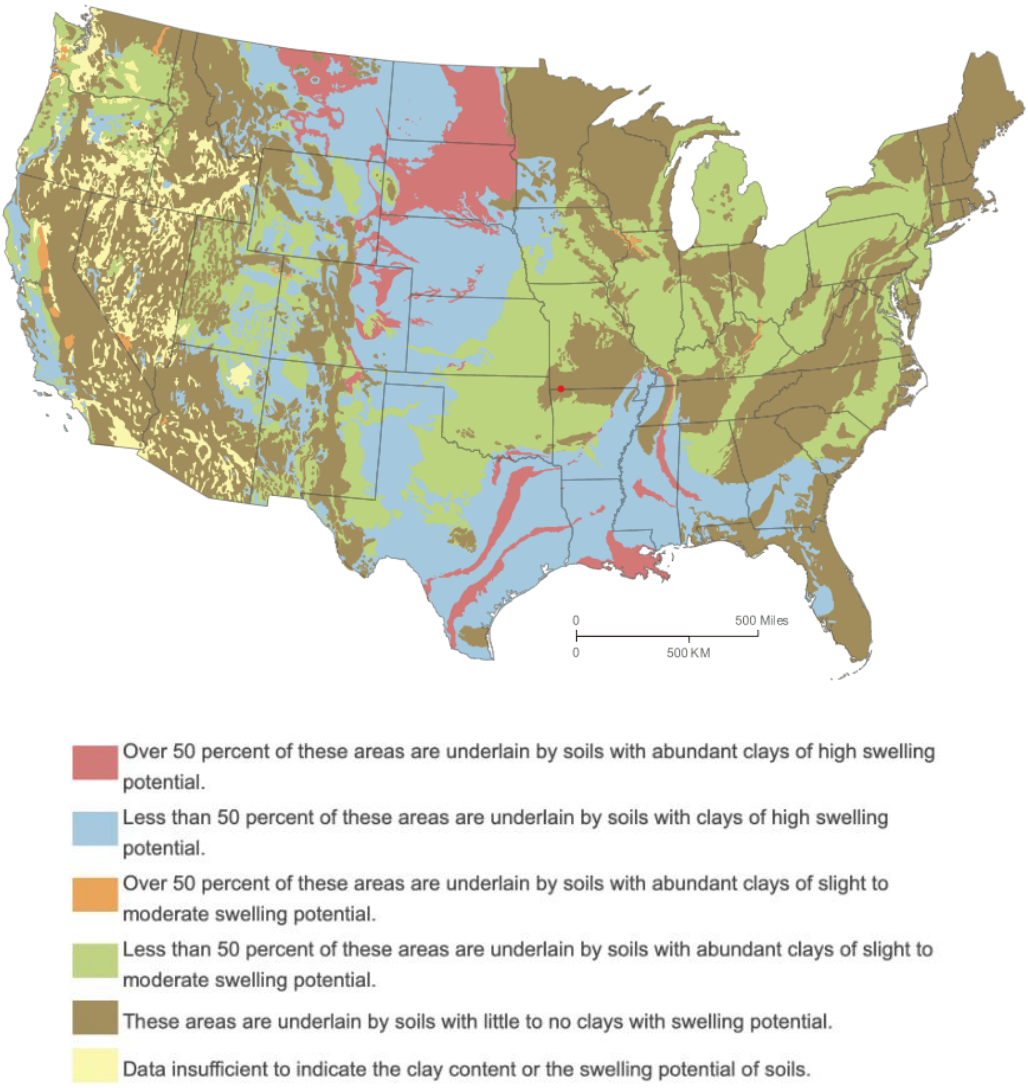

Figure 2.4: Distribution of expansive soil throughout the United States of America (Olive et al., 1989)

2.5 Expansive Soil in Alabama

The distribution of expansive soils across the United States is extensive, with significant concentrations in various regions, as illustrated in Figure 2.4. Among the states, Alabama stands

out as one of the states that contains expansive soils, particularly within the East Gulf Coastal Plain and the Blackland Prairie regions, as shown in Figure 2.5.

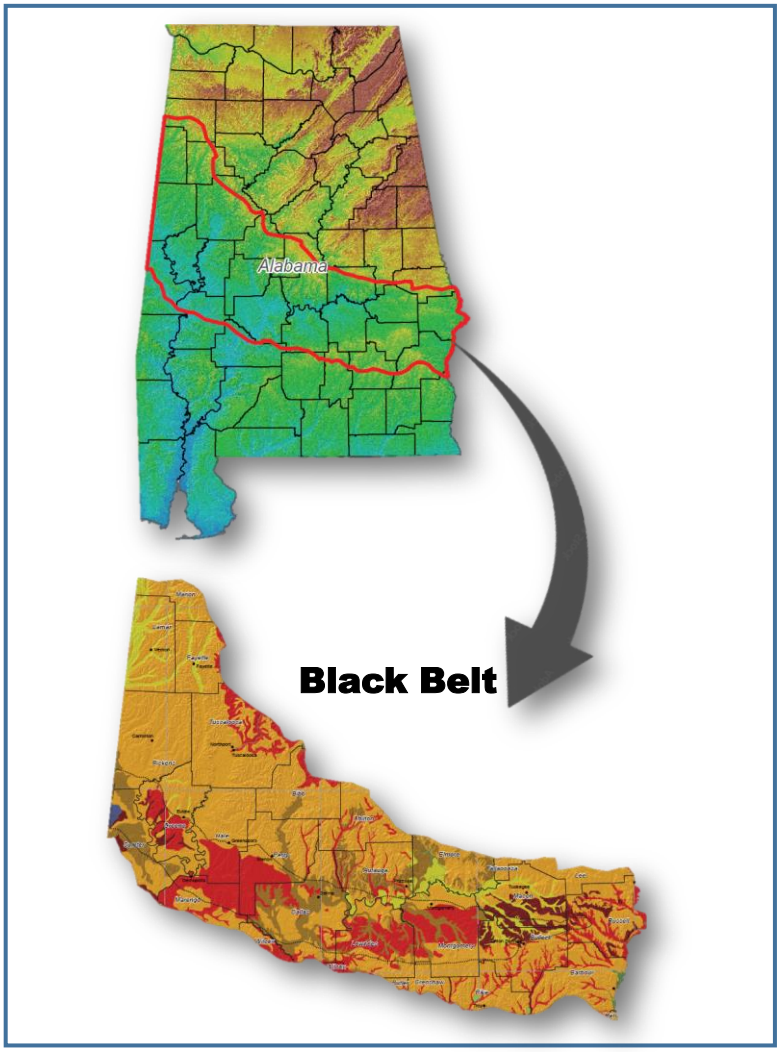

Figure 2.5: Balck belt area in Alabama (Dorina Murgulet 2009)

Alabama's diverse geological landscape is divided into five distinct physiographic provinces, which vary from south to north, as illustrated in Figure 2.6. These physiographic regions represent the largest-scale divisions based on rock type, age, structure, and geological history. North America is divided into eight such regions, which are further subdivided into provinces and sections, each characterized by similar landforms and distinguished by geographic location. In

Alabama, these provinces demarcate areas of similar geology and geomorphology, with soil types generally following the same distribution patterns (ALDOT, 2021). The five physiographic provinces of Alabama include:

- **East Gulf Coastal Plain**
- **Piedmont Upland**
- **Alabama Valley and Ridge**
- **Cumberland Plateau**
- **Highland Rim**

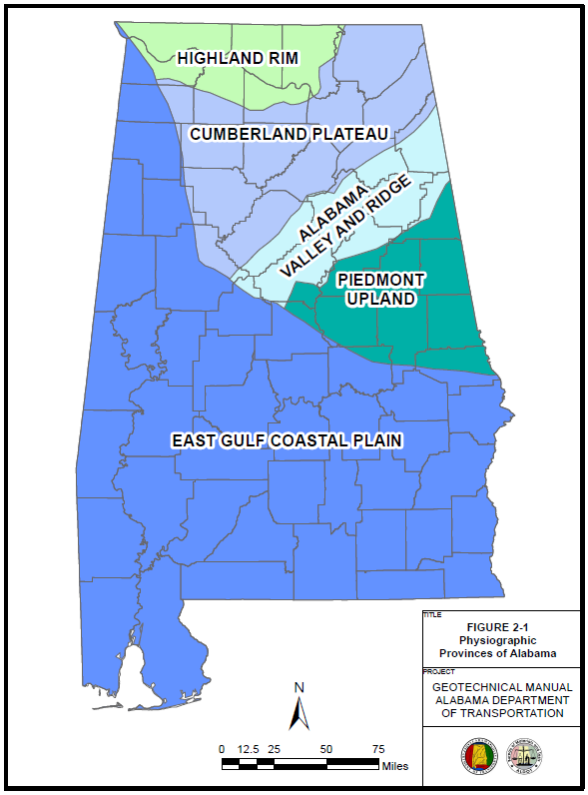

Figure 2.6: Physiographic Provinces of Alabama (ALDOT, 2021)

For the purposes of this study, our focus is on the expansive soils found in the East Gulf Coastal Plain. This area, also known simply as the Coastal Plain, is part of a larger region that spans over 42 million acres across five states, stretching from southwestern Georgia through the

Florida Panhandle into Alabama, and continuing across Mississippi into southeastern Louisiana and Arkansas. In Alabama, the East Gulf Coastal Plain encompasses approximately 60 percent of the state, covering portions of 40 out of 67 counties (ALDOT, 2021).

The geology of the East Gulf Coastal Plain reveals a sequence of rock units that become progressively younger towards the southern end. This Coastal Plain was formed on sedimentary rocks and sediment layers ranging from the Mesozoic era to recent times, dating back approximately 140 million years. The unconsolidated layers primarily consist of gravels, sands, silts, and clays. The soils in this area are classified into five distinct regions, each with unique characteristics, which we will explore in detail (ALDOT, 2021). Soils such as Smithdale, Luverne, and Savannah are predominant in the Upper Coastal Plains. These soils typically feature either a loamy or clayey subsoil or a sandy loam or loam surface layer. As one transitions to the **Lower Coastal Plains**, the soil profile changes. Here, Dothan and Orangeburg soils are prevalent in the eastern part, while Smithdale and Bama soils define the western section. The **Major Flood Plains and Terraces** are characterized by soils derived from alluvial deposits, indicative of the dynamic sedimentary processes at work in these areas. The **Coastal Marshes and Beaches**, located along the Mobile River, Mobile Bay, and the Gulf of Mexico, consist of deep, poorly drained soils situated near sea level and subject to regular tidal influences. The **Blackland Prairie**, often referred to as the "Black Belt" due to the dark coloration of its soils, is another significant region located in central and western Alabama, as shown in Figure 2.5. This area is characterized by its distinct curved shape and is notable for containing clayey soils with a high percentage of smectitic clays. These clays exhibit pronounced swelling and shrinking behaviors in response to moisture fluctuations, making the soils in this region particularly expansive (ALDOT, 2021). Figure 2.7 illustrates the diverse soil types across Alabama using two classification systems. The USGS map

on the left shows broad soil regions, with the Coastal Plain dominating the southern half, characterized by sandy and loamy soils. The Black Belt Prairie region stretches east-west across central Alabama, featuring a mix of clay and sandy clay soils. Northern Alabama includes Limestone Valleys and the southern edge of the Appalachian Plateau, with more varied soil compositions. The USDA map on the right provides a more detailed view at 200 cm depth, confirming the clay-rich nature of the Black Belt and revealing a diverse band of soil types running diagonally from the northeast to the southwest. This soil diversity reflects Alabama's varied geology and topography, significantly influencing agricultural practices and natural vegetation throughout the state.

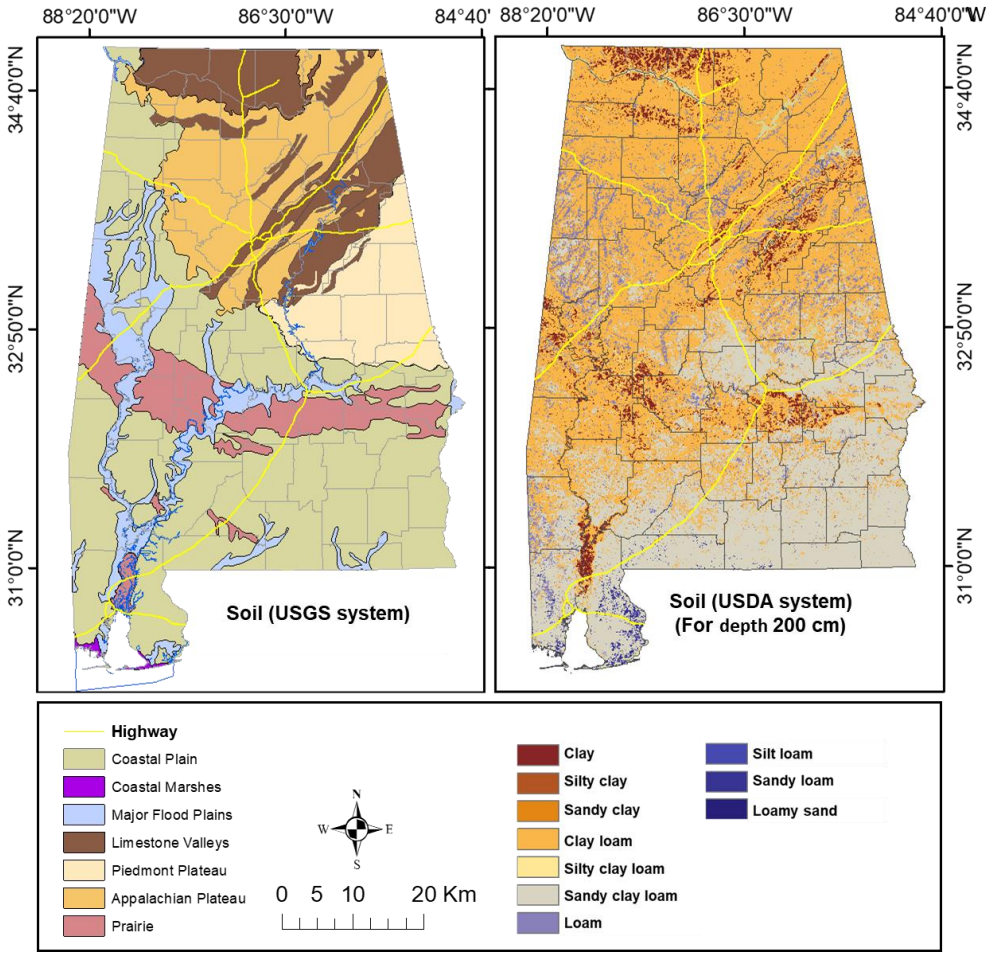

Figure 2.7. Alabama soil areas map (USGS and USDA systems)

2.6 Effect of Expansive Soil on Pavement

Changes in volume due to fluctuations in moisture content of the expansive soil within the subgrade can lead to road and highway deterioration, with an estimated annual cost exceeding $1.1 billion, notably affecting regions such as the western, central, and southeastern parts of the United States (Jones Jr & Holtz, 1973; Snethen et al., 1975). A survey conducted in 1972 of the highway departments across the 50 states, the District of Columbia, and Puerto Rico revealed that expansive soils are present within the geographical boundaries of 36 states (Lamb, 1973; Snethen et al., 1975).

Post-structure failure is inevitable in civil engineering, especially when construction is positioned on expansive soil. Expansive soil, known for its propensity to expand and contract significantly with changes in moisture content, poses a formidable challenge to houses and pavement. These soils absorb water during wet seasons, causing their clay particles to expand and push apart. This expansion increases the soil volume, reducing air-filled voids and creating upward pressure that can heave and deform the pavement above. Conversely, in dry periods, the soil loses moisture mainly through evaporation or transpiration in vegetated areas. Clay particles contract as water leaves the soil matrix, leading to overall soil shrinkage. This process not only increases air-filled voids between soil particles but also causes the soil mass to pull away from adjacent materials, often resulting in surface cracks and fissures in the pavement. This continuous cycle of hydration and dehydration, known as the swell-shrink cycle, subjects pavements to repeated stress as illustrated in figure 2.8. Over time, this can lead to significant structural damage, including uneven surfaces, cracks, and potentially complete pavement failure. Pavement damage from the expansive soil could be attributed to its low strength, high compressibility, and excessive volume change (Tanyıldızı et al., 2023).

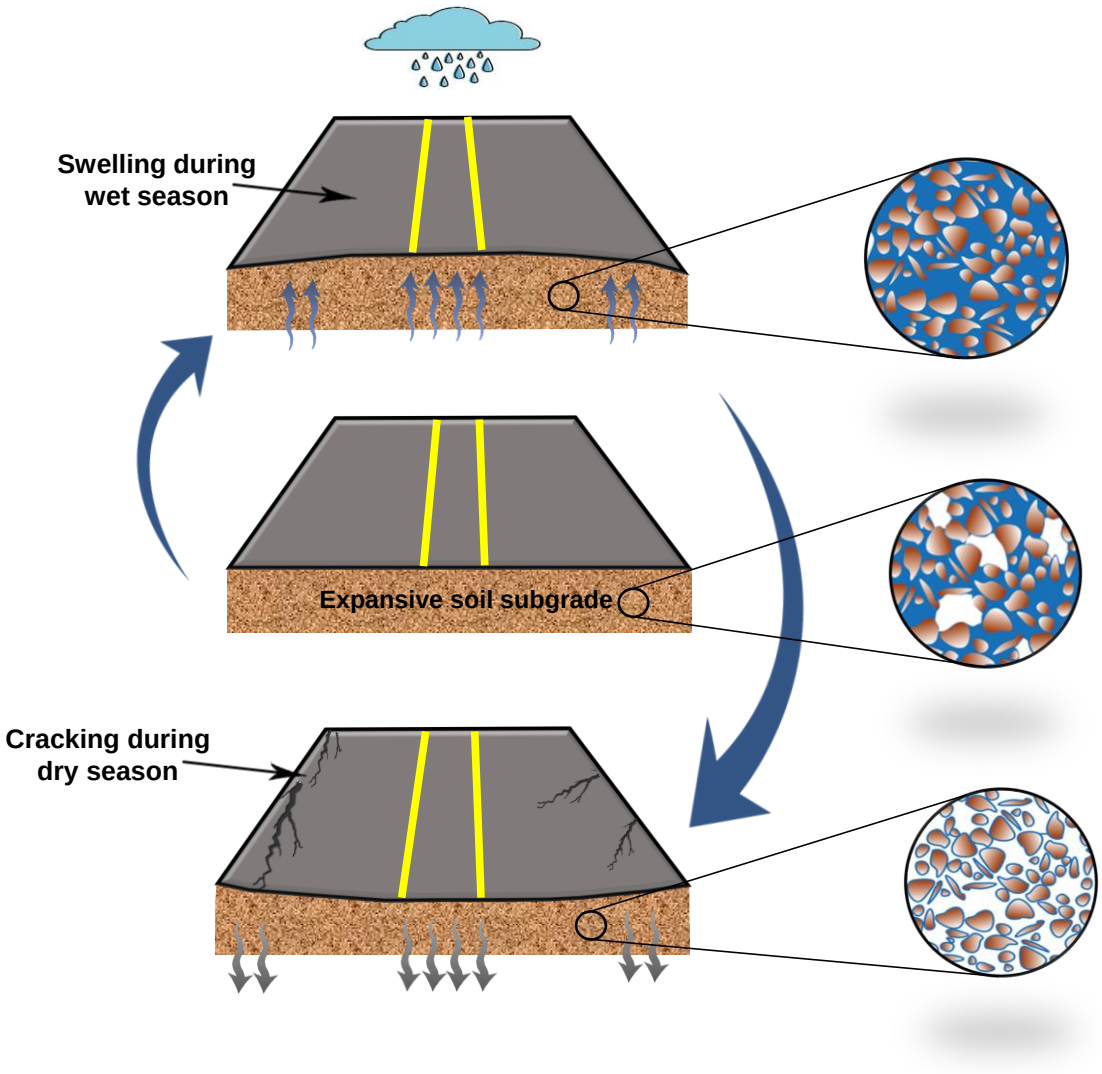

Figure 2.8: Seasonal Effects of Expansive Soils on Pavement Structure

Figures 2.9 a and b indicate an example of pavement failure. There's a large, sunken area in the middle of the paved road, creating a significant depression. The pavement has clearly buckled and collapsed, creating a hazardous condition for any vehicles (Figure 2.9a). Figure 2.9b shows crack running along the center of the road due to the expansive soil.

Figure 2.9: Pavement issues due to expansive soil **a**) pavement crack (U.S. Department of Transport) **b**) longitudinal crack (Zornberg and Gupta, 2009)

2.7 Stabilization Techniques to Mitigate Problems Associated with Expansive Soils

Mechanical, chemical, thermal, and electrochemical stabilization techniques have been developed over the years to address the challenges of expansive soils. Mechanical stabilization techniques include soil compaction, soil replacement, soil reinforcement, pre-wetting, and wetting-drying cycles (Barman & Dash, 2022; Zada et al., 2023). The mechanical expansive soil stabilization method does not fundamentally address the microscopic factors contributing to soil expansion and could be a reversible process. Chemical stabilization, on the other hand, induces complex physicochemical reactions, leading to physical, chemical, mineralogical, and microstructural changes (Barman & Dash, 2022; Croft, 1967; Diamond et al., 1963; Khattab et al., 2007; Rajasekaran & Rao, 2002). Chemical stabilization is divided into two categories: traditional

chemical stabilization, such as lime, cement, fly ash, or a mixture of cement and fly ash, and non-traditional stabilizers. Non-traditional expansive soil stabilizers include silica fume (Al-Gharbawi et al., 2022; Phanikumar & e, 2020; Singh et al., 2020), gypsum (Kuttah & Sato, 2015; Yilmaz & Civelekoglu, 2009; Zha et al., 2021), bottom ash (Melese, 2022; Tiwari et al., 2021b), cement kiln dust (Almuaythir & Abbas, 2023; Salahudeen et al., 2014; Sudheer Kumar & Janewoo, 2016), Ground Granulated Blast Furnace Slag (Kumar Sharma & Sivapullaiah, 2012; Mujtaba et al., 2018; Sharma & Sivapullaiah, 2016), Rice Husk Ash (Aziz et al., 2015; Jain et al., 2020), enzymes (Kushwaha et al., 2018; Pooni et al., 2019; Pooni et al., 2021), biopolymer stabilization (Bukhary & Azam, 2024; Hamid et al., 2022; Singh & Das, 2020), salts (Durotoye et al., 2016; Zumrawi et al., 2016), lignin stabilization (Sarker et al., 2023; Sarker et al., 2021), and nanoparticles (Coo et al., 2016; Krishnan & Shukla, 2019; Rosales et al., 2020; Zulfeqar et al., 2024). Figure 2.10 illustrates an overall diagram of different methods used for expansive soil stabilization. The following sections will discuss the most common stabilization methods used for expansive soils, including mechanical/physical and chemical methods, and their advantages and disadvantages.

2.7.1 Mechanical Stabilization Techniques

Mechanical stabilization is a process through which expansive soil's swell pressure and swell potential are reduced without fundamentally altering its chemical properties (Carraro et al., 2010). There are several techniques for mechanical stabilization, including compaction, soil replacement, soil reinforcement, surcharge loading, pre-wetting, and moisture control.

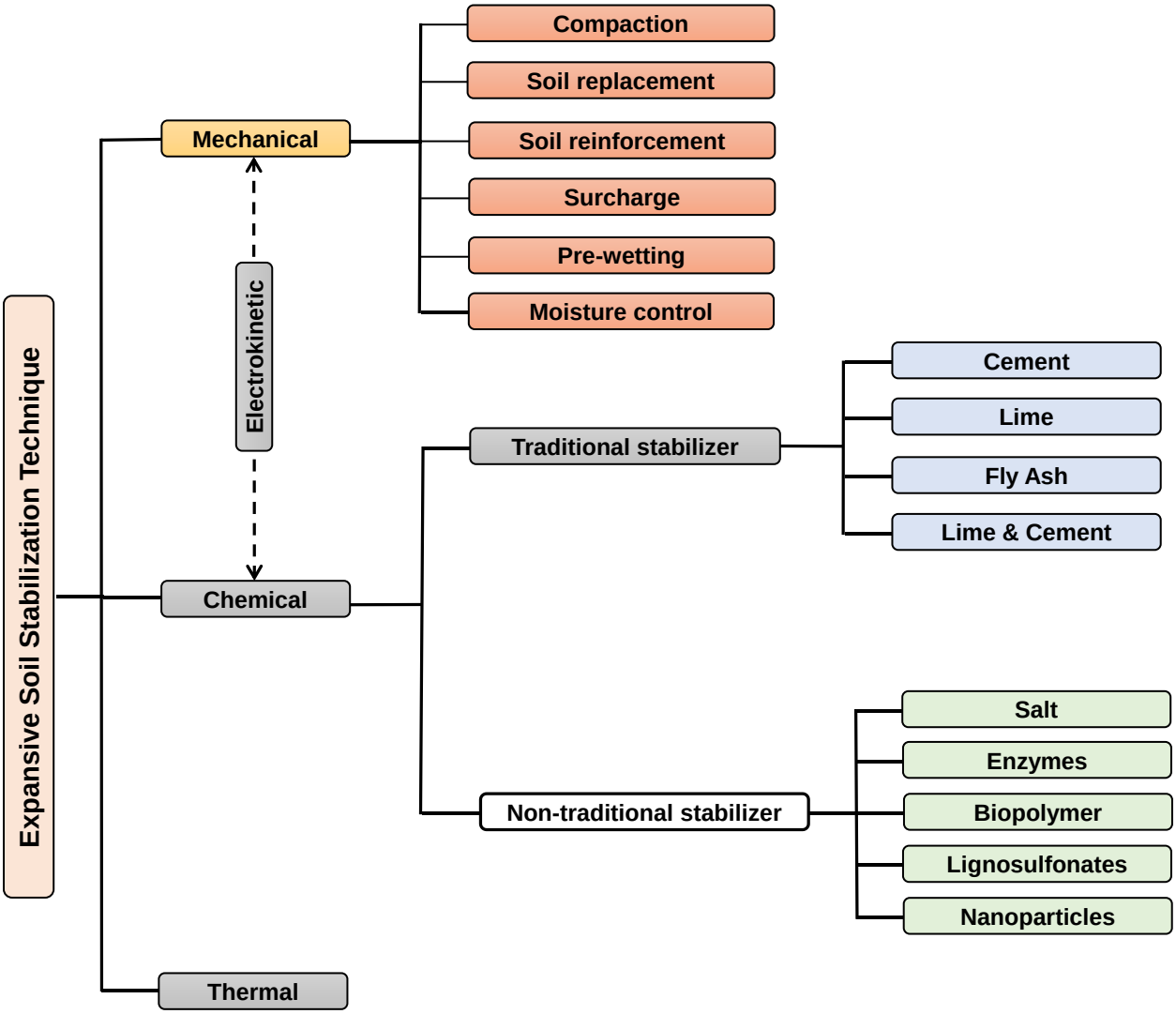

Figure 2.10: Expansive soil stabilization methods

2.7.1.1 Soil Removal and Replacement

Soil removal and replacement is a common and effective technique used to mitigate the problems associated with expansive soils. This method involves excavating the problematic expansive soil and replacing it with a more stable, non-expansive material. The goal is to eliminate the source of potential swelling and shrinkage, thereby providing a stable foundation for construction.

The process begins with a thorough site assessment to determine the extent and depth of the problematic soil. Once identified, the expansive soil is excavated to a sufficient depth where its swelling potential is negligible. After removal, the soil is replaced with a stable, non-expansive material, such as sand, gravel, or engineered fill. This replacement material is then placed in layers and compacted to achieve the required density, ensuring the stability and load-bearing capacity of the foundation. Soil replacement can be cost-effective and faster than other expansive soil treatments, needing no special equipment and allowing uniform additive mixing. This method may reduce construction delays by eliminating curing periods required by alternative approaches. While removing and replacing expansive soil can be highly effective in mitigating risks associated with shrinkage and swelling, this technique does have some limitations. In most cases, the expansive soil layer often extends too deep to make complete removal and replacement economically feasible. In such cases, a depth of excavation and non-expansive backfill must be determined to prevent excessive heave based on the swell potential of the test (Nelson & Miller, 1997). The depth of replaced soil depends on the active zone depth, soil profile, and construction standard. Chen (2012) suggested 3-4 ft (1 to 1.3 m) of non-expansive backfill, but it was found to be ineffective for sites with highly expansive soil. When the expansive soil is replaced with new material, the moisture fluctuations within the non-expansive backfill layer are carefully monitored and controlled to ensure that the moisture levels in the backfill do not trigger swelling or shrinkage in the underlying expansive materials. Due to the costs associated with importing impervious fill material, granular non-expansive soils, such as sand and gravel, are commonly used as backfill materials. These materials offer higher strength and bearing capacities, making them suitable for supporting overlying structures. However, a significant risk associated with granular fill is that it can act as a water reservoir, potentially supplying moisture to the underlying expansive soils over

time (Nelson & Miller, 1997). To mitigate this risk, proper drainage systems are essential to control moisture levels in the granular fill, preventing it from triggering the swelling behavior of the expansive soils beneath. Also, the soil removal and replacement technique's effectiveness largely depends on the underlying clay's expansion potential. This method can provide adequate stability for soils with low to moderate expansion potential. However, the technique may not be as effective for clays with high expansion potential, especially in situations with high water infiltration rates. Figure 2.11 shows the expansive soil replaced with new non-expansive soil in the subgrade of pavement.

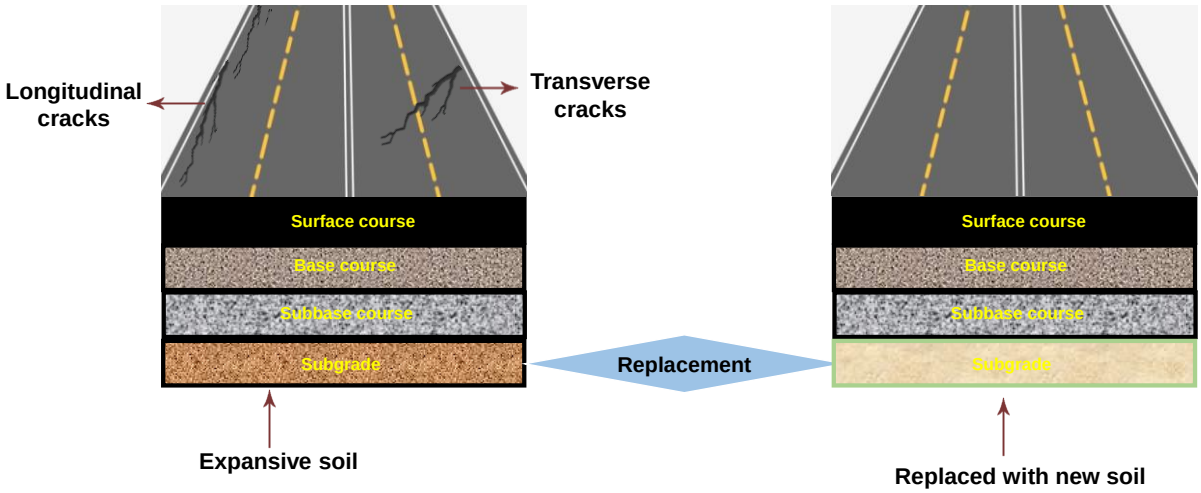

Figure 2.11: Expansive soil replacement in the subgrade of a pavement

2.7.1.2 Compaction

Compaction enhances soil properties by increasing its unit weight, strength, bearing capacity, and reducing undesirable settlement (Das & Sivakugan, 2017). The swell potential of expansive soils decreases when they are compacted at lower dry densities (Nelson & Miller, 1997). Expansive soils compacted at lower dry densities and with moisture contents higher than the optimum value

determined by the Standard Proctor test exhibit reduced expansion potential compared to those compacted at higher dry densities and lower moisture contents (Holtz, 1959).

In this technique, it is important to maintain the moisture content and the densities within a specified range. These values should be regularly checked to ensure soil uniformity. One advantage of this method is that proper compaction can minimize water movement into the underlying soil. Additionally, scarifying, pulverizing, and recompacting expansive soils can serve as an economically feasible stabilization method. While this technique can be effective in enhancing expansive soil stability, it also has certain drawbacks that need to be considered. Low-density compaction may not provide sufficient bearing capacity for heavier structures, though it is generally adequate for lighter buildings such as single-family houses. For certain highly expansive soils with a high swell potential for volume change, compaction alone may not adequately reduce swell potential and requires soil replacement instead. Furthermore, maintaining the specified densities and moisture contents during compaction requires frequent quality control testing, which can drive up the overall project cost (Nelson & Miller, 1997).

2.7.1.3 Surcharge Loading

Surcharge is a soil stabilization technique that uses a pre-load to consolidate and counteract the expected swell pressure. By applying a surcharge, the soil is pre-compressed, which reduces the potential for future swelling when moisture levels increase. This method is particularly effective in expansive clays that exhibit low to moderate swelling pressures. When an adequate load is applied, the surcharge can effectively prevent or significantly reduce swelling, thereby stabilizing the soil (Nelson & Miller, 1997).

However, the efficiency of the surcharge diminishes as swell pressures increase due to the nonlinear pressure-swell relationship. In other words, as the swell pressure increases, the surcharge required to counteract the swelling becomes disproportionately large, making the technique less effective. Therefore, field and laboratory testing that simulates actual site conditions is essential to accurately determine the swell characteristics of the soil and to design an appropriate surcharge load. This method is most suitable for low swell pressure and for projects where some degrees of heaving can be tolerated, such as secondary highways or other infrastructure where minor ground movement is acceptable. For larger projects where higher swell pressures are anticipated, surcharging may still be a viable option, provided the swell pressures remain within a low to moderate range. However, for expansive soils that exhibit very high swell pressures —sometimes reaching, up to 8000 psf (400 kPa)— the effectiveness of surcharging alone is limited. In these cases, the swell pressure may be too great to be fully controlled by surcharge loads, and additional stabilization methods may be necessary to achieve the desired soil stability (Nelson & Miller, 1997).

2.7.1.4 Pre-wetting

Prewetting or ponding is a stabilization approach that aims to induce heave in expansive soils before construction by increasing the moisture content. The underlying principle of this method is to induce the soil to reach its maximum potential heave before any structures are built. By doing so, the risk of further significant volume changes post-construction is minimized, thereby reducing the likelihood of damage to structures (Nelson & Miller, 1997; Nelson et al., 2015).

Prewetting involves saturating the expansive soil to the point where it swells to its maximum extent. This is typically achieved by applying water through methods such as ponding, where water is allowed to accumulate on the soil surface, or by using controlled irrigation systems.

The soil is kept wet until it achieves a near-saturation state, ensuring that any swelling occurs before the construction phase. Once the soil has been pre-wetted and allowed to heave, the theory is that no further appreciable swelling will occur, since the soil will already be in its fully expanded state. Consequently, any post-construction changes in moisture content should result in minimal additional volume changes, thus protecting the integrity of the built structures (Chen, 2012).

Despite its conceptual advantages, prewetting has several significant limitations: (1) Expansive soils, particularly those rich in clay, often exhibit low hydraulic conductivity. This means that moisture penetration through the soil is a slow process, requiring several weeks to months for water to adequately reach the entire depth of the active zone—the layer of soil that undergoes significant volume changes with moisture variations. (2) Extended ponding can result in severe loss of soil strength, leading to reductions in bearing capacity and slope stability concerns. (3) The wetting front —the boundary between wet and dry soil—often only advances to shallow depths, much less than the full depth of the active zone. This incomplete wetting can result in continued moisture redistribution to lower layers can still occur after construction, causing ongoing heave that the prewetting was intended to prevent. (4) In dense, low-permeability clay soils, the time required for effective moisture penetration can be exceedingly long, sometimes taking up to a year or more. This extended duration can make the prewetting process impractical for many projects. (5) Even after the soil has been pre-wetted, there is a risk that moisture will continue to migrate to deeper soil layers over time, leading to continued heaving after construction has been completed. (Nelson & Miller, 1997). Figure 2.12 illustrates the prewetting of a typical expansive soil before and after of construction of a living house.

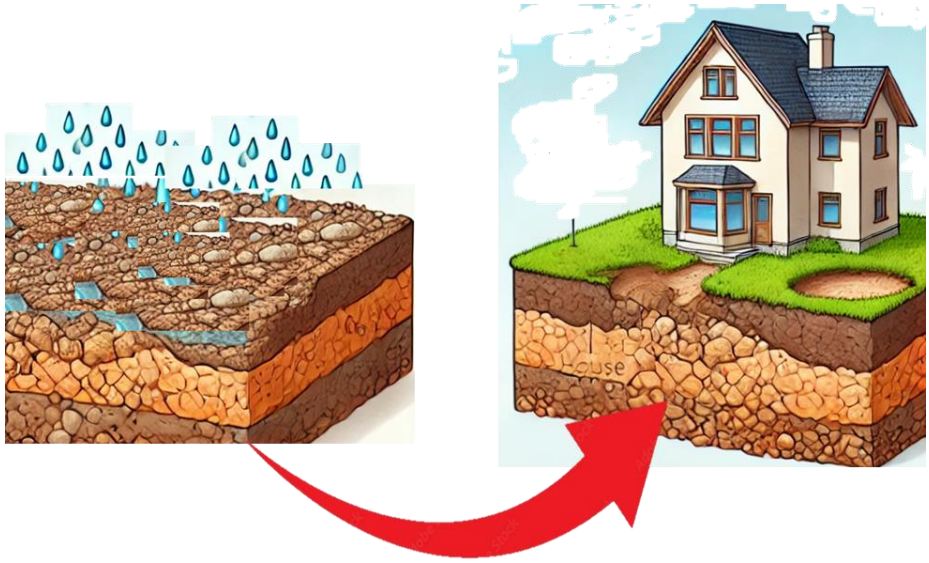

Figure 2.12: The pre-wetting of the soil pre and post-construction.

Despite challenges associated with this technique, prewetting has demonstrated success in specific cases, particularly in highly fissured, desiccated expansive clay soils that have relatively higher hydraulic conductivity. In such cases, the soil's natural cracks and fissures can facilitate quicker moisture penetration, making the prewetting process more effective. To further enhance the efficiency of prewetting, techniques such as the installation of sand drains can be employed. Blight and De Wet (1965) utilized sand drains to achieve around 90% of the estimated maximum heave in prewetted clay within two months. Felt (1953) increased moisture content in desiccated, fissured clay within one month of ponding, with continued swelling observed over six months of flooding. Steinberg (1981) conducted a prewetting experiment on a highway section in Texas, finding that most expected heave occurred within one month of ponding. McDowell (1965) ponded a highway section in Waco, Texas, achieving 4 ft of water penetration in just 24 days, without using sand drains. Van der Merwe et al. (1980) stabilized expansive fissured soils in South Africa for road construction using prewetting, placing a sand blanket for 50 days to increase saturation down to 40 inches and developing at least half the expected heave. Holtz and Gibbs (1956) used

ponding as a remedial measure to stabilize subgrade soils for the Friant-Kearn Canal. Ponding has also been coupled with lime stabilization for the surface soil to create a firm working base while preventing subgrade evaporation (Önal, 2015).

2.7.1.5 Moisture Control Alternatives

Controlling expansive soil moisture content is essential for mitigating its adverse effects and preserving pavement structural integrity. While it may be impossible to completely prevent water content increases in foundation soils, several strategies can be employed to minimize moisture fluctuations and stabilize moisture levels over time. One effective approach involves using horizontal and vertical barriers, such as parking lot slabs or moisture barriers placed around foundations. These barriers help regulate moisture infiltration and create more uniform heave patterns, thereby reducing differential movement and associated structural damage. In addition to barriers, proper surface (Nelson et al., 2015).

For pavements, a more advanced solution involves using Modified Moisture Barriers (MMBs), which combine geocomposite and geomembrane layers (Sapkota, 2019; Pandey et al., 2021). These MMBs have proven to be highly effective in isolating subgrade soils from environmental moisture, maintaining a consistent moisture content within the soil. By doing so, MMBs reduce the swelling and shrinkage cycles that often lead to pavement distress, such as cracking, rutting, and uneven surfaces. Field studies have demonstrated the effectiveness of MMBs in reducing seasonal deformation in pavements compared to untreated sections (Pandey et al., 2021). These studies indicate that MMBs improve pavement performance and lower maintenance costs by reducing the need for frequent repairs and surface treatments. The consistent moisture environment created by MMBs contributes to the long-term durability of pavements, making them

a practical and efficient solution for mitigating the adverse effects of expansive soils on infrastructure (Nelson et al., 2015; Pandey et al., 2021).

2.7.1.5.1 Horizontal Moisture Barriers

Horizontal barriers, whether flexible or rigid, often use impermeable membranes made from materials like polyethylene, PVC, and polypropylene. It's crucial to ensure these membranes have long-term chemical stability and avoid punctures, especially for those thinner than 20 mils. The surface must be prepared by removing any sharp objects and compacting them evenly. Most membranes degrade under sunlight, so they should be covered unless UV-resistant. Additionally, checking the chemical compatibility of the membrane with the soil is essential to prevent damage. Around buildings, these membranes should be protected by a 6 to 12-inch layer of earth (Johnson, 1979; Nelson et al., 2015).

2.7.1.5.2 Vertical Moisture Barriers

Vertical moisture barriers are more effective than horizontal barriers in minimizing lateral moisture migration and maintaining long-term uniform water content distribution. They are commonly used in highway pavements and new construction. A vertical moisture barrier typically consists of an excavated trench lined with impermeable materials such as polyethylene, concrete, asphalt, or impervious slurries, which must be durable enough to resist puncturing or tearing during placement (Chen, 2012; Steinberg, 1998). The trench is then backfilled with materials like grout or clay to ensure impermeability, although granular materials can be used in certain conditions to act as a capillary break (figure 2.13).

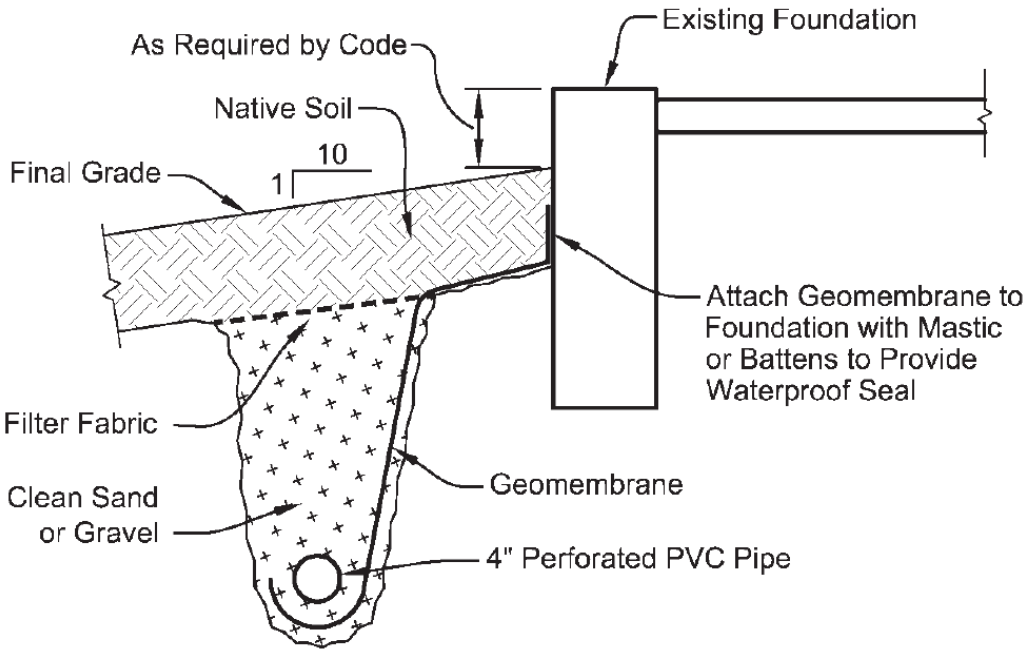

Figure 2.13: Configuration of a vertical moisture barrier (Nelson & Miller, 2015)

The depth of the vertical barrier should be based on the zone of water migration, typically extending one-half to two-thirds of the depth affected by seasonal moisture changes. Barriers less than 2 to 3 feet deep are generally ineffective (Chen, 2012; Nelson & Miller, 1997; Snethen, 1979). In highway projects, significant maintenance cost reductions are observed when vertical membranes are placed to a depth of 8 feet (Steinberg, 1998). If installation at the time of construction is not possible, barriers should be placed at least 3 feet away from the structure to allow equipment maneuvering and avoid soil disturbance and should be connected to the structure with horizontal barriers (US Department of the Army 1983). Field tests at Colorado State University showed that vertical barriers significantly reduce differential heave compared to slabs without barriers, although the total heave over several years was similar (Goode, 1982; Hamberg, 1985).

A study conducted by Pandey et al. (2021) at Texas A&M University-Commerce examined the effectiveness of a modified moisture barrier in stabilizing a damaged section of Farm to Market 639 road in Frost, Navarro County, Texas. The 91-meter section, which had developed a large crack along its center, was treated with a geocomposite and geomembrane barrier installed at the base-subgrade interface. Moisture sensors and inclinometers were used to monitor the performance of both the treated and untreated control sections. Initial results showed an 89% reduction in deformation in the barrier section compared to the control. The barrier effectively maintained consistent soil moisture levels and prevented seasonal variations observed in the control section. During a period of significant soil shrinkage in September 2019, the control section experienced 30.24 mm of movement, while the barrier section showed minimal movement. Visual inspections revealed cracking in the control section, whereas the barrier section remained intact.

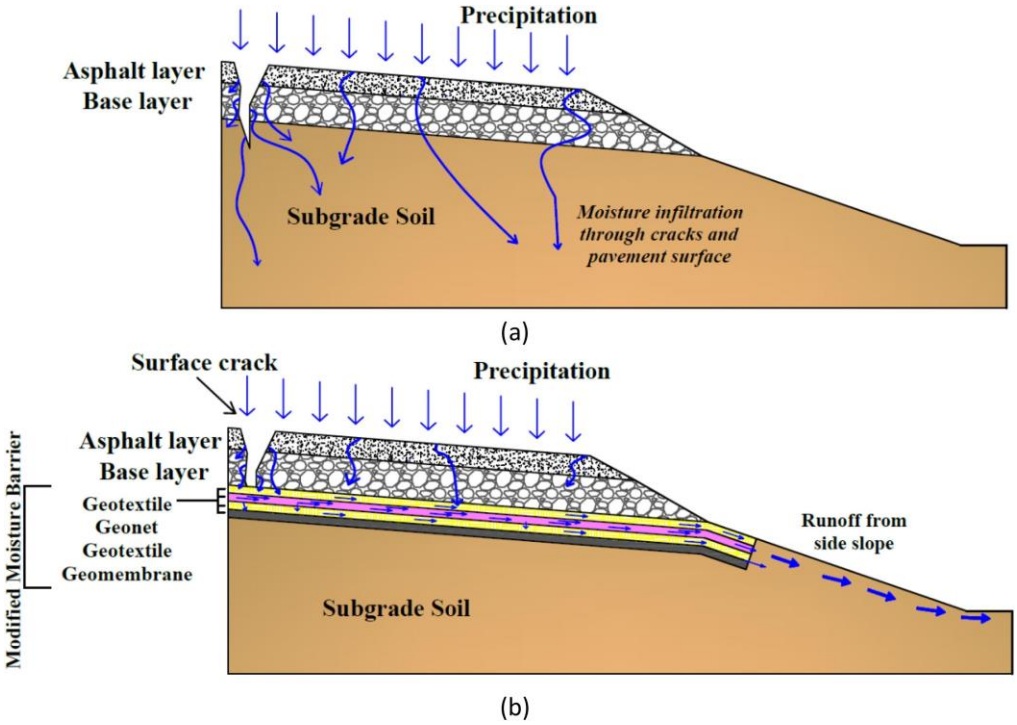

Figure 2.14: a) Moisture infiltration into subgrade soil, **b)** Modified moisture barrier isolating subgrade soil from infiltrating rainwater (Pandey et al. 2021)

2.7.2 Soil Reinforcement

Soil reinforcement is a technique for improving soil strength and stability by introducing reinforcing materials into the soil matrix. This method is particularly effective in improving shear resistance, reducing swell potential, and increasing the load-bearing capacity of soils, making it a valuable approach in various geotechnical applications.

Soil reinforcement involves integrating materials with higher tensile strength into the soil matrix. These materials work by absorbing and distributing the stresses within the soil, thereby enhancing its overall strength and stability. The fibers or geosynthetics increase the soil's resistance to shear forces, which is critical in preventing failures such as landslides or excessive settlement (Chegenizadeh & Nikraz, 2011; Viswanadham et al., 2009). Two commonly used methods of soil reinforcement are fiber reinforcement and geosynthetic reinforcement.

Fiber reinforcement involves incorporating discrete fibers, either synthetic or natural, into the soil to improve its mechanical properties. The fibers, typically made from materials such as polypropylene, polyester, or natural fibers, are mixed with the soil to create a composite material with enhanced tensile strength and ductility. Adding fibers increases the soil's resistance to deformation, thereby improving its load-bearing capacity and reducing issues such as shrinkage and swelling (Puppala & Musenda, 2000). Numerous studies have demonstrated the effectiveness of fiber reinforcement in improving soil properties (Abdi et al., 2008; Al-Akhras et al., 2008; Estabragh et al., 2016; Phanikumar & Singla, 2016; Puppala & Musenda, 2000; Soltani et al., 2018; Tang et al., 2007; Tiwari et al., 2021b; Wang et al., 2017). Puppala and Musenda (2000) used the two types of polypropylene fiber reinforcement on expansive soil. The soil was subjected to different dosages of (0, 0.3, 0.6, and 0.9 percent by dry weight of soil) fibers. The findings demonstrated that fiber reinforcement improved the unconfined compressive strength of the soil

while simultaneously decreasing both the volumetric shrinkage strains and swelling pressures of the expansive clay soils. A study done by Soltani et al. (2018) used two types of tape-shaped polypropylene fibers, i.e. fiber A (width fw = 2.5 mm) and fiber B (fw = 7.0 mm), were used as the reinforcements. The study shows that the fiber inclusions led to a significant reduction in swelling behavior, i.e. swelling potential and swelling pressure, with the reduction being dependent on fiber content and fiber length (or aspect ratio) as shown in Figure 2.14.

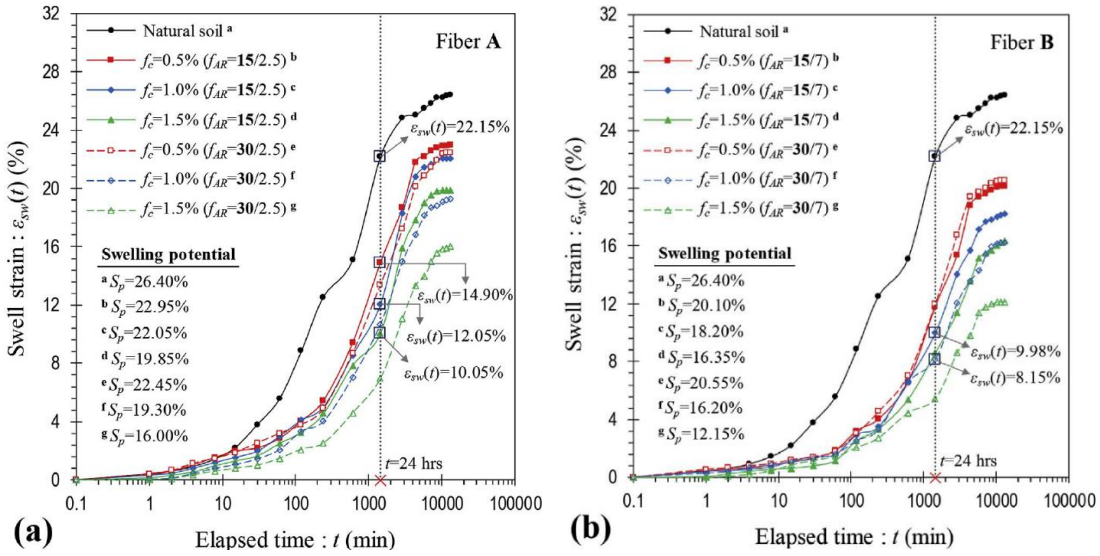

Figure 2.14: Swell strain–time curves for the natural soil and various fiber–reinforced samples, **a)** Fiber A, and **b)** Fiber B (Soltani et al. 2018).

Geosynthetic reinforcement uses geosynthetic materials, such as geogrids, geotextiles, or geomembranes, to reinforce the soil. These materials are placed within or on top of the soil layers to provide additional stability and strength. Geosynthetics are particularly effective in controlling soil erosion, improving slope stability, and reinforcing foundations (Cristelo et al., 2016; Onur et al., 2016; Tiwari et al., 2021a). Due to their high tensile strength characteristics, geosynthetics can serve multiple functions within paved structures, acting as separation layers, filtration media, stiffening elements, and reinforcement components, thereby enhancing the overall durability of

the pavement system. Various researchers have conducted in-depth investigations into the utilization of geotextiles in a range of geotechnical structures, including paved areas, residential buildings, slope stabilization projects, bridge pier construction, and landfill sites (King et al., 2017; Liu et al., 2015; Onur et al., 2016; Zornberg, 2017).

The paper by Bonaparte et al. (1987) discusses soil reinforcement applications using geosynthetics, particularly for slopes, retaining walls, and embankments on weak foundations. While not specifically addressing expansive soils, the principles and design methods presented can be adapted for use in expansive soil conditions. The authors detail various reinforcement mechanisms, including tensile resistance, soil-reinforcement interaction, and load distribution, which are all relevant to mitigating the challenges posed by expansive soils. For instance, the tensile reinforcement provided by geosynthetics can help resist the tensile stresses that develop during soil volume changes. The design considerations for reinforced slopes and embankments on weak foundations could be particularly useful when dealing with expansive soil sites, as they address stability issues and differential movements – common concerns in expansive soil environments. Additionally, the discussion on reinforcement properties and testing methods offers valuable insights for selecting appropriate geosynthetic materials for expansive soil applications, where factors such as long-term performance and soil-reinforcement interaction are important.

2.8 Chemical Stabilization

Chemical stabilization is a widely used method for improving the engineering properties of soils, particularly their strength, durability, and resistance to environmental conditions. Traditional chemical stabilization techniques typically involve the use of additives such as lime, cement, or fly ash, which react with the soil to enhance its load-bearing capacity and reduce plasticity and

swelling potential. These methods have been extensively studied and applied in various construction projects. In recent years, non-traditional techniques have emerged, utilizing innovative materials such as enzymes, polymers, and nano-additives to achieve similar or enhanced stabilization effects with potentially lower environmental impact. These modern approaches offer new possibilities for soil stabilization, particularly in challenging environments or for specialized applications.

2.8.1 Traditional Chemical Stabilization.

Traditional chemical stabilization methods are commonly employed for expansive soils due to their efficacy and widespread availability of stabilizing agents. These methods involve the addition of well-established additives that chemically interact with the soil to enhance its properties. Common traditional stabilization techniques include the use of lime, cement, and fly ash, each of which serves to modify the soil's structure and behavior. Lime is often employed to reduce plasticity and swelling, while cement increases soil strength and stiffness. Fly ash, a byproduct of coal combustion, enhances the soil's workability and compressive strength. Together, these traditional methods provide reliable solutions for managing expansive soils in various construction projects.

2.8.1.1 Lime Stabilization

The use of lime as a soil stabilizing agent has gained widespread acceptance and recognition worldwide, emerging as an extensively employed technique for enhancing soil properties. Stabilization of expansive soils with lime has proven successful, effectively minimizing swelling while improving soil plasticity and workability (Nelson et al., 2015). lime stabilization involves the process of stabilizing soils through the incorporation of calcined limestone products,

specifically either calcium oxide or calcium hydroxide (Bell, 1988). Among chemical additives employed for treating expansive soils, lime stands out as the most efficacious and extensively utilized option (Al-Mhaidib & Al-Shamrani, 1996; Al-Mukhtar et al., 2012; Al-Mukhtar et al., 2010; Belchior et al., 2017; Bhuvaneshwari et al., 2014, 2019; Biswas et al., 2021; Dafalla et al., 2015; Dash & Hussain, 2012; Kumar & Thyagaraj, 2021; Nalbantoglu, 2006; Nelson & Miller, 1997; Siddique & Hossain, 2011; Stoltz et al., 2012).

Generally, from 3 to 8 percent by weight of hydrated lime is added to the soil (Nelson & Miller, 1997). The primary reactions in the lime reaction include cation exchange, flocculation-agglomeration, lime carbonation, and pozzolanic reaction (Little, 1995; MANUAL, 2004; Nelson et al., 2015; Thompson, 1966). When water is introduced to lime, an exothermic (heat-releasing) reaction occurs, forming hydrated lime or $Ca(OH)_2$. The additional heat generated during this process, equivalent to 15.6 kcal/mol, aids in reducing the natural moisture content of soil. Moreover, upon dissolving in water, $Ca(OH)_2$ dissociates into OH^- and Ca^{2+} ions, which can replace the existing monovalent cation in the soil mineral and increase the interparticle attractive force soil (Barman & Dash, 2022), as shown in the following equations.

$$CaO + H_2O \longrightarrow Ca(OH)_2 + \text{heat} \qquad (15.6\,\text{kcal/mol}) \qquad (2-2)$$

$$Ca(OH)_2 \longrightarrow Ca^{2+} + 2OH^- \qquad (2-3)$$

Subsequently, the OH^- ions released from the hydrated lime make the soil matrix highly alkaline; under this high pH environment (pH $\geq$ 12.4), the silica and alumina from clay lattices become soluble and react with Ca^{2+} and OH^- ions, thereby forming cementitious compounds such as calcium silicate hydrate (C-S-H) and calcium aluminate hydrate (C-A-H), respectively. This series of reactions is known as the pozzolanic reaction (Federico et al., 2015; Nalbantoglu & Tuncer, 2001; Thompson, 1966). The reaction process is shown in detail as follows:

$$3Ca^{2+} + 6OH^{-} + 2SiO_2 \longrightarrow 3CaO \cdot 2SiO_2 \cdot 3H_2O \qquad (C-S-H) \qquad (2-4)$$

$$3Ca^{2+} + 6OH^{-} + Al_2O_3 \longrightarrow 3CaO \cdot Al_2O_3 \cdot 3H_2O \qquad (C-A-H) \qquad (2-5)$$

The mechanisms and effects of lime stabilization on expansive soils have been extensively studied by several researchers. Barman & Dash, (2022) performed a comprehensive study on key parameters affecting the lime stabilization process. Their study indicated that the effectiveness of this stabilization process is influenced by several key factors, such as soil type and mineralogy, lime type and amount, pH of the soil matrix, curing condition (time, temperature), organic compound, sulfate, and iron content. Researchers at Texas A&M University have developed a comprehensive framework, the Soil Stabilization Index System (SSIS), to support road maintenance and construction projects (Nelson & Miller, 1997). This system assists in selecting the most suitable soil stabilization technique by providing a decision-making flowchart based on the soil's Plasticity Index. The flowchart, illustrated in Figure 2.15, guides users through a step-by-step process, helping them determine the most effective method for stabilizing soils with varying plasticity characteristics. By considering the PI, the SSIS ensures that the chosen stabilization technique is tailored to the soil's specific needs, ultimately leading to more durable and stable road infrastructure.

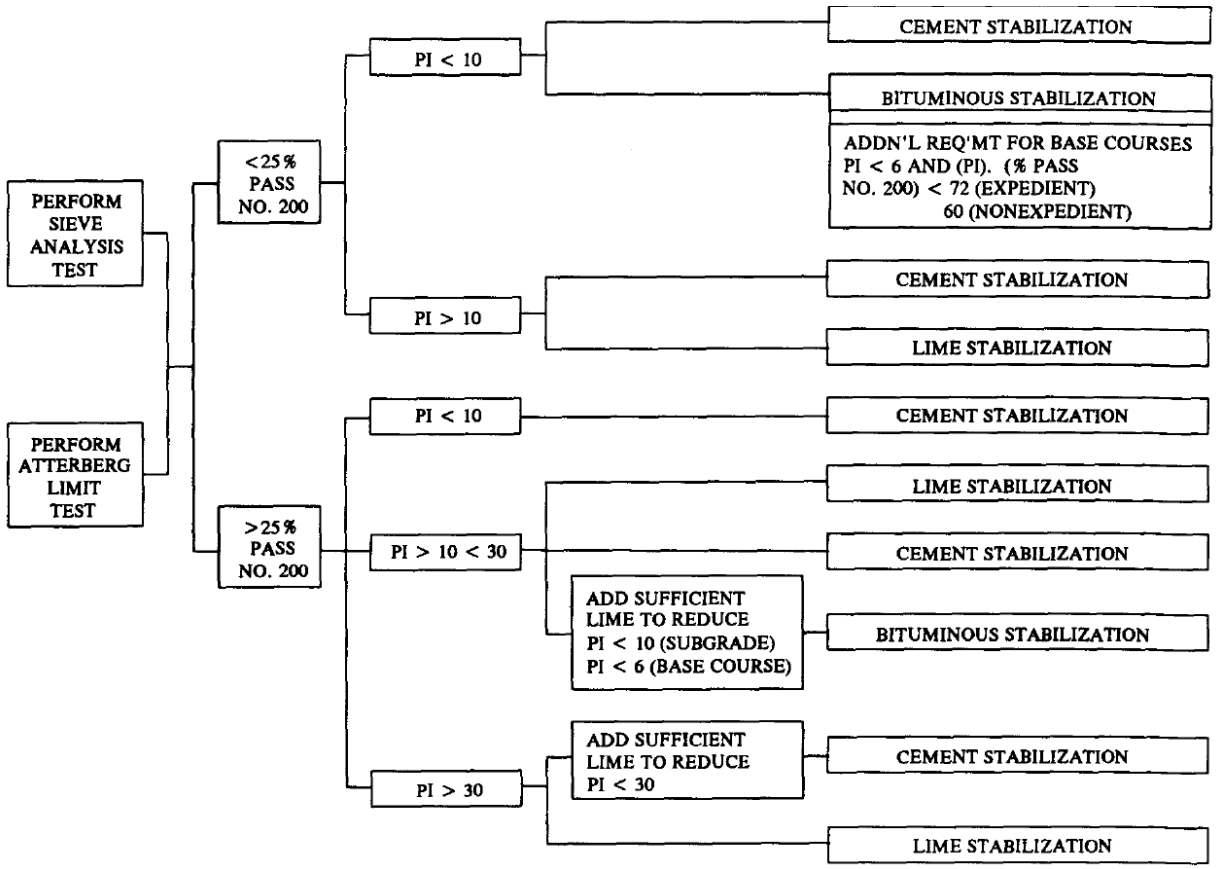

Figure 2.15: Selection of stabilization technique-SSIS Method (Nelson & Miller, 1997).

Zhao et al. (2015) investigated the lime stabilization mechanisms of expansive clay (Nanyang clay), finding that cation exchange, flocculation, and calcium hydroxide crystal formation occurred rapidly, leading to significant swelling reduction within one week. They noted that pozzolanic reactions and carbonation, contributing to long-term strength gains, became more prominent after 90 days. Figure 2.16 (a,b) indicates the SEM images of treated and untreated Nanyang clay with lime. Dash and Hussain (2012) provided insights into the complex relationship between lime content, soil type, and curing time in soil stabilization. The effectiveness of lime stabilization was evaluated on various soil types by measuring key geotechnical properties, including Atterberg limits (liquid and plastic limits), swelling potential, unconfined compressive strength, mineralogical composition, and microstructural characteristics. They observed that while

lime generally improves soil performance initially, excessive amounts can have adverse effects, particularly in silica-rich soils. Their research revealed an optimum lime content (5-9%, depending on soil type) beyond which strength decreased and swelling increased due to the formation of porous calcium silicate gels. Alternative approaches to lime stabilization have also been explored. Thyagaraj et al. (2012) investigated in-situ lime precipitation by sequentially mixing calcium chloride and sodium hydroxide solutions with expansive soil. This method effectively reduced swelling potential and plasticity index while increasing unconfined compressive strength. Sahoo and Pradhan (2010) examined the use of lime-stabilized soil cushions, finding that a red soil cushion stabilized with 8% lime and cured for 17 days significantly improved the strength and durability of underlying expansive soil.

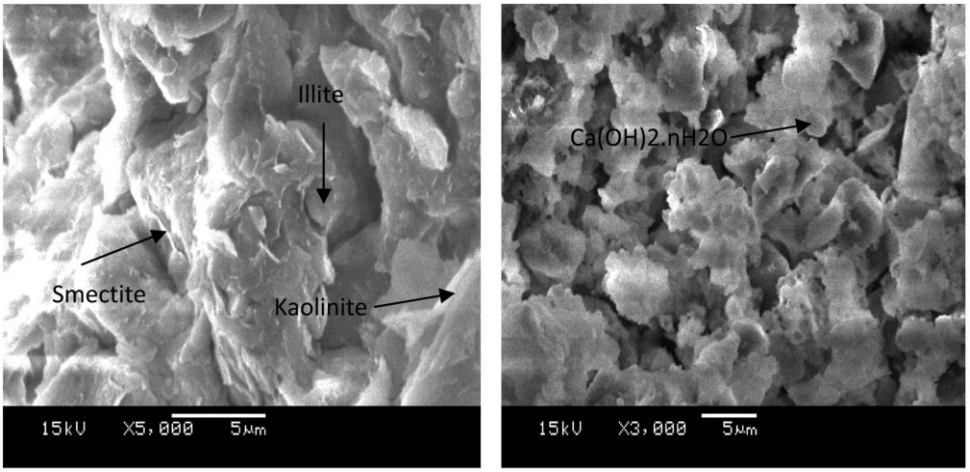

Figure 2.16: SEM image of **a)** compacted Nanyang expansive clay, **b)** lime-treated Nanyang expansive clay immediately after compaction (Zhao et al., 2015)

2.8.1.2 Cement Stabilization

Portland cement has been demonstrated to be effective in improving different soil types, including granular soils, silts, and clay soils (Nelson et al., 2015). When clay is mixed with cement and water, a complex process of hydration and chemical reactions occurs. The primary components of

cement, tricalcium silicate C_3S, and Di-calcium silicate C_2S react with water to form cementitious compounds such as calcium silicate hydrate (C-S-H) and calcium aluminum hydrate (Barman & Dash, 2022; Chew et al., 2004; Prusinski & Bhattacharja, 1999). These reactions, represented by equations are shown here as follows:

$$2C_3S + 6H_2O \longrightarrow C-S-H + Ca(OH)_2 \qquad (2-6)$$

$$2C_2S + 4H2O \longrightarrow C-S-H + Ca(OH)_2 \qquad (2-7)$$

The hydrated lime $Ca(OH)_2$ produced during this process further breaks down into OH^- and Ca^{2+} ions, promoting soil flocculation and reacting with pozzolanic materials in the soil to form additional cementitious compounds (Estabragh et al., 2014; Herzog & Mitchell, 1963). This process leads to the formation of stronger interparticle bonds and enhanced soil performance. It also decreases the soil's liquid limit, plasticity index, and susceptibility to volume fluctuations (Chen, 2012; Petry & Little, 2002).

Research by Zhao et al. (2013) on cement stabilization of highly expansive Handan clay provides concrete evidence of these enhancements in soil behavior and characteristics. Their research found that over a 7-day curing period, the physicochemical properties of the cement-treated clay underwent substantial changes. Notably, the plasticity index decreased substantially, while the swelling potential was almost eliminated after seven days. Scanning Electron Microscopy (SEM) analysis provided insight into the microstructural evolution of the treated soil. Initially, cement eroded clay particles, a process followed by the formation of new hydration products. These products developed into a chain-shaped, solid gel-like structure, which contributed to the stabilization and strengthening of the soil matrix. Chemical analysis further revealed complex alterations in the cation concentrations within the pore water and the soil's exchange complex, indicative of the ongoing pozzolanic reactions between the cement and the clay minerals.

These reactions contributed to the formation of stable, cementitious compounds that enhanced the soil's strength and durability. One of the most significant findings was the marked increase in the unconfined compressive strength of the cement-treated clay. The stress-strain behavior of the soil also shifted from a strain-hardening response, where the material continues to strengthen as it deforms, to a strain-softening behavior, where the material initially strengthens but then begins to weaken after reaching peak strength. This transition highlights the profound impact of cement stabilization on the mechanical performance of the soil.

The typical cement content for treating expansive soils usually falls between 2% and 6% of the soil's dry weight (Chen, 2012). However, cement is less effective than lime for highly plastic clays and is more suitable for non-lime-reactive soils (Mitchell & Raad, 1973). The mixing process is similar to lime stabilization but requires a shorter time between addition and final mixing due to cement's quicker hydration and setting time (Nelson et al., 2015). While cement treatment offers significant strength improvements, it may cause cracking, which can be minimized through proper construction techniques. These techniques include compacting at slightly drier than optimum water content, pre-cracking, delayed surface hot mix placement, reduced cement content, and use of interlayers (Little et al., 2000; Petry & Little, 2002). It's important to note that cement stabilization may not be suitable for all clay soils, particularly those with high water affinity, which may impede complete cement hydration (Nelson et al., 2015).

Various environmental and compositional factors play a critical role in determining the performance of cement-treated soils. The mineralogy of the soil is particularly influential in the stabilization process. For instance, soils rich in kaolinite and well-crystallized illite tend to be more resistant to cement treatment compared to those containing montmorillonite, which reacts more readily with cement (Bell, 1995; Herzog & Mitchell, 1963). The required cement content for

effective stabilization varies depending on soil properties, typically ranging from 3% to 16% for expansive soils (Bell, 1993; Rauch et al., 2002). The effectiveness of cement stabilization is also contingent upon several key factors, including the water-cement ratio, cement content, and the curing period (Barman & Dash, 2022; Horpibulsuk et al., 2010; Miura et al., 2001; Prusinski & Bhattacharja, 1999). According to the Portland Cement Association (2003), achieving a 7-day compressive strength of 2.1-2.8 MPa for treated clay generally requires an appropriate cement content. Elevated curing temperatures can significantly accelerate strength development in cement-treated soils (Zhang et al., 2014), whereas exposure to freeze-thaw cycles typically reduces both strength and stiffness, presenting a challenge in colder climates (Jamshidi et al., 2016). Organic matter in soil can hinder cement hydration, especially when the content exceeds 3-4% (Barman & Dash, 2022; Tremblay et al., 2001). Additionally, the presence of sulfates in the soil can induce ettringite formation, an expansive mineral that can cause heaving and cracking in stabilized soils (Nelson et al., 2015; Rajasekaran, 2005; Ramon & Alonso, 2013). Compaction is generally recommended within a 2-hour window after mixing to ensure optimal compaction and strength, as delays can negatively impact strength and density (Bell, 1995; Little & Nair, 2009). In recent years, the addition of nano-silica to cement-treated soils has been explored to enhance cement hydration and promote pozzolanic reactions. Even in small quantities, nano-silica has been shown to improve strength and reduce hydraulic conductivity, making it a promising additive for soil stabilization (Ghasabkolaei et al., 2016; Kulanthaivel et al., 2021). These factors collectively influence the effectiveness of cement stabilization, highlighting the importance of considering soil composition, environmental conditions, and additives in soil improvement projects.

2.8.1.3 Fly Ash Stabilization

Fly ash, a fine-grained residue from coal combustion in power plants has been used as an additive in soil treatment, particularly with lime (NLA 2004). It is classified into two major types: Class F, produced from anthracite or bituminous coal, and Class C, from lignite and subbituminous coal (Cokca, 2001). Both classes are pozzolanic, but Class C is also cementitious and often contains higher sulfate levels. Fly ash particles are spherical, non-plastic, and typically classified as 'silt' in the United Soil Classification System (Deka et al., 2015; Yarbaşı et al., 2007).

The addition of fly ash to the soil reduces plasticity index, permeability, and expansion potential while increasing stiffness, strength, and freeze-thaw resistance (Little et al., 2000; Nelson et al., 2015). Studies have shown significant reductions in swelling potential and pressure of expansive soils with fly ash treatment. Cokca (2001) reported a 68% reduction in swelling potential with Class C fly ash, while Puppala et al. (2006) observed up to 64% reduction in swelling pressures with Class F fly ash. The effectiveness of fly ash stabilization depends on factors such as soil type, fly ash content, and fly ash type, with optimal content typically ranging from 15-20% for Class C and 25-60% for Class F (Cokca, 2001; Mir & Sridharan, 2019; Misra, 1998; Solanki et al., 2009).

Research by Phani Kumar and Sharma (2004) demonstrated that fly ash addition reduces soil plasticity, with the liquid limit decreasing and plastic limit increasing as fly ash content increases. They observed a 50% reduction in the free swell index (FSI) of expansive soil with 20% fly ash addition. Both swell potential and swelling pressure were reduced by 50% at 20% fly ash content. The hydraulic conductivity of soil-fly ash mixtures decreased with increasing fly ash content, correlating with an increase in maximum dry unit weight. Compaction characteristics are also affected by fly ash addition. Phani Kumar and Sharma (2004) reported that the optimum moisture content decreased by 25%, while the maximum dry unit weight increased by about 5%

at 20% fly ash content. Compaction curves shifted upward and toward the left with increasing fly ash content, indicating improved soil stability. The undrained shear strength of soil-fly ash mixtures increased with fly ash content, showing a 27% increase at 20% fly ash for a water content of 20%. Environmental factors such as freeze-thaw cycles and the presence of organic matter or sulfates in the soil can impact the effectiveness of fly ash stabilization, necessitating careful consideration in design and implementation (Bin-Shafique et al., 2011; McCarthy et al., 2012; Nath et al., 2017).

Despite the advantages of using traditional stabilizers (lime, cement, and fly ash), they are also associated with several disadvantages. for example, lime treatment requires sustained temperatures above 70°F for 10-14 days to gain strength effectively, and its efficacy is reduced in soils containing organics, sulfates, or certain iron compounds. Additionally, lime-treated soils are vulnerable to strength loss if exposed to excessive water, as lime can be leached out when saturated, necessitating protection from both surface and groundwater to maintain the treatment's effectiveness. In the same way, cement treatment, while similar to lime treatment in application, may not be as effective as lime in treating highly plastic clays, potentially limiting its usefulness in certain soil types. Furthermore, cement-stabilized material is prone to cracking, which necessitates careful evaluation before use and may lead to long-term stability issues in treated soils (Nelson & Miller, 1997). Moreover, environmental challenges and energy intensiveness are additional factors. For example, manufacturing 1 tonne of Portland cement produces approximately 0.95 tonnes of CO_2 equivalent emissions and requires 5000 MJ of primary energy (Higgins, 2007).

2.8.2 Non-Traditional Chemical Stabilization

Expansive soil's non-traditional chemical stabilization involves using innovative or less conventional chemical additives to enhance the engineering properties of expansive soils. These methods are often explored as alternatives to traditional stabilizers such as lime, cement, and fly ash. Non-traditional chemicals for expansive soil can be used independently, in combination with traditional methods, or even synergistically with other non-traditional techniques. While there are various categories of these non-traditional stabilizers, a detailed exploration of all types is beyond the scope of this study. Instead, this section will focus on the most commonly used groups of non-traditional chemicals for stabilizing expansive soils.

2.8.2.1 Salt stabilization

The most common salts used in soil stabilization are sodium chloride (NaCl) and calcium chloride ($CaCl_2$) (Nelson & Miller, 1997). These inorganic salts, along with others like KCl, $MgCl_2$, and $AlCl_3$, play a significant role in soil modification (Turkoz et al., 2014). When expansive clay comes into contact with a salt solution, cation exchange occurs, with multivalent cations (e.g., Ca^{2+}, Al^{3+}) replacing weaker cations (e.g., Na^{+}, K^{+}) (Gleason et al., 1997). This process, along with increased salt concentration in soil pores, leads to particle flocculation and a reduction in the diffuse double layer (DDL) thickness, resulting in decreased liquid limit, plasticity, swelling potential, and swelling pressure of clay soils (Barman & Mishra, 2022; Di Maio, 1996).

The effects of sodium chloride on soil properties are variable but generally more pronounced in soils with a high liquid limit. It may increase the shrinkage limit, and shear strength, and provide some control over frost heave in reactive soils Calcium chloride, which has been used for frost heave control since the late 1920s, stabilizes moisture content changes in soils, reducing the potential for volume change. Typically, about 1% calcium chloride by weight of dry soil is needed for stabilization (Nelson & Miller, 1997). Treatment with $CaCl_2$ leads to an increase in

maximum dry density (MDD) and a decrease in optimum moisture content (OMC), contributing to improved initial and long-term soil strength (Zumrawi & Eltayeb, 2016). This strength improvement is attributed to cation exchange, formation of Calcium Silicate Hydrate (C-S-H) and (Calcium Aluminate Silicate Hydrate) CASH gels, and increased pore water surface tension (Shon et al., 2010; Tingle et al., 2007). For any type of salt, a concentration of 1 mol/L is typically sufficient to decrease the liquid limit and swelling potential to minimal levels (Di Maio, 1996). It's worth noting that the performance of $CaCl_2$ is generally superior to other salts (Abood et al., 2007), and the strength improvement increases with the curing period (Shon et al., 2010; Turkoz et al., 2014).

Despite their benefits, salt treatments have some drawbacks. Calcium chloride is easily leached from the soil and requires a relative humidity of at least 30% for effective use. Due to leaching, salt treatments generally need to be repeated every 3 years, which may affect their economic viability (Gromko, 1974). There is insufficient evidence that salts other than sodium chloride and calcium chloride have adequate soil stabilization capabilities to be economically justifiable.

2.8.2.2 Enzyme

Enzymes are organic molecules that catalyze specific chemical reactions under favorable conditions, typically used in low concentrations as they are not consumed by the reactions they facilitate. For an enzyme to be active in the soil, it requires mobility to reach a reaction site, which is provided by pore fluid, while the specific soil chemistry offers the reaction site (Tingle et al., 2007).

Enzymes like Renolith, PermaZyme, TerraZyme, and Fujibeton have emerged as potentially effective organic catalysts for stabilizing fine-grained soils, particularly expansive ones (Parsons & Milburn, 2003; Shankar et al., 2009; Tingle et al., 2007). These non-toxic, biodegradable liquids work by neutralizing the negative charge on clay surfaces, reducing water affinity, and producing cementitious products (Khan et al., 2020; Marasteanu et al., 2005). The enzyme coating on soil particles prevents further water adsorption, creates physical bonds between soil grains, and reduces void distribution in the soil matrix (Chitragar et al., 2019; Pooni et al., 2019). These effects can lead to improved soil strength, increased California Bearing Ratio (CBR) values, reduced permeability, and enhanced resistance to wet-dry cycles and desiccation cracking (Begum et al., 2020; Pooni et al., 2019; Rajoria & Kaur, 2014; Venkatasubramanian & Dhinakaran, 2011; Xie et al., 2020). The proposed mechanism for enzyme stabilization, resulting in reduced affinity for moisture, appears theoretically valid but has limited laboratory verification. Rauch et al. (2003) reported minor changes in X-ray diffraction results, specific surface area, and alumina/silica ratios for high enzyme quantities.

The effectiveness of enzyme stabilization depends on factors such as clay content, temperature, curing time, and environmental conditions (Barman & Dash, 2022; Tingle et al., 2007). Tingle and Santoni (2003) observed only minor improvements in wet, unconfined compressive strength of low-plasticity and high-plasticity clays with one enzyme product. Enzyme dosages generally range from 0.002% to 0.1%, depending on the soil's clay fraction (Blanck et al., 2014; Xie et al., 2020). Given this mechanism, enzymes may be most appropriate for use with clay materials that have an affinity for water, particularly high-plasticity clays with organic content. Silts and granular soils, which lack significant water affinity, would be unsuitable for enzyme stabilization. While enzyme stabilization offers potential benefits, including improved soil

performance and durability, its efficacy is limited in soils with inadequate clay content or at higher temperatures (Thomas & Rangaswamy, 2019).

2.8.2.3 Polymer Stabilizer

Polymer stabilizers, typically composed of vinyl acetates or acrylic copolymers suspended in an emulsion, work by coating soil particles and forming physical bonds as the water evaporates. The emulsifying agent in these stabilizers also acts as a surfactant, enhancing penetration and particle coating efficiency. The effectiveness of polymer stabilization depends on the ability to adequately coat soil particles and the physical properties of the polymer itself. This method is more suitable for granular materials than fine-grained soils due to the latter's high specific surface area, which reduces mixing efficiency. Polymers used in soil stabilization generally provide excellent tensile and flexural strength, creating robust physical bonds (Tingle et al., 2007). Similar to asphalt cement, these polymers are water-resistant, effectively waterproofing the coated particles and reducing moisture susceptibility (Tingle et al., 2007).

Polymer stabilization of expansive soil has been reported by researchers widely (Al-Atroush & Sebaey, 2021; Azzam, 2012; Hu et al., 2022; Liu et al., 2017; She et al., 2020; Singh & Das, 2020; Soltani, Deng, et al., 2022; Tiwari et al., 2020; Yazdandoust & Yasrobi, 2010; Zhang et al., 2019). Taher et al. (2020) conducted a study comparing commercially available polymer soil stabilizers to quicklime and Class C fly ash for expansive soil treatment. They found that while polymer treatment reduced the swelling potential of highly expansive soil by 70% and increased unconfined compressive strength by only 46 kPa, it was significantly less effective than lime and fly ash. Lime treatment achieved a 100% reduction in swelling potential and a 1260 kPa increase in UCS, while fly ash treatment resulted in a 97% reduction in swelling and a 380 kPa increase in UCS.

However, one notable advantage of the polymer treatment was its minimal impact on hydraulic conductivity, increasing it by only 2 times relative to untreated soil (2.9×10^{-11} m/s). In contrast, lime and fly ash treatments led to much larger increases, 52,000 and 1,100 times, respectively. Interestingly, when the polymer was applied as a spray-on coating, it effectively reduced hydraulic conductivity to below 1.9×10^{-12} m/s. In a related study, Ma et al. (2023) explored using polymer waterproof coatings to protect expansive soil slopes from instability caused by precipitation. Their findings demonstrated that polymer coatings were highly effective in reducing moisture content fluctuations and preventing rainwater infiltration in slopes. The effectiveness of coating increased with higher soil compaction density and was most pronounced when coverage exceeded 90%.

2.8.2.4 Lignosulfonates Stabilizer

Lignosulfonates, derived from lignin in wood and plant materials, are versatile soil stabilization products available in sodium, calcium, and ammonium forms. These compounds function primarily as cementing agents by coating soil particles with a thin adhesive film, and physically bonding them together (Tingle et al., 2007).

While their exact chemical composition varies due to diverse source materials, lignosulfonates also possess minor chemical effects and ion exchange capabilities that contribute to soil stabilization. These effects can vary, offering additional benefits based on the specific type of lignosulfonate used. Typically water-soluble, lignosulfonates are susceptible to leaching under wet conditions, but they remain highly effective as long as they are retained within the soil matrix. Obtained as a by-product from the wood and paper processing industry, lignosulfonates present a

sustainable option for soil stabilization, aligning with environmental and economic goals (Chavali & Reshmarani, 2020; Tingle et al., 2007).

Lignosulfonates are widely used to improve various soil properties, including strength, erosion resistance, compaction, and durability (Indraratna et al., 2008; Santoni et al., 2002; Telysheva & Shulga, 1995; Tingle & Santoni, 2003). For example, research conducted by Tingle and Santoni (2003) demonstrated that low plasticity clay (CL) treated with a lignosulfonate solution showed significant strength improvement under both dry and wet conditions after 28 days of curing. This finding underscores lignosulfonate's ability to enhance soil stability across different environmental conditions, making it a versatile stabilizing agent. Further research by Chavali and Reshmarani (2020) revealed that lignosulfonate significantly influences the strength behavior of expansive soils. The treatment with lignosulfonate reduces the negative surface charge of soil particles, leading to the formation of a polymer chain microstructure. This microstructure, coupled with the flocculation or aggregation of soil particles (as shown in Figure 2.17), contributes to the enhanced strength and stability of expansive soils. The study also highlighted that the fine content in the soil plays a crucial role in determining the optimum percentage of lignosulfonate required for effective stabilization. Higher fine content typically demands a greater amount of lignosulfonate to achieve the desired improvement in soil properties.

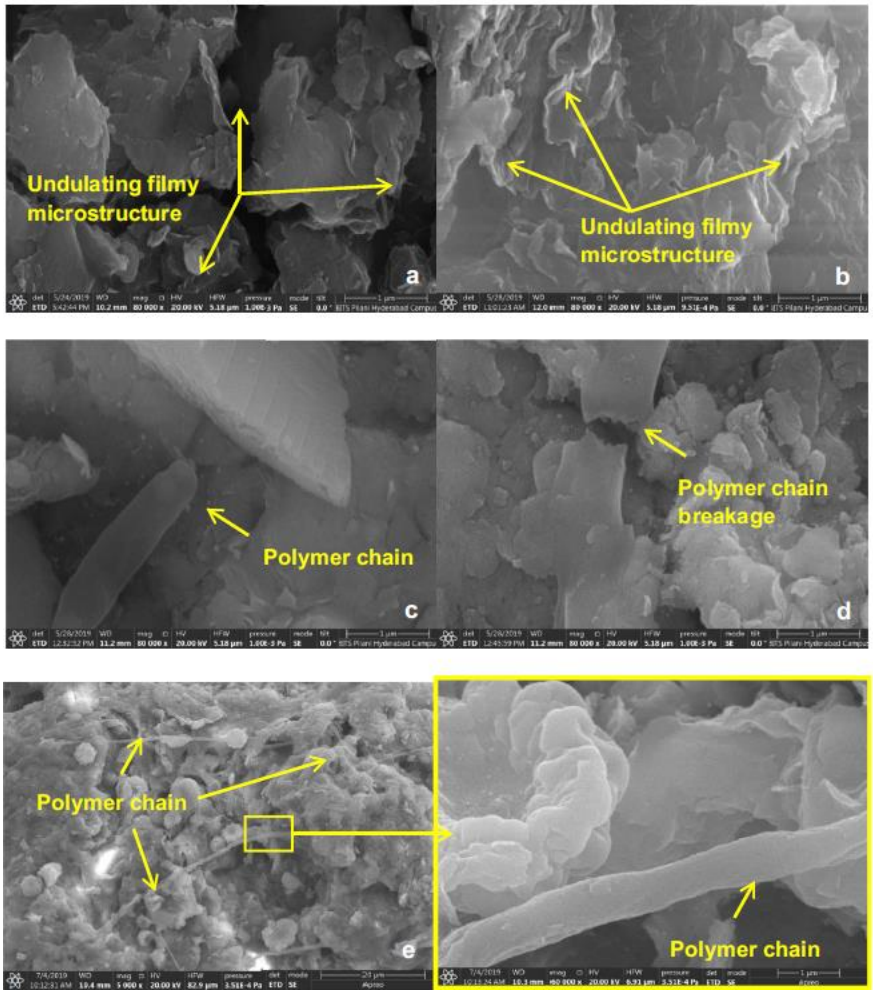

Figure 2.17: SEM images of Amaravathi soil treated with **a)** 0% Lignosulfonate, **b)** 0.5% Lignosulfonate, **c)** 1% Lignosulfonate, **d)** 2% Lignosulfonate, **e)** 4% LS (Chavali & Reshmarani, 2020)

2.8.2.5 Nanoparticle Stabilizers

Nanoparticles are extremely small particles with dimensions typically ranging from 1 to 100 nanometers (nm) (Krishnan & Shukla, 2019). Due to their small size and relatively large SSA compared to conventional soil additives, these particles can interact significantly with the soil matrix, and even a small amount of these particles can notably modify soil physiochemical properties including strength, stiffness, and hydraulic conductivity (Kong et al., 2018; Samala &

Mir, 2020; Yong et al., 2019). Nanoparticles can effectively penetrate into the soil pores upon integration, affecting water flow through the soil matrix. This integration will impact drainage efficiency and the potential for water accumulation, which subsequently can change the swelling potential in expansive soils (Alsharef et al., 2016; Ng & Coo, 2015; Yong et al., 2019). In terms of mechanical behavior, due to the large SSA of nanoparticles, stronger adhesive forces are expected between the nanoparticles and the soil matrix, thereby yielding a consequential increase in soil strength (Kalhor et al., 2019) and stiffness (Changizi & Haddad, 2016; Ghasabkolaei et al., 2016; Ghavami et al., 2018). Furthermore, due to the chemical interactions of nanoparticles with the soil, significant changes in the chemical properties of the soil would occur. These changes encompass variations in pH and cation exchange capacity, which ultimately would improve the swell-shrink characteristics of the soil (Coo et al., 2016; Naval et al., 2017).

Given the limited information available on the effects of nano-conditioning on expansive soils, Zulfiqar et al. (2024) conducted an extensive literature review to gather data and studies related to the use of nano-conditioning in general soil treatment, with a particular emphasis on factors relevant to the behavior of expansive soils. In this review, soil parameters were categorized into three distinct groups: physical (e.g., plasticity index), mechanical (e.g., elastic modulus, unconfined compressive strength, and shear strength parameters), and hydraulic characteristics (e.g., hydraulic conductivity, saturated volumetric water content, and soil water retention curves). Each of these parameters is crucial for effective soil stabilization, particularly in the context of expansive soils, where a comprehensive understanding is essential for appropriately modifying the soil under varying hydro-mechanical loading conditions. Table 2.2 provides a summary of the data and nanoparticles considered for this research, with index numbers used in Figures 2.18-2.21 to

facilitate the interpretation of data across these studies. The subsequent sections discuss the impact of nano-conditioning on these various soil parameters.

Table 2.2: Index number, soil type, and nanoparticles used in Figures 2.18-2.21

Index No	Soil Type	NPs	References
1	SC	MWCNT, CNFs	(Alsharef et al., 2016)
2	CH	CuO, γ-Al_2O_3	(Coo et al., 2016)
3	CL-ML	Nanoclay	(Tabarsa et al., 2018)
4	CH	MgO , Al_2O_3	(Naval et al., 2017)
5	CL	Silica Fume,SiO_2	(Ghavami et al., 2018)
6	CL	$CaCO_3$	(Choobbasti et al., 2019)
7	CL	SiO2	(Kalhor et al., 2019)
8	CL	Nano Clay	(Karumanchi et al., 2020)
9	CL	Bentonite	(Ghasemipanah et al., 2014)
10	CL	SIC	(Alsabhan et al., 2023)
11	CL	SiO_2	(Ghasabkolaei et al., 2016)
12	Silty clay	ZnO	(Khodaparast et al., 2021)
13, 14	CL	SiO_2	(Samala & Mir, 2020)
15	Loess	SiO_2	(Kong et al., 2018)
16, 17	CH	SiO_2	(Thomas & Rangaswamy, 2020)
18	CL	SiO_2	(Changizi & Haddad, 2016)
19	Soft soil	MgO	(Gao et al., 2018)
20	CL	iron oxide	(Rajabi et al., 2021)
21	CL	SiO_2	(Moayed & Rahmani, 2017)
22	CL	Nanocaly, SiO_2	(Zomorodian et al., 2017)

2.8.2.5.1 Impact of Nanoparticle Stabilizers on Physical Characteristics of Soil

Studies on the effect of nano-conditioning on the physical characteristics of soil often focus on its impact on the soil's plasticity index. The plasticity index is a key indicator of a soil's tendency to undergo volume changes due to swelling and shrinkage, which is particularly critical in expansive soils. Soils with a high PI are especially prone to significant volume fluctuations as they absorb and release water. Nano-conditioning presents a promising approach to modifying the plasticity index, potentially improving soil stability. However, the effectiveness of nano-conditioning in

altering the PI of soils can vary depending on factors such as the type, concentration, and surface characteristics of the nanoparticles used. For example, as shown in Figure 2.18, the incorporation of nanoparticles like carbon nanofibers, nanotubes, and nanoclays can lead to a significant increase in the PI. This increase can range from 15.38% with the addition of 0.2% carbon nanotubes (Alsharef et al., 2016) to approximately 96% with the inclusion of 1% nanoclay (Karumanchi et al., 2020).

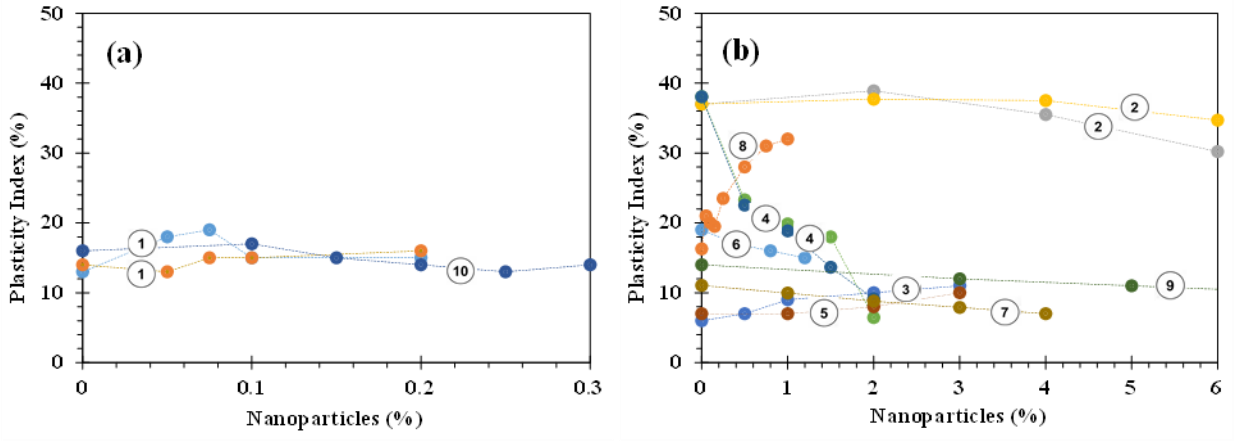

Figure 2.18: Plasticity index of different soil at varying percentages of nanoparticles

Naval et al. (2017) explored the integration of MgO and Al_2O_3 nanoparticles into expansive soil and consistently observed a reduction in PI with different nanoparticle percentages. Specifically, adding 2% MgO (light green – curve 4) and Al_2O_3 (yellow – curve 4) nanoparticles resulted in a PI reduction of around 83% and 76%, respectively. Similar trends were reported when incorporating other nanoparticles, such as $CaCO_3$ in curve 6, bentonite in curve 9, and SIC in curve 10. As presented in Figure 2.18(b), the results reported by Ghavami et al. (2018) – curve 5 suggest that the incorporation of 3% nano-SiO_2 into Kaolinite clay can lead to an increase in soil PI, while Kalhor et al. (2019) – curve 7 reported an opposite trend, where a decrease in PI was observed with 3% nano-SiO_2 concentration. These conflicting results highlight the complexity of

nanoparticle-soil interactions and suggest that factors such as soil chemical composition and physical characteristics can also play a significant role.

2.8.2.5.2 Impact of Nano-conditioning on Mechanical Behavior of Soil

The effect of nano-conditioning on the mechanical behavior of expansive soils has primarily been studied through variations in Unconfined compressive strength, elastic modulus, and shear strength parameters, including cohesion (c) and friction angle (ϕ'). Figures 2.19(a), (b), and (c) illustrate the UCS of the soil at varying curing periods and nanoparticle dosages. As observed in these figures, the effect of nanoparticles on soil's compressive strength can be different depending on the type of soil and the nanoparticles used for treatment. For example, a direct correlation is noted between the increase in the percentage of nano-SiO_2 and the corresponding enhancement in the UCS of soil (curves 5, 7, 13, 14, 15, and 16). However, there is a saturation point beyond which the strength starts to decline. This decline in strength can be attributed to SiO_2 aggregation and disruption of the cementitious matrix, which varies depending on the soil type. Furthermore, these findings suggest a significant increase in UCS when soil is conditioned for an extended period of time (Ghavami et al., 2018; Kalhor et al., 2019; Kong et al., 2018; Samala & Mir, 2020; Thomas & Rangaswamy, 2020).

Curve 6 illustrates the effect of $CaCO_3$ nanoparticles on soil strength. The highest UCS was achieved when clay was incorporated with 1.2% $CaCO_3$. The UCS of the soil increased from 250 kPa with no additives to 362 kPa, 372 kPa, and 408 kPa for curing periods of 7, 14, and 28 days, respectively. This increase in UCS is attributed to the formation of cementitious material between the stabilizer and soil, which enhances inter-particle bonds and fills the voids. Additionally, the presence of $CaCO_3$ crystals further strengthened the inter-particle bonds, contributing to the overall increase in soil strength (Choobbasti et al., 2019). Curve 11

demonstrates the effect of incorporating different percentages of nano-SiO_2 as additives into the soil, along with 9% cement as co-additive (Ghasabkolaei et al., 2016). The inclusion of co-additive was observed to facilitate a chemical reaction between co-additive and nanoparticles and further improve the soil strength. A similar trend was noted when different percentages of ZnO nanoparticles were combined with 6% lime, as shown in curve 12 (Khodaparast et al., 2021).

Cohesion and friction angle are also necessary measures of soil strength. Cohesion represents the internal molecular attraction between soil particles. A higher cohesion value indicates that the soil particles adhere more strongly and possess greater resistance to shear forces. Figure 2.19(d) illustrates the relationship between soil cohesion and various dosages of nanoparticles at different time intervals. As presented in this figure, contrasting findings have been reported regarding the impact of nanoparticles on soil cohesion. In some cases (curves 18, 19, 3, and 10), an increasing trend in soil cohesion is observed at higher doses of nanoparticles. For example, Tabarsa et al. (2018) found that mixing varying percentages of nanoclay (1%, 2%, and 3%) can significantly increase soil cohesion when it is cured for 16 hours. Specifically, the cohesion of the low-plasticity clay and silt increased from an initial value of 23 kPa to values as high as 52.2 kPa (Curve 3 in Figure 2.19d).

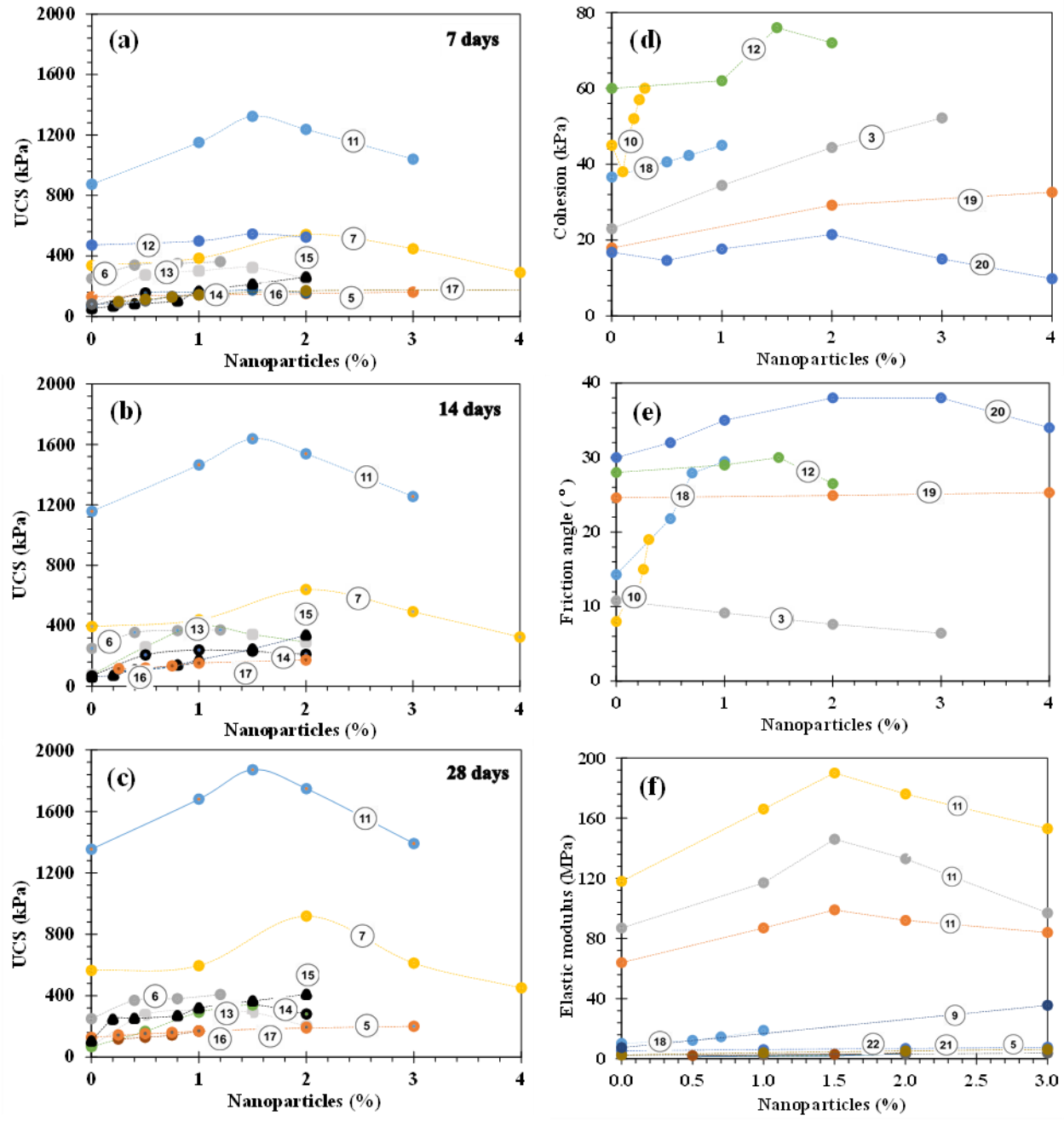

Figure 2.19: Unconfined compressive strength, cohesion, friction angle, and elastic modulus of soil at different dosages of nanoparticles

Rajabi et al. (2021) related this behavior to the formation of cement-like compounds in the presence of nano-iron oxide which can result in increased van der Waals forces between the nanoparticles and soil particles and improved cohesion. However, in the cases of curves 12 and 20, variations of soil cohesion to nanoparticle percentage do not follow the same pattern. For these cases, cohesion initially increases but then declines beyond a certain dosage. Similar to cohesion, the relationship between nanoparticle percentage and friction angle can vary widely depending on the specific types of soil and nanoparticles involved. In some cases (curves 10 for nano-SIC and 18 for nano-SiO_2), the presence of nanoparticles corresponds with a substantial increase in the soil's friction angle. However, a marginal change was noted in the friction angle for cases where nanoparticles such as nanoclay – curve 3, ZnO – curve 12, MgO – curve 19, and nano-iron oxide – curve 20, were employed for soil conditioning. Consequently, drawing a universal conclusion regarding the effect of nanoparticles on the soil friction angle and cohesion is challenging.

Elastic Modulus offers valuable insights into soil stiffness and deformation. Soil with a higher Young's modulus (E) is stiffer and more resistant to an applied force, thereby minimizing the settlement potential. Figure 2.19(f) compares the elastic modulus of the soils treated with various nanomaterials and different percentages. As presented in this figure, for soils treated with SiO_2 (Changizi and Haddad, 2016 – curve 18) and nanobentonite (Ghasemipanah et al. 2014 – curve 9), a proportional increase in the soil's E_{50} was noted as the dosage of nanoparticles increases. A similar trend in Young's modulus of soils can be observed for other nanoparticles such as SiO_2 (Ghavami et al., 2018– curve 5), SiO_2 (Moayed & Rahmani., 2021 – curve 21), and nanoclay & SiO_2 (Zomorodian et al., 2017– curve 22). In one case where nano-SiO_2 was mixed with chemical agents such as cement (Ghasabkolaei et al. 2016 – curve 11), elastic modulus initially increased, but decreased once the percentage exceeded a certain threshold.

2.8.2.5.3 Impact of Nanoparticle Stabilizers on Hydraulic Characteristics of Soil

Hydraulic conductivity refers to the soil's ability to transmit water and defines drainage conditions in soils. Nanomaterials can influence hydraulic conductivity by altering soil structure, pore characteristics, and surface properties. Studies conducted by Alsharef et al. (2016) and Ng and Coo (2015) reported a decrease in hydraulic conductivity as the percentage of nanoparticles in soil increased, as indicated in Figures 2.20a and b. The rate of changes in hydraulic conductivity decreased at higher nanoparticle concentrations. This behavior can be caused by pore clogging, increased soil aggregation, surface tension effect, and nano-coating. The effect of nanoparticles on hydraulic conductivity was highly dependent on the type of nanoparticles and the duration of the treatment. For example, in soil treated with γ-Al_2O_3, around 40% reduction in hydraulic conductivity was reported with a nanoparticle concentration of 6% (Ng & Coo, 2015). However, when carbon nanofiber was used, the treated soil experienced a reduction of approximately 60% in hydraulic conductivity (Alsharef et al., 2016). The study results by Yong et al. (2019) further indicated a decrease in hydraulic conductivity values over time for soils treated with nanoparticles (as shown in Figure 2.20c). This can be due to the formation of cementing compounds and soil pore clogging resulting from the chemical reactions between nanoparticles and soil (Yong et al., 2019). As the reaction progresses, the production of cementing compounds can reduce the effective pore size and pore connectivity, thereby decreasing the hydraulic conductivity of the treated soil.

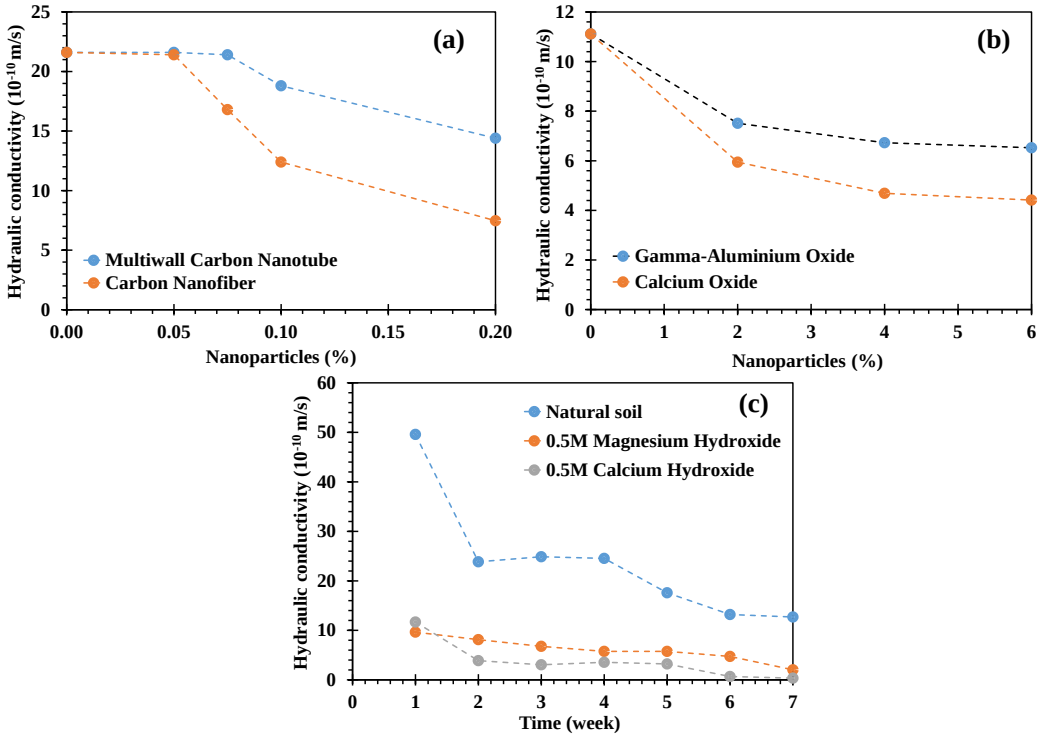

Figure 2.20: Hydraulic conductivity **a,b)** different nanoparticle percentages, **c)** different curing time

The soil water retention curve (SWRC) represents an essential hydraulic soil characteristic describing its water retention capacity. It shows how the soil's moisture content changes in response to changes in soil water potential or suction (Khosravi & McCartney, 2012). Understanding the SWRC is crucial to studying various aspects of the behavior of expansive soils. Chen et al. (2022) conducted a study to investigate the impact of different percentages of nano biochar (NBC) on the soil water retention curve (SWRC), as depicted in Figure 2.21. The results indicate that the application of NBC led to a reduction in the air-entry value. A lower air-entry value facilitates the easier escape of water from the soil pores, thereby negatively affecting the soil's water-holding capacity. A ≥ 0.7% NBC concentration causes soil water repellency, mainly because the solid-liquid contact angle of the soil mixture exceeded 90°. This phenomenon hinders the infiltration and retention of water in the soil, and reduces the soil's ability to hold water. A contact angle below 90° typically shows that the soil is relatively hydrophilic, indicating that the

soil particle readily absorbs and retains water. Another study by Zhou and Chen (2017), suggests that the addition of nano-carbons in the soil improves its water retention capability to some extent. Further study would be needed to understand the impact of the dosage of nanoparticles to avoid undesirable effects on SWRC and to ensure optimal water management in geotechnical systems.

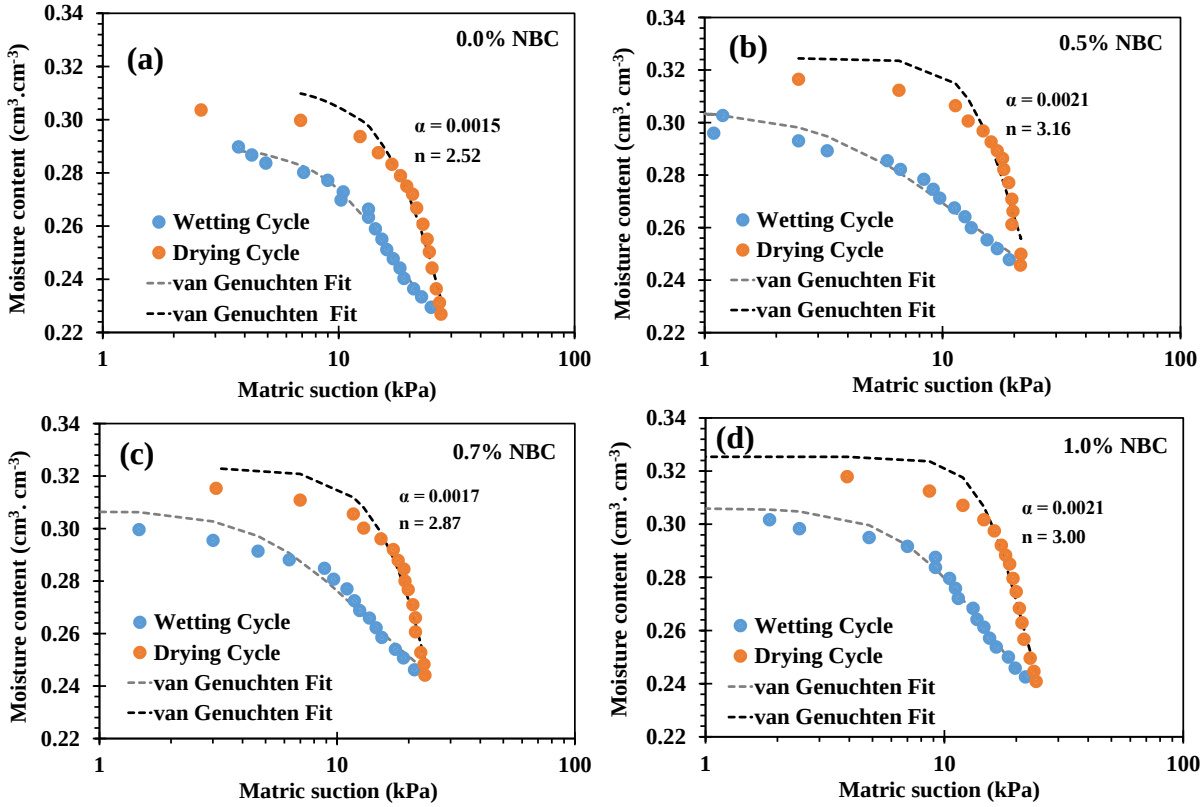

Figure 2.21: Soil water retention curve treated with different percentages of biochar nanoparticles (van Genuchten 1980 fit) (Chen et al. 2022)

Utilizing nanomaterials for soil conditioning offers several advantages that make them attractive compared to other additives such as lime or cement. Nanoparticles have demonstrated the ability to efficiently modify soil's physical, mechanical, and hydraulic characteristics due to their small size, large SSA, reactivity, and CEC. These unique properties allow nanoparticles to effectively enhance soil behavior (strength and deformation) and characteristics (SWRC, Hydraulic conditicvity, soil plasticity). However, we must also acknowledge the limitations

associated with nanoparticle-based soil stabilization approaches. One major limitation is the absence of standardized guidelines and protocols for their application. The effectiveness of nanoparticles can vary significantly depending on factors such as soil type, initial conditions (void ratio, moisture content, pH), nanoparticle type and concentration, curing time and method, and the inclusion of other chemical additives. Thus, we need to investigate further the optimal conditions for employing nanoparticles in different soil types. Another factor to consider is the cost associated with manufacturing and using nanoparticles on a large scale, which can be higher than conventional chemical additives. Addressing the cost aspect and exploring ways to enhance production techniques and reduce costs is essential for making nanoparticle-based soil stabilization more commercially viable and economically competitive. Advancing soil conditioning using nanoparticles and stability enhancement, requires additional research to fill these knowledge gaps.

2.8.2.6 Combination of Different Additives

Different additives are often combined for expansive soil stabilization to leverage their complementary properties and address multiple aspects of soil behavior. This synergistic approach can lead to more effective and long-lasting stabilization, as each additive may target specific soil characteristics. For instance, while cement alone may not improve clay workability and lime alone may not sufficiently strengthen highly expansive clays, a 1:1 combination of cement and lime can provide higher strength with better workability (Abu-Farsakh et al., 2015). In the same way, in soils with low pozzolanic content, lime or cement alone may provide insufficient strength improvement (Ji-ru & Xing, 2002; Voottipruex & Jamsawang, 2014). To address this issue, pozzolanic materials like fly ash (FA) are often added as co-additives. The addition of FA with lime to expansive soils enhances performance compared to using FA alone (Barman & Dash, 2022; Nicholson & Kashyap, 1993), as it provides additional pozzolanic phases of aluminates and

silicates that react in the highly alkaline environment created by lime to form cementitious compounds (Bakharev et al., 1999; Brough & Atkinson, 2002; Kukko, 2000). This combination accelerates strength gains and improves the overall stability of the treated soil. Similarly, industrial waste materials such as ground granulated blast furnace slag, cement kiln dust, and silica fumes have been used alongside lime to enhance the performance of treated soils by furnishing additional reactive materials for pozzolanic reactions (Cokca, 2001; Kumar & Gupta, 2016; Peethamparan et al., 2008; Wild et al., 1999). The use of these additives aims to improve the kinetics of pozzolanic reactions and the formation of cementitious compounds without resorting to uneconomical or unsustainable high stabilizer dosages (Bell, 1996; Dash & Hussain, 2012; Kumar et al., 2007).

The effectiveness of combined additives depends on factors such as additive content, curing period, temperature, and water content (Barman & Dash, 2022). For example, higher dosages (7%) of calcium carbide residue (CCR) can increase unconfined compressive strength (UCS) up to 7 days of curing, while adding a small proportion (3%) of FA can extend this increase up to 28 days (Horpibulsuk et al., 2012). The presence of cement or lime in soil-FA mixes promotes the formation of cementitious gels, leading to continued strength improvement for up to 150 days of curing (Kolias et al., 2005; Mahedi et al., 2018; Show et al., 2003). Additionally, in sulfate-rich environments, the addition of FA or ground-granulated blast furnace slag (GGBS) to lime or cement-treated soil can help mitigate the deleterious effects of sulfates (McCarthy et al., 2014; Seco et al., 2011; Sukmak et al., 2015).

2.8.3 Electrochemical Stabilization

The electrokinetic soil stabilization is based on the dewatering and hardening of the soil through electroosmosis (Nelson & Miller, 1997). During the electrokinetic phenomenon, an electric field

is applied to a wet soil mass, causing the migration of ions towards the oppositely charged electrode. This process occurs through three distinct mechanisms: electromigration, electroosmosis, and electrophoresis (Abdullah & Al-Abadi, 2010; Eykholt & Daniel, 1994; Gray & Mitchell, 1967). Electromigration is the transport of charged species (ions and ionic complexes) towards the electrode of opposite charge under the influence of an applied electric field. Positively charged species (cations) migrate towards the cathode, while negatively charged species (anions) migrate towards the anode (Figure 2.22). Electroosmosis is the movement of pore fluid within the soil matrix from the anode toward the cathode due to the applied electric field. Finally, electrophoresis is another phenomenon that involves the migration of charged colloidal particles, such as clay particles, suspended in soil-water suspension.

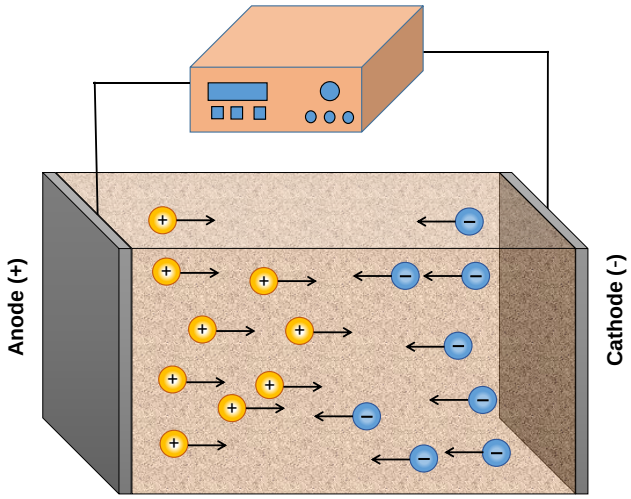

Figure 2.22: The ion transport due to electrokinetic towards the opposite electrodes

During the electrokinetic pH is lower near the anode, indicating an acidic condition due to oxygen evolution reaction (OER) and production of H^+ ions as shown in equation 2-8. The pH near the cathode is alkaline due to hydrogen evolution reaction (HER) and generation of OH^- as shown in equation 2-9. The generation of OH^- ions and relatively slower migration toward the

anode leads to a localized increase in the pH near the cathode and creates an alkaline environment. Acar and Alshawabkeh (1993) found that the mobility of a proton under an electric field is 1.8 times the hydroxyl ion mobility.

$$\text{Anode}: \quad 2H_2O - 4e^- \longrightarrow O_2 + 4H^+ \qquad (2-8)$$

$$\text{Cathode}: \quad 2H_2O + 2e^- \longrightarrow H_2 + 2OH^- \qquad (2-9)$$

Electrokinetic soil has been previously used for soil dewatering and consolidation (Adamson et al., 1966; Esrig, 1968; Fetzer, 1967; Fu et al., 2019; Shang & Lo, 1997; Shang, 1997; Sutar & Rotte, 2022). Moreover, the electrokinetic process can be combined with the addition of chemicals to enhance soil strength. The study conducted by Adamson et al. (1966) revealed that applying direct electric (DC) current through soil samples, sometimes in combination with chemical additives like calcium chloride or aluminum sulfate, can effectively remove water from saturated soils, increase shear strength and cohesion, and reduce the swelling and cracking tendencies of expansive clays. Their research demonstrated impressive results, including a reduction in soil water saturation by 52% through electro-osmosis, an increase in cohesion from 225 to 425 psf, and an improvement in the internal friction angle from 25° to 28° in treated samples. Additionally, they observed a significant reduction in shrinkage cracking in expansive clays by introducing aluminum ions.

In the same vein, the study by Jayasekera (2015) explores the effects of electrokinetic (EK) processing on the compressive strength of two types of soils: soft alluvial soil (Soil S1) and basaltic soil (Soil S2) from central Victoria, Australia. Laboratory experiments involved passing a direct current through the soil using electrodes under various voltage gradients (0.5, 1.0, 2.0 V/cm) for periods of 7, 14, 30, and 60 days. Throughout these experiments, the soil samples were maintained with a continuous water flow via the hollow core anode. The results indicated that soil compressive

strength increases with longer processing times and higher voltage gradients, with strength increases of up to 200% observed under certain conditions (Figure 2.23). The increase in soil strength during EK processing is due to electroosmotic advection reducing water content and electromigration altering soil structure by moving charged ions. Even after the EK processes end, ionic diffusion and aging continue to enhance strength through ongoing ionic changes and cementation bond formation.

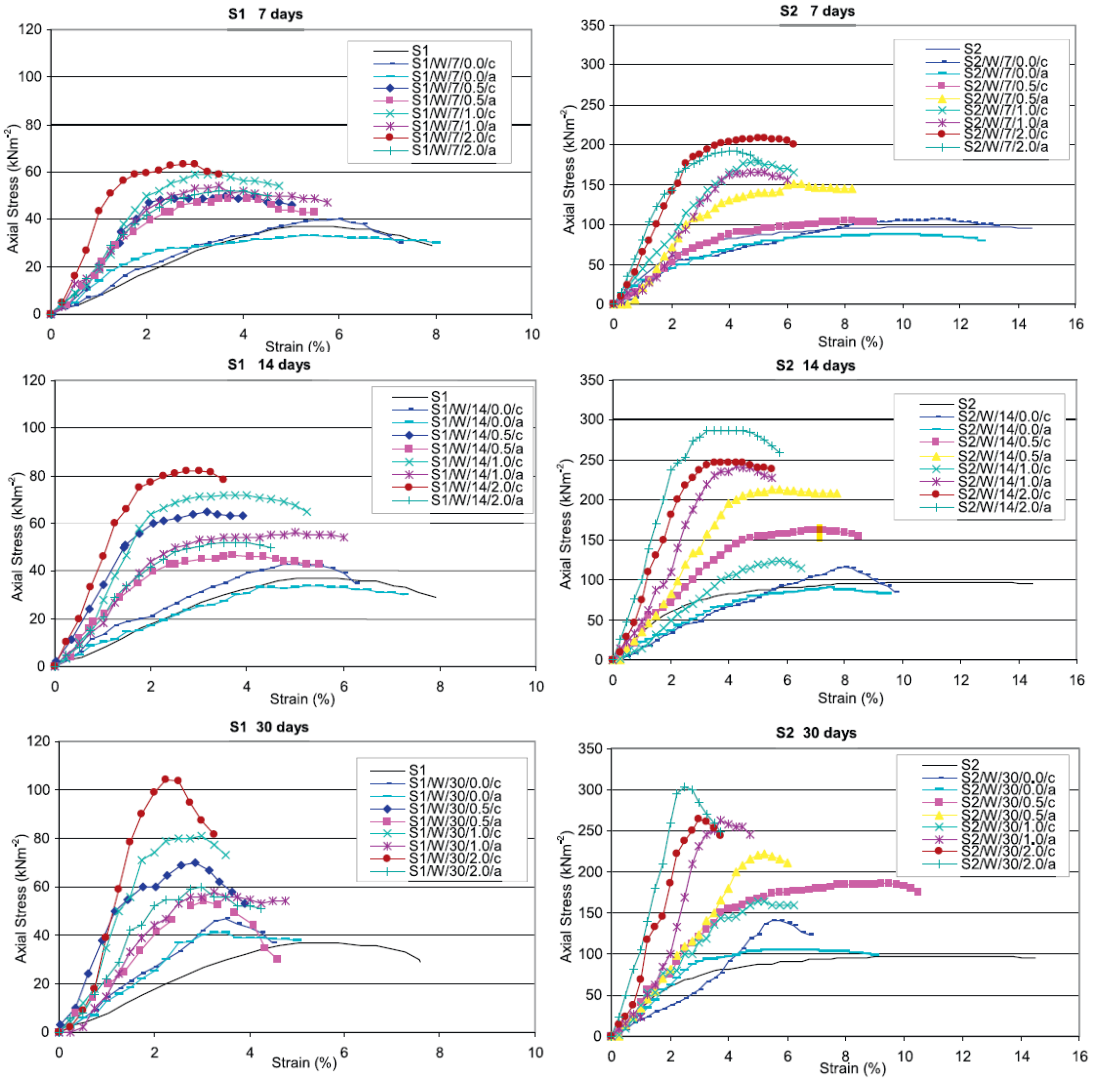

Figure 2.23: Stress-strain relationship at cathode and anode positions for soil S2 and S2 after 7 days, 3 days, and 30 days with and without EK processing (Jayasekera .2015)

Research conducted by Ou et al. (2018) tested various combinations of chemical solutions, including calcium chloride ($CaCl_2$), potassium hydroxide (KOH), and sodium silicate, under specific conditions to optimize the treatment process. The results indicated that using a fresh sodium silicate solution and continuously injecting deionized water significantly enhanced the pozzolanic reaction and increased the clay's strength near the cathode. This comprehensive approach resulted in substantial strength improvement across the entire soil sample, achieving cone resistance values ranging from 1 to 5 MPa.The findings demonstrate that electrochemical treatment can effectively improve clay strength by leveraging the combined effects of electroosmosis, chemical solution injection, and the pozzolanic reaction. The study revealed that the presence of Ca^{2+} ions and a highly alkaline environment facilitated the formation of cementing agents, which contributed to the soil's increased strength. In the same way, a study by Abdullah and Al-Abadi (2010) explored the electrokinetic (EK) enhancement of expansive soils using cationic stabilizing agents, specifically potassium (K^+) and calcium (Ca^{2+}) ions. Through EK processes, these ions are driven into the soil, aiming to reduce its plasticity and swell potential while increasing its shear strength. The results demonstrated that potassium ions significantly reduce the soil's plasticity index (PI) from 40 to 8, transforming the soil from a highly expansive state to one of low expansiveness. Additionally, the free swell percentage decreased dramatically from 14% to 0.4% for K^+-stabilized soil. The investigation also revealed that EK processes effectively distribute cationic stabilizing agents uniformly throughout the soil, resulting in homogeneous improvement in soil properties (figure 2.24).

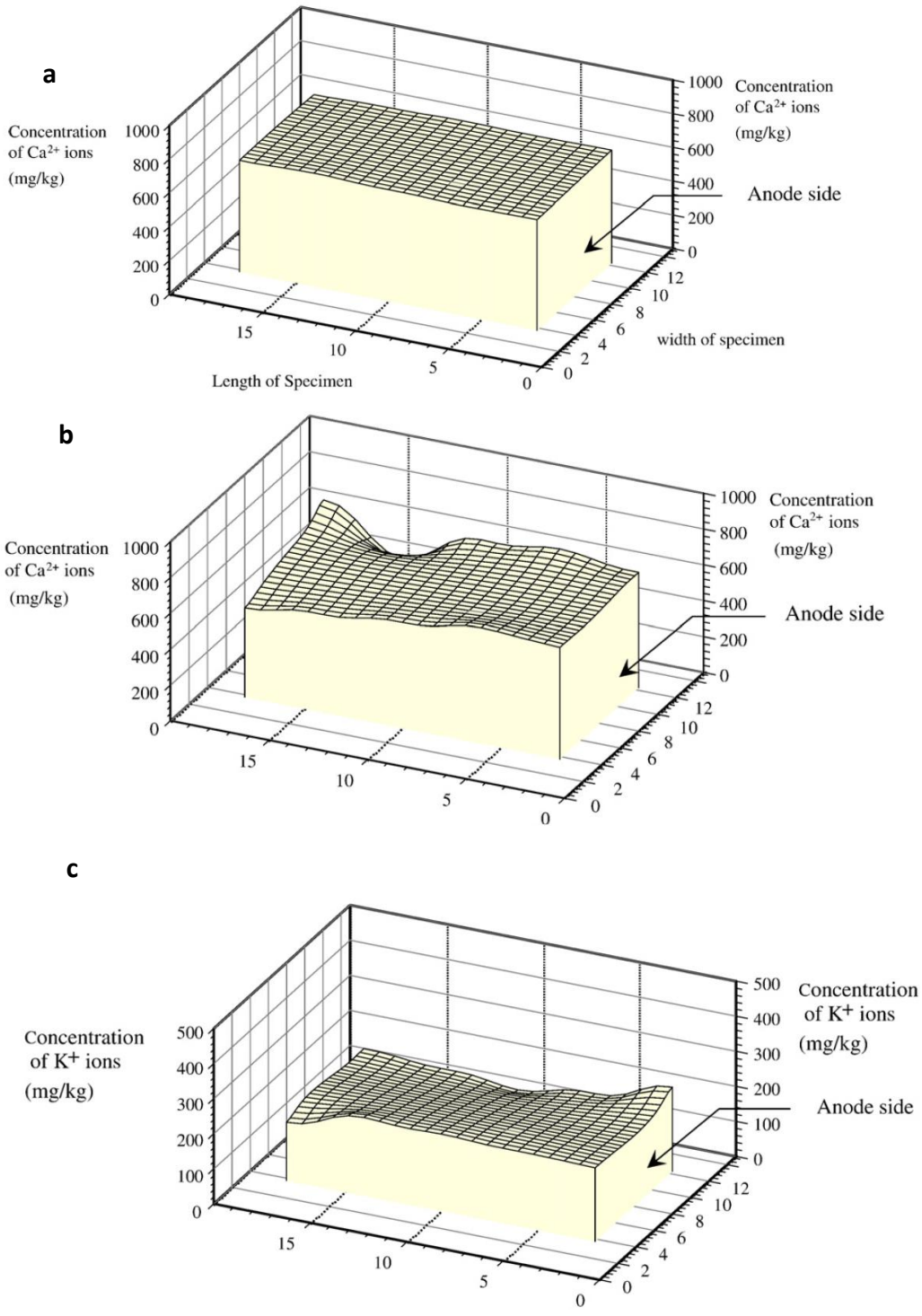

Fiure 2.24: Distribution of ions **a)** Ca^{2+} ions— source is $Ca(OH)_2$, **b)** Ca^{2+} ions— source is $CaCl_2$, **c)** K^+ ions— source is KOH (Abdullah & Al-Abadi, 2010)

Electrokinetic techniques have also been used in environmental engineering, primarily for their effectiveness in soil decontamination and remediation of heavy metals. This method has proven particularly useful in treating fine-grained soils contaminated with various pollutants, including heavy metals, organic compounds, and radionuclides (Kim et al., 2001; Pamukcu & Kenneth Wittle, 1992; Wang et al., 2021). Its application in distributing nanoparticles for expansive soil remediation is novel and could be a promising approach.

2.8.4 Other Soil Stabilizers Additives

Researchers have used and studied various materials for expansive soil stabilization. These emerging options often utilize industrial by-products, naturally occurring substances, or engineered materials to improve the expansive soil engineering properties. While many of these methods require further research to fully understand their long-term performance and environmental impacts, they represent potential sustainable solutions for soil stabilization in various geotechnical applications. For example, bottom ash (Galvín et al., 2021; Jamsawang et al., 2023; Le et al., 2019; Melese, 2022; Puppala et al., 2002), sulfonated oil (Park et al., 2006; Soltani, Deng, et al., 2019; Soltani, Raeesi, et al., 2022), marble dust (Abdelkader et al., 2021; Jain & Jha, 2020; Sakr et al., 2021), eggshell powder (Mehmood et al., 2023) have been reported.

2.8.5 Heat Stabilization of Expansive Soil

Heat stabilization/thermal of expansive soil is a technique used to reduce the soil swell potential significantly by applying high temperatures. This process reduces the soil's tendency to expand and contract with moisture changes, making it more stable for construction purposes. Abu-Zreig et al. (2001) investigated the effects of heat treatment (100-400°C) on clayey soils. They found that temperatures above 100°C dramatically reduce the soil liquid limit, plastic limit, optimum

water content, unconfined compressive strength, and swelling pressure of the tested soils. At 400°C, the liquid limit decreased by 80%, the plastic limit reached zero, the optimum water content reduced by 65%, swelling pressure decreased by 94%, and unconfined compressive strength was eliminated, as shown in Figure 2.25. These changes were attributed to soil organic matter's destruction and cohesion loss at high temperatures. In the same way, research by Wang et al. (1990) examined the effects of heat treatment (up to 600°C) on kaolin and bentonite clays. They found that kaolin showed dramatic changes at 500°C, including increased particle size, strength, and cohesion, while decreasing plasticity and swelling. Bentonite required 600°C to become non-expansive and non-plastic, with only moderate strength gains. Both clays experienced increased internal friction angles with heating. The research by Wohlbier and Henning (1969) examined the effects of heat treatment (up to 600°C) on kaolinite clay, focusing on changes in shear strength and other properties. Significant changes occurred above 400°C, coinciding with the transformation of kaolin to metakaolin. At 500°C, the clay became non-plastic and non-swelling, with a sharp drop in specific gravity and increased shear strength for dry samples. Samples heated to 600°C showed further strength increases and behaved more like brittle rocks. For water-saturated samples, significant strength increases were observed only above 400°C. The researchers used various analytical methods and developed a new approach to describe the curved Mohr's envelope. They concluded that heat treatment could effectively stabilize cohesive soils, with the most substantial changes occurring above 400°C, while noting that additional factors would need consideration for in-situ applications. Even though thermal stabilization can reduce the soil swell properties, it proves to be energy-intensive and impractical for on-site operations.

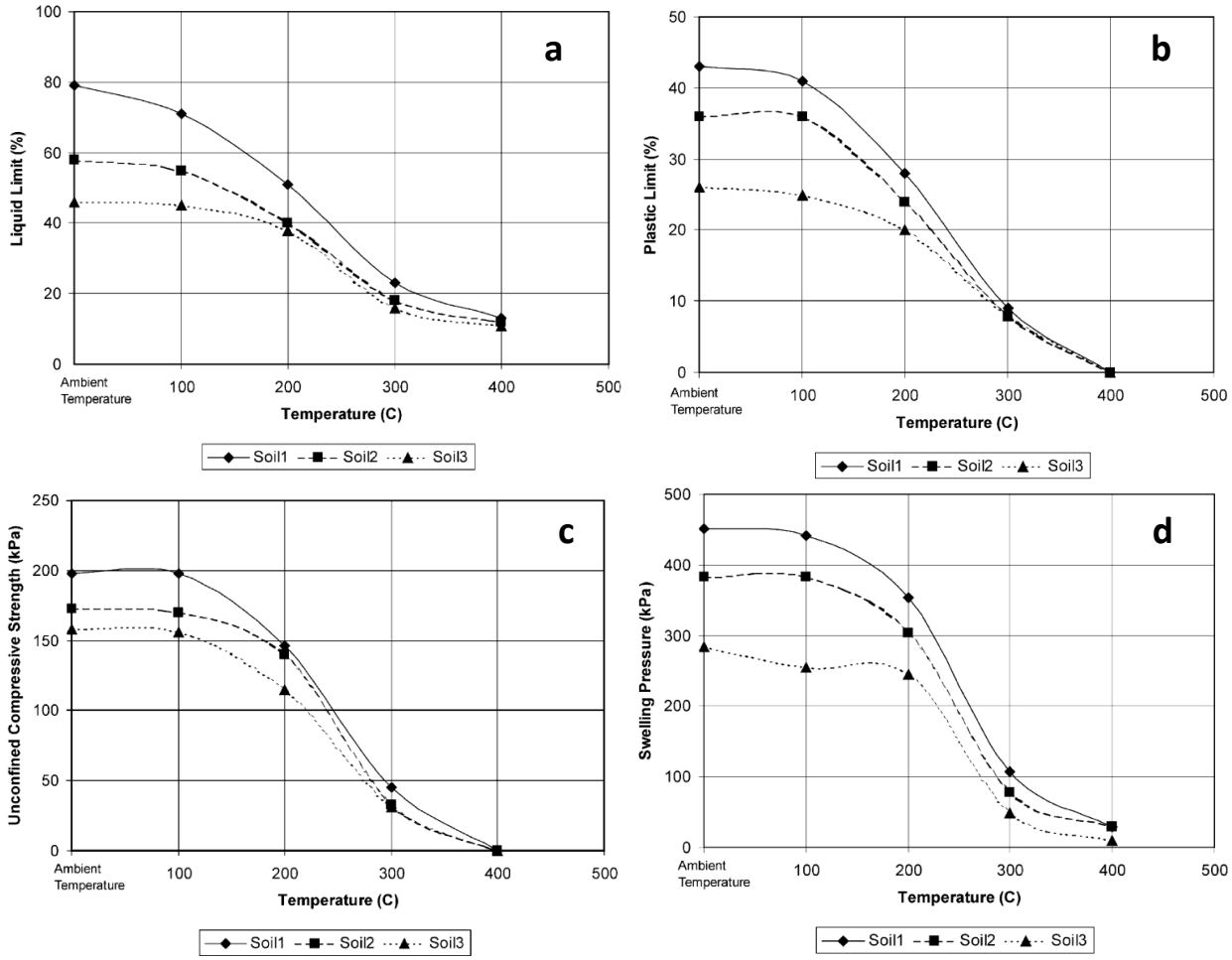

Figure 2.25: the effect of temperature on three different clay soil parameters: **a)** liquid limit, b) Plastic limit, **c)** Unconfined compressive strength, **d)** Swelling pressure (Abu-Zreig et al. 2001)

2.9 Established Expansive Soil Treatments in Alabama

Various stabilization techniques have been implemented to improve the expansive soil in Alabama, specifically along the AL-5 highway. Alabama Highway 5, known as AL-5 hereafter, serves as an important highway connecting Mobile and Birmingham. Al-5 is a farm-to-market highway that lacks the necessary support for contemporary trucking demands, as it was constructed directly over expansive clay without a proper aggregate base. Consequently, frequent resurfacing and maintenance are required due to the rapid deterioration of the pavement structure, often occurring

nearly every year. As a result, expansive subgrade clay and surrounding vegetation cause repetitive shrinkage and swelling of the subgrade (Stallings, 2016).

Research conducted by Stallings (2016) wanted to identify the root cause of pavement distress along the AL-5, as shown in Figure 2.26. The investigation found that the seasonal moisture demand variation of large trees growing near the roadway plays a crucial role in the subgrade's instability. These trees, located within a zone of influence of the road, contribute to the shrinking and swelling of expansive clays in the subgrade, subsequently causing localized pavement distress. To verify this hypothesis, a comprehensive survey was conducted of trees over 6 inches in diameter within approximately 60 feet of the roadway, establishing correlations between observed pavement distress and the trees' moisture demands. The list of trees observed is shown in Table 2.3.

Table 2.3: Summary of Common Trees Surveyed and their Size (Stallings, 2016)

Tree Common Name	Count of Trunk Diameter (inches)	Average of Trunk Diameter (inches)	Max of Trunk Diameter (inches)
American Elm	52	12.6	32.0
Black Willow	3	11.7	20.0
Eastern Red Cedar	123	10.2	27.0
Green Ash	93	10.0	27.0
Laurel Oak	51	12.0	40.0
Loblolly Pine	538	10.8	36.0
Pecan Tree	31	12.9	42.0
Post Oak	6	14.2	18.0
Red Oak	30	15.6	32.0
Slippery Elm	130	9.1	24.0
Sugarberry	406	10.2	27.0
Sweet Gum	106	8.4	18.0
Water Oak	108	12.2	52.0
White Ash	119	9.3	24.0
White Oak	8	10.9	22.0
Willow Oak	100	14.6	54.0
Winged Elm	33	8.7	15.0

The reseach found that loblolly pines (with small root systems and low moisture demand) were the most common trees, followed by Sugarberry trees (Elm family, with large root systems and high moisture demands). The largest tree surveyed was a 41.1-inch diameter willow oak, as shown in Figure 2.26.

Figure 2.26: Willow Oak, Diameter 41.1 inches (Stallings, 2016)

The shoulder slope geometries encouraged root growth towards the roadway, leading to subgrade soil desiccation during dry seasons. This cyclical shrinking and swelling, exacerbated by

large deciduous trees, resulted in subgrade rutting and longitudinal shrinkage cracks. Laboratory tests were also performed to identify the soil properties. These tests included one-dimensional swell tests, soil water characteristic curves (SWCC) development, and standard AASHTO classification tests. The results demonstrated that the soils along Alabama Highway 5 possess considerable swell potential, generating pressures between 500 and 1500 psf. This shrink-swell cycle is predominantly driven by suction pressures from the soils and nearby vegetation.

Similarly, research conducted by Jackson (2016) aimed to evaluate the shrink-swell behavior of the subgrade soil along the AL-5 highway. The study also examined several remediation techniques, including improved drainage, vertical moisture barriers, lime stabilization, and paved shoulders (detailed in Jones' 2017 report). The researcher installed field instrumentation to assess the effectiveness of these test sections and further characterize soil behavior. This included soil moisture sensors, soil suction sensors, pore water pressure sensors, and asphalt strain gauges. All the instruments used for the research are shown in Figure 2.27, and the tests' results can be found in the Jackson 2017 report. Six monitoring locations were established along AL-5, corresponding to five remediation techniques and a control section. Sensors were placed in the pavement, subgrade, and shoulder to measure soil moisture, matric suction, pore water pressure, and asphalt strain. A seventh location was added to monitor vegetation effects. The locations of these instruments and remediation sites are shown in Figure 2.28.

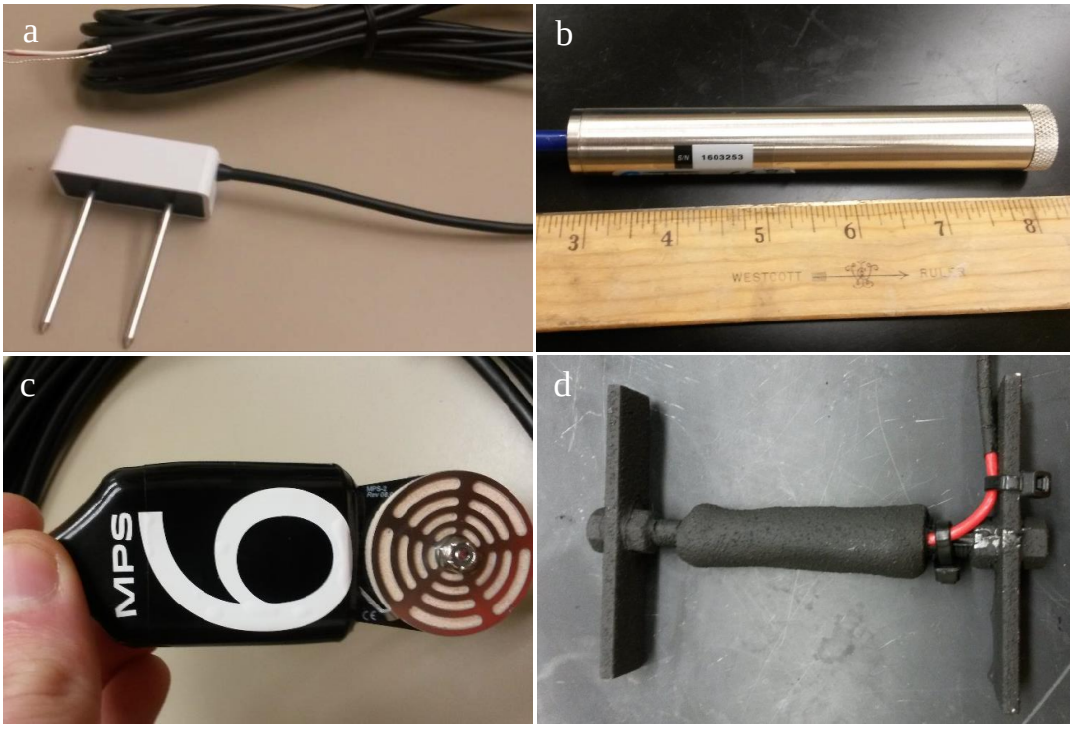

Figure 2.27: instrument used installed along the test section: **a)** Moisture Sensors, **b)** Piezometers, **c)** Suction Sensors, **d)** Asphalt Strain Gages (Jackson, 2016)

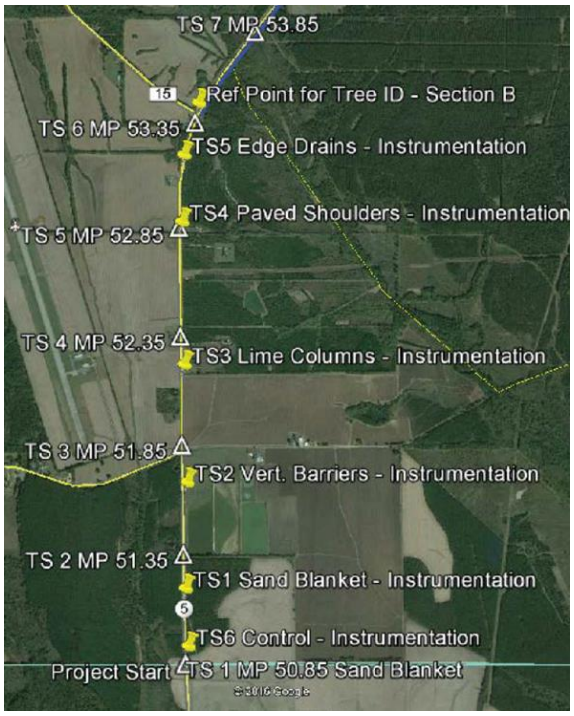

Figure 2.28: Instrumentation Locations

As mentioned in Jackson (2016) report, the vertical moisture barriers, sand blanket and lime columns, paved shoulders, edge drainage and deep mixing remediation techniques were discussed briefly, with limited details on their construction and implementation. Jackson (2016) primarily focused on the instrumentation setup for these sections. Jones (2017) provided more comprehensive information on the construction process and initial performance of these remediation techniques. The research was conducted on a 4-mile section of Alabama State Highway 5, located approximately 20 miles west of Selma, AL, in Perry County, to understand the effect of various treatment techniques common in Alabama for expansive soils. These treatment techniques included increasing drainage, installing vertical moisture barriers, lime stabilization, and paving shoulders. The site is located between the mile points 0.85 and 54.85 and is divided into eight sections for different remediation techniques, as shown in Table 2.4. The map of the area with the research site is shown in Figure 2.29 a and b. The research site features Vaiden-Okolona-Sucarnoochee soils, characterized as poorly to moderately well-drained, brown to olive-gray clayey soils, with underlying Mooreville Chalk Foundation as the predominant parent material. Additionally, certain areas near the creek exhibit clayey alluvium deposits (Harris, 1997).

Table 2.4: Test sections on AL-5 (Jones, 2017)

Test section	Remediation Technique	Milepost
1	Sand Blanket	50.85 – 51.35
2	Vertical moisture Barriers	51.35 – 51.85
3	Lime Columns	51.85 – 52.35
4	6’ Paved Shoulders	52.35 – 52.85
5	Edge Drains	52.85 – 53.35
6	Control	53.35 – 53.85
7	Deep Mixing-Canceled	53.85 – 54.35
8	Control	54.35 – 54.85

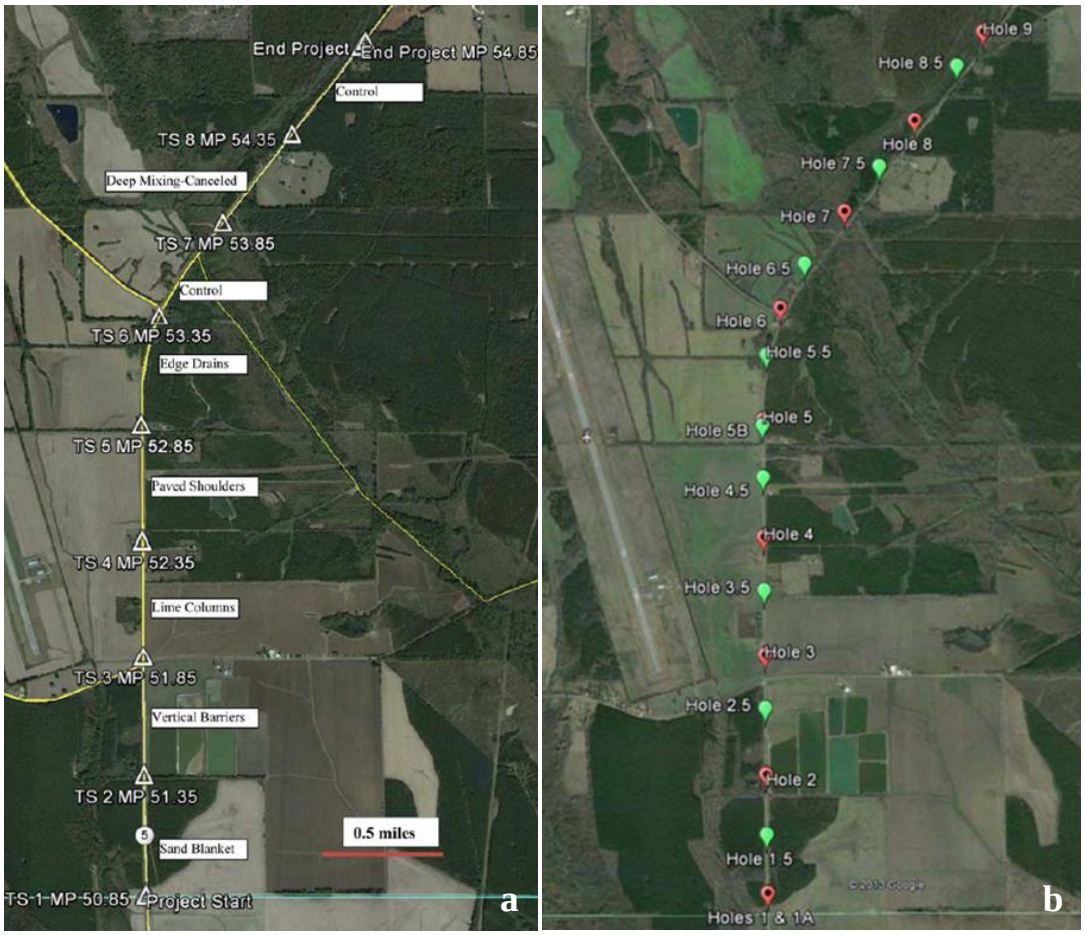

Figure 2.29: Boring and remediation locations for the studied sites on the Al-5 (jones, 2017)

It is worth mentioning that before discussing the various remediation techniques implemented along the AL-5 highway, it is crucial to gain a comprehensive understanding of the geotechnical properties of the soil at the site. Table 2.5 provides detailed information on these properties, including borehole designations, sampling depths, Atterberg limits (Liquid Limit and Plastic Limit), water content, percentage passing the No. 200 sieve (which indicates the fines content and helps classify the soil), dry density, specific gravity, and swell pressure. These parameters offer valuable insights into the soil's behavior and potential challenges for construction and remediation efforts. The percentage passing the No. 200 sieve is particularly important, as it reflects the proportion of fine-grained particles (silt and clay) in the soil, which significantly

influences its engineering properties of the soil including the swell potential. For more comprehensive information regarding these geotechnical properties of the soil, readers are encouraged to reader the report by Stallings (2016). This section provides a concise overview of the remediation techniques implemented along the AL-5 highway, as Jones (2017) documented.

Table 2.5: Summary of AL-5 Laboratory Data (Stallings 2016)

Borehole	Depth (ft)	LL	PI	%<#200 Sieve	Water Content (%)	Dry Density (pcf)	Specific Gravity	Swell Pressure (psf)
B-1A	1.5	70	46					
B-1A	3.5	88	58					
B-1A	5.5	110	83					
B-1A	7.5	79	50					
B-1A	9.5	103	74					
B-1.5A	1.5	97	68					
B-1.5A	3.5	66	42	98	37.0	84.0	2.75	736.0
B-1.5A	7.5	91	66					
B-1.5A	9.5	85	61	98	32.9	87.5	2.62	1301.0
B-2A	3.0	83	52					
B-2A	5.0	73	48					
B-2A	7.0	86	59					
B-2A	9.0	95	68					
B-2.5A	1.5	70	46					
B-2.5A	3.5	84	58	93	31.9	90.1	2.75	927.0
B-2.5A	5.5	79	47					
B-2.5A	7.5			98	29.2	92.4	2.72	1560.0
B-3A	1.5	93	67					
B-3A	3.5	65	41					
B-3A	7.5	74	49					
B-3.5A	1.3	68	40	99	38.6	82.5	2.70	1035.0
B-3.5A	3.3	87	59					
B-3.5A	5.3	84	57					
B-3.5A	7.3			97	41.5	77.7	2.74	1073.0
B-4A	1.8	72	47					
B-4A	5.8	93	70					
B-4.5A	1.2	68	40	97	38.8	81.5	2.72	1082.0
B-4.5A	5.2	97	69					
B-4.5A	7.2			96	33.3	84.4	2.73	
B-5A	1.5	50	26					
B-5A	7.5	91	68					
B-5.5A	1.0	86	60	96	39.6	81.0	2.75	871.0
B-5.5A	7.0	88	61	96	33.3	87.7	2.70	1393.0

Borehole	Depth (ft)	LL	PI	%<#200 Sieve	Water Content (%)	Dry Density (pcf)	Specific Gravity	Swell Pressure (psf)
B-Tree C	3.0			94	39.6	79.3		622.0
B-Tree C	7.0			94	32.2	89.8		1374.0
B-6A	1.5	97	73					
B-6A	7.5	80	50					
B-6.5A	1.5						2.69	
B-6.5A	3.5	71	47	60	28.2	90.2		509.0
B-6.5A	5.5	57	39					
B-6.5A	7.5	50	35					
B-6.5A	8.8			45				
B-7A	3.5	57	40					
B-7A	5.5	58	38					
B-7A	7.5	63	42					
B-7.5A	5.0	67	49	81	29.2	93.9	2.72	608.0
B-7.5A	7.0	60	42	78	27.8	95.4	2.81	709.0
B-8A	5.0	64	48					
B-8A	7.0	50	34					
B-8.5A	1.0			90				
B-8.5A	3.0			78				

2.9.1 Sand Blanket – Test Section 1

A sand blanket was constructed in Test Section 1 to create a drainage layer beneath the pavement surface and act as a flexible barrier between the expansive clays and the pavement. The purpose was to keep the subgrade at a more constant moisture content and minimize differential heave across the pavement, which can lead to cracking. The construction involved removing the existing pavement, placing a geotextile on the subgrade, and then adding a 6-inch layer of sand. Perforated drainage pipes were installed on either side of the sand blanket layer under the shoulders to collect water and route it to the ditch line. A trench was dug along the edge of the pavement, lined with geotextile, and backfilled with the sand blanket material. After completing both lanes with the sand blanket, a final wearing course of asphalt was paved over the top, as shown in figure 2.30a-d.

Figure 2.30: a) North Bound Lane- Edge Drain and Sand Blanket, **b)** North Bound Lane – Application of Sand Blanket, **c)** North Bound Lane – Placement of Tack Coat on Granular Base, **d)** Rainwater flowing out of Sand Blanket (Jones, 2017).

2.9.2 Vertical Barriers – Test Section 2

Vertical moisture barriers are composed of impermeable geosynthetic material sheets installed in ditches along the edge of the pavement to limit the literal flow of water in and out of the subgrade. According to Nelson and Miller (1997), it's usually not feasible to install vertical moisture barriers for the full depth of the active zone. They propose opting for a depth between one-half to two-

thirds of the active zone instead. Figure 2.31 represents a cross-section of the vertical barriers section.

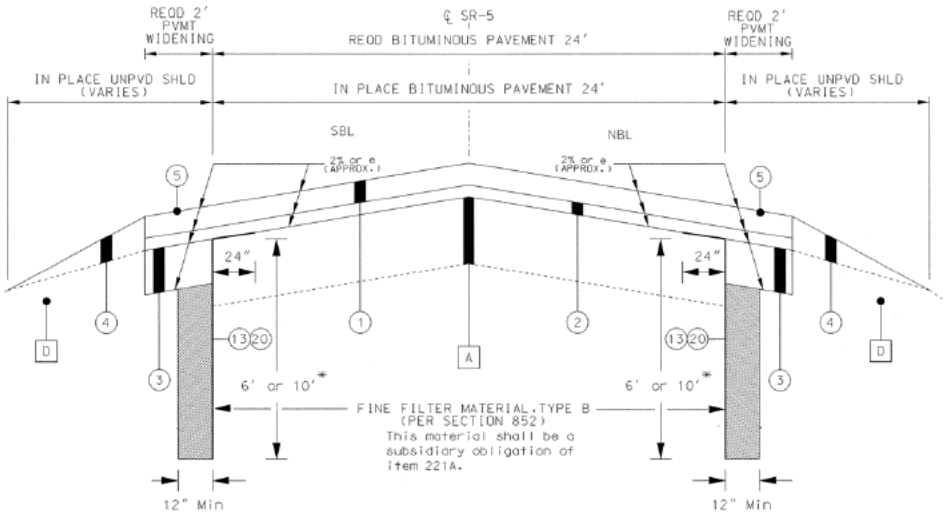

Figure 2.31: Vertical Barriers Cross Section (ALDOT 2015)

Jones (2017) placed six-foot trenches along the entire test section following excavation, the trench was backfilled with fine sand, as depicted in Figures 2.32a and 2.32b. Subsequently, a layer of asphalt was applied directly on top of the sand, as illustrated in Figures 2.32c and 2.32d.

Figure 2.32: a) Backfilling of Vertical Barriers **b)** Sand Backfill of Vertical Barriers **c)** Paving over Vertical Barrier Trench **d)** Leveling Asphalt over Vertical Barriers (Jones 2017).

2.9.3 Lime Columns – Test Section 3

Lime stabilization of soil is a chemical stabilization method used to alter the physicochemical properties of soil. For the section 3 of AL-5, lime was used to chemically stabilize the subgrade. Lime was inserted into drilled holes in both the pavement and shoulder of the road, reaching a depth of one foot below the ditch line. The Figure 2.33 a and b shows display the cross-section and the layout of the lime columns. Figure 2.34 a and b shows the drilling and cloum installation.

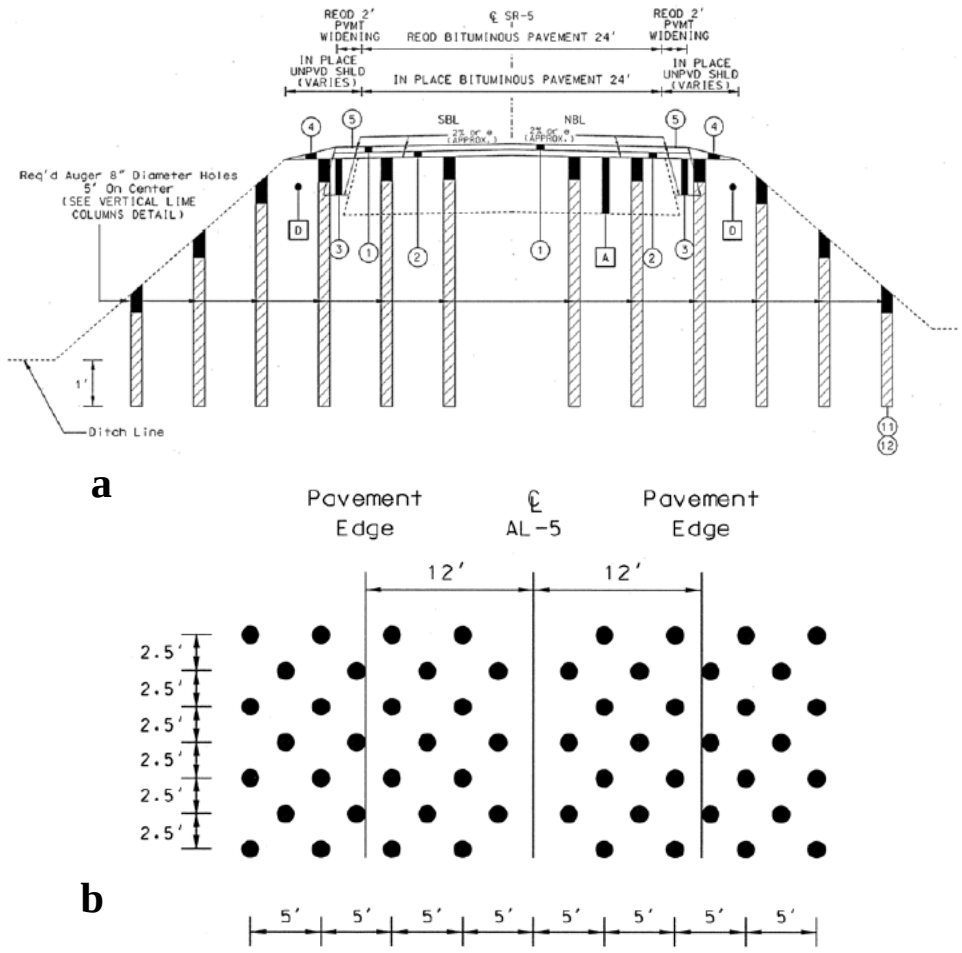

Figure 2.33: a) Lime Columns Cross Section **b)** Lime Columns Plan View Detail (ALDOT 2015)

Figure 2.34: a) Drill Used for Lime Column Installation **b)** Auger used for Lime Column Installation (Jones 2017).

2.9.4 Paved Shoulders – Test Section 4

The initial field investigation revealed frequent longitudinal cracks along the outer wheel path, as shown in Figure 2.35a. To address this issue, it was suggested to employ paved shoulders in Test Section 4, aiming to divert longitudinal crack development from the wheel path to the shoulder. The proposed remediation involved paving six-foot-wide shoulders on both sides of the road, as depicted in Figure 2.35 b.

Figure 2.35: a) Longitudinal Cracking at AL-5 (Herman 2015) **b)** After paving of Paved Shoulders (jones 2017)

2.9.5 Edge Drains – Test Section 5

In Test Section 5 the drains were installed at the edge of the pavement ot control the mostirue content of the subgrade. For this purpose, a corrugated pipe with a diameter of 4 inches was placed alongside the pavement within a 1-foot wide by 1-foot deep trench backfilled #57 stone as backfill as shown in figure 2.36.

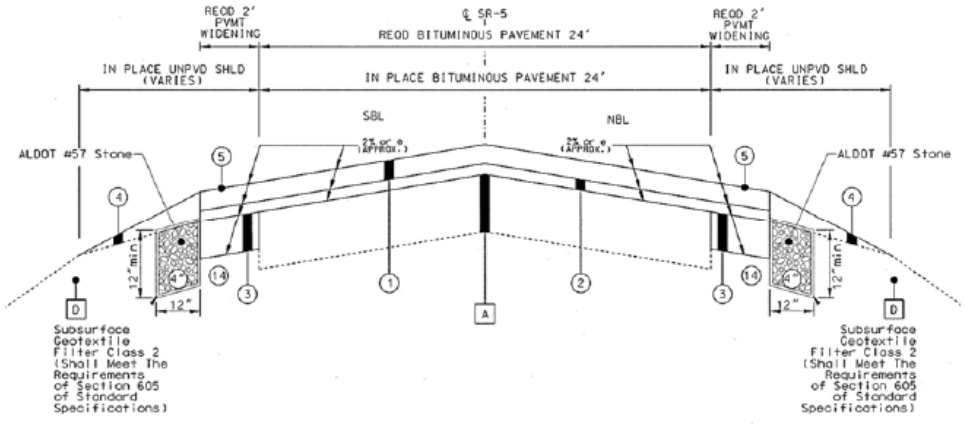

Figure 2.36: Edge Drain Cross-Section at AL-5 (ALDOT 2015)

Figure 2.37: Edge Drains after Backfilling with Stone (jones 2017)

2.9.6 Deep Mixed Columns – Test Section 7

It was suggested to utilize deep soil mixing in Test Section 7 to stabilize expansive clay soils by blending Portland cement with the existing soil. The layout of the columns, with a required diameter of 2 feet, is depicted in figure 36. According to the plans, the southern half of Test Section 7 was designated to have columns with a depth of 6 feet, while the northern half was planned for columns with a depth of 15 feet. But it was canceled due to construction issues.

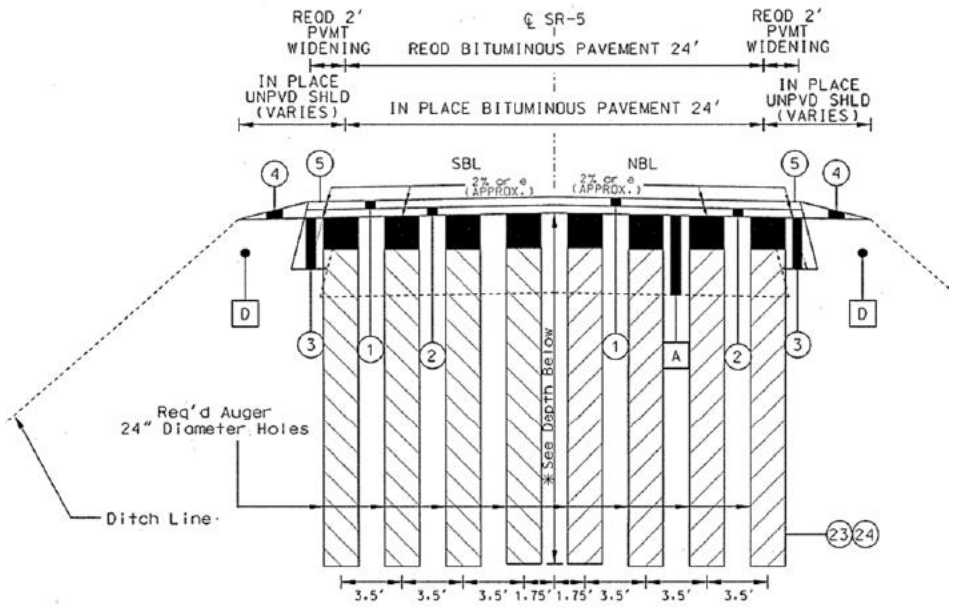

Figure 2.38: Deep Mixed Columns Cross Section (ALDOT 2015)

2.9.7 Control Sections

To assess the efficiency of the different remediation techniques implemented on AL-5, control sections were integrated. These sections underwent a sole modification of widening the road's shoulder by 2 feet on each side. Importantly, a final layer of asphalt was applied across the entire project area, encompassing the control sections as well.

Following Jones (2017) and Jackson (2016) works which implemented various remediation techniques on Alabama Highway 5 (AL-5) to address pavement distress caused by expansive clay subgrade. Kennedy (2019) conducted ring shear tests to further characterize the subgrade behavior. Torsional ring shear tests were performed to determine the drained residual strength of the soil. Specimens from each remediation section were consolidated and subjected to torsional shear in the ring shear device to assess the shear strength of the subgrade soils that may have contributed to pavement distress. Continuous pavement and subgrade instrumentation monitoring has

improved pavement distress over the past few years, with the lime column test section showing the most improvement. The torsional ring shear tests revealed very low peak and residual resistance angles for the subgrade, indicating that the material was weak and likely contributed to the pavement distress. Slope stability analyses concluded that while the roadway embankments were stable at the end of construction, they quickly began to fail as the peak and residual shear strength values were reached.

As discussed, various remediation techniques have been implemented to address the pavement distress due to expansive soils along Alabama Highway 5 (AL-5), including sand blankets, vertical moisture barriers, lime columns, paved shoulders, and edge drains. While these methods have shown some effectiveness in mitigating pavement distress, they each have limitations. For instance, the sand blanket and edge drains focus primarily on moisture control but may not adequately address the fundamental chemical properties of the expansive clay. Lime columns, while effective in altering soil properties, require extensive excavation and can be labor-intensive with localized effects. Vertical moisture barriers and paved shoulders may help redistribute stresses but do not directly tackle the expansive nature of the soil. Given these limitations, there is a need for innovative approaches that can more comprehensively address the issues of expansive soils while potentially offering more efficient and non-disruptive in-situ implementation. One such promising technique is electrokinetic nanoconditioning for soil stabilization. This method can modify soil properties at the molecular level, potentially providing more lasting stabilization effects. The following discussion will explore the application of electrokinetic nano conditioning as an alternative approach to soil stabilization, addressing its principles, potential advantages, and how it might overcome some drawbacks associated with the previously implemented techniques along AL-5.

CHAPTER 3

Materials and Methods

3.1 Soil Collection and Characterization

The soil utilized in this study was collected from Perry County (AL, USA), specifically alongside Alabama Highway 5, an area known for its expansive clay composition. This area is part of the "Black Belt" region, also known as the Blackland Prairie, due to the dark surface colors of its soil. The region is characterized by expansive clay soils, particularly those with a high percentage of smectitic clays. Smectites are three-layered clay minerals capable of absorbing water within their interlayer spaces (ALDOT, 2021). As a result, clayey soils in this region are known for their pronounced swelling and shrinking properties under moisture fluctuations, contributing significantly to pavement distress over the years. To ensure a comprehensive analysis of these soil properties, both disturbed and undisturbed samples were collected from the site, as illustrated in Figure 3.1.

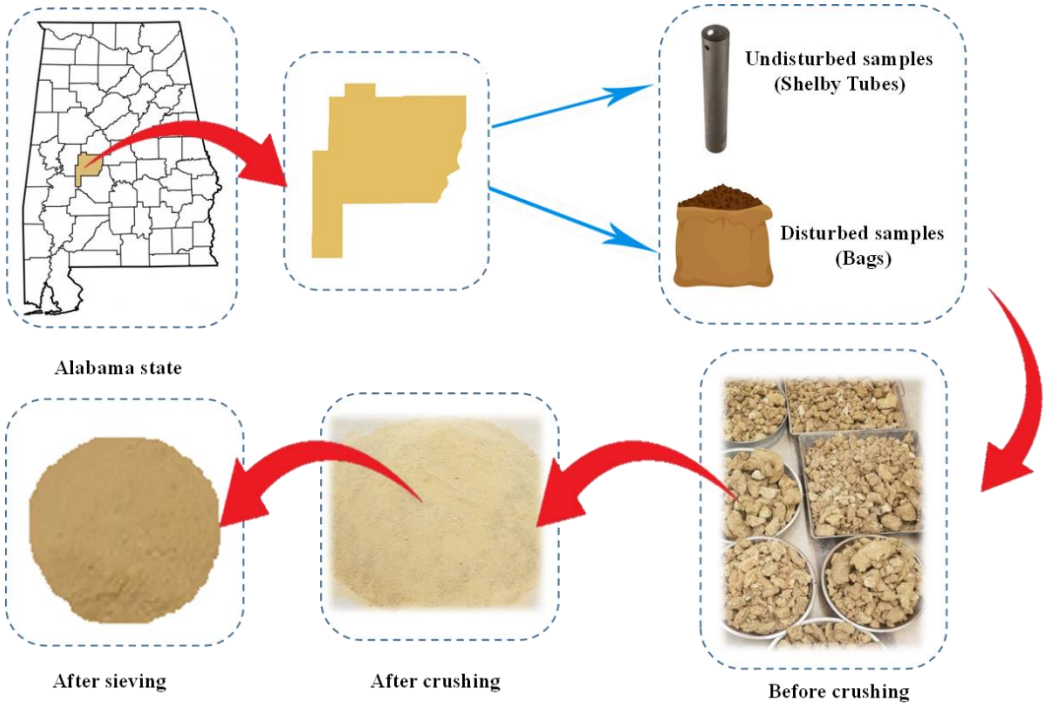

Figure 3.1: Soil collection and crushing procedure

The disturbed samples were initially oven-dried at 105°C for 24 hours, then crushed, sieved through a #40 mesh, and mixed well together to ensure homogeneity (Figure 3.1). These samples underwent a series of standard tests, including specific gravity (ASTM D854), sieve analyses (ASTM D6913), Atterberg Limits (ASTM D4318), and pH measurement (ASTM D4972. Table 3.1 presents the basic soil characterization results, and Figure 3.2 illustrates the grain size distribution (Figure 3.2a) and the XRD data for of the disturbed sample (Figure 3.2b).To accurately replicate the site conditions in the lab, undisturbed samples were used to measure dry unit weight (ASTM D7263) and soil moisture content (ASTM D2216).

Table 3.1. Basic characterization of clayey soil used in this research

Property	**Magnitude**
Specific gravity (ASTM D854)	2.72
Liquid limit (ASTM D4318)	64.78
Plasticity index (ASTM D4318)	37.22
pH (D4972 ASTM D4972)	7.80
dry unit weight (kN/m^3)(ASTM D7263)	12.46
Moisture content (ASTM D2216)	40%
USCS soil classification (ASTM D2487)	CH

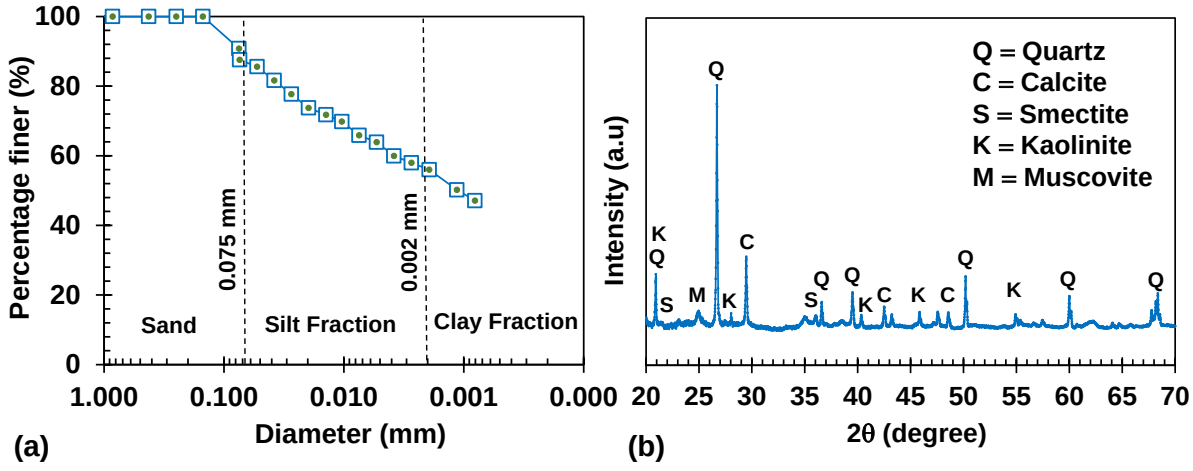

Figure 3.2: a) Grain size distribution of the untreated CH soil and **b)** X-ray diffractogram of untreated soil

3.2 Strength and Soil Characteristics Tests

3.2.1 The Consistency Limit tests

The Atterberg limits test was performed according to ASTM D4318-17 standards. For this test, soil samples were obtained from different sources depending on the experimental condition. In the case of physical mixing samples, soil was taken from Ziploc bags after 7 days of conditioning. For the electrokinetic treatments (both with and without nanoparticles), soil samples were extracted from three positions within the electrokinetic chamber after 7 day conditioning period.

3.2.2 Unconfined Compressive Strength Tests

The unconfined compressive strength (UCS) test was conducted in accordance with ASTM D2166-06 standards using a GeoJac Automated Loading System by GEOTAC. The test was performed with a target axial strain of 15% and a strain rate of 1% per minute. Remolded soil samples were prepared for physical mixing with nanoparticles, whereas undisturbed soil samples were extracted and utilized for the electrokinetic and electrokinetic nano-conditioning tests. Initially, three distinct undisturbed samples were extracted from the electrokinetic chamber using a nickel tube with a diameter of around 4 cm and a length of 15 cm. Subsequently, the samples were carefully trimmed to achieve a diameter of around 3.3 cm and a height of 7.1 cm, maintaining a height-to-diameter ratio between 2 and 2.5. Figure 3.3 shows the sample extractor and GeoJac system.

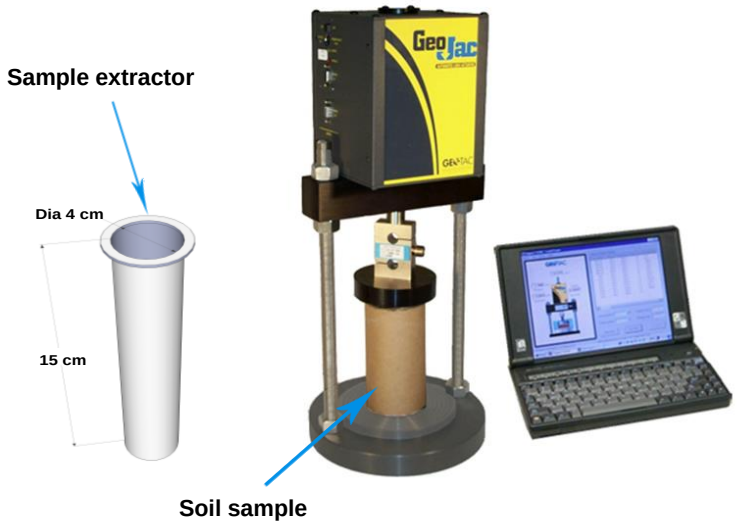

Figure 3.3: Steel tube for extracting undisturbed samples for UCS testing

3.2.3 One-Dimensional Swell Test

The one-dimensional swell test was conducted in accordance with ASTM D4546-21 standards using a GeoJac as used for the UCS test. The samples were remolded in the soil sampler after 7 days of conditioning for the physical mixing. Electrokinetic soil samples were extracted from the electrokinetic chambers and remolded for the swell test. The soil sample was placed between two porous stones in the oedometer apparatus, measuring 2.54 cm (1 in.) in diameter and 6.35 cm (2.5 in.) in height. An initial seating pressure of 1 kPa (20 psf) was applied to the specimen. The automated linear variable displacement transducer (LVDT) was then calibrated to zero to establish a baseline measurement. Following this setup, the sample was left undisturbed for one hour. After this initial period, water was added to the oedometer to initiate swelling. The specimen was then left undisturbed for a minimum of 24 hours, during which time it was allowed to undergo vertical displacement. This period ensured that the soil had sufficient time to react to the added moisture and reach equilibrium. Throughout the test, the LVDT continuously monitored the vertical displacement of the specimen.

3.2.4 Soil Water Retention Curve

The soil water retention curve was established following ASTM D6836-16 guidelines (Method D). The upper section of the curve was determined using Hyprop2 (METER Group, Inc., USA), while WP4C equipment was used for the lower part. Remolded samples were compacted into stainless steel cylinders measuring 8 cm in inside diameter and 5 cm in height. The Hyprop-2 allows for the measurement of water retention characteristics in the matric potential range from saturation to approximately -100 kPa. Through the chilled-mirror dew point technique, the WP4C covered the matric potential range from -0.5 to -300 MPa. Figures 3.4 a and b Hyprop and WP4C systems, respectively.

Figure 3.4: Equipment used for measuring soil water retention curve (SWRC): **a)** Hyprop system used for the upper section of the SWRC. **b)** WP4C device used for the lower section of the SWRC curve.

3.2.5 pH and Electric Conductivity Measurement

The soil pH was measured using a Mettler-Toledo pH meter Seven Compact S210-Kit, following ASTM D4972 standards. Before measuring the soil pH, the samples were air-dried, then crushed, and prepared following the standard procedure for testing. For the electrical conductivity, the ratio of dried soil to distilled water was kept at 1:5, as reported by Hussain et al. (2023).

3.3 Nanomaterials Characterization

The commercial MgO and SiO_2 nanoparticles utilized for this study were purchased from Skyspring Nanomaterials, Inc., based in Houston, TX 77082, USA. Detailed physical and chemical properties of the nanoparticles are shown in Tables 3.2 and 3.3, while the zeta potential of the nanoparticles is shown in Figure 3.5.

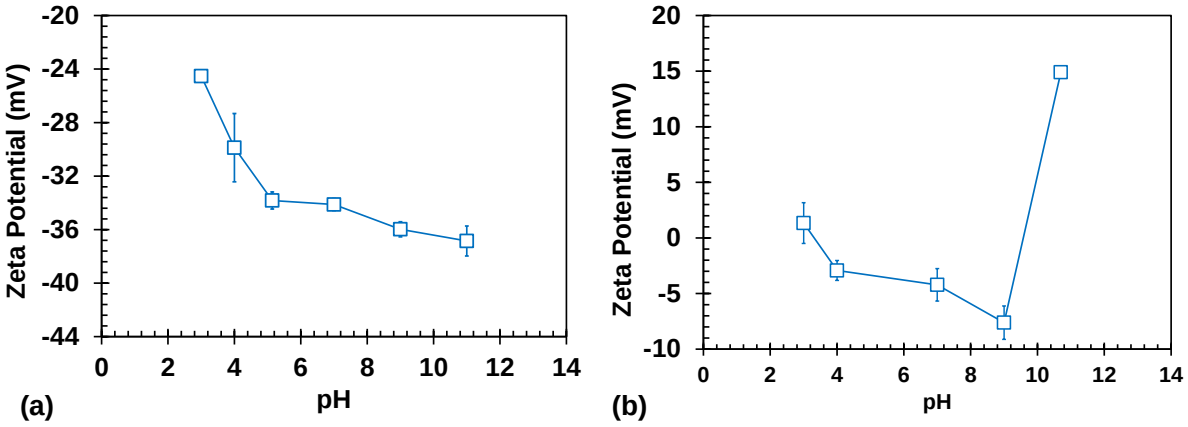

Figure 3.5: Zeta potential of **a)** SiO_2 and **b)** MgO nanoparticles with respect to pH

Table 2: Physical and chemical properties of nano MgO

Nanomaterial	**MgO**	**Typical Impurities**	**Values**
Purity	99%		
Appearance	white nanopowder	Ca	0.15%
APS	20 nm	K	0.015%
SSA	50 m^2/g	Na	0.20%
Morphology	polyhedral	Hg	0.01ppm
Bulk density	0.13-0.16 g/cm^3	Pb	0.02ppm
True density	3.58 g/m^3		

Table 3: Physical and chemical properties of nano SiO_2

Nanomaterial	**SiO_2**	**Typical Impurities**	**Values (%)**
Purity	99.5		
Appearance	white nanopowder	Al	≤ 0.002
APS	15-20 nm	Fe	≤ 0.001
SSA:	640 m^2/g	Ca	≤ 0.002
Bulk density:	0.08~0.10g g/cm^3	Mg	≤ 0.001
True density:	2.648 g/m^3	Cl	≤ 0.001

3.4 Electrokinetic Experimental Setup and Procedure

A series of characteristics and strength tests were initially performed to evaluate the impact of nanoparticles on the expansive soil parameters, including plasticity index, swell potential, and strength and soil water retention curve (SWRC), and select the most effective material for electrokinetic nano-conditioning. For these experiments, soil prepared in Section 3.1 was physically mixed with varying percentages of nanoparticles. Specifically, the soil was mixed with 1%, 2%, and 3% of MgO or SiO_2 NP solution, which was chosen based on the soil's dry weight. To mimic the natural water content of the soil, a predetermined amount of DI water was added to a beaker containing a magnetic stir bar. The nanoparticles were then introduced into this water. The solution was then placed on a magnetic stirrer plate and stirred at 350 rpm for 30 minutes to ensure a homogeneous dispersion of the nanoparticles. Subsequently, the nanoparticle solution was added to a predetermined amount of oven-dried, pre-weighed soil, and mixed thoroughly by hand for 30 minutes to achieve a homogeneous mixture. The solution pH for MgO NPs was 10.78 ± 0.02, and for the SiO_2, it was 5.14 ± 0.02. The soil mixture was then transferred into Ziploc bags, vacuumed, and placed in a controlled environment to prevent moisture loss as shown in Figure 3.6. After 7 days of curing, the soil samples were subjected to testing. All tests were performed at room temperature (25°C ± 2°C).

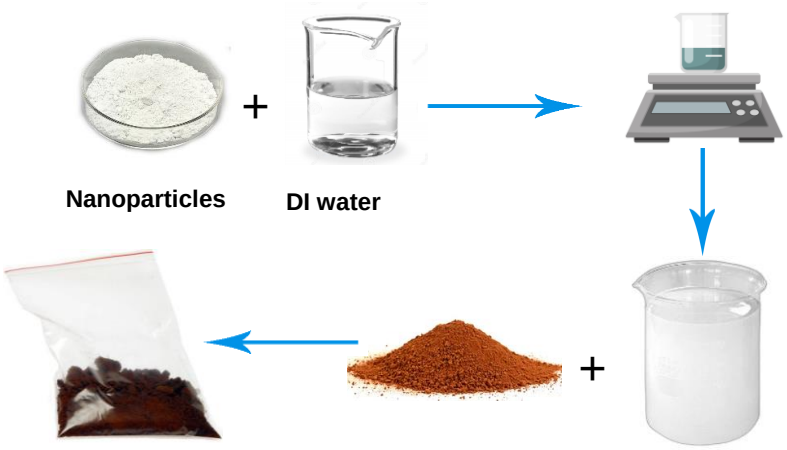

Figure 3.6: Physical mixing procedure of the soil with nanoparticles

Secondly, we explored the sole effect of electrokinetics on the expansive soil matrix. For these experiments, rectangular electrokinetic soil conditioning cells with length, width, and height of 15 cm, 10 cm, and 12 cm were made from acrylic plates, as presented in Figure 3.7. Each cell featured a single drainage hole with a diameter of approximately 1 cm positioned above the bottom at one end of the cell. A Whatman No. 42 ashless filter paper was used to prevent soil particle washout from the setup. Graphite plates (12 cm × 9cm × 3 mm, Gold/Silver color, LEISHENT brand, Amazon, USA) with an effective area of 90 cm^2 were used as the working electrode. The cathode plate was modified with a 1 cm diameter hole drilled into it to align with the drainage hole in the cell, while the anode plate remained solid. The soil sample, which was prepared 30 minutes prior, was then remolded in the electrokinetic cell with dimensions of 15 cm × 10 cm × 10 cm. Each remolded specimen was compacted in five layers to minimize trapped air and achieve a targeted dry unit weight of 12.46 kN/m^3 and a moisture content of 40%. Subsequently, the electrodes were connected to a DC Power Supply (0 to 60V, 0 to 5 A, Model 3644A), and a data logger (model DAQ6510) was employed for monitoring the current. Soil conditioning was conducted at three distinct electric potentials: 10V, 15V, or 25V. Notably, at this phase, no holes were created on top of the soil sample near the anode for the injection of water or nanoparticles. Instead, a single

drainage hole was positioned near the bottom of the cathode for water collection, as depicted in Figure 3.7. Following the conditioning period, three undisturbed samples were extracted from the electrokinetic cell using a thin nickel sampler with a diameter of 4 cm and a length of 15 cm. These samples were taken from positions located 2.5 cm, 7.5 cm, and 12.5 cm away from the anode, as illustrated in Figure 3.8. The extracted samples underwent comprehensive testing, including moisture content, UCS, Atterberg limits, and pH. The water used in these experiments was obtained from a Millipore Milli-Q system.

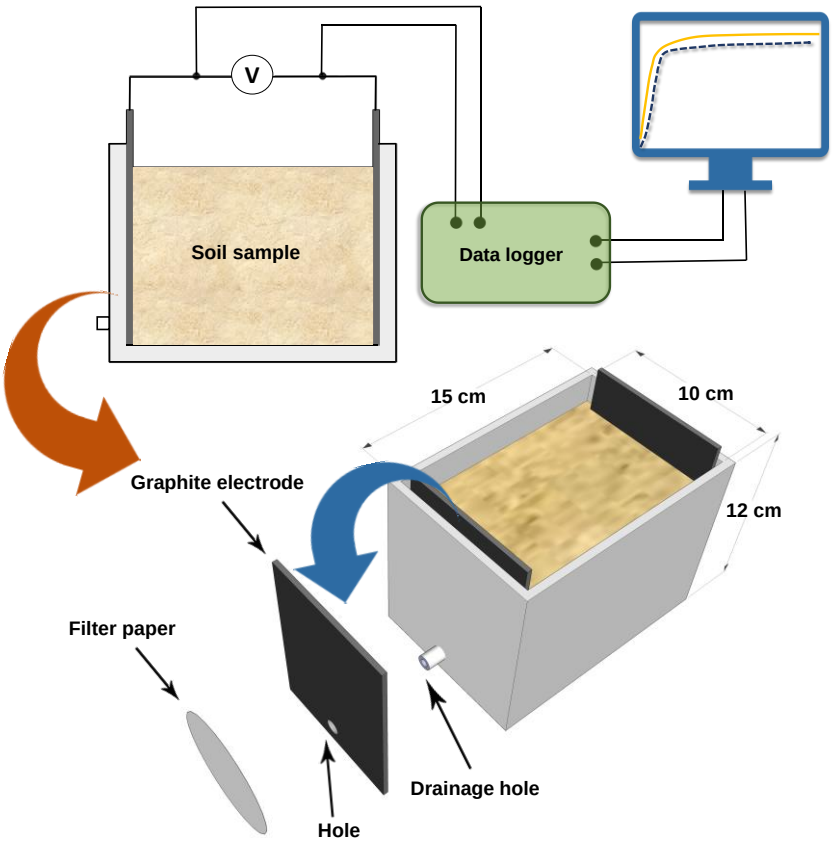

Figure 3.7: Experimental setup for electrokinetic soil conditioning

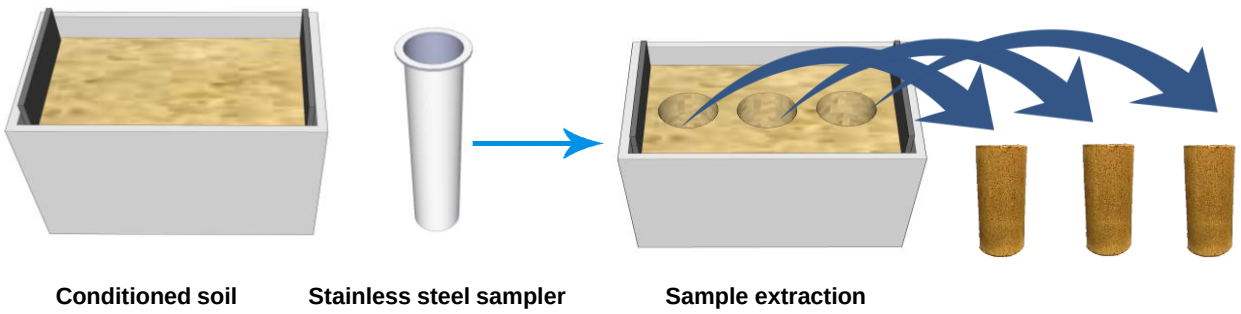

Figure 3.8: undisturbed sample extraction from the treated soil

Lastly, we incorporated nanoparticles into the soil matrix by injecting them into the soil and distributing them throughout using an electric field. After the preparation of soil samples inside the electrokinetic cell, as previously, three injection holes, each with a diameter of approximately 1 cm, were positioned about 0.5 cm from the anode electrode face (figure 3.9). These holes were spaced around 3 cm apart from center to center. The holes were created using a threaded steel bar, slowly inserted vertically into the soil while gently rotating to minimize sample disturbance. To refine the injection channels, a 1 cm diameter PVC pipe was temporarily inserted into each hole and rotated to smooth the walls without compromising the soil structure. The PVC pipes were then removed, leaving behind well-formed injection channels. After removing the PVC pipes, a 1% MgO nanoparticle solution was prepared by suspending 18,750 mg of MgO in 200 mgL^{-1} sodium hexametaphosphate (99.8% purity, Thermo Scientific), stirred at 350 rpm on a magnetic stirrer to maintain a homogeneous solution throughout the injection. Injections were conducted at 12-hour intervals using a 10 mL pipette. After the injection and a 7-day conditioning period, undisturbed soil samples were extracted from positions 2.5 cm, 7.5 cm, and 12.5 cm from the anode and tested for moisture content, UCS, Atterberg limits, and pH. Different nanoparticle-to-water ratios (1:10, 1:15, and 1:20) were tested to account for real-world conditioning applications. It should be noted that the soil was subjected to an electric potential of 15V throughout the 7-day curing period.

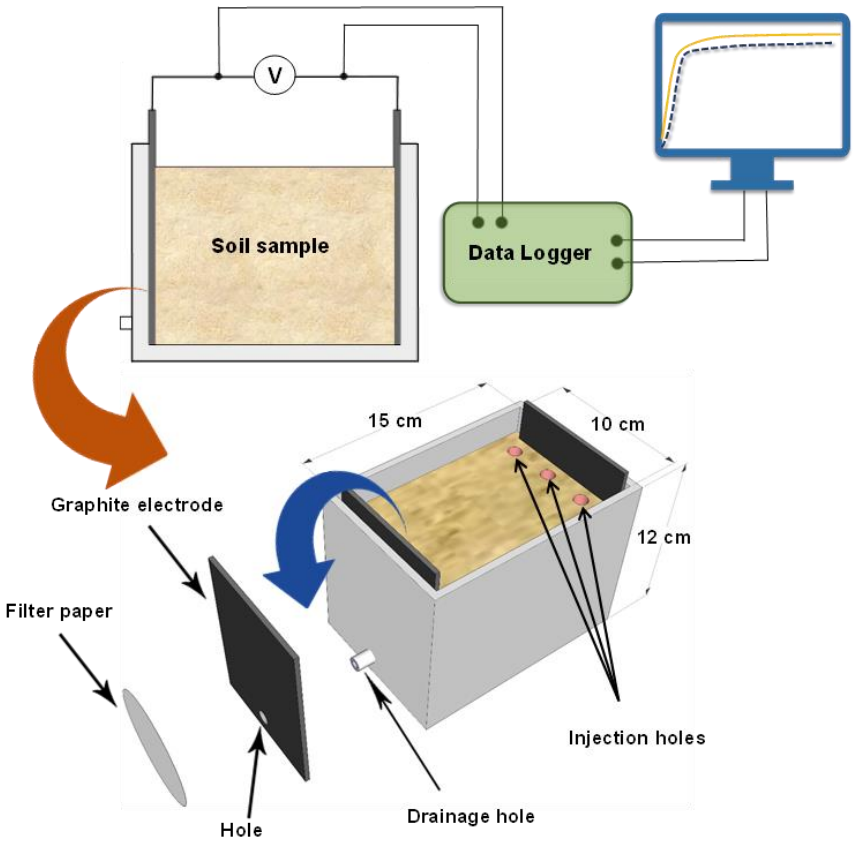

Figure 3.9: Experimental setup for nano-electrokinetic soil conditioning

3.5 Analytical methods

For the XRF and XRD analysis, soil samples were crushed into powder and sieved through a #40 sieve. The chemical composition of the soil was then evaluated using a benchtop Epsilon 1 XRF machine (Malvern Panalytical, Worcestershire, WR14 1XZ UK). The offers an Omnian standardless measurement, with source excitation from 7kV to 50kV, allowing measurements from Sodium in the periodic table down to Americium. Sample cells were prepared using polypropylene films, and the cells were loaded with the soil samples. X-ray diffraction testing was performed on the powdered sample using an AXRD powder diffraction system (Proto Manufacturing, Ypsilanti, MI, USA) with Cu Kα radiation (λ = 1.5418 Å). For the SEM (Carl Zeiss Microscopy, LLC, White Plains, NY 10601 USA), undisturbed soil samples were used with

a approximately 1 cm^2 in area and 3-4 mm in thickness. These samples were mounted directly onto aluminum support stubs covered with double-stick carbon tape. All samples were sputter coated with gold using an EMS Q150R Sputter Coating Device (Electron Microscopy Sciences, Hatfield, PA 19440, USA) and then imaged at 20kv using a Zeiss EVO50 scanning electron microscope. Qualitative and quantitative EDS analysis was performed on each sample using an Oxford INCA EDS analysis system (Oxford Instruments America, Inc., Concord, MA 01742 USA).

CHAPTER 4

Results and Discussions

This chapter will discuss the results obtained from our laboratory experiments. The first section will cover the Atterberg limits for both disturbed and undisturbed soil samples collected from the site. These tests were conducted to confirm the collected soils' high plasticity and expansive nature. After crushing and mixing the soil, the vertical swell strain test was performed under different moisture contents to simulate how the mixed soil would swell under various seasonal conditions throughout the year. In the second part, we will examine soil conditioned with different percentages of nanoparticles (MgO and SiO_2) when physically mixed with the soil, typically 1%, 2%, and 3% nanoparticles. Then, we will discuss electrokinetic soil conditioning to evaluate the isolated effect of electrokinetics (electroosmosis and electromigration) on soil matrices. Finally, we will assess the effect of electrokinetic nano-conditioning of expansive soil, using 1% MgO nanoparticles with different MgO to water ratios under 15V (100V/m).

4.1 Evaluate the Swell Potential of the Tested Soil

As previously discussed, various techniques are available to evaluate the expansive potential of soils. In this study, we employed two complementary approaches to assess the expansive characteristics of the soils under investigation. The first approach involved the measurement of plasticity and plasticity index (PI), which are key indicators of a soil's propensity to undergo volume changes. The plasticity index, derived from the difference between the liquid limit and plastic limit of the soil, provides valuable insights into the soil's behavior under varying moisture conditions. Soils with a high PI are typically more prone to significant expansion and contraction, making this measurement essential for predicting potential soil movement. The second approach utilized swell strain tests, which directly measure the soil's ability to expand when exposed to

moisture. In these tests, the soil sample is subjected to controlled moisture conditions, and the resulting strain or expansion is recorded. Swell strain tests are particularly useful for quantifying the degree of swelling that may occur in situ, offering a more practical assessment of the soil's expansive potential.

4.1.1 Plasticity and PI Measurement

The Seed et al. (1962) approach to classifying soils based on the plasticity index (PI) is a recognized method in geotechnical engineering for assessing the expansiveness of soils. Expansive soils are those that undergo significant volume changes in response to moisture fluctuations—expanding when wet and shrinking when dry. This behavior can cause substantial damage to structures if not properly managed. In the Seed et al. (1962) classification system, soils are categorized based on their PI values into different expansiveness classes, which indicate the likely degree of swelling and shrinkage that the soil might experience:

1. **Low Expansive (PI < 10):** Soils with a PI of less than 10 are considered to have a low potential for expansion and contraction. These soils are generally more stable and pose less risk of causing structural damage due to volume changes.
2. **Moderately Expansive (10 ≤ PI ≤ 20):** Soils with a PI between 10 and 20 are classified as moderately expansive. These soils may experience noticeable volume changes under varying moisture conditions, which could affect structures built on them if not properly accounted for.
3. **Highly Expansive (20 < PI ≤ 35):** Soils with a PI between 20 and 35 are classified as highly expansive. These soils have a significant potential for swelling and shrinkage, which can lead to more severe structural issues if not mitigated.

4. **Very Highly Expansive (PI > 35):** Soils with a PI greater than 35 are considered very highly expansive. These soils are most prone to extreme volume changes and pose a high risk for causing significant structural damage, requiring careful engineering solutions to manage their behavior.

To determine the plasticity index (PI) values, soils extracted from both disturbed and undisturbed Shelby tubes collected from the field, were crushed and sieved as described in the previous chapter, and then Atterberg limit tests were conducted to measure LL and PL of soils, following the procedures detailed in Chapter 3. The plasticity index (PI) was then calculated as the difference between LL and PL. For disturbed samples, as illustrated in Figure 4.1a, there is a noticeable variation in the liquid limits (LL) among the soil samples. The majority of samples, specifically those from bags 1, 3, 4, 5, and 6, exhibit liquid limits exceeding 60%, indicating a relatively high moisture content at which these soils transition from a plastic to a liquid state. In contrast, the sample from bag 2 has a notably lower LL of 57.65%, suggesting differences in soil composition or mineral content. Similarly, as shown in Figure 4.1b, the plastic limit (PL) also varies among the samples, revealing further differences in soil properties. The soil samples from bags 1 and 2 demonstrate a PL of less than 30%, indicating that these soils require less water to transition from a semi-solid to a plastic state. Conversely, the samples from bags 3, 4, 5, and 6 have higher plastic limits, all exceeding 30%, suggesting that these soils need a higher water content to reach the plastic state. Using the PI values derived from these tests, we classified the soils according to the expansiveness classification proposed by Seed et al. (1962). Most of the samples fall into the "very highly expansive" category (PI > 35), indicating a significant potential for soil expansion and contraction. The exception is the soil from bag 2, which is classified as

"highly expansive" (20 < PI ≤ 35), reflecting a somewhat lower, though still considerable, risk of expansive behavior.

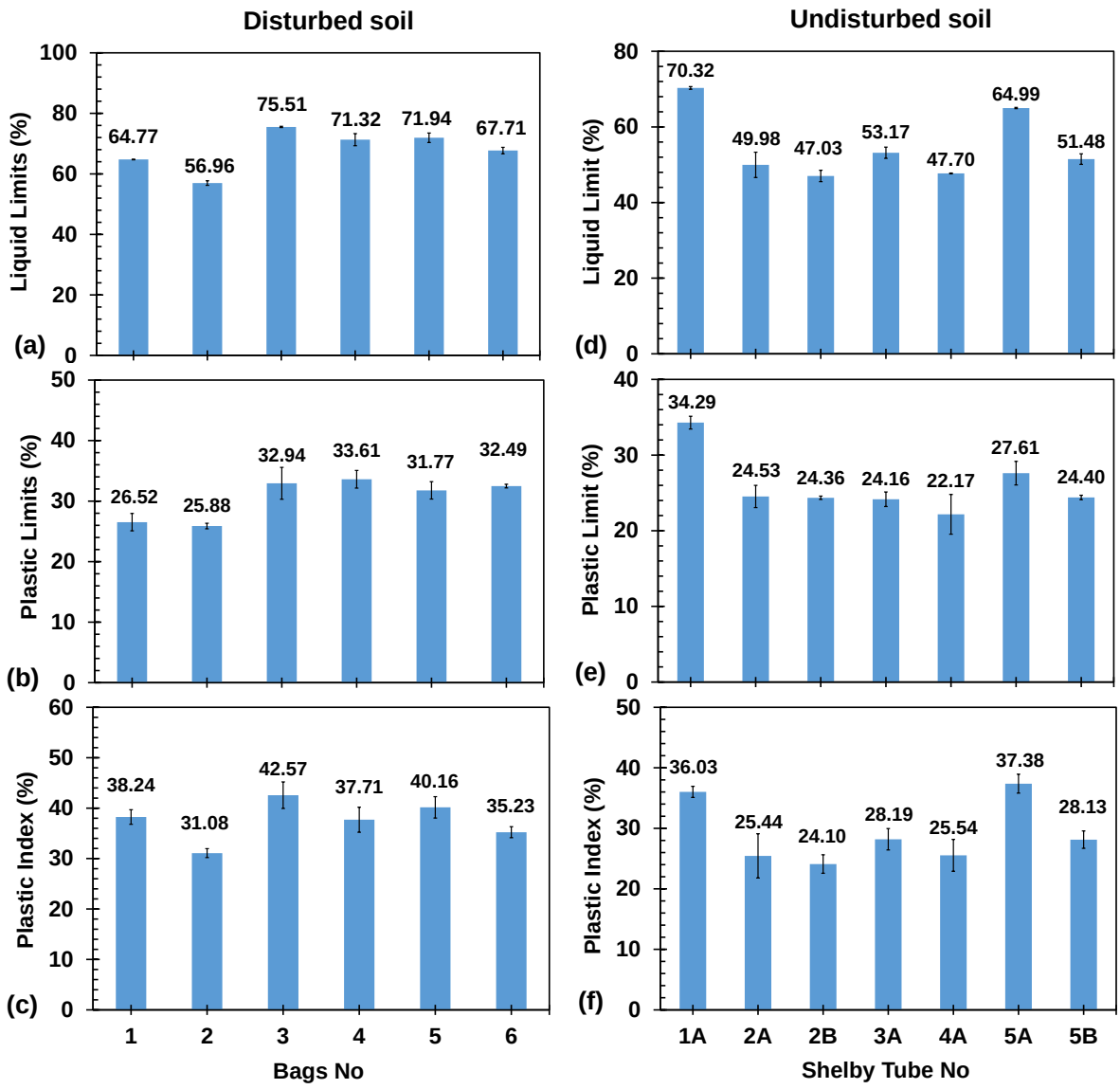

Figure 4.1: Plasticity index of disturbed and undisturbed soil **a)** Liquid Limit, **b)** Plastic Limit, **c)** Plasticity Index, **d)** Liquid Limit, **e)** Plastic Limit, **f)** Plasticity Index

For soils extracted from the Shelby tubes, as shown in Figures 4.1d, 4.1e, and 4.1f for liquid limit, plastic limit, and plasticity index, respectively, results similar to those from the disturbed samples were observed. Tubes 1A and 5A, both extracted from a depth of 5.5-7.5 ft, exhibit LL

values exceeding 60 (Figure 4.1d). In contrast, the other Shelby tube samples—2A (5.5-7.5 ft), 2B (7.5-9.5 ft), 3A (5.5-7.5 ft), 4A (5.5-7.5 ft), and 5B (7.5-9.5 ft)—have LL values below 60. Figure 4.1e presents the plastic limit (PL) data. Tube 1A shows a PL greater than 30, while the remaining tubes have PL values below 30. Consequently, the soil's plasticity index (PI) varies, depending on the LL and PL of each tube. Notably, tubes 1A and 5A have a PI exceeding 35, classifying them as very highly expansive soils. The other tubes, with PI values below 35, fall into the highly expansive soil category according to the Seed et al. (1962) expansive soil classification system.

Figure 4.2: Soil colors observed from different bags after oven-drying and sieving

The variations in Atterberg limits among the soil samples are particularly intriguing, especially considering that they were collected from nearly the same site. These differences in PI, as well as in the liquid and plastic limits, suggest significant heterogeneity in soil properties, which could be influenced by several factors such as localized stratification, varying moisture levels, or the presence of fill material from previous site activities. After oven-drying and sieving, further distinctions were observed in soil color, as shown in Figure 4.2. Notably, the soil from bags 2 and 6 exhibited a light brown hue, while the remaining samples had a brownish-yellow color. These

color variations underscore the differences in soil composition and further highlight the potential influence of factors like weathering, organic matter content, and soil texture on the expansive characteristics of the soil.

Figure 4.3 presents the color variations among soils extracted from different Shelby tubes, further emphasizing the diversity in soil properties even within a localized area. For instance, Figure 4.4a shows a cylindrical soil sample extracted from Shelby tube 2A, displaying multiple horizontal fissures along its length, indicative of the soil's tendency to fracture along these planes. This sample also has a light yellow color, contrasting with other samples in terms of both physical appearance and internal structure. Figure 4.4b provides cross-sectional views of the soil, revealing dark, crack-like features that are likely root traces or organic matter inclusions. These features, while not actual cracks, suggest the presence of decomposed plant roots or organic material within the soil matrix. It's important to note that for our experiments, we did not use soil extracted from any of the Shelby tubes for the main testing procedures. These samples were solely used for basic characterization, such as determining moisture content and unit weight.

Figure 4.3: Soil colors observed from different Shelby tubes after oven-drying and sieving

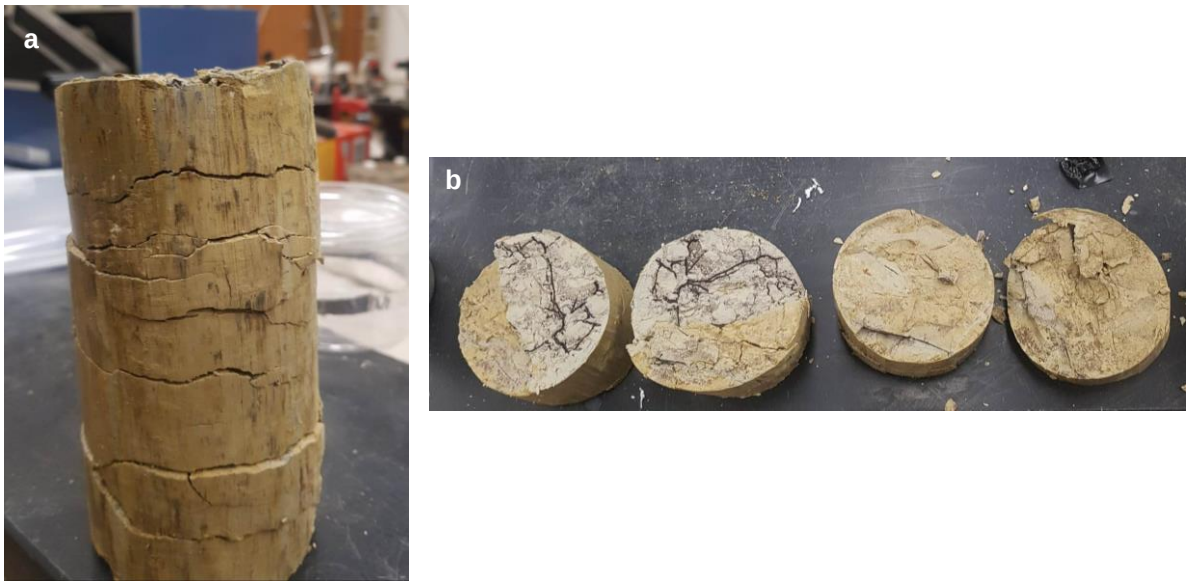

Figure 4.4: Soil sample from Shelby tube 2A**, a)** Full cylindrical sample with horizontal fissures. **b)** Cross-sectional slices showing internal structure and organic traces.

4.1.2 Vertical Swell Strain Tests

Soil samples prepared from disturbed specimens were mixed with water to conduct swell strain tests, and the quantity of water was determined based on the targeted moisture content for testing. Four different initial moisture contents—15%, 20%, 30%, and 40%—were selected to evaluate the effect of initial moisture content on the swelling potential of expansive soils. The specimens were compacted into cylindrical molds of 25.4 mm in height and 63.5 mm in diameter. A dry density of 12.46 kN/m^3 was considered for all specimens, representing the actual density in the field. Swell strain tests were then conducted following the procedure explained in the previous chapter.

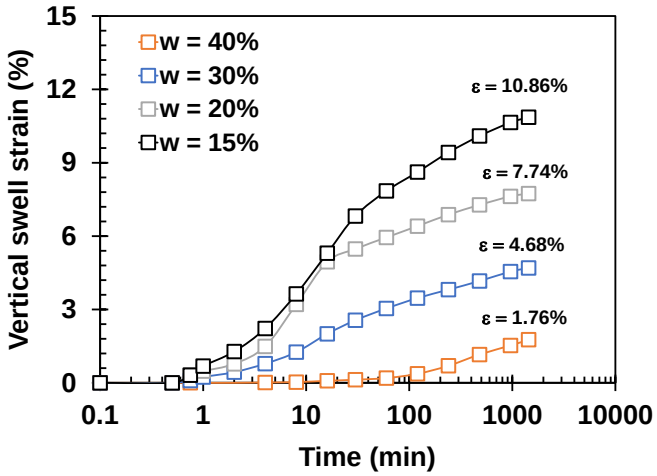

Figure 4.5: Vertical swell strain of the soil

Figure 4.5 illustrates the vertical swell strain over time for specimens prepared with varying initial moisture contents. The results indicate the great tendency of the tested soil to expand, though less pronounced in specimens prepared at lower moisture content. The soil specimen with an initial moisture content of w = 0.4 (or 40%) demonstrates the lowest vertical swell strain among the tested specimens, reaching a maximum strain of 1.76% after the testing period. The soil specimens with lower initial moisture contents (15% and 20%) exhibit significantly higher vertical swell strains, reaching 10.86% and 7.74%, respectively. This indicates that the soil has a high swell potential when it starts off drier. The soil's initial moisture content directly influences expansive soils' expansion behavior. When soil has a low initial moisture content, it is relatively dry, meaning it has a higher capacity to absorb additional water when exposed. This water absorption causes the soil particles to swell, leading to a greater vertical swell strain. On the other hand, when the soil's initial moisture content is higher (30% and 40%), the soil is closer to saturation. In this state, the soil has already absorbed a significant amount of water, leaving less capacity to take in more. As a result, less additional water is absorbed by the soil, leading to a lower degree of expansion.

Figures 4.6a and 4.6b provide a visual comparison of the soil sample prepared at an initial moisture content of 40% before and after the vertical swell strain test. In Figure 4.6a, the soil sample is shown in its initial state, prior to inundation. The surface is smooth and level, with no visible signs of swelling or structural disturbance, representing the controlled baseline condition at the start of the experiment. At this point, the soil's original volume and structure remain intact, establishing a reference for subsequent observations. In contrast, Figure 4.6b depicts the same soil sample after 24 hours of inundation. The surface now clearly shows signs of swelling, with a visibly increased volume. This change is the result of water absorption by the soil particles, particularly the clay minerals, which leads to an expansion in inter-particle spacing and an overall increase in volume. The comparison between these two figures highlights the impact of moisture on the soil's physical behavior, demonstrating the significant expansion that occurs when expansive soils absorb water.

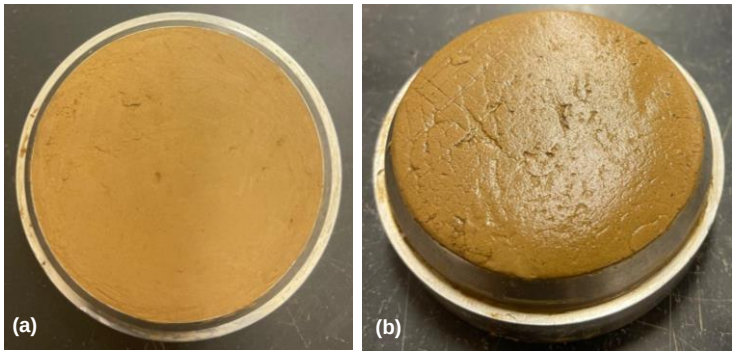

Figure 4.6: a) before the swell test, **b)** after the swell test

4.2 Effect of Nanomaterials on Swelling and Mechanical Behaviors of Expansive Soils

A series of experiments were conducted to evaluate the effects of nanomaterials on soil properties, including Atterberg and swell potential to assess plasticity and expansion characteristics, unconfined compressive strength, SWRC and hydraulic conductivity measurements to evaluate the soil's water retention capabilities and permeability, and XRD to evaluate the formation of M-

S-H and to identify the mineral composition, in the treated soil. For the tests, nano-silica (SiO_2) and nano-magnesium oxide (MgO) were used, and nano-conditioning was performed using mechanical mixing. This process involved evenly dispersing the nanomaterials solution into the soil following the procedure explained in Chapter 3, which ensured a homogeneous distribution of nanoparticles throughout the soil matrix. For the mechanical tests, such as unconfined compressive strength (UCS) , the soil specimens were prepared using static compaction of the moist soil, creating cylindrical specimens with a height of 76 mm and a diameter of 38 mm.

4.2.1 Atterberg Tests

Figure 4.7a illustrates the correlation between the consistency limits and the amount of MgO nanoparticles (MgO-NPs) added to the soil. With the addition of 1%, 2%, and 3% MgO-NPs, the soil's liquid limit (LL) increased by 1.91%, 3.47%, and 5.31%, respectively. Similarly, the plastic limit (PL) rose by 16.11%, 24.38%, and 43.25%. Notably, the increase in PL was substantially higher than the increase in LL, which led to a corresponding decrease in the plasticity index (PI = LL - PL). Specifically, the PI decreased from 37.22 to 34.02, 32.75, and 28.74 with the incorporation of 1%, 2%, and 3% MgO nanoparticles, respectively. These reductions in PI correspond to decreases of 8.59%, 12.01%, and 22.78%. As a result, according to Seed et al.'s (1962) expansive soil classification, the addition of MgO nanoparticles shifted the soil from a "very highly expansive" category (PI > 35%) to a "highly expansive" category (20% < PI < 35%), even with just a 1% addition of nano MgO. Similarly, when the soil was treated with 1%, 2%, and 3% nano SiO_2, both the LL and PL increased, as shown in Figure 4.7b. However, unlike MgO nanoparticles, the LL increased at a higher rate compared to the PL when nano SiO_2 was added. Specifically, the PI decreased slightly from 37.22 to 36.63 with the addition of 1% SiO_2, but then increased to 38.87 and 41.00 with 2% and 3% SiO_2, respectively.

The different behaviors of SiO_2 and MgO in soil conditioning are primarily due to their distinct surface areas, chemical reactivities, and interactions with water and soil particles. SiO_2, with its high surface area and strong hydrophilicity (Xu & Zhang, 2021), tends to increase both LL and PL, with a greater impact on LL, resulting in a higher PI at higher concentrations. MgO, with its moderate surface area and specific interactions with soil, tends to increase PL more than LL, leading to a lower PI and more stable soil at higher concentrations. As the percentage of SiO_2 exceeds 1%, the LL increases more rapidly than the PL, causing the gap between them (which defines the PI) to widen. This behavior suggests that while the soil can hold more water overall when treated with nano SiO_2, it particularly retains more water in its plastic state before transitioning to a liquid state as the SiO_2 concentration increases beyond 1%.

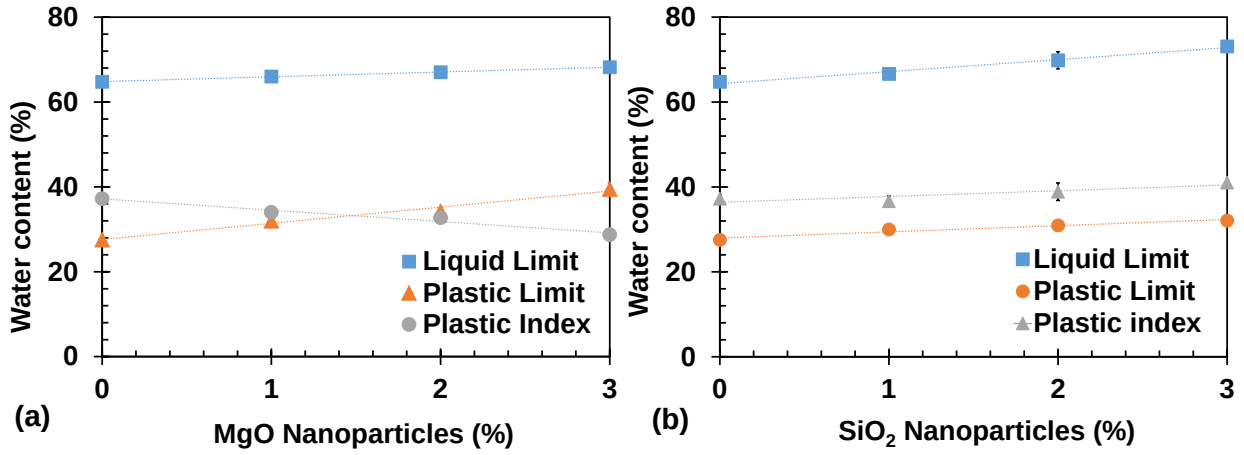

Figure 4.7: The soil Atterberg's limits conditioned with different percentages of nanoparticles**.** **a)** MgO nanoparticles **b)** SiO_2 nanoparticles

4.2.2 Vertical Swell Strain of Treated Soil

Figure 4.8 shows the one-dimensional vertical swell strain of soil specimens treated with MgO (Figure 4.8a) and SiO_2 (Figure 4.8b). As presented in Figure 4.8, different swelling behavior is observed in specimens treated with MgO and SiO_2. The stabilized soil loaded with MgO NPs decreases the vertical swell strain of the soil (Figure 4.8a). The addition of MgO NPs significantly

reduced the soil's swell potential. The untreated soil exhibited a strain of 1.76%, which decreased to 0.29% when treated with 1% MgO nanoparticles, representing an 83.52% reduction. As the concentration of MgO nanoparticles increased, the swell potential continued to decline. Treatment with 2% MgO nanoparticles resulted in a 94.32% reduction in strain, while 3% MgO nanoparticles almost eliminated swelling, achieving nearly 100% reduction compared to the untreated soil sample.

The reduction in the swell potential of soil can be attributed to several interconnected mechanisms. When MgO nanoparticles are introduced into the soil, they react with water to form $Mg(OH)_2$ (Wang et al., 2022). Due to their small size, these nanoparticles have a high SSA and reactivity, allowing for efficient interaction with clay particles. In the interlayer spaces, $Mg(OH)_2$ undergoes hydrolysis and polymerization, forming positively charged monomers and small polymers that can diffuse and create hydroxy-Mg-interlayers. These interlayers effectively transform the expanding clay minerals into non-expanding, chlorite-like structures, preventing water from entering the interlayer spaces. Simultaneously, the external precipitation of $Mg(OH)_2$ coats the clay particles, further reducing water absorption and promoting aggregation (Xeidakis, 1996). This coating effect, combined with the internal structural changes, significantly reduces the soil's ability to absorb water and expand. Over time, additional processes such as physical adsorption, hydrogen bonding, and pozzolanic reactions (M-S-H formation) further stabilize the soil structure, resulting in a sustained reduction of swell potential (Xeidakis, 1996).

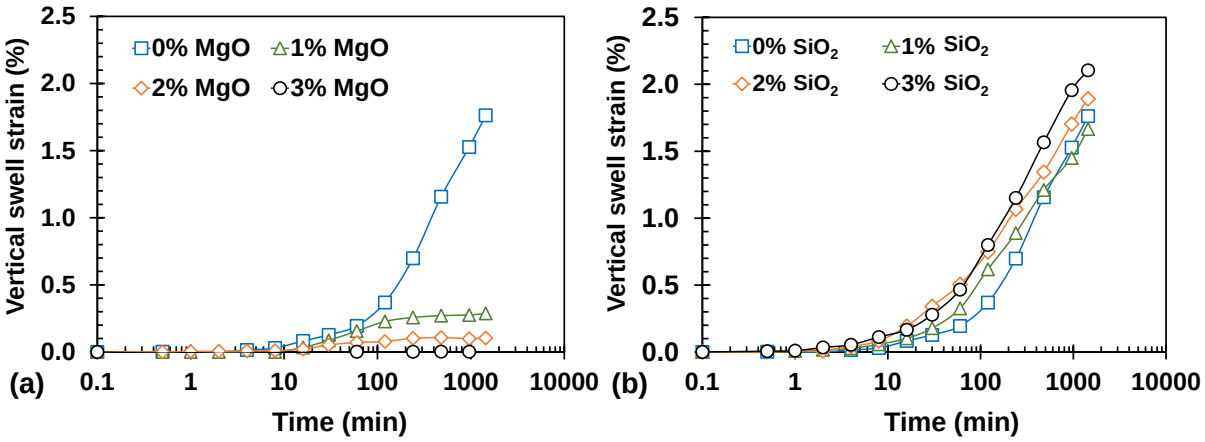

Figure 4.8: The soil vertical swell strain with different percentages of nanoparticles**. a)** MgO nanoparticles **b)** SiO_2 nanoparticles

For the soil treated with nano SiO_2 (Figure 4.8b), the swell strain of the soil decreases after 24 hours from 1.76% to 1.67%, which only shows a 5.11% reduction in the soil swell. However, going beyond 1% SiO_2, the soil vertical swell increases from 1.76% to 1.89% and 2.10% with the addition of 2% and 3% SiO_2 nanoparticles respectively. The swelling and shrinking behavior of expansive soils is governed by two key aspects: the swelling and shrinking of the montmorillonite clay mineral itself, and the change in the average spacing between soil particle units. Nano-SiO_2 particles, when uniformly dispersed in the soil, adhere to the surface of soil particles through the condensation of silanol groups, forming siloxane bonds. This imparts molecular-level hydrophobicity to the modified soil surface, making it water-repellent. Consequently, the hydrophobic surface hinders the absorption and loss of water from the soil. Moreover, the incorporation of nano-SiO_2 particles reduces the pore volume and size within the soil matrix, thereby decreasing the change in the average spacing between particle units during swelling and shrinking processes. These mechanisms collectively contribute to the reduction in soil expansion when nano-SiO_2 is introduced into expansive soils. Too much nanoparticle causes nano-SiO_2 particle agglomeration, leading to a low aspect ratio and a low contact surface area, resulting in

weak adhesion forces between the clustered nanoparticles and clay (Luo et al., 2022). Adding nanoparticles beyond a certain amount may lead to the agglomeration of nanoparticles and increase the void ratio of the soil mixture (Iranpour, 2016; Luo et al., 2022). As a result, beyond a threshold value, the swell potential of the soil may increase.

4.2.3 Unconfined Compressive Strength

Figure 4.9a illustrates the strain-stress curves of soil treated with 1%, 2%, and 3% MgO nanoparticles. As shown in the figure 4.9a, the soil stress increases progressively with the addition of MgO NPs, rising from 60.30 kPa in untreated soil to 84.91 kPa, 120.36 kPa, and 121.75 kPa with the incorporation of 1%, 2%, and 3% MgO NPs, respectively. These increases correspond to strength improvements of 40.81%, 99.60%, and 101.91%. The enhanced soil strength can be primarily attributed to changes in the soil's density, void ratio, and water content. Due to their hydrophilic nature and high surface area, MgO NPs adsorb water from the soil, filling the voids within the soil matrix and increasing the density, consequently leading to an enhancement in strength (Sadiq et al., 2023; Taha et al., 2015). Moreover, due to the high reactivity of MgO NPs when integrated with soil, chemical reactions between the silica (SiO_2) in the soil and MgO NPs take place, producing magnesium silicate hydrate (M-S-H) gel, as shown in equations (4-1) and (4-2).

$$MgO + H_2O \longrightarrow Mg(OH)_2 \qquad (4-1)$$

$$Mg(OH)_2 + SiO_2 \longrightarrow \text{M-S-H}\left(\text{Magnesium Silicate Hydrate}\right) \qquad (4-2)$$

This process facilitates the formation of strong bonds within the soil matrix, resulting in increased soil strength (Lang et al., 2021; Sadiq et al., 2023; Wang et al., 2022). The stabilization of expansive soils using $Mg(OH)_2$, a product of MgO hydration, has been well-documented. Xeidakis (1996a, 1996b) reported that the adsorption mechanism of $Mg(OH)_2$ by clay includes

physical adsorption, chemical bonding, cementation through crystallization, and long-term pozzolanic reactions. Similarly, Yi et al. (2016) found that the stabilization mechanisms of $Mg(OH)_2$ are akin to those of $Ca(OH)_2$, involving dissolution, cation exchange, and pozzolanic reactions, with the latter playing a crucial role in strength improvement.

The improvement in soil strength appears to become marginal beyond the addition of 2% MgO NPs, potentially due to the limited availability of reactive sites and the lack of further bonding opportunities within the soil matrix. This phenomenon is consistent with findings from Chen et al. (2023), who observed that the maximum strength in loess soil was achieved with the addition of 2% MgO NPs.

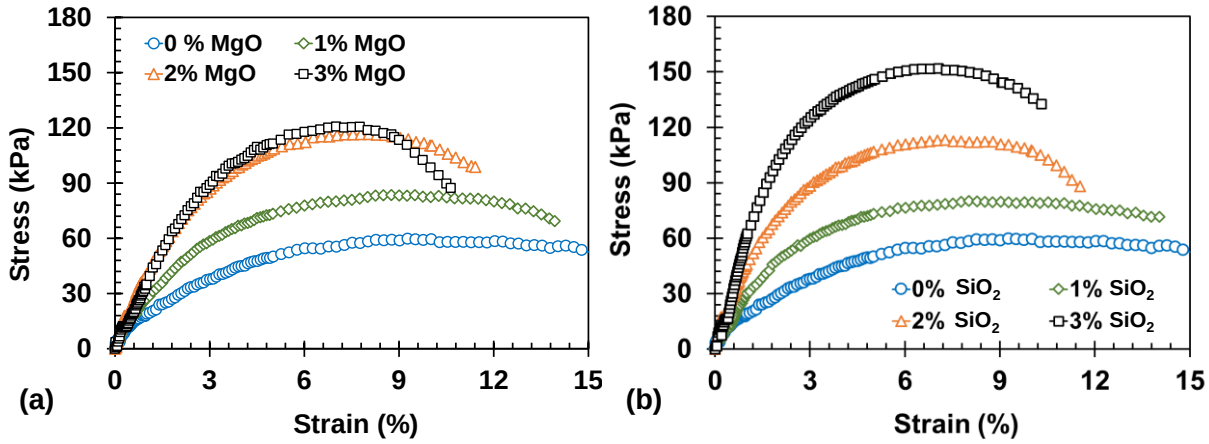

Figure 4.9: The soil unconfined compressive strength with different percentages of nanoparticles**. a)** MgO nanoparticles **b)** SiO_2 nanoparticles

Figure 4.9b presents the stress-strain behavior of soil treated with silica nanoparticles (SiO_2 NPs). The unconfined compressive strength of the soil exhibits a notable increase with the addition of nano-SiO_2. For the untreated soil sample with 0% SiO_2 NPs, the UCS is 60.30 kPa. Upon incorporating 1% nano-SiO_2, the soil strength increases to 82.12 kPa, representing a 36.18% enhancement compared to the untreated soil. Further increasing the nano-SiO_2 content to 2% results in a UCS of 113.89 kPa, corresponding to an 88.87% increase relative to the untreated soil.

Notably, the soil treated with 3% SiO_2 NPs achieves a maximum UCS of 153.83 kPa, indicating a substantial 155.12% improvement in strength compared to the untreated soil sample. The increase in the UCS of the soil could be attributed to the high surface area of SiO_2 NPs and small size can fill the voids in the soil and improve the packing density of the soil (Liu et al., 2023). The SiO_2 NPs can also act as nucleation sites for the formation of hydration products, such as C-S-H gel, during the cementitious reactions in the soil. This can form a denser matrix with the soil and better distribution within the soil, and therefore increase the soil strength (Hou et al., 2012; Liu et al., 2023). The same trend was observed by Ahmadi and Shafiee (2019), they found that by increasing the SiO_2 NPs, the soil peak strength increased.

4.2.4 Soil Water Retention Curves of Treated Soil

Soil water retention curve (SWRC), also known as the soil water characteristics curve (SWCC), is a graphical representation that describes the relationship between a soil's degree of saturation and its water potential or matric suction (Eyo et al., 2022). The key characteristics of the SWRC are the air entry suction (ψ_{ae}) and residual suction (ψ_{res}). Air entry suction is the point at which air begins to enter the soil's voids, displacing water to neighboring water-filled voids. Water contents associated with these suctions are saturated (θ_s) and residual (θ_{res}) water contents; residual suction corresponds to the condition where water remains only as thin films around soil particles. Based on these characteristics, the SWRC can be divided into three distinct regions (Figure 4.10): the boundary effect zone (saturation zone), which occurs at suctions below the air entry suction; the transition zone, for suctions between the air entry and residual suctions; and the residual zone, where suctions exceed the residual suction (Fredlund et al., 2011; Hussain et al., 2020; Soltani, Azimi, et al., 2019). Treating soil with nanoparticles can alter these regions, thereby affecting the

hydro-mechanical behavior of the treated material. This can change the soil's water retention capacity, stability, and performance under different moisture conditions.

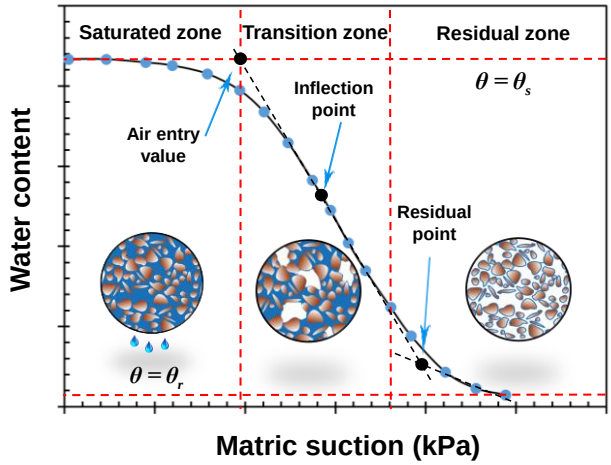

Figure 4. 10: Different regions of the SWRC

The SWRC graphs in Figures 4.11 and 4.12 illustrate the impact of varying concentrations of MgO and SiO_2 nanoparticles on the matric suction behavior of expansive soil. These graphs also present the van Genuchten (1980) fitting curves and the corresponding fitting parameters, including the shape factor "n" and a fitting parameter related to the air entry suction "α". The van Genuchten model is described by the following equation, which relates the soil's volumetric water content (θ) to the matric suction (ψ):

$$\theta(\psi) = \theta_r + \frac{\theta_s - \theta_r}{\left[1 + (\alpha\psi)^n\right]^{1-\frac{1}{n}}} \qquad (4-3)$$

where θ(ψ) is the volumetric water content at matric suction ψ, θ_r and θ_s are residual and saturated volumetric water contents, α is the fitting parameter that controls the position of the SWRC on the suction axis and is the inverse of the air entry suction (in kPa^{-1}), a parameter, and n is a dimensionless shape parameter that affects the slope of the SWRC in the transition zone between saturation and residual conditions.

Starting with air entry suction, the pure soil (Figure 4.11a) exhibits air entry at a relatively low matric suction value, indicating that air begins to replace water in the soil voids at lower suction levels. For both MgO and SiO_2 treatments, the addition of nanoparticles shifts the air entry suction (ψ_{ae}) towards higher values, particularly at concentrations of 2% and 3%. Specifically, for MgO-treated soils, the air entry suction increases from 62.5 kPa in untreated soil to 200 kPa and 143 kPa for soils treated with 2% and 3% MgO, respectively. This shift suggests an enhanced ability of the treated soils to retain water at lower suction levels, delaying the entry of air into the soil voids. In comparison, SiO_2-treated soils also show an increase in air entry suction, but the changes are more moderate, with values of 167 kPa and 143 kPa for soils treated with 2% and 3% SiO_2, respectively.

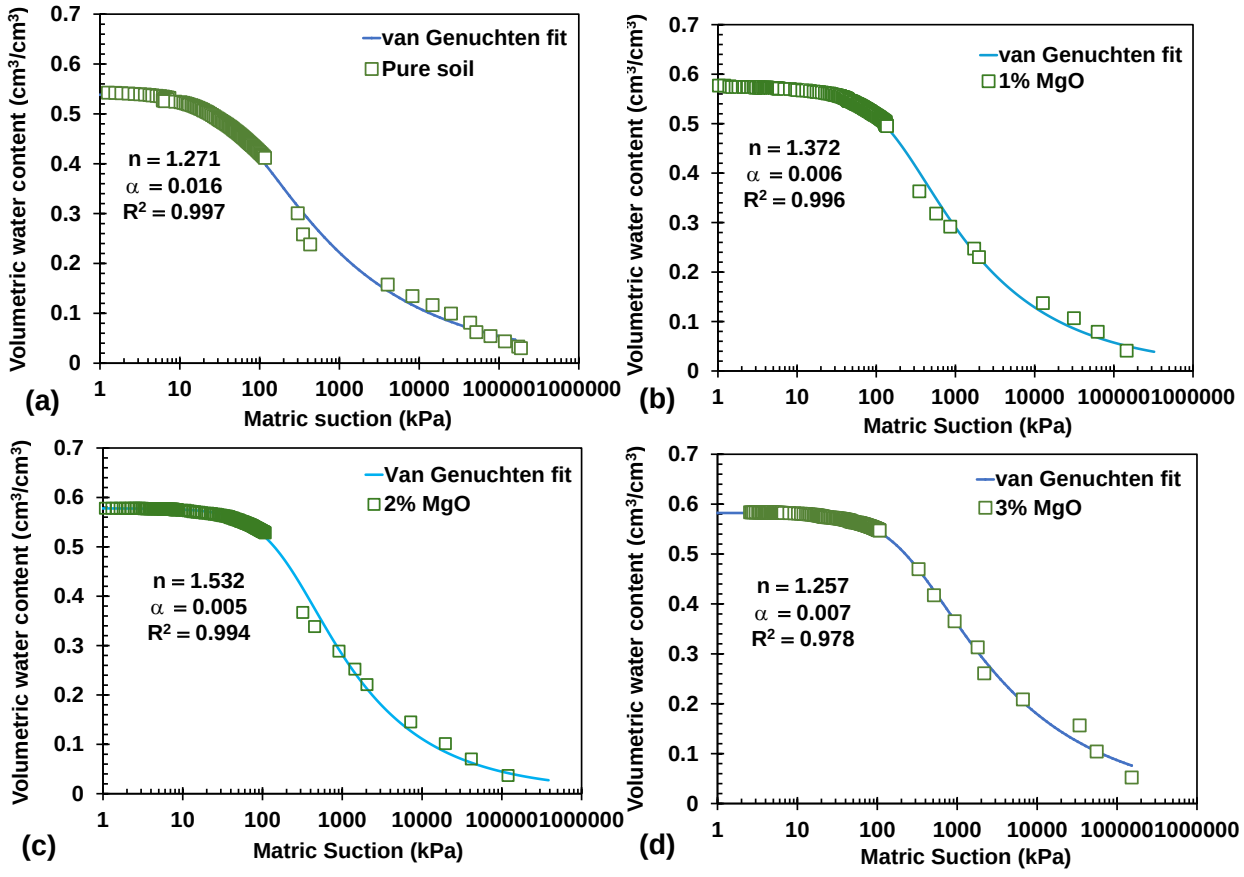

Figure 4.11: The soil water retention curve treated with different percentages of MgO nanoparticles **a)** Untreated soil **b)** 1% MgO **c)** 2% MgO **d)** 3% MgO

For residual suction, the pure soil's curve (Figure 4.11 a) shows residual suction at a moderate matric suction level, where the soil retains only thin water films around its particles. With the addition of MgO and SiO_2 nanoparticles, particularly at higher concentrations, the residual suction increases, as seen in Figures 4.11d and 4.12d.

The slope of the SWRC curves, which represents the rate at which water is released as suction increases, also changes with the addition of nano-MgO and SiO_2. In the pure soil (Figure 4.11a), the curve has a relatively steep slope, indicating a rapid transition from saturation to residual moisture content as matric suction increases. However, with increasing nano-MgO and SiO_2 contents, the slope, indicated by the van Genuchten "n" parameter, increases from 1.271 in untreated soil to 1.532 and 1.257 for soils treated with 2% and 3% MgO, respectively. This gradual change suggests that MgO-treated soils exhibit a more consistent release of water across a broader range of suction levels. In contrast, the slopes for SiO_2-treated soils are steeper, with "n" values of 1.372 and 1.257 for 2% and 3% SiO_2 treatments, indicating a more abrupt water release as suction increases. This steeper slope in SiO_2-treated soils suggests that water is released more quickly, which could lead to less uniform moisture retention compared to MgO-treated soils.

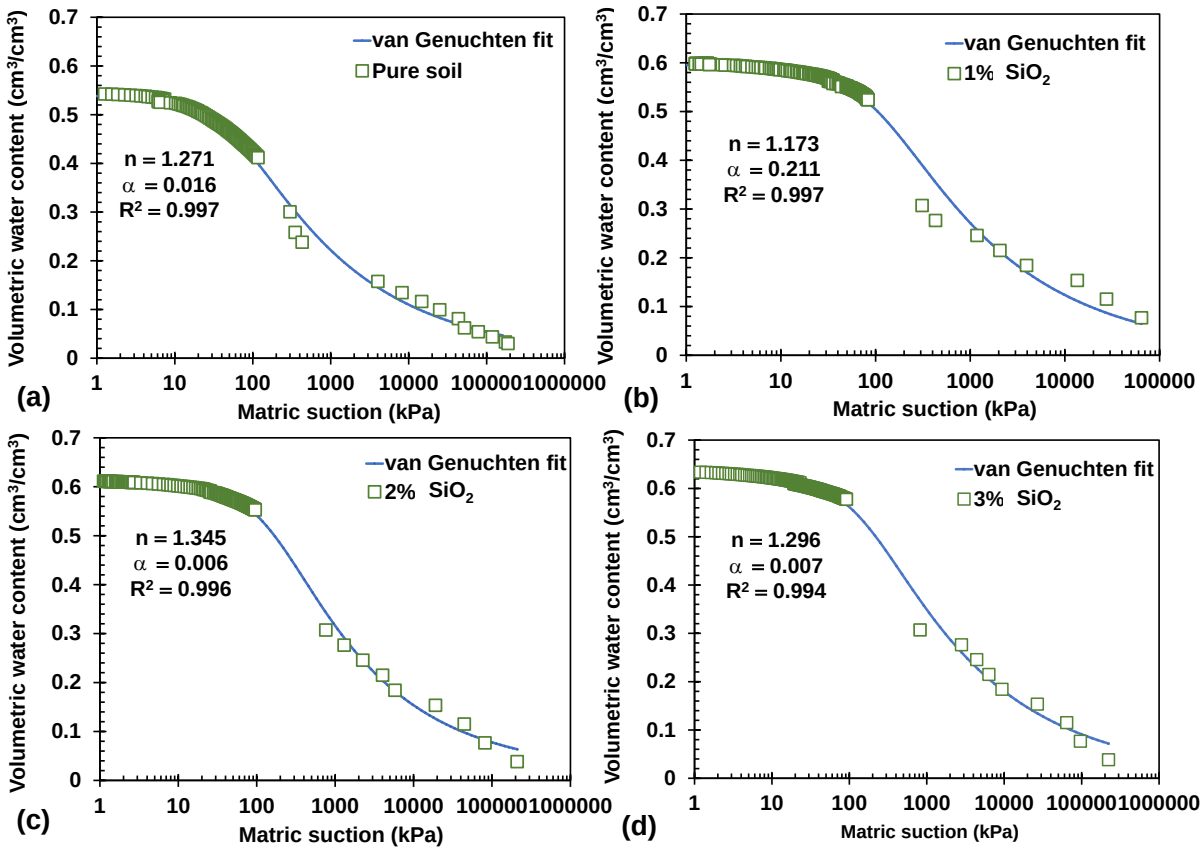

Figure 4.12: The soil water retention curve treated with different percentages of SiO_2 nanoparticles **(a)** Untreated soil **(b)** 1% SiO_2 **(c)** 2% SiO_2 **(d)** 3% SiO_2

The differences in the effects of MgO and SiO_2 nanoparticles on the soil water retention curves (SWRC) and the associated hydro-mechanical properties of expansive soils can be attributed to their distinct physical and chemical characteristics. SiO_2 nanoparticles generally have a significantly higher specific surface area than MgO nanoparticles, allowing for more extensive interactions with water molecules. This leads to higher water retention at lower suctions but also results in a quicker release of water as suction increases, causing a steeper slope in the SWRC for SiO_2-treated soils. In contrast, MgO nanoparticles, with their smaller surface area, promote a more moderate pattern of water retention and release, contributing to a more gradual slope in the SWRC. Additionally, SiO_2's strong hydrophilicity, due to the presence of numerous hydroxyl groups on

its surface (Xu & Zhang, 2021), enhances water adsorption, resulting in more abrupt changes in water content when suction levels rise. On the other hand, MgO nanoparticles react with soil minerals to form magnesium silicate hydrate (M-S-H) gel, stabilizing the soil structure and moisture content and leading to more consistent water retention.

4.2.5 Hydraulic Conductivity of Treated Soil

Hydraulic conductivity is a crucial property that determines how easily water can flow through soil, significantly influencing the soil's behavior under various environmental conditions. Figure 4.13 illustrates the variations in hydraulic conductivity by adding 1%, 2%, and 3% of MgO and SiO_2 nanoparticles.

For MgO-treated soils, the results demonstrate a significant linear decrease in hydraulic conductivity as the soil is treated with 1% and 2% MgO nanoparticles. Specifically, the hydraulic conductivity decreases from 6.815×10^{-7} cm/s for untreated soil to 3.832×10^{-7} cm/s with the addition of 1% MgO, and further to 1.184×10^{-7} cm/s with 2% MgO, reflecting a substantial reduction in water flow through the soil matrix. However, increasing the MgO concentration beyond 2% yields only marginal additional reductions in hydraulic conductivity, suggesting a threshold point at 2% MgO, beyond which no substantial further decrease occurs. This indicates that 2% MgO could be considered an optimal concentration, where the effectiveness of additional MgO in reducing hydraulic conductivity diminishes. Notably, a similar pattern was observed in the unconfined compressive strength (UCS) of MgO nanoparticle-treated soil, reinforcing the existence of this threshold effect across multiple soil properties. The reduction in hydraulic conductivity is primarily attributed to the nanoparticles' ability to occupy interstitial voids and alter the soil's pore structure, effectively restricting water flow pathways within the treated matrix.

The blue curve in Figure 4.13 represents the relationship between soil hydraulic conductivity and SiO_2 nanoparticle concentration. The data reveal that the lowest hydraulic conductivity was observed when the soil was treated with 1% SiO_2, reducing the hydraulic conductivity from 6.815×10^{-7} cm/s (untreated) to 2.205×10^{-7} cm/s. Interestingly, beyond this concentration, the hydraulic conductivity begins to increase, reaching 4.202×10^{-7} cm/s with 2% SiO_2 and 3.921×10^{-7} cm/s with 3% SiO_2. This trend aligns with the observed changes in the soil's plasticity index (PI) and vertical swell strain when treated with SiO_2 nanoparticles. The initial reduction in soil hydraulic conductivity at lower SiO_2 concentrations can be attributed to the nanoparticles' ability to fill the voids between soil particles, thereby reducing the pathways available for water flow. However, the subsequent increase in hydraulic conductivity at concentrations above 1% SiO_2 may be due to soil agglomeration and solidification processes, as Bahmani et al. (2014) suggested. These processes could potentially create new pore networks that facilitate water flow, counteracting the initial reduction in hydraulic conductivity.

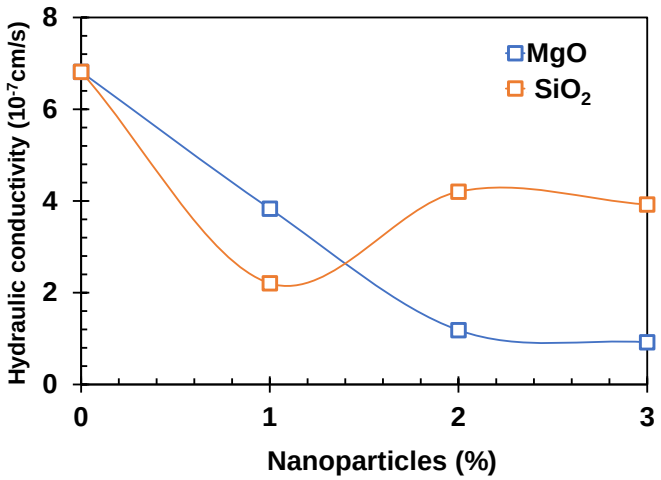

Figure 4.13: The saturated hydraulic conductivity of the soil treated with different percentages of MgO and SiO_2 nanoparticles

4.2.6 Effect of MgO on Soil pH and the pH Effect on the Soil Strength

As part of the study, a series of tests were conducted to evaluate the effect of nano-conditioning with nano-MgO on soil pH and how these changes in pH influence soil compressive strength. The initial soil pH was measured at 7.45, which falls within the neutral range. Upon treatment with MgO nanoparticles, the soil pH increased significantly, rising to 10.06, 10.83, and 11.51 with the addition of 1%, 2%, and 3% nano MgO, respectively, as illustrated in Figure 4.14. This marked increase in pH is attributed to the alkaline nature of MgO, which dissociates in water to form magnesium hydroxide $Mg(OH)_2$, a compound known for its basic properties. Introducing MgO nanoparticles into the soil matrix creates an environment that raises the overall pH, influencing both the chemical interactions within the soil and its physical properties.

The relationship between soil strength and pH was further investigated during the physical mixing of soil with a 2% MgO nanoparticle solution, as shown in Figure 4.15. The experiment revealed that the optimal soil strength was achieved at a pH of 10.58, which corresponds to the pH of the MgO solution when it first interacts with the soil. This pH level appears to be ideal for promoting the formation of strong bonds within the soil matrix. Lower pH levels, such as 7 and 4, were found to be less effective in promoting these beneficial chemical reactions. Based on these findings, the subsequent electrokinetic injection treatment aimed to maintain the MgO solution at approximately pH 10.58 throughout the process. This strategy was designed to replicate the conditions that produced the highest soil strength in the baseline physical mixing tests. By maintaining this optimal pH during the electrokinetic treatment, the process could consistently promote the formation of M-S-H gel and maximize the benefits of nano MgO stabilization, thereby ensuring that the soil's compressive strength was enhanced to its fullest potential.

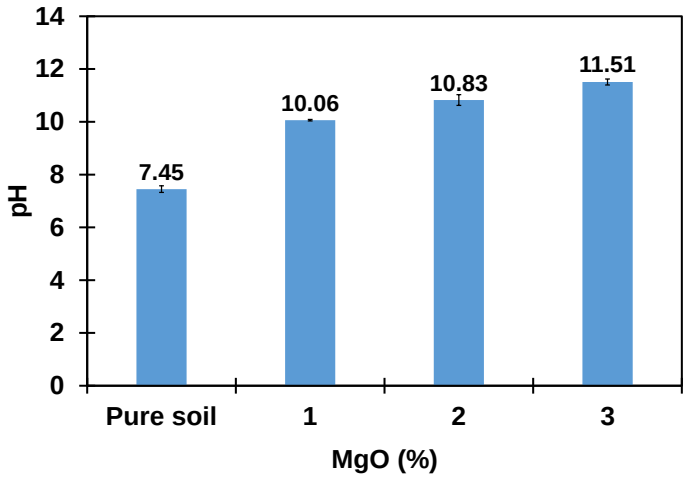

Figure 4.14: The soil pH after being treated with different percentages of MgO nanoparticles

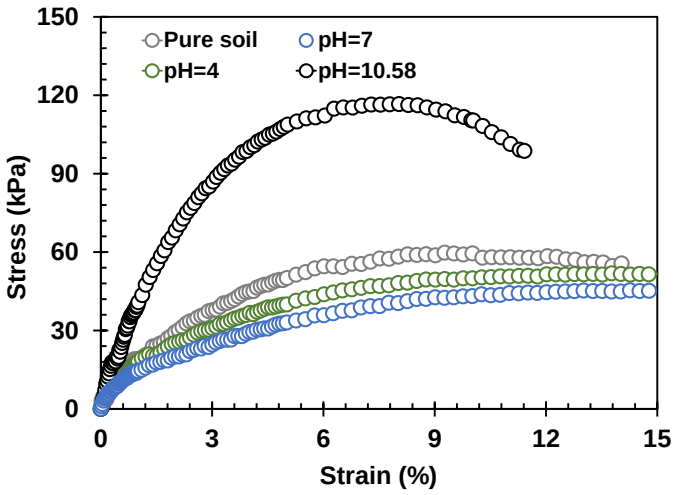

Figure 4.15: The treated soil unconfined compressive strength treated 2% MgO, with different solution pH during the mixing process

4.2.7 XRD Analysis of the Treated Soil

XRD analysis was performed to evaluate the formation of M-S-H and to identify the mineral composition and crystallinity of the soil. The X-ray diffraction (XRD) results for MgO nano-conditioning are presented in Figure 4.16. Figure 4.16a shows the characteristic XRD pattern of pure MgO nanoparticles, displaying prominent diffraction peaks at 2θ angles of approximately 36.9°, 42.9°, and 62.3°, corresponding to the (111), (200), and (220) crystallographic planes,

respectively. These sharp and well-defined peaks indicate the crystalline nature of the MgO nanoparticles used in this study.

Figure 4.16b illustrates the XRD patterns of soil samples treated with varying concentrations of MgO nanoparticles (1%, 2%, and 3%), alongside the untreated (pure) soil sample for comparison. The XRD pattern of the untreated soil exhibits broad and less intense peaks, indicative of the amorphous or poorly crystalline nature of the original soil material. The results indicate no significant alterations in soil peak patterns following MgO treatment. Several factors may contribute to this observation: (1) the relatively low concentrations of nano MgO utilized (1%, 2%, and 3%) may be insufficient to induce detectable changes in the soil's overall crystalline structure; (2) the reaction between MgO and soil SiO_2 in the presence of water might produce extremely small crystallites or amorphous gel-like structures (M-S-H) that are below the detection threshold of XRD analysis; and (3) the nanoscale dimensions of the MgO particles and the limited reaction time may also influence the lack of observable changes in the XRD patterns. These findings suggest that the soil stabilization effects of nano MgO at these concentrations likely occur primarily through physicochemical interactions rather than significant alterations to the soil's crystalline structure.

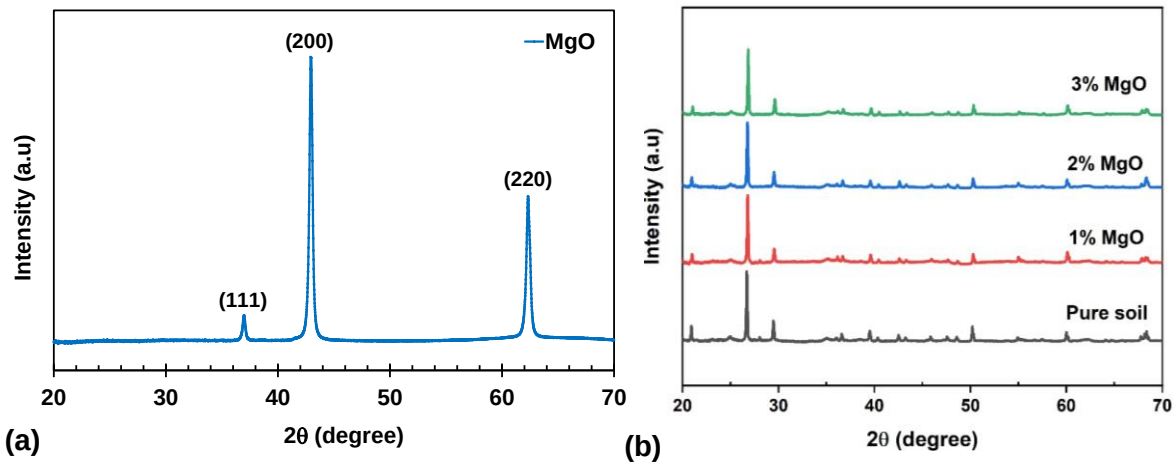

Figure 4.16: XRD patterns of **a)** MgO nanoparticles and **b)** soil samples treated with different percentages of MgO nanoparticles (0%, 1%, 2%, and 3%).

4.3 Effect of Electrokinetic on Soil Matrices

A series of experiments were conducted to investigate the effects of electrokinetics on expansive soils in isolation. For these experiments, soils were subjected to direct current (DC) electricity at three different voltage levels: 10 V (67 V/m), 15 V (100 V/m), and 25 V (167 V/m) over a 7-day curing period. Following the treatment, several parameters were analyzed to assess the impact of electrokinetics on the soil's physical and chemical properties. These parameters included Atterberg limits and vertical swell strain to evaluate plasticity and expansion characteristics, unconfined compressive strength (UCS) to determine the soil's mechanical stability, changes in moisture content, pH variation, electrical conductivity, and microstructural analysis using Scanning Electron Microscopy (SEM). X-ray fluorescence (XRF) analysis was also conducted to evaluate the soil's chemical composition post-treatment. Each of these parameters will be discussed in detail in the following sections. For these tests, samples were taken from the electrokinetic cell, following the procedure described in Chapter 3.

4.3.1 Effect on Soil Swell Potential

To evaluate the effect of electrokinetics on soil swell potential, we first measured variations in soil moisture throughout the specimen during the electrokinetic process. This initial step was crucial to understanding how the electric field influenced moisture distribution within the soil. Following this, we conducted Atterberg limit tests and vertical swell strain tests to assess the changes in the soil's expansive potential in response to the applied electric field. These tests provided a comprehensive analysis of how the moisture redistribution, induced by electrokinetics, affected the soil's plasticity, liquid limit, and overall tendency to swell.

4.3.1.1 Moisture Content of Treated Soil

During the electrokinetic process, the applied electric field interacts with the ions present in the soil, establishing a net water flow that typically moves from the anode to the cathode (Acar & Alshawabkeh, 1993; Rittirong, 2007; Sivapullaiah & Prakash, 2007). This movement causes significant changes in soil moisture content throughout the specimen. The extent of these changes is influenced by several factors, including the magnitude of the electric field, the type and characteristics of the soil, and the initial moisture content within the soil. To analyze the effect of electrokinetics on soil moisture distribution, soil samples were extracted from different locations within the electrokinetic cell after applying varying electric field intensities (10 V, 15 V, and 25 V), as described in Section 3.4. The moisture content was measured at each location to assess how the electric field influenced water movement through the soil matrix.

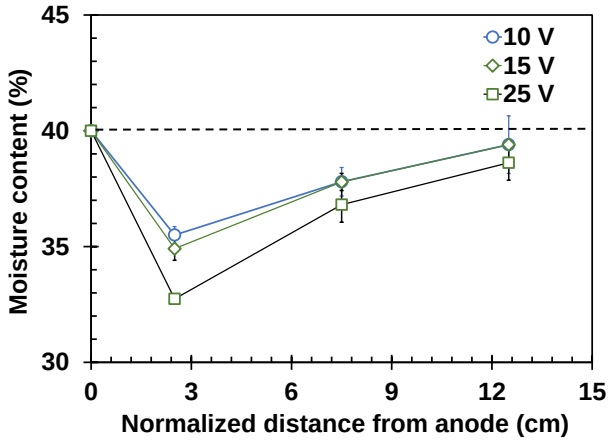

Figure 4.17: Moisture variation in the soil treated under different electric field intensities for days

The data presented in Figure 4.17 reveals a distinct pattern of moisture redistribution within the soil. The dashed line indicates the initial soil moisture content of 40%. As the electric field is applied, a clear trend emerges: moisture content decreases near the anode and increases toward the cathode, demonstrating water movement from the anode toward the cathode.

At a voltage of 10 V, the moisture content near the anode decreases from its initial value of 40% to 35.50%. Conversely, moving toward the cathode, the moisture content increases to 39.40%, indicating water migration under the influence of the electric field. As the voltage is increased to 15 V, the effect becomes more pronounced. The moisture content near the anode further decreases to 34.91%, while near the cathode, it remains almost the same as at 10 V (39.40%). The most significant changes are observed at the highest voltage of 25 V. Here, the moisture content near the anode drops to approximately 32.74%, while near the cathode, it reaches 38.62%. This figure clearly illustrates the strong influence of the electric field on moisture redistribution, with higher voltages leading to more pronounced water movement from the anode to the cathode.

Figure 4.18 visually demonstrates treated soil samples with —10 V, 15 V, and 25 V—after 7 days of electrokinetic treatement. The images show clear evidence of moisture redistribution and its effects on the soil structure as a result of the applied voltages. In the 10 V sample, the soil appears relatively intact, with a smooth surface and minimal visible cracking. This suggests that the lower voltage induced some moisture migration, but the overall structural integrity of the soil was largely maintained. The modest changes in moisture content likely led to a relatively uniform shrinkage across the sample. At 15 and 25 V, the soil sample exhibits noticeable cracking, indicating more significant moisture migration from the anode to the cathode. The cracks suggest that the soil near the anode has lost a substantial amount of moisture, leading to shrinkage and subsequent cracking. The soil near the cathode, meanwhile, has likely absorbed additional moisture, though this is less visually apparent in the image.

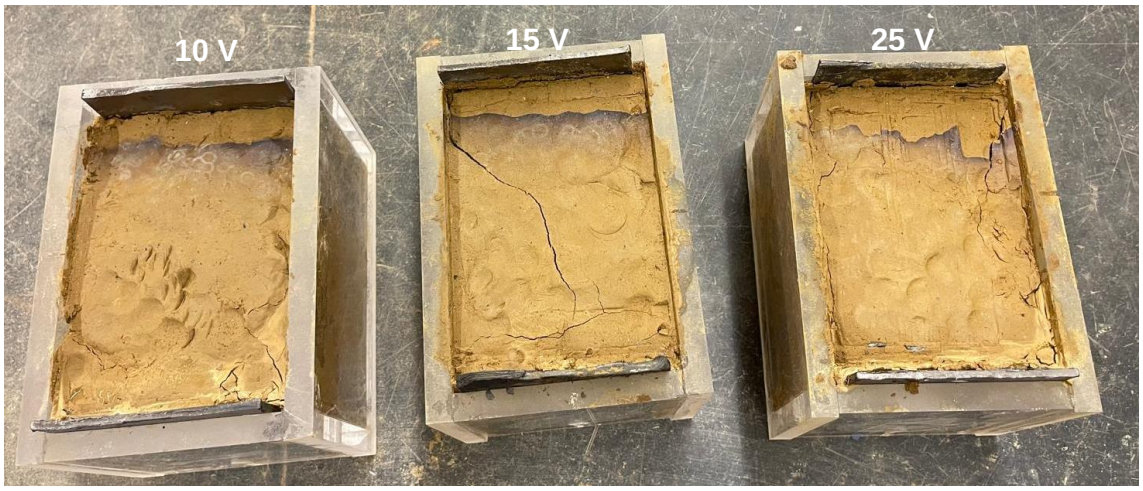

Figure 4.18: Treaded samples after 7 days under different electric potentials.

4.3.1.2 Atterberg's Limits of Treated Soil

Figure 4.19 presents the results of Atterberg limit tests conducted to evaluate the plasticity and swell potential of expansive soils subjected to electrokinetics. The graphs display the variations in liquid limit (LL), plastic limit (PL), and plasticity index (PI) as a function of the normalized

distance from the anode. The tests were performed under three different voltages: 10 V (a), 15 V (b), and 25 V (c), over a 7-day curing period.

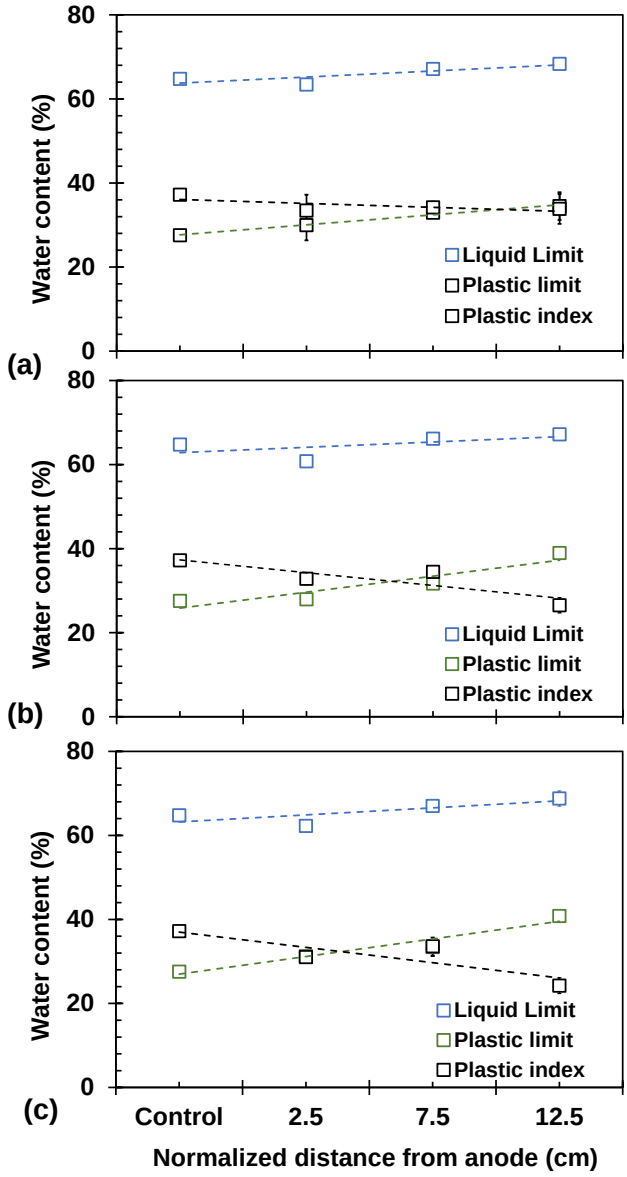

Figure 4.19: Atterberg's limits of soil treated under different electric field intensities for 7 days **(a)** 10 V **(b)** 15 V **(c)** 25 V

In all three cases, a general trend can be observed where the liquid limit (LL) and plastic limit (PL) increases slightly with increasing distance from the anode, while the plastic index (PI) tends to decrease. This trend is more pronounced at higher voltages, particularly in the 25 V test

(Figure 4.19c). The plasticity index (PI), which is the difference between the LL and PL, generally decreases with distance from the anode, indicating a lower swell potential further from the anode. At 10 V (Figure 4.19a), the liquid limit increased from around 63.43% near the anode to about 68.34% at the furthest distance (12.5 cm). The plastic limit changes slightly from 29.98% to 34.50%, leading to small changes in the plasticity index from approximately 33.45% to 33.84%. The changes are more noticeable at 15 V (Figure 19b). The liquid limit increases from approximately 60.78% to 67.21%, while the plastic limit increases from 27.95% to 38.98%. This decreases the plasticity index from about 32.83 % near the anode to 26.52 % at 12.5 cm. The most pronounced changes are observed at 25 V (Figure 19c). The liquid limit rises from 62.27% to 68.78%, and the plastic limit increases from 31.24% to 40.81%. Consequently, the plasticity index substantially decreases from 31.04% near the anode to 24.24% at the furthest distance. These results indicate that electrokinetic treatment significantly influences the Atterberg limits of expansive soils. As the distance from the anode increases, both the Liquid Limit and Plastic Limit tend to rise, while the Plasticity Index generally decreases, particularly at higher voltages. This suggests that the soil's water-holding capacity increases, but its susceptibility to volume changes may decrease further from the anode.

These changes in LL and PL are closely linked to variations in soil pH, which also tends to increase towards the cathode during electrokinetic treatment (Rittirong, 2007). Near the anode, the pH is lower, reflecting acidic conditions due to the Oxygen Evolution Reaction (OER) and the production of H^+ ions. Conversely, the area near the cathode becomes alkaline, resulting from the Hydrogen Evolution Reaction (HER) and the generation of OH^- ions (equation 4-4 & 4-5).

$$\text{Anode}: \quad 2H_2O - 4e^- \longrightarrow O_2 + 4H^+ \qquad (4-4)$$

$$\text{Cathode}: \quad 2H_2O + 2e^- \longrightarrow H_2 + 2OH^- \qquad (4-5)$$

As the soil pH increases towards the cathode, the plastic limit (PL) rises in a linear fashion. For instance, under 15V conditioning, the LL increased from 60.78 (pH 6.65) near the anode to 67.21 (pH 10.86) near the cathode, while the PL increased from 27.95 (pH 6.65) near the anode to 38.98 (pH 10.86) near the cathode. These shifts in LL and PL correspond with a decrease in the soil's PI towards the cathode. This trend was consistently observed under 10V and 25V treatments over the same 7-day curing period. These findings align with previous research, which indicates that both LL and PL increase with rising soil pH (Esrig & Gemeinhardt Jr, 1967; Nettleton, 1960; Rittirong, 2007).

4.3.1.3 Swell Potential of the Treated Soil

Figure 4.20 presents soil samples' vertical swell strain behavior subjected to different electric potentials of 10V, 15V, and 25V over 7 days. The results are shown for three different positions within the electrokinetic cell: (a) near the anode, (b) in the middle, and (c) near the cathode. The effects of electrokinetic treatment on soil swelling potential vary across the soil profile, from anode to cathode, and under different applied voltages. The results show that the swell potential of the soil increases near the anode compared to the untreated soil as the voltage increases from 10V to 15V and 25V. In the middle region, the potential remains relatively stable while, near the cathode, the swell potential decreases.

Near the anode, the soil samples exhibit a significant increase in vertical swell strain as the electric field intensity increases. The control sample, which was not subjected to any electric field, shows the lowest swell strain, with a final strain of around 1.76%. However, when a 10 V electric field is applied, the swell strain decreases steadily, reaching approximately 1.15% by the end of

the test. The 15 V and 25 V treatments show even more pronounced swell behavior, with the 25 V sample reaching a maximum strain of around 3.01%. This indicates that the soil near the anode is highly sensitive to the applied electric field, with higher voltages leading to greater expansion. This behavior can be attributed to several factors. Firstly, the soil near the anode has a lower water content due to electro-osmosis. During inundation, soil with lower initial water content tends to exhibit higher swelling potential compared to soil with higher water content due to the hydration process. Additionally, the dissolution of soil minerals and cation exchange processes during electroosmosis may play a role. Near the anode, acidification my breakdown organic matter and weakening the inter-particle bond and potentially altering the soil's swelling characteristics. However, further research is needed to confirm these hypotheses.

The swelling potential remains relatively stable in the middle region, showing no significant changes compared to untreated soil. This lower change in the swelling behavior of expansive soils is mainly due to the balance between electrochemical reactions occurring at the anode and cathode, with the middle region experiencing minimal effects from the electrokinetic process. Towards the cathode, the behavior is markedly different from the other regions. For samples taken from this region, the swelling potential decreases as the voltage increases, with samples subjected to 15 V and 25 V showing minimal or no swelling strain.

This decrease could be due to several complex changes occurring in the soil matrix. As previously mentioned, the soil water content increases near the cathode, which can reduce swelling potential. Moreover, cation movement towards the cathode results in a higher percentage of Ca^{2+} in this region, as shown in Table 4.1. These Ca^{2+} ions could participate in cementation reactions, producing C-S-H hydrate products in the soil. It is worth noting that the decrease in swelling potential aligns with the reduction in the soil's plasticity index towards the cathode. Consequently,

the cation concentration and diffuse double layer (DDL) thickness are reduced, reducing soil swelling potential (Barman & Dash, 2022). These observations indicate the complex interplay of electrochemical processes, moisture content changes, and ion migration during electrokinetic treatment of expansive soils. Further research is needed to fully understand the mechanisms behind these changes and optimize the treatment process for different soil types and conditions.

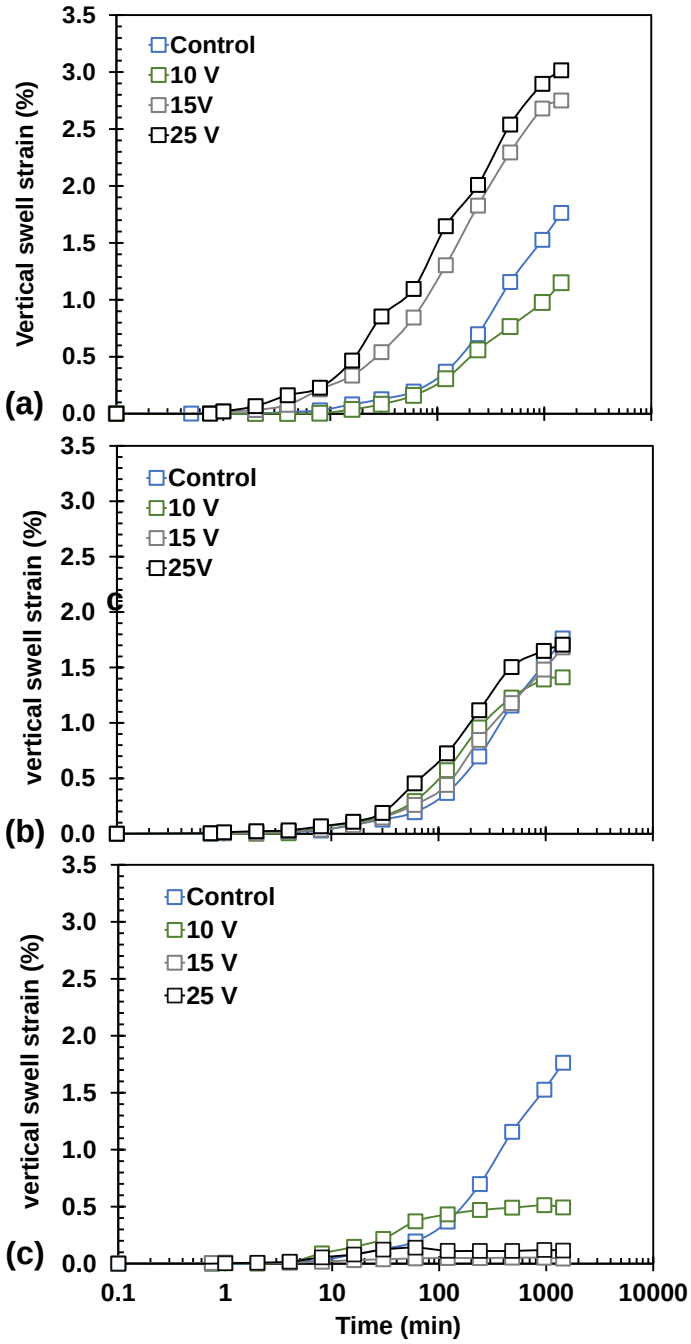

Figure 4.20: Vertical swell strain of the soil treated under different electric field intensities (**a)** Near the anode (**b)** in the Middle (**c)** near the cathode.

Table 4.1: XRF analysis of the soil samples

Voltage	Compound	Mg	Al	K	Ca	Fe	Si	Ti
	Pure soil	0.46	19.91	2.07	10.86	18.01	45.55	2.13
10V	Anode	0.66	20.53	2.00	9.54	18.10	45.90	2.07
	Middle	0.85	19.98	1.98	11.23	17.47	45.41	2.04
	Cathode	0.43	19.80	1.97	13.39	17.14	44.27	2.02
15V	Anode	0.86	20.42	2.05	9.06	18.08	46.37	2.10
	Middle	0.96	19.81	2.01	11.57	17.94	44.59	2.05
	Cathode	0.91	19.55	1.99	13.45	17.15	43.92	2.03
25V	Anode	0.76	21.10	2.11	5.40	19.06	48.38	2.13
	Middle	0.87	19.78	2.03	11.64	18.07	44.40	2.08
	Cathode	0.91	19.33	1.92	15.05	16.56	43.23	2.01

4.3.2 Unconfined Compressive Strength of Treated Soil

A series of unconfined compressive strength tests were performed to evaluate the strength characteristics of soil subjected to an electric field. As described in Section 3.4, the soil within the electrokinetic cells was exposed to voltages of 10 V, 15 V, and 25 V. Following the curing process, cylindrical samples were extracted from the soil using the procedure shown in Figure 4.21 and described in Section 3.4. These samples were then analyzed to determine how the applied electric field influenced the soil's compressive strength, with particular attention to the effects of different voltage intensities on soil stabilization and strength enhancement.

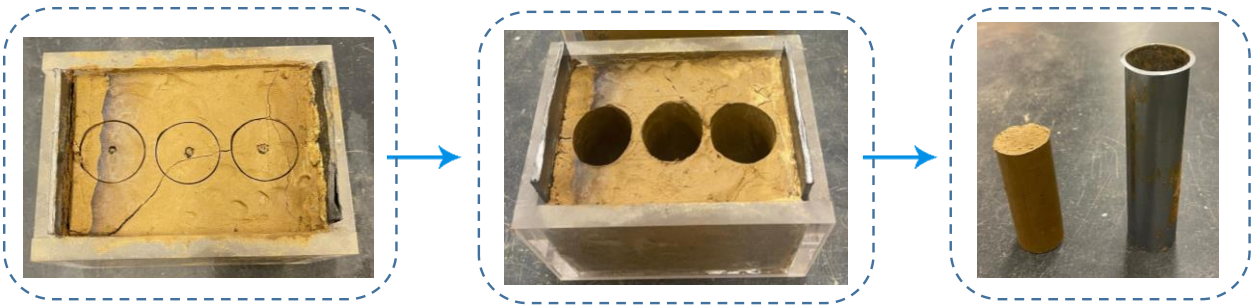

Figure 4.21: Sample procedure extraction images of the samples

The stress-strain curves shown in Figure 4.22 represent the results of unconfined compressive strength (UCS) tests conducted on soil samples subjected to different voltages during the electrokinetic treatment process. The figure comprises three plots—(a), (b), and (c)—each

corresponding to soil samples extracted from different positions within the electrokinetic cell: near the anode, in the middle, and near the cathode, respectively.

Electrokinetic soil stabilization leads to non-uniform strength improvements throughout the soil specimen, primarily due to variations in moisture content and the chemical reactions induced by the applied electric field. Near the anode, the stress-strain curves indicate that the soil treated with 10 V, 15 V, and 25 V electric fields displays significantly higher compressive strength compared to the control sample. The control sample, represented by blue circles, exhibits the lowest peak stress, around 60.30 kPa. As the applied voltage increases, the peak stress also increases, reaching 147.86 kPa, 157.97 kPa, and 175.43 kPa for applied voltages of 10V, 15V, and 25V, respectively. These increases represent improvements of 145.21%, 161.97%, and 190.93% over the control sample. This suggests that the soil near the anode benefits considerably from the electrokinetic treatment, with higher voltages yielding stronger soil. For the sample taken from the middle of the cell, the trend remains consistent with the observations from the anode region. The control sample continues to show the lowest strength, while the samples treated with 10 V, 15 V, and 25 V demonstrate progressively higher peak stresses.

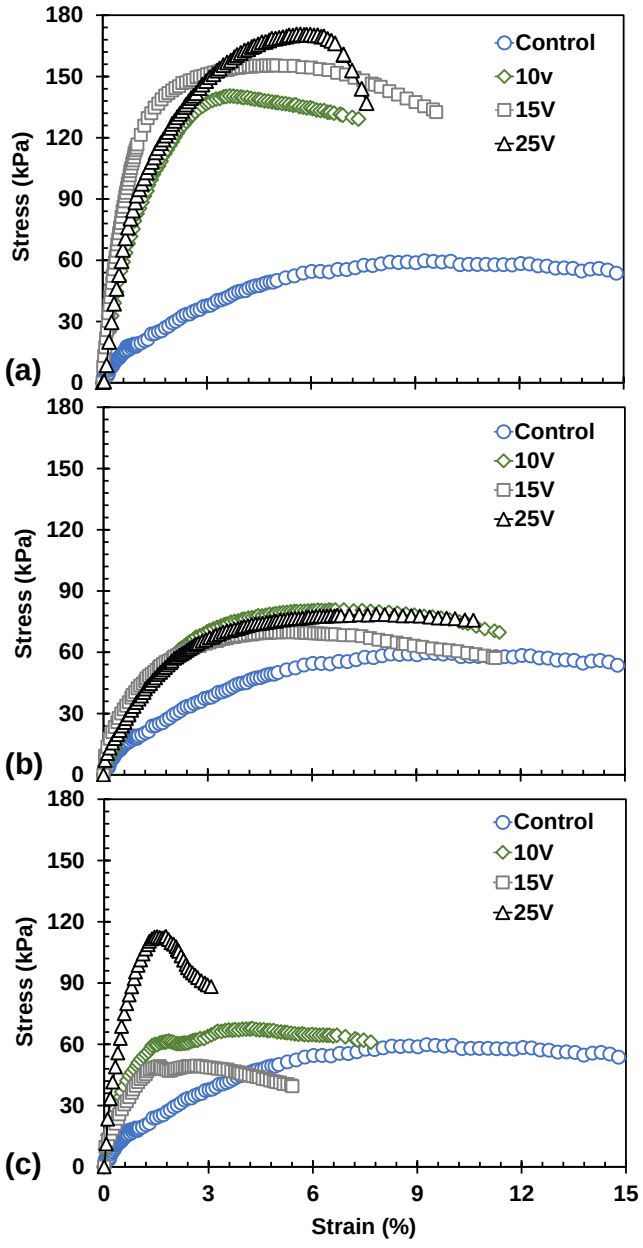

Figure 4.22: UCS test in the soil treated under different electric field intensities. **a)** Near the anode **b)** in the Middle **c)** near the cathode.

However, the strength improvement in this middle region is slightly less pronounced compared to the anode region, with peak stresses reaching approximately 102.42 kPa, 71.11 kPa, and 83.87 kPa for 10V, 15V, and 25V applications, respectively. Although these increments are less dramatic than those observed near the anode, they still represent substantial improvements of

69.85%, 17.93%, and 39.09% over the control sample, as shown in Figure 4.19b. These changes are likely due to this region's relatively higher water content than the area near the anode.

For soil samples near the cathode, The treated samples show enhanced strength, with peak stresses of 65.88 kPa, 47.51 kPa, and 114.19 kPa for applied voltages of 10V, 15V, and 25V, respectively. Notably, the soil near the cathode shows the least improvement in strength compared to the anode and middle regions, suggesting that the effectiveness of electrokinetic treatment diminishes slightly as the distance from the anode increases. This shift can be attributed to two primary factors: the high pH (>7.5) conditions near the cathode, which promote the development of face-to-face (F-F) clay particle associations, as documented by Gratchev and Sassa (2009), leading to increased particle contact; and the physical alterations induced by these chemical changes.

These modifications manifest in the soil's mechanical properties and visual appearance, transitioning from ductile to brittle behavior compared to specimens from the anode and middle sections. Figure 4.23 presents a visual comparison of soil samples taken from the electrokinetic cell's form near the anode, middle, and cathode regions, showcasing their appearance before the unconfined compressive strength (UCS) test, immediately after the test, and following the drying process. These visual observations indicate the complex mechanism involved in electrokinetically treated soil by changing their color and its physical properties from anode to cathode. The soil demonstrates increased stiffness near the anode, characterized by higher stress values and a clearly visible failure plane after the UCS testing. In contrast, the middle section displays characteristics of a more plastic nature, exhibiting higher strain capacity and a tendency to deform without a distinct failure plane. This behavior suggests a more uniform stress distribution throughout the sample during loading. The soil transitions to a more brittle state as we approach the cathode. In

this region, failure predominantly occurs near the specimen ends, deviating from the well-defined failure plane typically observed in more ductile samples, as shown in Figure 4.23. The extraction and preparation of samples from the cathode area posed significant challenges due to the soil's fragile/brittle nature. These spatial variations in mechanical behavior highlight the complex physicochemical reactions induced by the electrokinetic process, resulting in a heterogeneous soil matrix with significantly altered properties along the anode-cathode axis.

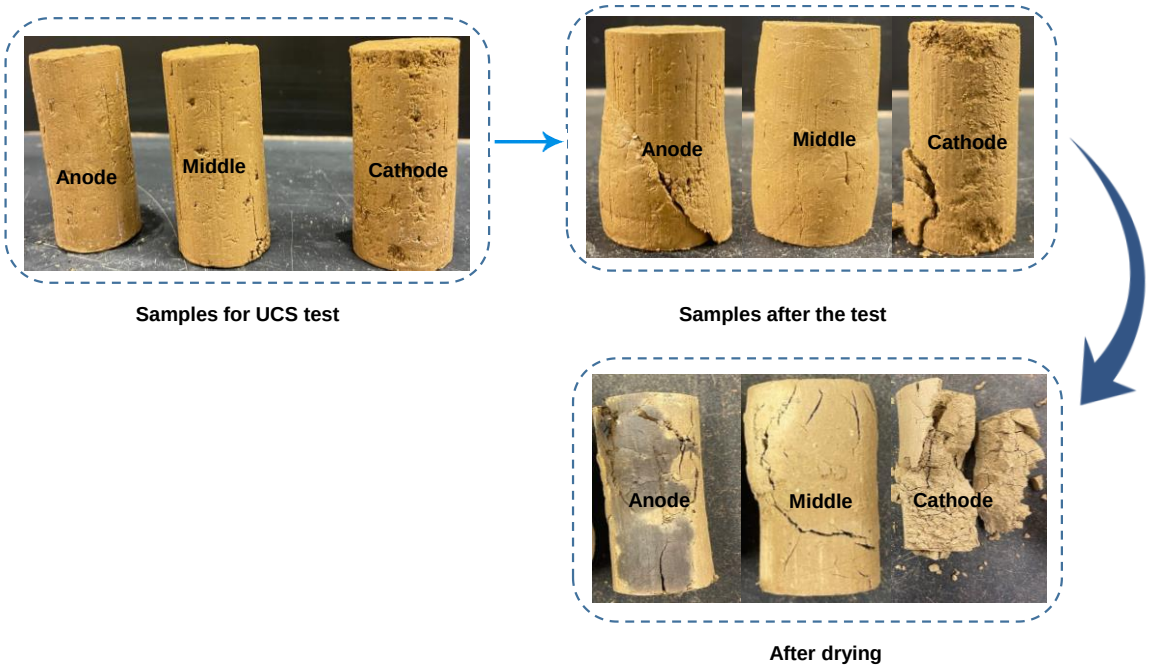

Figure 4.23: UCS samples shown at three stages: before testing, after testing, and following oven drying

4.3.3 Current Gradient and Collected Water

Electroosmosis is a key mechanism in soil conditioning under an electric field, where the movement of water plays a critical role in altering soil properties. Understanding the relationship between applied voltage and electroosmotic flow is essential for optimizing soil treatment methods and ensuring effective soil stabilization through electrokinetics. This section presents an analysis of the variations in current flow and cumulative water movement during the electroosmosis

process, focusing on the impact of different applied voltages. The results are based on a 7-day conditioning period with applied voltages of 10 V, 15 V, and 25 V, and the subsequent effects on current and water movement are illustrated and discussed.

Figures 4.24a and 4.24b provide detailed insights into how current varies over time and how cumulative water movement progresses under different voltage conditions. In Figure 24a, the current variation of the system is presented. Initially, the current rises rapidly in all three voltage cases. For the 25 V case, the peak current is the highest, followed by 15 V and 10 V. However, after reaching the peak, the current begins to decline over time. This decrease in current is more rapid in the higher voltage cases (25 V and 15 V), while the 10 V case shows a relatively steady decline. By the end of the experiment, the current stabilizes at similar lower values across all voltages, with 25 V reaching a slightly lower plateau compared to the other two voltages. The initial high current is likely due to the dissolution of salt precipitates in the pore fluid, which is associated with the negatively charged clay particles (Reddy & Saichek, 2004). As the conditioning period progresses, the reduction in current can be attributed to several factors, including concentration polarization, activation polarization, and a decrease in ion concentration in the pore solution as a result of electromigration. Additionally, the ingress of acidic and alkaline environments into the soil specimen further contributes to the current reduction (Hussain et al., 2023; Reddy & Cameselle, 2009; Reddy & Saichek, 2004; Virkutyte et al., 2002; Zhou et al., 2021). The observed current decline is more pronounced at higher voltages, whereas at lower voltages, the current remains relatively stable throughout the process.

In Figure 4.24b, the cumulative water movement is depicted. The data reveal that water movement increases progressively with time, and the total cumulative water displacement is significantly influenced by the applied voltage. The highest cumulative water movement is

observed in the 25 V case, followed by the 15 V and 10 V cases. The 25 V curve shows a rapid increase in cumulative water movement early on, with a steady rise throughout the experiment. The 15 V case demonstrates a similar trend but at a slightly lower rate. The 10 V case shows the slowest cumulative water movement, suggesting that lower voltages generate less effective electroosmotic flow over time. This finding is consistent with electrokinetic principles and other research findings (Fu et al., 2019).

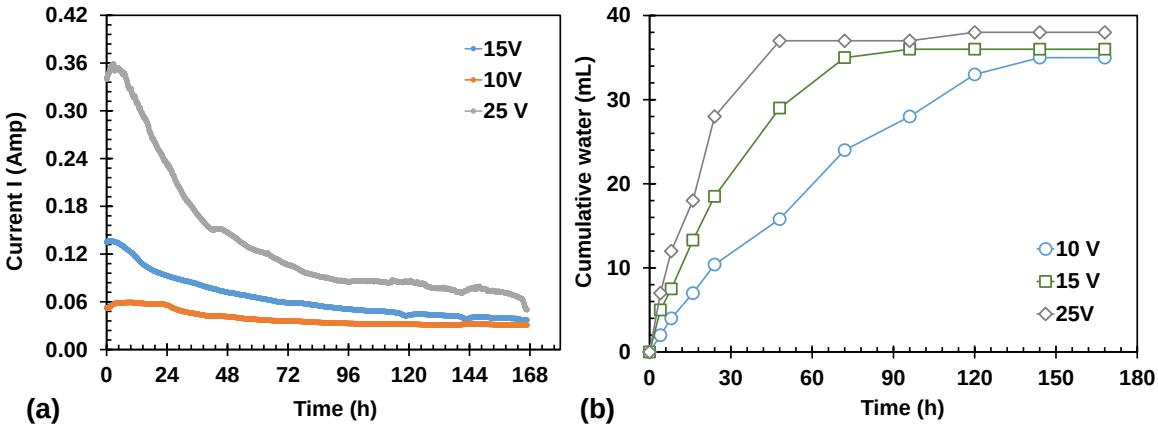

Figure 4.24: Current changes and water collected from the samples during the electrometric soil conditioning **a)** Current changes **b)** Cumulative water collected

4.3.4 pH Changes and Electric Conductivity

During electroosmosis, changes in soil pH and electrical conductivity (EC) are intrinsically linked to the electrochemical reactions occurring at the electrodes and the transport of ions within the soil. These changes significantly impact the ion exchange capacity, particle flocculation, and overall soil stability. Figure 4.25a highlights the variation in soil pH, with the dashed line representing the pristine soil's pH for comparison. At the anode, the oxygen evolution reaction (OER) generates oxygen gas and hydrogen ions (H^+), as described in Equation 4-4, lowering the pH and creating acidic conditions. Conversely, at the cathode, the hydrogen evolution reaction (HER) reduces water molecules to produce hydrogen gas and hydroxide ions (OH^-), as outlined in Equation 4-5, resulting in a rise in pH and the formation of an alkaline environment. This pH gradient across the soil profile—lower pH near the anode and higher pH near the cathode—can

significantly alter the soil's ion exchange capacity, which in turn affects the movement and concentration of ions within the soil.

These variations in pH directly influence the soil's electrical conductivity (EC), as shown in Figure 4.25b. The ion exchange capacity, which is highly dependent on pH, affects how freely ions can move within the soil matrix. At lower pH values near the anode, the increased presence of H^+ ions leads to a higher concentration of charge carriers in the pore fluid, elevating the soil's EC in this region. This elevated conductivity is further driven by the dissolution of salts and minerals under the acidic conditions created by the OER. As the pH rises toward the cathode, the interaction between migrating cations (such as H^+) and hydroxide ions (OH^-) reduces the availability of free ions in the pore fluid, resulting in a decrease in EC in the cathode region (Acar et al., 1993).

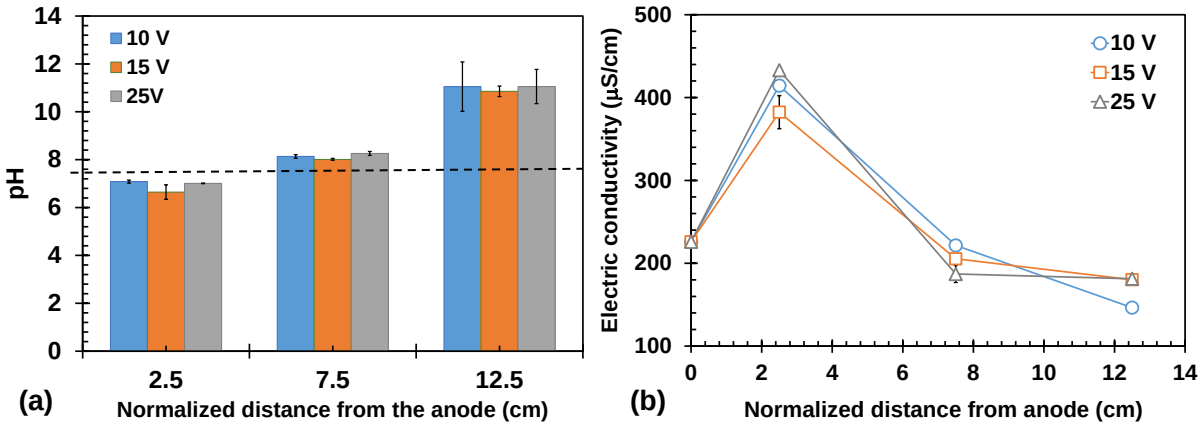

Figure 4.25: (**a)** pH changes (**b)** Electric conductivity

In essence, the changes in soil pH affect the ion exchange capacity, which subsequently alters the soil's bulk conductivity (Acar et al., 1993; Reddy & Cameselle, 2009). As the ion concentration shifts throughout the soil—enhanced near the anode due to increased acidity and reduced near the cathode due to alkaline conditions—the EC mirrors these trends. The gradual decrease in EC from anode to cathode is a direct result of the dynamic interaction between the

generated ions and the electrochemical reactions taking place in different regions of the soil. This interplay between pH, ion exchange, and conductivity is crucial for understanding the overall behavior of soils undergoing electrokinetic treatment.

4.3.5 XRD Analysis and Mineralogical Composition

X-ray diffraction (XRD) is a powerful technique for identifying the soil mineralogy. It can analyze the mineral composition, basal spacing of different clay minerals, and the change that occurs in the basal spacing of smectite caused by the different interlayer cations (Wu et al., 2016). The XRD test was performed to compare the mineralogical changes and composition of treated and treated soil.

The XRD patterns displayed in Figure 4.26a, b, and c show the crystalline structures of soil samples subjected to electrokinetic treatment with different voltages. The x-axis shows the shows degree (2θ) in degrees from 10 to 70, and the y-axis shows the intensity. The samples were extracted from three distinct regions: near the anode, in the middle, and near the cathode, with untreated (pure) soil included for comparison (2.5cm, 7.5cm, and 12.5 cm). The XRD analysis reveals several important insights into how the crystalline structure of the soil changes across these regions due to electrokinetic processes. The pure soil sample presents a distinct XRD pattern with clearly defined peaks at various angles, indicating the presence of well-crystallized minerals typical of expansive soils. These peaks serve as a reference for comparing the impact of electrokinetic treatment on the crystalline structure in different regions of the soil. In the anode region, the XRD pattern reveals some attenuation of peak intensity compared to the untreated soil. The reduction in crystallinity near the anode may be attributed to the acidic conditions generated by the oxygen evolution reaction (OER) during electrokinetic treatment. The presence of H^+ ions

can dissolve certain minerals or alter their crystalline structure, leading to a reduction in peak intensity.

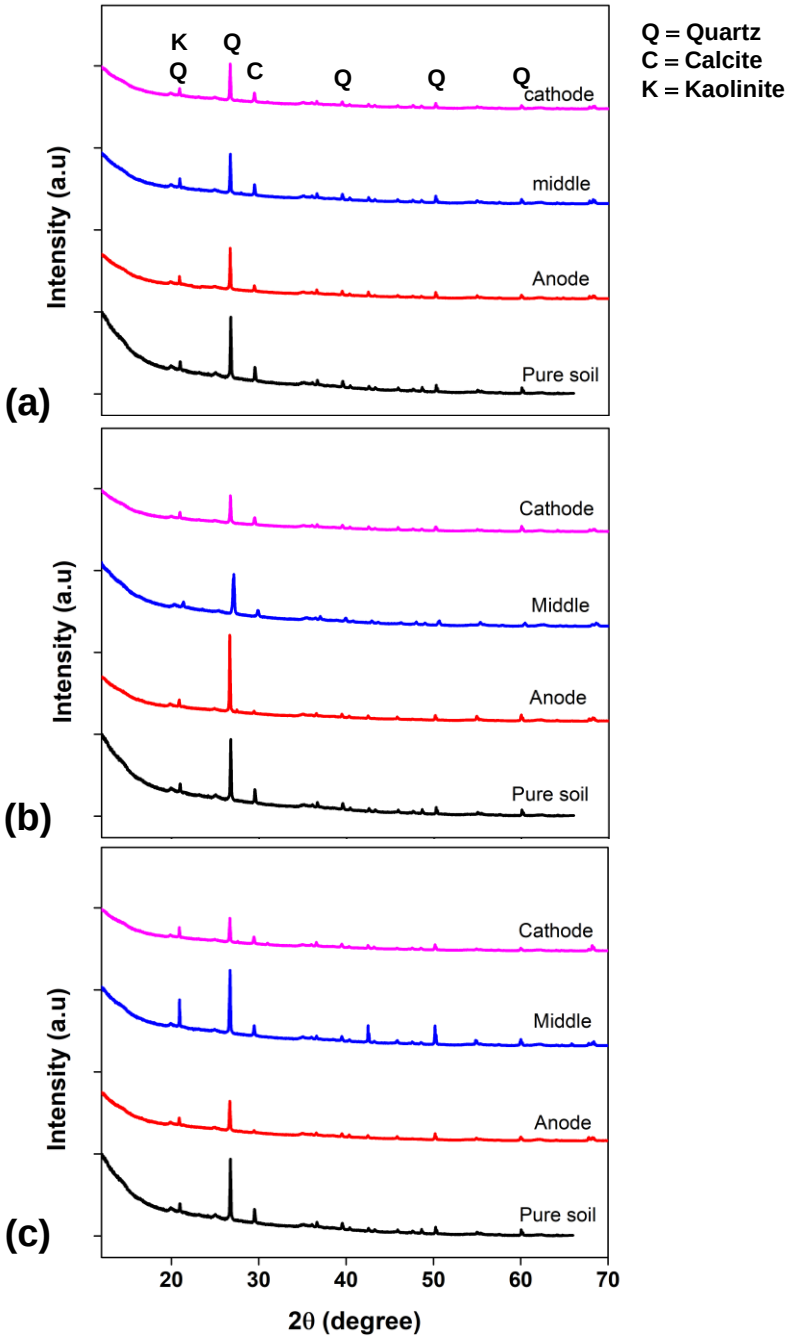

Figure 4.26. XRD analysis of samples **a)** conditioned 10 V **b)** conditioned with 15 V **c)** conditioned with 25V

The middle region shows XRD patterns with less dramatic changes compared to the anode and cathode regions. Although some alteration in peak intensity is observed, the crystalline structure remains largely similar to the untreated soil. This indicates that the middle zone is less affected by the electrochemical reactions occurring at the anode and cathode, resulting in a relatively stable mineral composition. Near the cathode, some changes are observed in the XRD peak intensity, which could be due to the reduction in crystallinity. This effect is likely due to the alkaline environment created by the hydrogen evolution reaction (HER) near the cathode, where hydroxide ions (OH^-) may induce mineral dissolution or form new phases, such as amorphous precipitates. The XRD pattern in the cathode region suggests the formation of face-to-face (F-F) clay particle associations, which may increase the amorphous content in the soil, reducing the intensity of the crystalline peaks.

4.3.6 SEM Analysis

To further explore the effect of electrokinetic treatment of the expansive soil microstructure and morphology, scanning electron microscopy (SEM) analysis was performed on the soil samples. Figure 4.27 presents SEM images illustrating the microstructural characteristics of soil samples subjected to electrokinetic conditioning at different positions within the electrokinetic cell under 15v, focusing on the distribution of voids and the overall morphology of the soil matrix.

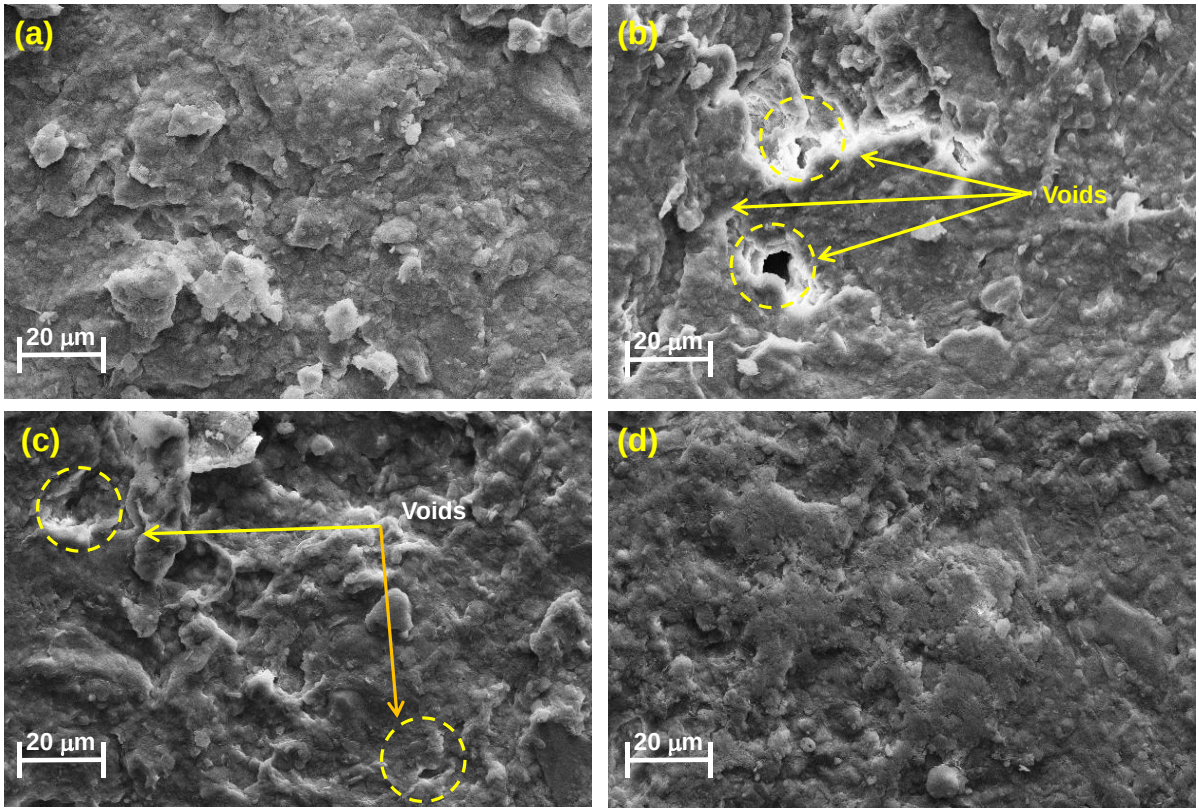

Figure 4.27. SEM images of treated and untreated soil under an electric field (100V/m) for 7 days, **a)** Pure soil, **b)** Near the anode, **c)** Middle, **d)** Near the cathode

Image 4.27a represents the pure soil sample, showing a relatively compact and dense structure with few visible voids. The matrix appears well-consolidated, indicating minimal porosity and reflecting the natural state of the soil without any electrokinetic treatment or nano-conditioning. Image 4.27b shows the soil sample taken from the area near the anode. Distinct voids are visible, as indicated by the arrows, showing that the soil in this region has undergone electrokinetic changes, likely resulting in particle displacement and swelling. The presence of voids suggests that the soil in this area is less compacted, likely due to the acidic environment created near the anode during electrochemical reactions. Image 4.27c corresponds to the soil sample taken from the middle region of the electrokinetic cell. In this case, voids are still present but are smaller and more dispersed compared to those near the anode. This suggests that the soil in the middle zone has undergone intermediate changes, reflecting a balance between the acidic

conditions near the anode and the alkaline conditions near the cathode. Image 4.27d illustrates the soil sample collected near the cathode. This region displays a more homogeneous and consolidated structure with minimal voids, indicating better compaction and reduced porosity. The alkaline environment near the cathode likely contributes to particle flocculation, leading to a denser soil matrix that enhances strength and reduces swelling potential.

4.4 Soil Conditioning Using Electrified Nanoparticles

Initial physical mixing experiments and preliminary results demonstrate that MgO nanoparticles exhibit superior performance compared to SiO_2 in improving expansive soil properties. This enhanced effectiveness is evident in MgO's ability to reduce soil expansiveness, increase strength, and improve water retention characteristics, leading to more consistent and reliable soil improvement outcomes. Beyond these mechanical advantages, the electrokinetic transport properties of nanoparticles, assessed through zeta potential behavior, further support MgO's selection as the preferred conditioning agent. Unlike SiO_2, which maintains a negative charge across the pH spectrum, MgO exhibits a positive charge at both low and high pH levels, making it particularly suitable for electrokinetic transport (Fig. 3.5). Based on these combined advantages in both mechanical properties and electrokinetic behavior, MgO was selected as the optimal nanoparticle for electrokinetic soil conditioning in this study.

For investigating the effect of MgO nanoparticle conditioning, two parallel sets of experiments were conducted: control samples treated with water injection only (using the same volume of water as required for the MgO solution), and treatment samples using 1% MgO nanoparticle solution at varying water-to-MgO ratios (1:10, 1:15, and 1:20). The solutions were injected into the soil through three strategically placed injection holes, as described in Figure 3.9. A 15 V voltage was applied across the electrokinetic cell for a 7-day conditioning period to

distribute the MgO NP. Following the conditioning phase, a comprehensive analysis was conducted on key soil parameters, including pH levels, moisture content, unconfined compressive strength (UCS), and swelling behavior. These measurements provided detailed insights into the effectiveness of electroosmosis and electromigration in enhancing nano-conditioning for soil stabilization.

4.4.1 Moisture Content Measurement

Figure 4.28 illustrates the moisture content of soil treated with 1% MgO at different MgO-to-water ratios (1:10, 1:15, and 1:20) and subjected to an electric potential of 15 V for 7 days. Unlike the electrokinetic treatment alone, the moisture distribution in the soil when water or nanoparticles are injected into the system does not follow a uniform pattern.

Figure 4.28a illustrates the moisture content distribution in soil treated with 1% MgO at a 1:10 ratio. The moisture content varies across different soil regions, with values of 42.04% near the anode, 45.26% in the middle section, and 40.27% near the cathode. This variation is primarily attributed to the electrokinetic movement of nanoparticles and water from the anode towards the cathode, driven by the applied electric field. Over time, as the pH of the soil changes, this movement gradually slows, reducing the transport of water and nanoparticles. Furthermore, forming almost an impermeable layer near the cathode during the electrokinetic process inhibits further water dissipation from the system. Figure 4.28b illustrates the moisture content distribution in soil treated with 1% MgO at a 1:15 ratio. The moisture content is measured at 43.87% near the anode, 46.80% in the middle, and 41.84% near the cathode. This distribution contrasts with that of the control sample, where the moisture content decreases linearly towards the cathode. The observed difference can be attributed to the faster movement of the MgO solution compared to

water alone, as noted during the experiment. In the control sample, water movement occurs solely due to electroosmosis, whereas in the MgO-treated sample, the nanoparticles are driven by both electroosmosis and electromigration, owing to their positive surface charge. After 4 days, as electroosmosis slows down, the water content near the anode increases, while it decreases towards the cathode due to the reduced movement and the pH gradient.

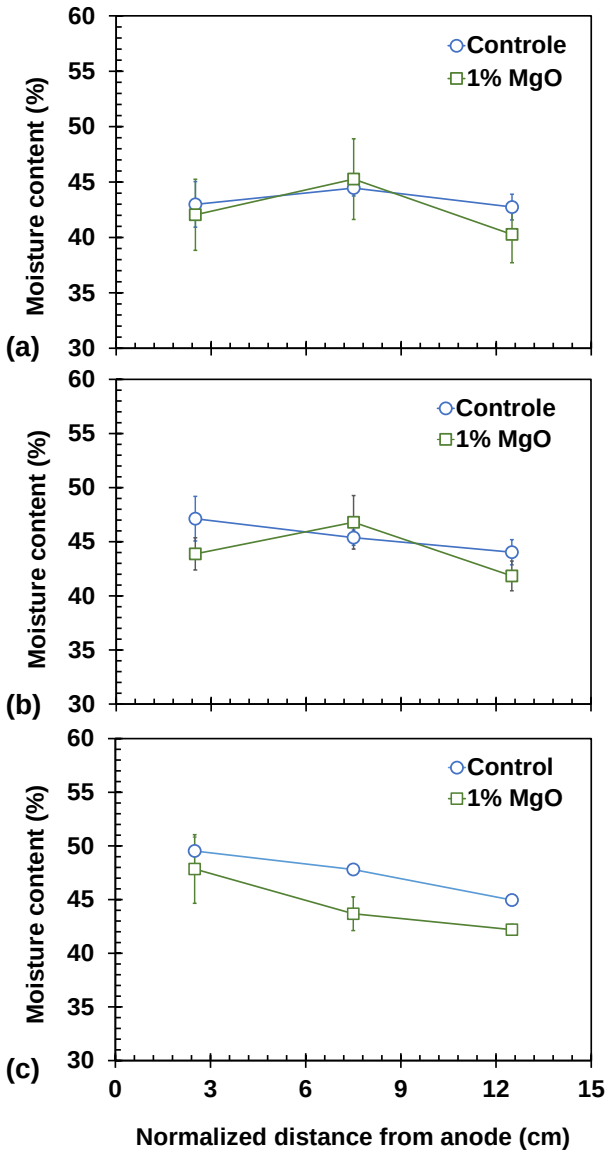

Figure 4.28: Moisture content of soil treated with 1% MgO at different MgO-to-water ratios: **(a)** 1:10, **(b)** 1:15, and **(c)** 1:20

Figure 4.28c shows the moisture content of soil treated with 1% MgO at a 1:20 ratio. The moisture content decreases towards the cathode in the control and 1% MgO samples: 47.85%, 43.68%, and 42.19% near the anode, middle, and cathode, respectively. This pattern suggests that, at higher MgO-to-water ratios, it becomes increasingly difficult to move water from the anode to the cathode. Consequently, moisture content remains higher near the anode. It is worth noting that the injection process continued for approximately 5 days during the experiment.

4.4.2 Atterberg Limit of Treatd Soil

Figure 4.29 illustrates the Atterberg limits of post-treated soil with 1% MgO at different nano MgO-to-water ratios (1:10, 1:15, and 1:20) over a 7-day curing period. A consistent variation in Liquid Limit (LL), Plastic Limit (PL), and Plasticity Index (PI) is visible across Figures 4.29a, b, and c. In the control sample (Figure 4.29a), moving toward the cathode, the LL increases from 64.22 near the anode to 65.05 in the middle and further to 67.53 near the cathode. This aligns with previously discussed electrokinetic results. Similarly, the PL increases from 28.96 near the anode to 43.59 near the cathode, which leads to a reduction in PI from 35.26 near the anode to 23.93 at the cathode.

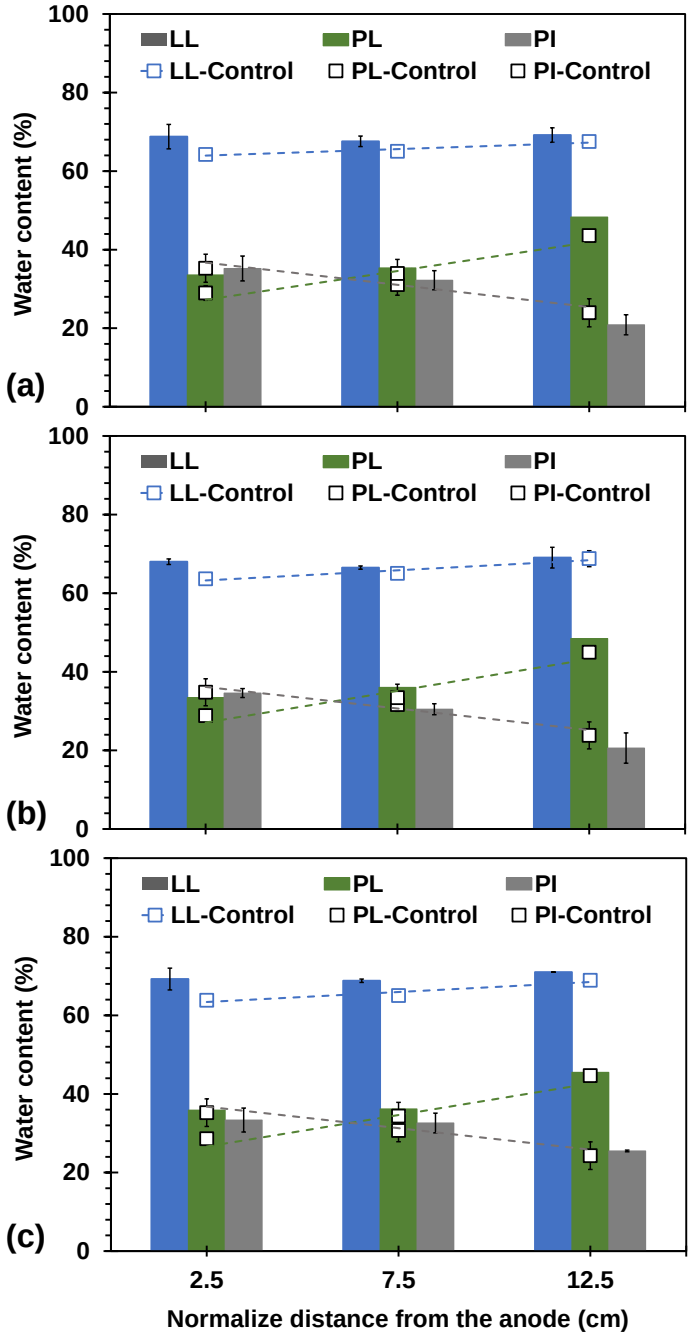

Figure 4.29: The soil conditioned with the 1% MgO but with a different MgO to water ratio. **a)** MgO to water (1:10) **b)** MgO to water (1:15) **c)** MgO to water (1:20).

After the injection of 1% MgO with a 1:10 ratio, the LL of post-treated soil also increases toward the cathode, changing from 68.78 near the anode to 67.59 in the middle and 69.18 near the cathode. Correspondingly, the PL changes from 33.57 near the anode to 35.37 in the middle and

48.31 near the cathode. These changes result in the PI decreasing from 35.21 near the anode to 32.22 in the middle and 20.87 near the cathode. Compared to the control, all positions where samples were taken exhibited lower LL, PL, and PI values. For the 1:15 nano MgO-to-water ratio (Figure 4.29b), the PI value decreases from 34.60 near the anode to 30.48 in the middle and 20.59 near the cathode. The PI values in all sampling points were lower than those of the control sample. In Figure 4.29c, for the 1:20 nano MgO-to-water ratio, the PI follows a similar trend, decreasing from 33.36 near the anode to 32.61 in the middle and 25.50 near the cathode. Notably, for the highest water content (1:20 ratio), the PI values are lower than those observed for the 1:10 and 1:15 ratios.

Regardless of the nano MgO-to-water ratio, in all three cases, the soil transitioned from very expansive to highly expansive based on the PI values, as noted by Seed et al. (1962). These changes in PI can be attributed to the introduction of MgO nanoparticles, which not only alter the soil's chemistry but also reduce its expansiveness by modifying the PI value. This observation is consistent with the XRF data (Table 4.2), which show an increase in Mg and MgO concentrations in the soil compared to the control samples. Therefore, it can be concluded that the distribution of MgO into the soil occurred due to both electroosmosis and electromigration, as MgO has a positive surface charge at a pH of 10.78.

Table 4.2: XRF analysis of treated soil with 1% MgO from anode to cathode with 1:15 ratio

Sample	Mg	Al	K	Ca	Fe	Si	Ti	MgO	Al_2O_3	SiO_2	CaO	Fe_2O_3
	Major elements (%)							Major compound (%)				
Pure soil	0.46	19.91	2.01	10.86	18.01	45.54	2.13	0.40	18.25	41.62	5.25	7.78
Control	0.94	20.90	2.07	7.97	18.10	46.85	2.07	0.78	18.92	42.01	3.78	7.72
Anode	1.14	20.86	2.13	6.89	18.29	47.47	2.10	0.93	18.20	40.94	3.15	7.52
Control	0.79	19.97	1.97	11.72	17.30	45.21	2.03	0.68	18.71	42.19	5.79	7.63
Middle	1.26	20.21	2.00	11.24	17.43	44.83	2.01	1.08	18.72	41.39	5.51	7.62
Control	0.44	16.54	2.16	17.65	20.86	38.71	2.39	0.32	12.78	30.85	7.59	7.97
Cathode	0.90	19.67	1.96	14.77	16.52	43.25	1.94	0.80	18.99	41.86	7.59	6.81

4.4.3 Swell Potential of Treated Soil

Figure 4.30 illustrates the vertical swell strain in soil treated with 1% MgO at different MgO-to-water ratios (1:10, 1:15, 1:20) over a 7-day curing period under an applied electric field of 15V. A decreasing trend in soil swell potential is observed towards the cathode, indicating a gradient effect in response to the movement of ions and the distribution of MgO particles under the influence of the electric field.

Near the anode, where the MgO solution is injected (Figure 4.30 a, d, and g), the treatment effectiveness shows promising results across different MgO-to-water ratios. In Figure 4.30 a, the soil treated with 1% MgO demonstrates a reduced vertical swell strain (0.33%) compared to the control sample (0.46%), indicating a positive treatment effect. In Figure 4.30 d, which represents the 1:15 ratio condition, although the MgO-treated soil shows a marginally higher swell strain (0.43%) than the control (0.35%), this difference is relatively minor and may be attributed to the natural variability in soil response rather than a significant adverse effect of the treatment. The most notable improvement is observed in Figiure 4.30 g, where the MgO treatment substantially reduced the vertical swell strain to 0.27% compared to the control's 0.57%, representing approximately a 53% reduction in swelling potential. These results collectively suggest that MgO

treatment is generally effective in reducing soil swell potential, with the 1:15 ratio showing a slight deviation from the trend, though not substantial enough to negate the overall positive impact of the treatment across different conditions.

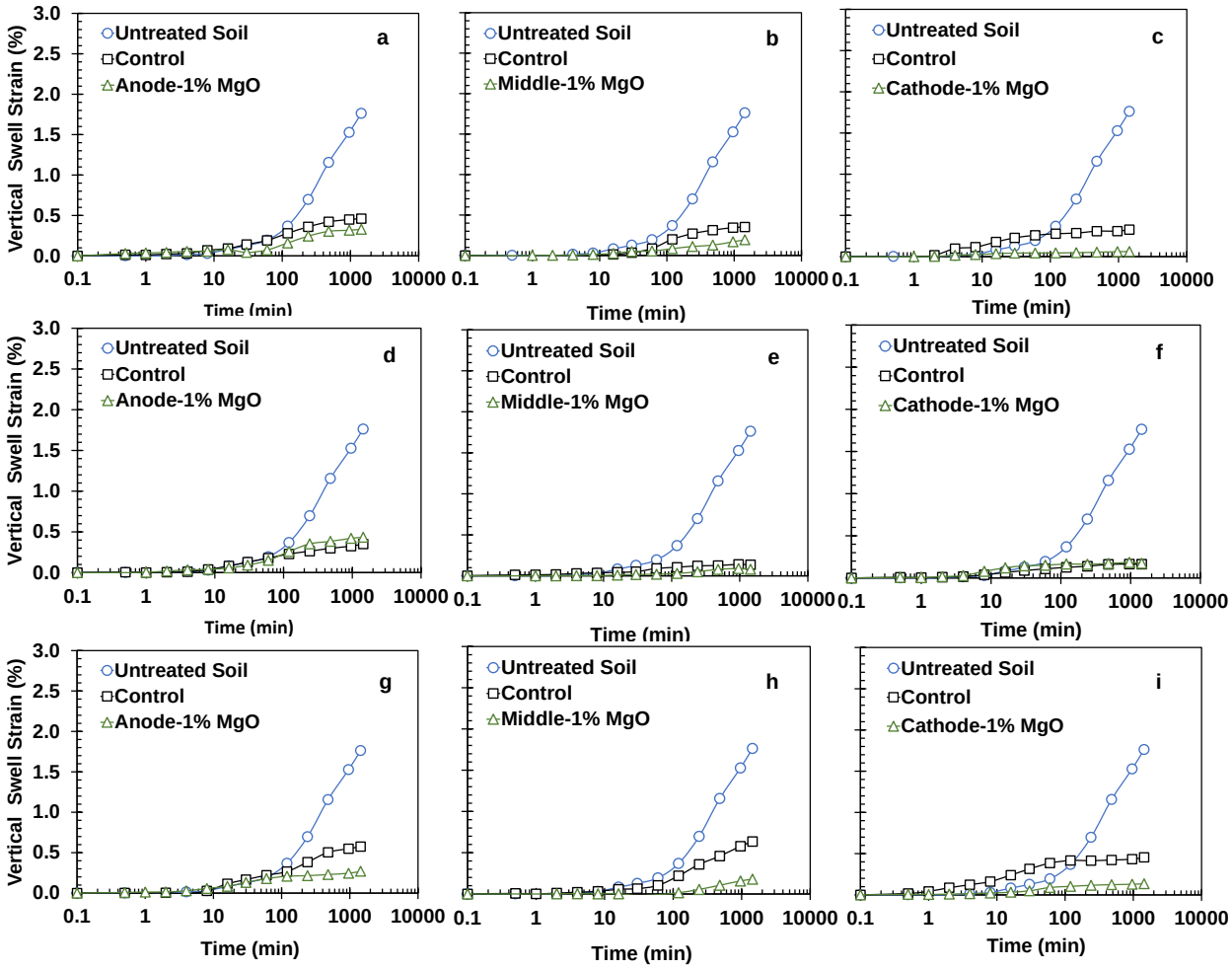

Figure 4.30: Swell strain of electrokinetic-MgO conditioned soil (1% MgO, 15V for 7 days) at different MgO-to-water ratios **a)** Anode (1:10), **b)** Middle) (1:10), **c)** Cathode (1:10), **d)** Anode (1:15), **e)** Middle) (1:15), **f)** Cathode (1:15), **g)** Anode (1:20), **h)** Middle (1:20), and **i)** Cathode (1:20).

In the middle section (Figiure 4.30 b, e, and h), all tested MgO-to-water ratios consistently reduce swell strain compared to the control and untreated samples, demonstrating the effectiveness of the 1% MgO treatment at this distance. In Figiure 4.30 b, the treated soil shows a reduction of

43% in swell strain (treated soil = 0.20%, control = 0.35%), followed by Figure 4.30 e with a reduction of 38% (treated soil = 0.08%, control = 0.13%). The most significant improvement is observed in Figiure 4.30 h, where the treatment achieved a 72% reduction in swell strain (treated soil = 0.18%, control = 0.64%). These findings highlight the stabilizing effect of MgO on soil in this region, regardless of the specific MgO-to-water ratio used.

Near the cathode (Figure 4.30 c, f, and i), the electrokinetic MgO-treated soil continues to exhibit lower swell strain compared to both the control and untreated samples, demonstrating that the treatment is effective across the entire soil profile. In Figure 4.30 c, the treated soil shows a significant reduction in swell strain, achieving an 82% decrease (treated soil = 0.06%, control = 0.33%). In Figure 4.30 f, the results show a slight increase in swell strain with the treated soil (0.17%) compared to the control (0.16%), though this difference is minimal. The treatment effectiveness is again demonstrated in Figure 4.30 i, where the swell strain is reduced by 71% (treated soil = 0.13%, control = 0.45%). These results suggest that MgO particles are transported through the soil matrix toward the cathode due to the combined effects of electroosmosis and electromigration. This distribution of MgO throughout the soil, even in areas far from the injection point at the anode, contributes to the overall reduction in swell strain and improved soil stability.

Figure 4.31 presents photographs of soil samples collected from three distinct regions within the electrokinetic cell: near the anode (A), middle (M), and cathode (C). These samples were treated with 1% MgO at different MgO-to-water ratios (1:10, 1:15, and 1:20) over a 7-day period under a 15 V (100 V/m) electric field. After the electrokinetic treatment, the samples were oven-dried for 24 hours to assess their swell potential and shrinkage characteristics. As shown in Figure 4.31, the cracking patterns in the samples result from moisture loss during the oven drying process. When moisture evaporates, it induces shrinkage and internal tension within the soil,

leading to the formation of cracks. The control samples, which were not treated with MgO, exhibit more extensive and wider cracking compared to the MgO-treated samples. This suggests that the MgO treatment helps to reduce the soil's tendency to crack upon drying.

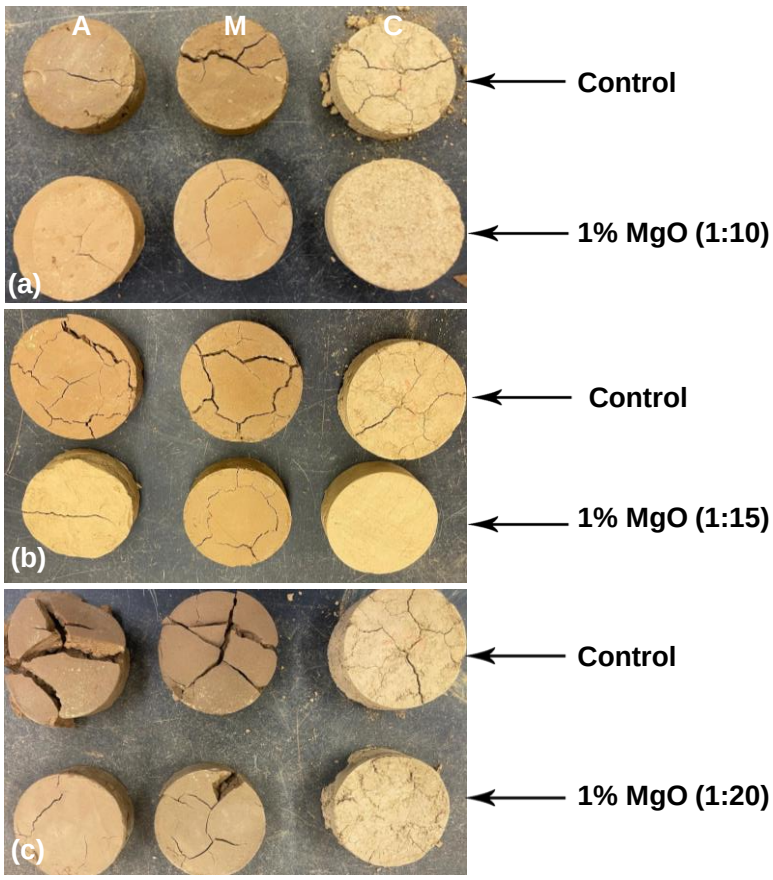

Figure 4.31: The 24-hour oven-dried sample of swell test (A=anode, M=middle, C=cathode) **a)** MgO to water (1:10) **b)** MgO to water (1:15) **c)** MgO to water (1:20).

In Figure 4.31a, which represents the samples treated with a 1:10 MgO-to-water ratio, the anode region (A) shows the most significant cracking, likely due to the higher rate of ion migration and moisture loss near the anode during electroosmosis. The cathode (C) region displays fewer cracks, indicating better moisture retention and reduced shrinkage. In Figure 4.31b, showing the 1:15 MgO-to-water ratio treatment, the cracking is less severe compared to the 1:10 treatment. The

middle (M) and cathode (C) regions demonstrate more uniform distribution of cracks, suggesting that this ratio allowed for better moisture management and more effective soil stabilization throughout the sample. In Figure 4.31c, where a 1:20 MgO-to-water ratio was used, the cracking patterns are even less pronounced, especially in the anode region (A). The higher water content in this treatment likely helped mitigate shrinkage and cracking. The cracks are smaller and more uniformly distributed across the sample, suggesting that this higher MgO-to-water ratio helped reduce the drying-induced tension in the soil. Overall, the MgO treatment across different ratios appears to significantly alter the soil's moisture retention and structural properties, reducing the extent of shrinkage-induced cracking during the drying process.

4.4.4 Unconfined Compressive Strength of Treated Soil

Figure 4.32 illustrates the unconfined compressive strength (UCS) of soil treated with 1% MgO at various MgO-to-water ratios (1:10, 1:15, 1:20) over a 7-day curing period under an applied electric field of 15V (equivalent to 100V/m). The data consistently demonstrate an increase in UCS towards the cathode, with each region showing different degrees of strength improvement depending on the MgO-to-water ratio.

Near the anode, as depicted in Figures 4.32a, d, and g, soil treated with 1% MgO exhibited higher UCS compared to both the untreated and control samples across all MgO-to-water ratios. The untreated soil presented a baseline stress value of 60.30 kPa. At a 1:10 ratio, the treated soil displayed the highest UCS of 90.21 kPa, representing a 49.60% increase over the untreated soil. The effectiveness of the MgO treatment reduced as the ratio increased, with the 1:15 ratio resulting in a UCS of 68.62 kPa, still higher than the control (28.88 kPa), and the 1:20 ratio yielding a stress of 32.41 kPa, only slightly surpassing the control sample at 25.54 kPa. These results indicate that

the MgO treatment, particularly at a lower MgO-to-water ratio (1:10), significantly enhanced the soil's strength near the anode. The observed trend of increased strength is likely due to stable moisture content near the anode during electrokinetic treatment and aggregation of MgO particles, which contributes to greater stress resistance.

In the middle section (Figures 4.32b, e, and h), the strength performance varied with different MgO-to-water ratios. The 1:15 ratio was most effective, increasing the UCS to 69.34 kPa, which represents a 14.99% increase compared to untreated soil (60.30 kPa) and is significantly higher than the control (22.66 kPa). Similarly, the 1:10 ratio increased the UCS to 66.56 kPa, which is higher than both untreated soil and control (46.23 kPa). The 1:20 ratio yielded the lowest UCS values, with the treated soil measuring 36.99 kPa and the control sample at 26.45 kPa. These results suggest that in the middle region, the 1:15 ratio is optimal for improving soil strength. The variations in UCS between different ratios can be attributed to differences in the moisture content distribution and migration of MgO during the electrokinetic process. Notably, all MgO-treated soils exhibited higher UCS values than the control samples, supported by X-ray fluorescence (XRF) data indicating an increase in MgO and Mg^{2+} concentrations throughout the treated samples.

Near the cathode (Figures 4.32c, f, and i), the UCS results revealed the most substantial improvements, with all MgO-treated soils outperforming the untreated and control samples. At a 1:10 ratio, the treated soil achieved the highest UCS of 193.80 kPa, representing a remarkable 221.39% increase over the untreated soil and significantly higher than its control at 139.77 kPa. The 1:15 ratio also showed substantial improvement with a UCS of 170.47 kPa, compared to its control at 104.51 kPa. Even the 1:20 ratio maintained high strength, with a UCS of 147.18 kPa versus the control at 78.79 kPa. This consistent and significant strengthening effect near the

cathode is likely due to the combined effects of electromigration of MgO and the presence of Ca^{2+} ions. XRF results confirmed higher concentrations of Ca^{2+} near the cathode than in other regions. The formation of an impermeable cementitious material, possibly magnesium silicate hydrate (M-S-H) and calcium silicate hydrate (C-S-H), was also observed near the cathode, contributing to the increased strength. This material likely reduced electroomotic flow and moisture content near the cathode, further enhancing soil stability and strength.

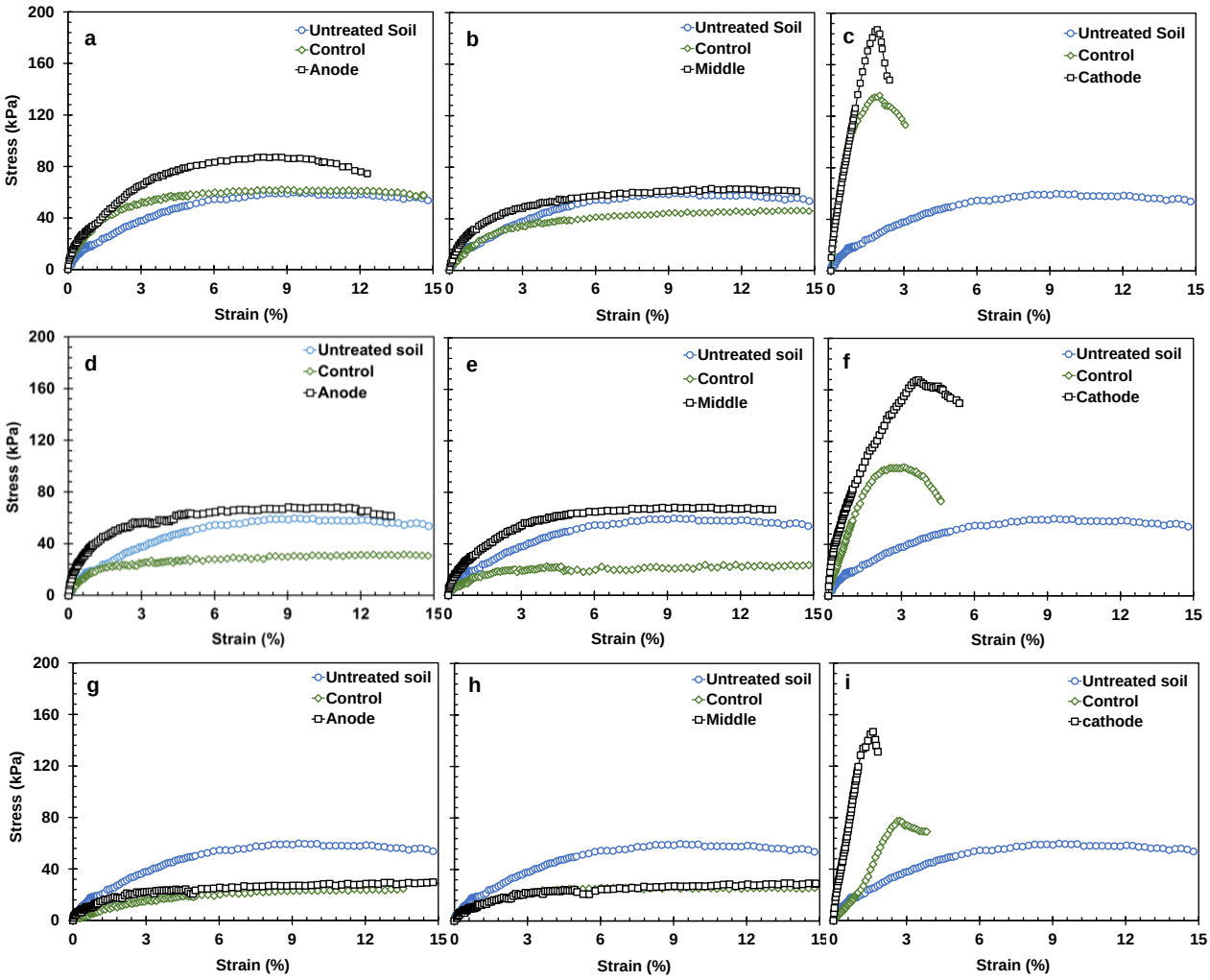

Figure 4.32: Unconfined compressive strength of or treated soil with 1% MgO and 100 V/m electric field for 7 days: **a)** Anode (1:10), **b)** Middle) (1:10), **c)** Cathode (1:10), **d)** Anode (1:15), **e)** Middle) (1:15), **f)** Cathode (1:15), **g)** Anode (1:20), **h)** Middle (1:20), and **i)** Cathode (1:20)

4.4.5 pH of Treated Soil

Figure 4.33 illustrates the pH variations in soil samples treated with 1% MgO at different MgO-to-water ratios (1:10, 1:15, and 1:20) compared to control samples, measured at normalized distances of 2.5, 7.5, and 12.5 cm from the anode. The pH is lower near the anode, indicating an acidic condition due to oxygen evolution reaction (OER) and production of H^+ ions as shown in equation 4-4. The pH near the cathode is alkaline due to hydrogen evolution reaction (HER) and generation of OH^- as shown in equation 4-5. The generation of OH^- ions and relatively slower migration toward the anode leads localized increase in the pH near the cathode and creates an alkaline environment.

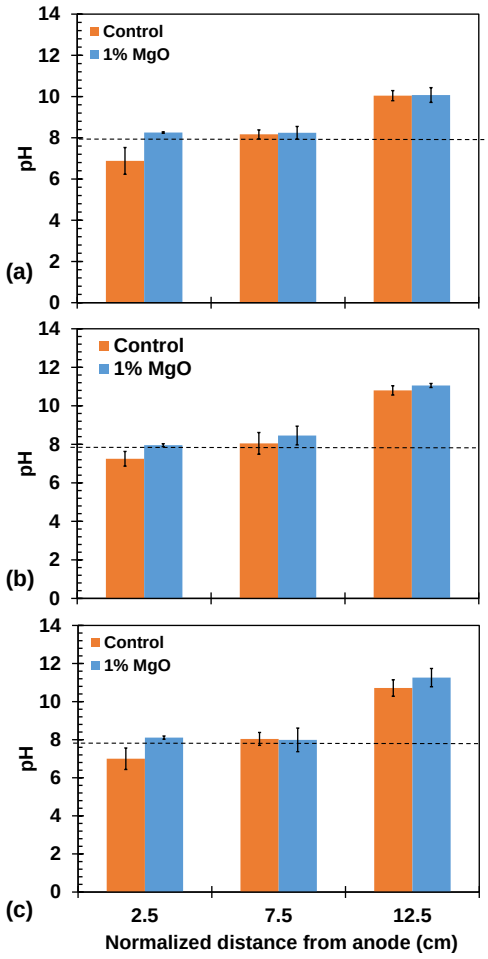

Figure 4.33: The soil pH conditioned with the 1% MgO but with a different MgO to water ratio. **a)** MgO to water (1:10) **b)** MgO to water (1:15) **c)** MgO to water (1:20).

In all cases, the MgO-treated soil exhibits a higher pH than the control, with the most pronounced difference observed near the anode (2.5 cm). For the 1:10 ratio (Figure 4.33a), the pH increase is most significant near the anode, with values rising from approximately 6.8 in the control to 8.3 in the treated soil. The 1:15 ratio (Figure 4.33b) shows a similar trend but with a slightly smaller pH increase near the anode. The 1:20 ratio (Figure 4.33c) demonstrates the least pronounced pH difference between treated and control samples, particularly at the 7.5 cm point. Across all ratios, the pH generally increases from anode to cathode, with both control and treated samples reaching their highest pH values of 11.3 near the cathode. The consistent pH elevation in MgO-treated samples, especially prominent at lower water ratios, suggests that MgO treatment effectively increases soil alkalinity, with the magnitude of this effect moderated by the MgO-to-water ratio.

4.4.6 Current Measurement during the Electrokinetic Conditioning

Figure 4.34 illustrates the current variation over time for soil samples treated with 1% MgO at different MgO-to-water ratios compared to control samples. In the 1:10 ratio (Figure 4.34a), the treated soil shows slightly lower current values than the control, with both following a similar decreasing trend over the 168 hours. For the 1:15 ratio (Figure 4.34b), the treated soil maintains a higher current than the control, especially after the 72-hour mark, indicating a more sustained conductivity. Interestingly, the 1:20 ratio (Figure 4.34c) demonstrates a reversal in trend, where the MgO-treated soil exhibits higher current values than the control, particularly beyond the 96-hour point. This suggests that increasing water content in the MgO treatment may enhance the soil's electrical conductivity over time. All three scenarios show an overall decreasing current trend, but the rate and pattern of decrease vary with the MgO-to-water ratio, implying that the

water content plays a crucial role in the electrokinetic behavior of MgO-treated soils. It is important to note that the observed fluctuations in current coincide with injection times, highlighting the immediate impact of MgO introduction on soil conductivity.

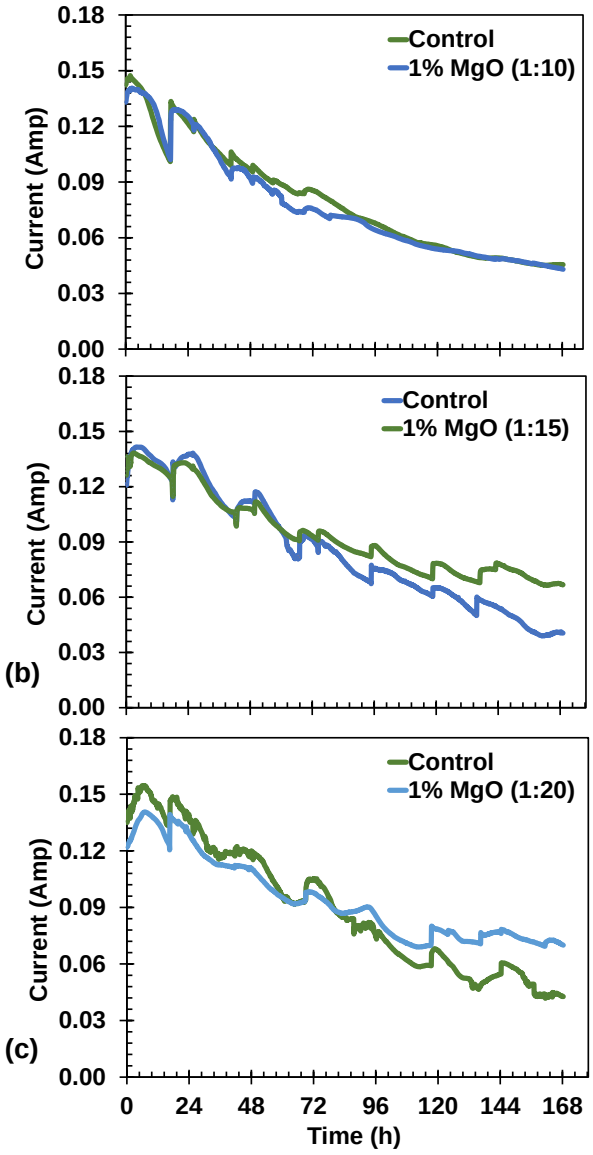

Figure 4.34: The soil current conditioned with the 1% MgO but with a different MgO to water ratio. **a)** MgO to water (1:10) **b)** MgO to water (1:15) **c)** MgO to water (1:20).

CHAPTER 5

Numerical Modeling

5.1 Introduction

Electrokinetic (EK) methods have been proposed and used across various scientific and engineering fields to enhance the movement of dissolved substances and chemical species through porous materials (Acar et al., 1993; Kim et al., 2001; Lear et al., 2004; Reddy et al., 1997; Sprocati et al., 2019; Yeung et al., 1997). This method has been used for soil dewatering and consolidation (Lockhart and Stickland, 1984; Adamson et al., 1966; Esrig, 1968; Fetzer, 1967; Fu et al., 2019; Shang & Lo, 1997; Shang, 1997; Sutar & Rotte, 2022), soil desalination (Akram et al., 2024; Hussain et al., 2023), heavy metal decontamination (Kim et al., 2001; Pamukcu & Kenneth Wittle, 1992; Wang et al., 2021) and soil strength improvement with salt injection (Abdullah & Al-Abadi, 2010; Chien et al., 2009; Chien et al., 2004). Besides the experimental result, numerical modeling can be a useful tool for understanding and predicting the processes that influence the efficiency of electrokinetics and optimizing and designing the system properly. However, implementing electrokinetic improvements is a time-consuming process involving numerous complex variables. To address this challenge, modeling before initiating operations has become crucial. This pre-implementation modeling significantly reduces the time and cost associated with electrokinetic processes by enabling accurate predictions of potential outcomes, especially when dealing with complicated and challenging variables (Han et al., 2021). Researchers and engineers can optimize their approach by integrating modeling into the electrokinetic application process, leading to more efficient and effective implementations in diverse scientific and industrial contexts.

Electrokinetic numerical modeling has garnered considerable attention in recent decades, with various studies advancing the understanding and application of electrokinetic remediation

(EKR) processes in contaminated environments. Researchers like Yang et al. (2022) and Mao et al. (2018) have developed sophisticated models that couple the Nernst-Planck-Poisson and Navier-Stokes equations to simulate the transport of contaminants in porous media under an electric field. Yang et al. (2022) focused on how ion concentration, pH, and zeta potential variations influence electroosmotic flow (EOF) and EKR efficiency, revealing the nonlinear behavior of EOF. In contrast, Mao et al. (2018) enhanced the EKR of ^{137}Cs-contaminated kaolin soils by employing non-uniform electric intensity and polarity reversal in their model, significantly improving contaminant removal efficiency and optimizing energy consumption.

Researchers have expanded electrokinetic modeling in more complex and heterogeneous environments to account for variable density effects, physical heterogeneities, and geochemical interactions. Sprocati et al. (2023) and Gallo et al. (2022) used models that combine the Nernst-Planck-Poisson formulation with geochemical codes like PHREEQC to study the impact of Coulombic interactions and density-driven flows on transport dynamics in porous media. These studies demonstrated that electrokinetic transport is significantly affected by buffer conditions and pore-scale interactions, leading to changes in contaminant plume shapes and mixing behavior. Similarly, Sprocati and Rolle (2022) developed a reactive transport model that integrates the Nernst-Planck equation with Darcy's law to simulate solute movement in heterogeneous media, highlighting the critical role of physical heterogeneities and pore water chemistry in influencing electroosmotic flow and contaminant degradation.

Several studies have applied these advanced models to specific environmental contexts, optimizing EKR strategies for various soil and sediment conditions. López-Vizcaíno et al. (2019) developed the M4EKR model, implemented in COMSOL Multiphysics, to simulate EKR

processes in calcareous soils contaminated with clopyralid. Their study showed that calcite dissolution-precipitation dynamics significantly influence pH distribution and EKR effectiveness. Similarly, Zheng et al. (2024) used a multi-physics coupled numerical model to simulate uranium removal from groundwater, demonstrating that electric fields can delay uranium migration and enhance remediation efficiency. Masia et al. (2017) and Masi et al. (2017) focused on optimizing the electrokinetic treatment of metal-contaminated marine sediments and dredged materials, respectively, by incorporating comprehensive geochemical reactions such as adsorption, precipitation, and dissolution into their models.

The practical application of electrokinetic modeling has also been explored in foundation pit leakage detection. Yu-Feng et al. (2022) developed a three-dimensional forward modeling approach to analyze the response characteristics of leakage electric fields in foundation pits, considering both conduction and electrokinetic effects. Their study demonstrated that electrokinetic effects could significantly enhance electric field signals at leakage points, improving detection accuracy and efficiency in complex underground environments. Sprocati et al. (2020) further expanded the scope of electrokinetic modeling by creating a process-based framework to analyze the interactions between physical, electrostatic, and biogeochemical processes during electrokinetic-enhanced bioremediation (EK-Bio) of chlorinated ethenes. Their model showed that electromigration and electroosmosis could significantly improve amendment distribution and contaminant biodegradation in low-permeability porous media.

Building on these foundations, we plan to use numerical modeling to explore the transport and distribution of MgO nanoparticles in soil using electrified as a driving force. This approach is intended to deepen our understanding of how nanoparticles can be effectively delivered into the

soil matrix, potentially offering innovative solutions for advanced stabilization techniques. Laboratory experiments have been conducted to investigate nano MgO's distribution under the influence of an electric field. To further this understanding, a series of two-dimensional (2D) numerical simulations were performed using COMSOL Multiphysics™ software, employing finite element method (FEM) modeling. This chapter discusses the development and application of a two-dimensional numerical model using COMSOL Multiphysics™ to simulate the electrokinetic transport of MgO nanoparticles in soil. The model aims to provide insights into the distribution patterns and transport mechanisms of MgO nanoparticles under the influence of an electric field.

5.2 Model Parameterization

The relevant parameters for these simulations are detailed in Table 5.1, providing a basis for optimizing the use of MgO nanoparticles in soil remediation efforts.

Table 5.1: Parameters used in the numerical investigation

Parameters	Values	Unit
Nanoparticles	MgO	-
Applied voltage	15	V
NPs size	20	nm
Density of soil	1270	kg/m^3
Density of liquid	1000	kg/m^3
Porosity	0.52	-
Soil water content	40 (almost saturated)	%
Dynamic viscosity	1.01×10^{-3}	Pa·s
Temperature	298.15	K
Concentration	1653	mol/m^3

The numerical simulation process in COMSOL Multiphysics™ for modeling soil behavior under an electric field involves several interconnected steps, as illustrated in Figure 5.1. The process begins with defining geometry and materials, which form the foundation for all subsequent calculations. COMSOL Multiphysics provides various drawing tools that enable the construction or importation of model geometry, allowing for a precise definition of the system's dimensions. Once the geometry is established, the materials used in the model are specified.

Following the establishment of the physical model, the next critical step involves setting up the boundary conditions and loading parameters. This includes specifying the electric field strength, initial nanoparticle concentration, and other relevant conditions at the simulation domain boundaries. These boundary conditions are essential for accurately representing the experimental setup and ensuring that the simulation reflects real-world scenarios. Once these parameters are defined, the system is discretized into a mesh, dividing the continuous domain into smaller, finite elements where the governing equations are solved. Integrating physics, boundary conditions, and mesh leads to formulating a matrix equation representing the discretized form of the governing partial differential equations. Solving this matrix equation yields the solution, describing the distribution of nano MgO particles over time and space within the soil under the applied electric field.

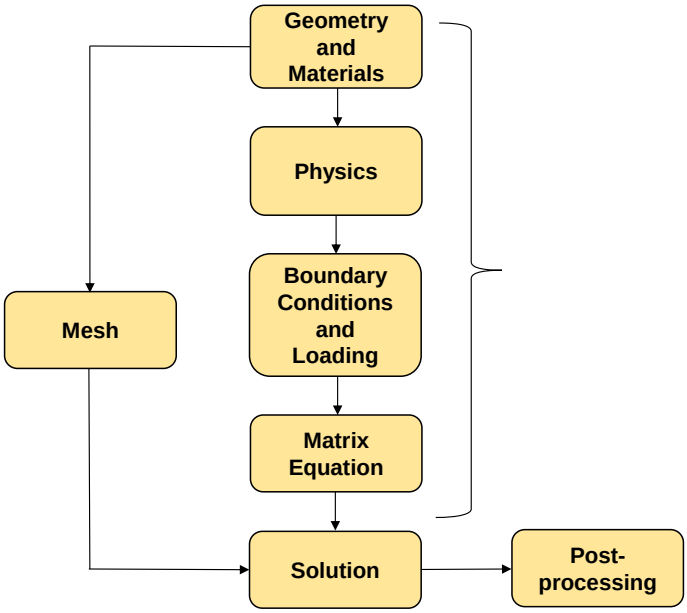

Figure 5.1: Workflow for Finite Element Analysis in Electrokinetic Soil Conditioning (COMSOL Multiphysics ®)

Several key assumptions and idealizations were necessary to address the complex nature of nanoparticle behavior in soil and develop a feasible model. These assumptions allow for approximating the system's essential physics while maintaining computational feasibility. The primary assumptions and parameters used in this modeling approach include: (1) the soil is considered isotropic and isothermal, (2) electrophoresis is assumed negligible compared to electroosmotic flow, (3) the pore geometry is assumed constant over time (porosity and tortuosity), and (4) the zeta potential and electric field are assumed to remain uniform throughout the soil (Han et al., 2021). (5) The nanoparticle was assumed to be an entity particle rather than a cation (Zhang et al., 2017). It is important to note that this model may change significantly if other parameters are considered or if these assumptions are refined. The results presented here are initial/preliminary and serve as a starting point for understanding the behavior of nano MgO in soil under an electric field. Further refinement of the model, incorporation of additional physical phenomena, and

validation against a broader range of experimental data would enhance the accuracy and applicability of these simulations. As this is an ongoing study, further refinements and validation of the model are anticipated, which may lead to substantial changes in the findings and conclusions presented here.

5.3 Modeling approach. Mathematical models of Electrokinetic nano conditioning of the soil

5.3.1 Model flow: In a soil system under the influence of an electric field, fluid movement during electrokinetic processes, characterized by creeping flow, is governed by the modified Navier-Stokes equations. The continuity equations describe laminar and incompressible electro-osmotic flow within the soil or porous media (Yang et al., 2022; Chun, 2002)

$$\rho\frac{\partial \boldsymbol{u}}{\partial t}+\rho\left(\boldsymbol{u}\cdot\nabla\right)\boldsymbol{u}=\nabla\cdot\left[-p\bar{\boldsymbol{I}}+\mu\left(\nabla\boldsymbol{u}+\left(\nabla\boldsymbol{u}\right)^{T}\right)\right]+\boldsymbol{F} \qquad (5-1)$$

In a steady-state condition, the time-dependent term $\frac{\partial \boldsymbol{u}}{\partial t}$ becomes zero because the velocity field does not change with time. Therefore, the Navier-Stokes equation simplifies to:

$$\rho\left(\boldsymbol{u}\cdot\nabla\right)\boldsymbol{u}=\nabla\cdot\left[-p\bar{\boldsymbol{I}}+\mu\left(\nabla\boldsymbol{u}+\left(\nabla\boldsymbol{u}\right)^{T}\right)\right]+\boldsymbol{F} \qquad (5-2)$$

and the continuity equation

$$\rho\nabla\cdot\boldsymbol{u}=0 \qquad (5-3)$$

In those equations, ρ (kg·m^{-3}) is the density, $\boldsymbol{u}$ (m·s^{-1}) is the fluid velocity vector, μ (Pa·s) is the liquid viscosity, p (Pa) is the pressure, I (unit less) is the direction vector, and $\boldsymbol{F}$ is the body-force vector introduced by an electrical field, ∇ (unit less), divergence operator, which when applied to a tensor or vector field, gives a scalar or vector field.

5.3.2 Species transport model: Besides convection caused by a pressure gradient, the external electric potential gradient can induce species convection by an electro-osmotic mechanism. Nernst-Planck equation (NPE) considers three main processes: diffusion, electromigration, and convection:

$$J_i = -D_i \nabla c_i - D_i \frac{z_i F}{RT} c_i \nabla \Phi + u c_i \qquad (5-4)$$

J_i ($molm^2s^{-1}$) is the flux of species i represents the amount of substance passing through a unit area per unit of time. D_i ($m^2 \cdot s^{-1}$) is the diffusion coefficient, c_i ($mol \cdot m^{-3}$) is species concentration, z_i (unit less) is the valence of species, F ($A \cdot s \cdot mol^{-1}$) is Faraday's constant; R ($J \cdot mol^{-1} \cdot K^{-1}$) universal gas constant is the molar gas constant, and T (K) is the temperature. The u is controlled by two driving forces, pressure, and electric potential, the same as macro-scale simulation (Yang et al., 2024).

$$u = -K_h \nabla h - k_{eo} \nabla \Phi \qquad (5-5)$$

K_h is the hydraulic conductivity ($m \cdot s^{-1}$), ∇h hydraulic gradient ($m \cdot m^{-1}$), k_{eo} ($m^2 \cdot V^{-1} \cdot S^{-1}$) electroosmotic permeability, typically ranging from 10^{-8} - 10^{-9} for soil with a pH value near neutral (Casagrande, 1952; Sprocati et al., 2019). $\nabla \Phi$ ($V \cdot m^{-1}$) is the applied voltage gradient. For more microstructural details, we also have the following equation.

$$u = -\frac{\varepsilon_p a^2}{8\mu\tau} \nabla p + \frac{\varepsilon_p \varepsilon_w \xi}{\mu\tau} \nabla \Phi \qquad (5-6)$$

ε_p (unit less) denotes the porosity, a (m) is the average radius of the pores, μ (Pa·s) is the dynamic viscosity, τ (unit less) represents the tortuosity of the porous structure, ∇p (Pa) is the pressure gradient, ε_w (F·m^{-1}) is the relative permittivity, ξ (V) is zeta potential.

The hydraulic conduccity K_h (m·sec^{-1}) could also be represent in terms of the permeability k (m^2) which is considered an intrinsic properties of porouse media, as follow:

$$K_h = \frac{k \cdot \rho \cdot g}{\mu} \qquad (5-7)$$

Where ρ (kg· m^{-3}) Fluid density, typically the density of wate; g (m· sec^{-2}) acceleration due to gravit, μ (Pa·s) is the dynamic viscosity.

In porous media, the permeability can be represented in terms of the Darcy number (D_a), a dimensionless number, as follows:

$$D_a = \frac{k}{L^2} \qquad (5-8)$$

In the above equation, L (m) represents the characteristic length, which in this case is the length of the electrokinetic chamber.

The governing transport equation of multicomponent species is derived from the mass conservation equation:

$$\frac{\partial c_i}{\partial t} + \nabla \cdot J_i = R_i \qquad (5-9)$$

R_i (mol·m^{-3}·s^{-1}) is a production or consumption rate expression.

5.3.3 Electric Current Density: The following equation has been used for the steady-state current density.

$$\nabla \cdot \mathbf{i} = \nabla \cdot \mathbf{J} = Q_{j,v} \qquad (5-10)$$

Where i ($A \cdot m^{-2}$) represents the current-density vector, it is mentionable that for calculating the value of the Diffusion coefficient, we have to use the **Stokes-Einstein–Sutherland** equation:

$$D = \frac{k_B T}{6\pi\eta r} \qquad (5-11)$$

Where:

- Boltzmann constant $k_B = 1.38 \times 10^{-23}\ J/K$
- Room temperature $T = 298.15\,K$
- Dynamic viscosity of water at room temperature $\eta = 0.001\ Pa \cdot s$
- Radius of the MgO nanoparticle $r = 10 \times 0^{-9}\ m$

5.3.4 Boundary Conditions

- **Outflow:** Ensures that species exit the domain without any diffusive flux across the boundary

$$n \cdot D_i \nabla C_i = 0$$

- **Electric Insulation:** specifies that no electric current crosses insulated boundaries.

$$n \cdot \mathbf{u} = 0$$

- **Zero Flux:** Ensures no flux across certain boundaries for mass or species transport.

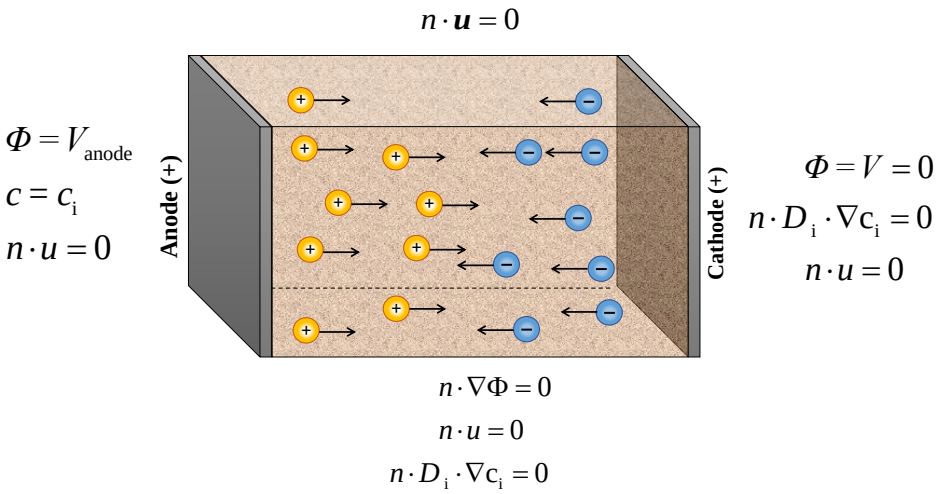

Figure 5.2: The boundary condition of the system

5.4 Results and Discussion

A series of analyses were performed to investigate the electrokinetic transport and distribution of MgO nanoparticles in soil using a two-dimensional numerical model developed in COMSOL Multiphysics™. The effects of MgO-to-water ratio and , hydraulic conductivity parameters were investigated, with a aim to provide insights into the distribution patterns and transport mechanisms of MgO nanoparticles under the influence of electric field.

5.4.1 Mesh Definition, Electric Potential, and Electric Field Distribution

Figure 5.3 illustrates the mesh configuration employed in our modeling process. We utilized the finest mesh in the software to ensure an accurate representation within our simulation. This fine mesh allows for a detailed and precise capture of the soil's complex behavior, particularly under the electrokinetic processes under investigation. Using such a mesh is crucial for minimizing numerical errors and ensuring that the simulation results closely replicate the actual physical

phenomena. Figure 5.3 indicates the 2D schematic of the model domain and mesh used for the modeling. Additionally, it is important to note that the dark black circles in the figure represent the injection points used to introduce nano MgO during the electrical process.

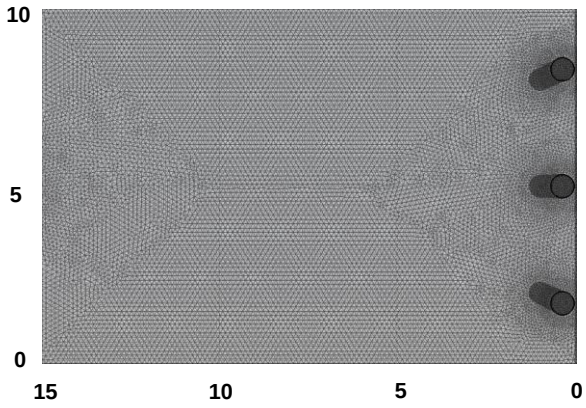

Figure 5.3: A 2D Schematic of the model domain and mesh

Figure 5.4a depicts the electric potential distribution across the system. The color gradient ranges from blue (0V) to red (15V), indicating a smooth voltage transition from one end of the volume to the other. This linear voltage distribution is characteristic of a uniform electric field applied across the sample. The potential increases steadily along one axis, suggesting the presence of electrodes at opposite ends of the sample, creating this potential difference. Figure 5.4b shows the corresponding electric field distribution within the same volume. The predominantly uniform teal color throughout most of the volume indicates a constant electric field strength of approximately 100 V/m, which aligns with the stated applied field of 15V across the 15 cm length. Interestingly, small localized regions of higher field strength are visible as yellow spots, which may correspond to areas of injection boundary effects within the sample.

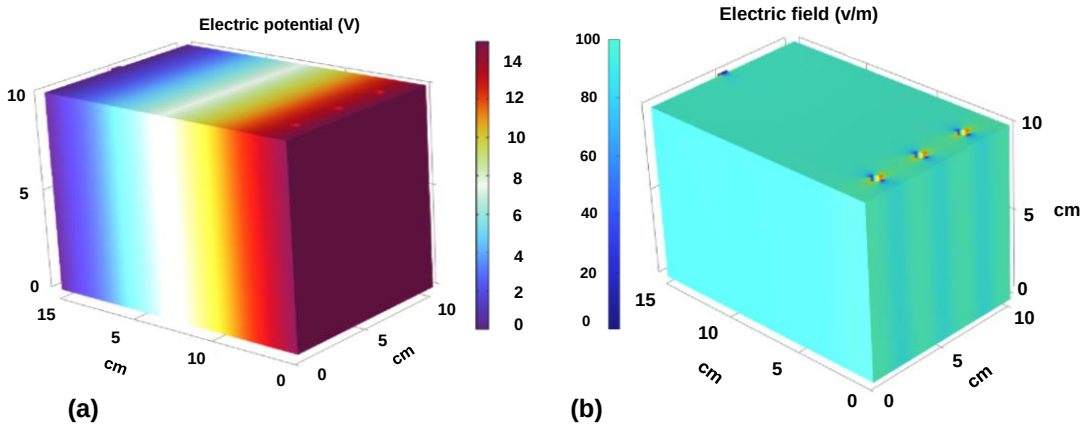

Figure 5.4: Schematic of 3D model under 15 V voltage **a)** electric potential, **b)** electric field

Figures 6.5a and 5.5b present the preliminary findings on the soil's electric field distribution and the resultant MgO nanoparticle distribution under an applied potential of 15V, respectively. Figure 5.5a illustrates the electric field intensity within the experimental chamber under an applied voltage of 15V. The field strength approximates 100 V/m, extending from the anode (right side) to the cathode (left side). The superimposed vectors in this figure denote the direction of the electric field, demonstrating a uniform orientation from the anode to the cathode across the soil matrix.

Figure 5.5b illustrates the distribution of MgO nanoparticles within the soil, based on a nano-MgO to water ratio of 1:15. The simulation reveals that MgO nanoparticles are dispersed throughout the system under the influence of an electric field, with a particularly higher concentration observed near the anode. This increased concentration is likely due to the aggregation and accumulation of nanoparticles in that region. This pattern is consistent with experimental observations, where significant aggregation and settling of MgO nanoparticles near the anode were noted. Figure 6 further supports this finding, providing visual evidence from a soil

sample extracted after the conditioning period, which clearly shows the accumulation and aggregation of MgO nanoparticles near the anode, likely influenced by gravitational forces.

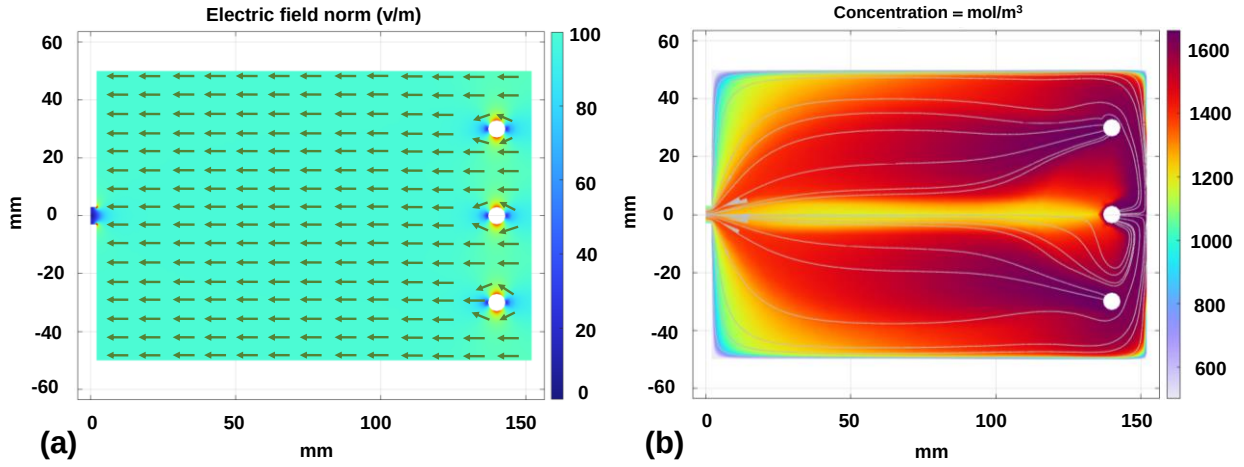

Figure 5.5: a) Electric field normal **b)** Distribution of nanoparticles MgO

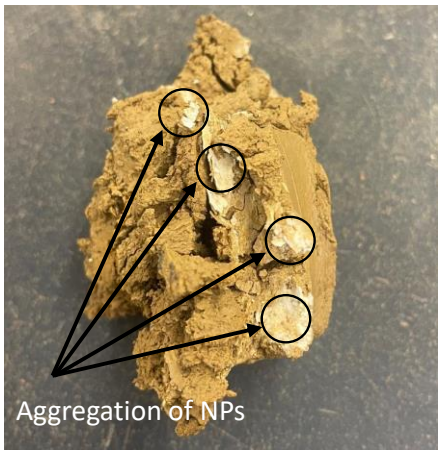

Figure 5.6: Aggregation of MgO nanoparticles was observed at the end of the test near the injection points

5.4.2 Evaluation of Different Nano-MgO to Water Ratio

Figures 5.7 illustrate the distribution of 1% MgO nanoparticles in soil under an applied voltage of 15V, with different MgO-to-water ratios. Both images depict the top view of the soil sample, with the concentration of MgO represented by a color gradient ranging from purple (lowest

concentration) to red (highest concentration). The white dots on the right side of each figure represent the nanoparticle injection points.

Figure 5.7a shows the distribution pattern for a 1:20 MgO-to-water ratio. The concentration gradient appears more gradual and spread out, with lower overall concentrations as indicated by the predominance of cooler colors (blues and greens). The MgO seems to have diffused more widely through the soil, creating a broader but less intense distribution pattern. There is a noticeable central band of lower concentration, flanked by areas of higher concentration towards the injection points of the sample. In contrast, Figure 5.7b depicts a 1:15 MgO-to-water ratio distribution. Here, we observe a markedly different pattern characterized by higher concentrations overall, as evidenced by the dominance of warm colors (reds and oranges). The distribution is more concentrated and localized, with distinct high-concentration pathways emanating from the injection points. This suggests that the reduced water content has led to less diffusion and more concentrated movement of the MgO nanoparticles through preferential pathways in the soil. The comparison between these two scenarios highlights the significant impact of the MgO-to-water ratio on nanoparticle distribution in soil under an electric field. With more water (1:20 ratio), the nanoparticles disperse more evenly but at lower concentrations throughout the soil matrix. Conversely, with less water (1:15 ratio), the nanoparticles form more concentrated channels, potentially following paths of least resistance in the soil structure. Since the distribution of MgO occurs due to electroosmosis and electromigration, migration is more pronounced in low water content.

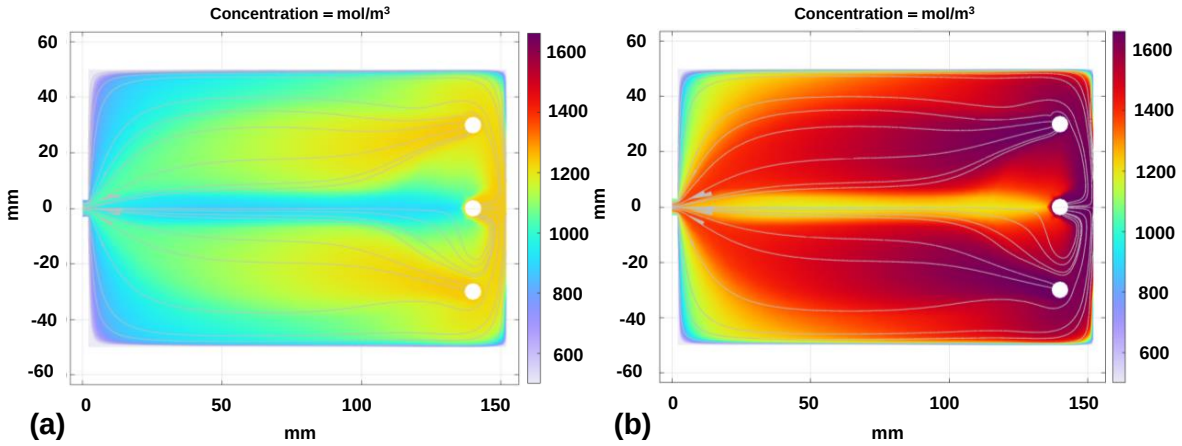

Figure 5.7: 1% MgO distribution in the soil with two different MgO-to-water ratios, **a)** 1:20 MgO to water ratio, c_i = 1240 mol/m^3 **b)** 1:15 MgO to water ratio c_i = 1653 mol/m^3

The model's prediction of an increased death zone with higher water content can be attributed to several interrelated factors. Adding more water likely extends the injection time, allowing for more extensive electrochemical reactions at the electrodes. This prolonged process can lead to significant pH changes in the soil, with a decrease near the anode and an increase near the cathode due to water oxidation and reduction, respectively (Acar & Alshawabkeh, 1993). These pH alterations can significantly impact the soil's zeta potential, consequently affecting the electroosmotic flow (Vane & Zang, 1997) and, as a result, affecting the distribution of nanoparticles.

5.4.3 Evaluation of the Hydraulic Conductivity

Figure 8 illustrates the distribution of 1%MgO nanoparticles in soil under an applied voltage of 15 V and an initial concentration of c_i =1653 mol/m³ across different hydraulic conductivity values. These preliminary modeling results demonstrate that in soils with lower hydraulic conductivity, the electrokinetic treatment leads to a more uniform and effective distribution of nanoparticles throughout the soil matrix. The color gradient in the image represents the concentration of MgO

nanoparticles, ranging from purple (lowest concentration, around 600 mol/m³) to deep red (highest concentration, approximately 1600 mol/m³). Regions with dark red color, particularly near the injection points, indicate the highest concentrations (> 1600 mol/m³).

The nanoparticle distribution shows a strong correlation with soil hydraulic conductivity. Figure 5.8a indicates the 1% MgO distribution in soil with lower hydraulic conductivity (K = 6.816 $\times 10^{-8}$ cm/s). The MgO nanoparticles are relatively well dispersed throughout the soil matrix, though not entirely uniform. Notably, we do not observe a dead zone near the cathode (left side of Figure 8a). The figure shows that the concentration is lower near the anode surface (right side), as indicated by the blue color. The concentration of MgO is highest near the injection points, shown in dark red, and gradually decreases towards the cathode, transitioning from red to orange to green. This pattern suggests a gradual diffusion of nanoparticles from the injection points towards the cathode. No pronounced dead zone was observed near the cathode, and the distribution of MgO is relatively widespread throughout the soil. However, concentration variations are evident, with higher levels near the injection points and gradual decreases towards the cathode.

Figures 8b and c show the soil with K = 6.816 × 10^{-7} cm/s and K = 6.816 × 10^{-6} cm/s, respectively, exhibiting different patterns of nanoparticle distribution in the soil. Figure 8b indicates that the MgO concentration decreases toward the cathode, with lower concentrations

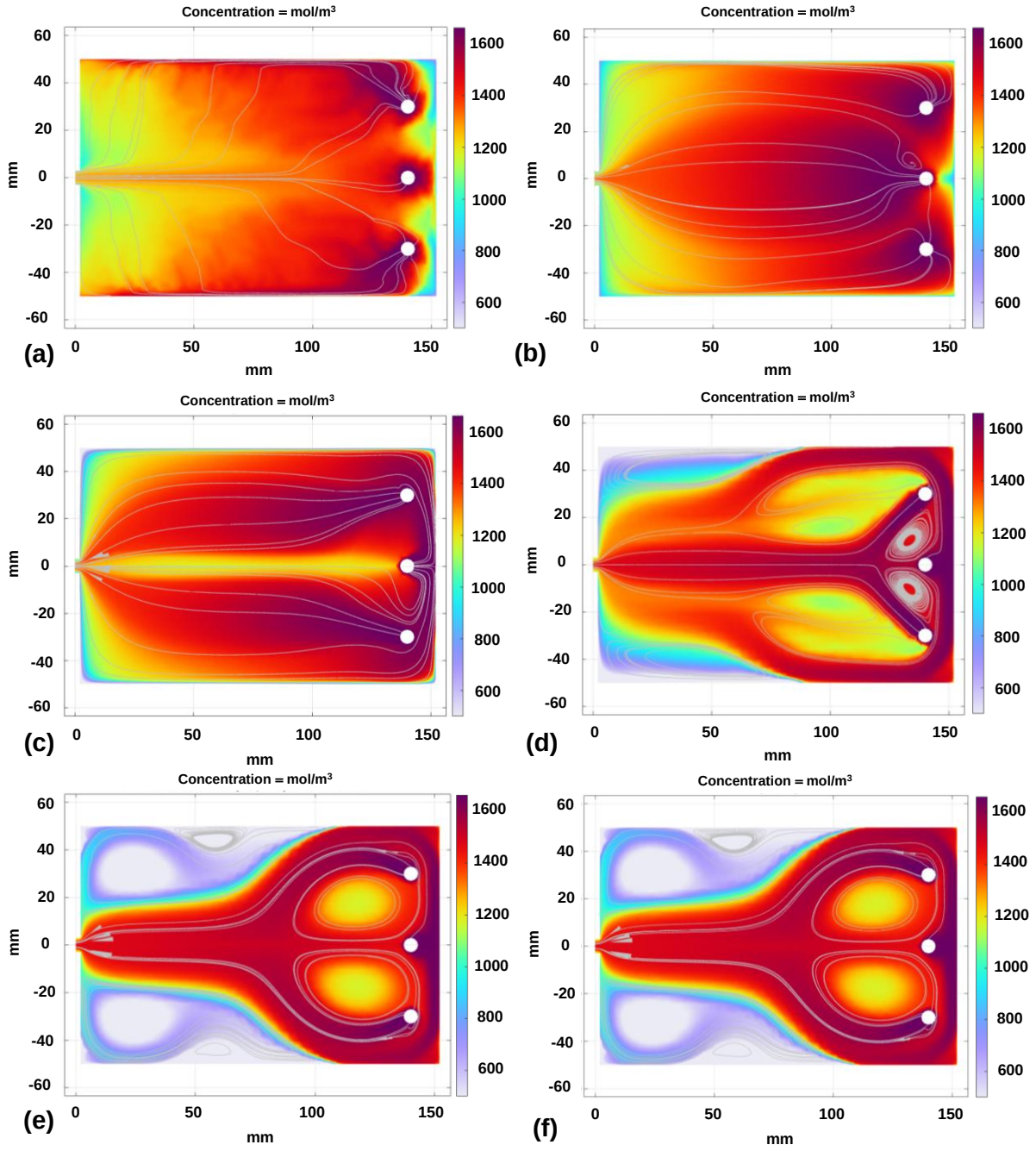

Figure 5.8: The MgO nanoparticle distribution in the system with different hydraulic conductivity values. Initial concentration c_i = 1653 mol/m^3; MgO to water ratio = 1:15; applied voltage V=15V. **a)** K = 6.816 × 10^{-8} cm/s, **b)** K = 6.816 × 10^{-7} cm/s, **c)** K = 6.816 × 10^{-6} cm/s, **d)** K = 6.816 × 10^{-5} cm/s, **e)** K = 6.816 × 10^{-3} cm/s, **f)** K = 6.816 × 10^{-1} cm/s.

(around 1000-1200 mol/m³) near the front. The concentration decreases relatively uniformly toward the cathode, with some areas of slightly lower concentration visible near the corners. In Figure 8c, the distribution pattern is noticeably different. A more pronounced central path of lower concentration flows toward the cathode, flanked by areas of higher concentration on both sides. These higher concentration zones also show a gradual decrease toward the cathode. The corners near the cathode display areas of lower concentration, though not as pronounced as in Figure 5.8b.

As we progress through Figures 5.8d to 5.8f, we observe the soil's hydraulic conductivity increasing from $K = 6.816 \times 10^{-5}$ cm/s to $K = 6.816 \times 10^{-1}$ cm/s, significantly affecting the distribution of MgO nanoparticles. In Figure 5.8d, areas of lower concentration (around 800-1000 mol/m³, shown in blue-green) appear near the cathode corners and along the edges. The concentration near the injection points is higher, decreasing towards the cathode through distinct pathways, creating a pattern of higher concentration zones surrounded by areas of lower concentration. As hydraulic conductivity increases, these patterns become more pronounced. In Figure 8e ($K = 6.816 \times 10^{-3}$ cm/s), we observe larger areas of low concentration near the cathode corners and along the chamber walls. Two distinct high-concentration zones (red-orange) form near the center, extending from the injection points towards the cathode.

Figure 5.8f shows a similar pattern to 8e, with even more pronounced areas of low concentration (blue-purple) near the edges and corners. The high-concentration zones in the center are more defined and compact. This evolution in distribution patterns can be attributed to the increasing influence of hydraulic flow competing with electrokinetic forces as soil permeability

increases. The result is a more non-uniform particle distribution, with clear preferential flow paths and particle accumulation areas contrasting with lower concentration zones.

These preliminary results indicate that the distribution of nanoparticles is more effective in fine-grained soils with lower hydraulic conductivity, such as clays and silts, compared to coarser-grained soils like sand. It is clear that soil with $K = 6.816 \times 10^{-8}$ cm/s likely represents clay or silt, while soil with $K = 6.816 \times 10^{-3}$ cm/s indicates coarser-grained material. This finding is consistent with the literature that has reported electrokinetic treatments working more effectively in fine-grained soils such as clay compared to coarse materials like sand (Alshawabkeh & Sheahan, 2003; Bjerrum et al., 1967; Lockhart, 1983; Malekzadeh et al., 2016; Vane & Zang, 1997). The superior performance in clay soils can be attributed to their unique physicochemical properties, including high surface charge, small pore sizes, and low hydraulic conductivity, which collectively enhance electrokinetic transport mechanisms.

5.4.4 Discussion

The preliminary results of this study offer valuable insights into the distribution of MgO nanoparticles in soil under various conditions, with a particular focus on the effects of hydraulic conductivity and MgO to water ratio. These findings provide a foundation for understanding nanoparticle behavior in electrokinetic soil stabilization. However, it is crucial to acknowledge the several simplifications and assumptions made in our modeling approach. This study employed the extremely fine mesh in COMSOL Multiphysics to ensure the highest possible resolution within the software's constraints. We assumed a homogeneous soil medium to establish baseline behaviors. Our model did not incorporate the effects of soil zeta potential changes over time or nanoparticles' temporal variation and tracking. Additionally, we utilized a 2D model for

simplification. While these simplifications were essential for our preliminary work, a more comprehensive understanding of real-world scenarios requires the consideration of additional factors in future simulations.

5.4.5 Factors to Consider for Future Research Modeling

Future research should consider several important parameters in their modeling for a more realistic understanding of nanoparticle movement, tracking, and distribution in soil systems. These include:

1. Incorporating soil heterogeneity and different particle sizes to reflect natural soil conditions accurately.
2. Modeling dynamic changes in soil pH and their effects on nanoparticle behavior, particularly the zeta potential changes over time.
3. Investigating interactions between nanoparticles and soil constituents, including adsorption-desorption processes and the potential for nanoparticle aggregation under various soil conditions.
4. Implementing 3D modeling to provide a more comprehensive and accurate representation of nanoparticle distribution, accounting for complex flow patterns and spatial variations not captured in 2D simulations.
5. Future research should focus on enhancing model accuracy by integrating laboratory data and visual validation of MgO nanoparticle movement, potentially utilizing fluorescent-tagged MgO nanoparticles to capture their distribution under UV light, thereby providing direct visual evidence for comparison with model predictions and refinement of simulation results.

Future Research Directions: Future studies should explore the effects of varying electric field strengths and configurations and the impact of different nanoparticle types and sizes on distribution patterns. Incorporating temperature variations and geochemical reactions would refine our understanding of nanoparticle behavior in electrokinetic soil stabilization. These advancements will lead to more accurate predictive models and more effective and efficient improvement strategies for expansive soils.

In conclusion, while our preliminary results provide valuable insights, they also underscore the need for more comprehensive modeling approaches incorporating a wider range of parameters and processes. By addressing these factors in future studies, researchers can develop more accurate and reliable models for predicting nanoparticle distribution in electrokinetic soil stabilization.

CHAPTER 6

Preliminary Cost Estimation

6.1 Introduction

Cost estimation is an important part of construction projects, providing stakeholders with a clear understanding of the budget required for a specific project or site. Accurate preliminary cost estimates are essential before implementation, as they influence decision-making, resource allocation, and feasibility. State Departments of Transportation (DOTs) typically rely on established guidelines and historical data to develop cost estimates for conventional highway construction, repair, and maintenance projects.

However, this particular scenario demands a more sophisticated and tailored method for initial cost assessment. For instance, we should consider applying nano-conditioning through electrokinetic processes to stabilize expansive soil in highway subgrades. Since large-scale field applications of this nano-conditioning technique are unprecedented, cost estimates mostly rely on small-scale trials and laboratory scales. This preliminary estimation is a starting point, acknowledging that unforeseen factors may arise during field implementation. Having said that, any preliminary cost estimate for novel construction techniques is subject to various uncertainties is important. As the project moves from concept to field application, additional needs may become apparent, potentially affecting the overall cost. Furthermore, material availability, price fluctuations, project location, and timing can significantly impact the final expenses. Therefore, this preliminary estimation would be a rough estimation of the project cost if implemented in the field. We aim to initiate an investigation into highway project cost estimation methods, focusing primarily on the preliminary cost estimates developed during the planning phase of electrokinetic nano conditioning.

For this cost estimate, we'll focus on a specific portion of the highway known for its problematic subgrade. We have selected a section of the AL-5 highway in Alabama, known for its expensive soil in the subgrade. Using this location as our case study, we'll calculate the potential costs of applying electrokinetic nano-conditioning to stabilize the subgrade. This approach will give a concrete example, allowing for a more accurate and realistic cost projection. Figure 6.1 shows the location of the AL-5 highway, which is the proposed site for potential implementation.

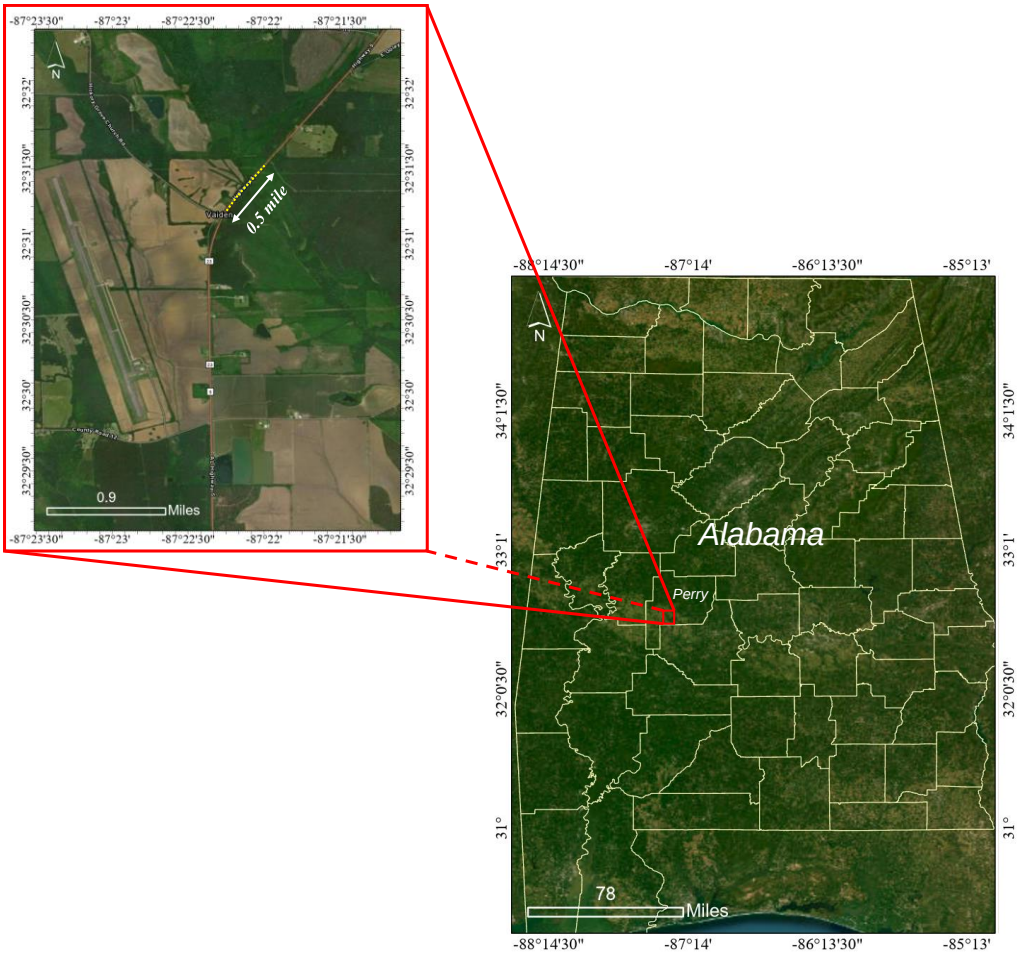

Figure 6.1: Map showing the location of the proposed study area

6.2 Estimation Approach

We will employ a systematic approach to estimate the cost of the proposed study area. Our process begins by focusing on a representative portion of the highway, as illustrated in Figure 6.2. This section serves as our baseline for calculations and analysis. The section under consideration spans 7.2m in total width from shoulder to shoulder, with 3.6m extending from the centerline to each shoulder. At the pavement centerline, an anode electrode measuring 2.4m in width and 0.30m in depth is to be installed. The design incorporates three injection holes on each side of this anode electrode for nanoparticles (NPs) introduction. Two cathode electrodes are to be positioned at the pavement shoulders, each 3.6m from the centerline anode. As illustrated in Figure 6.2, this configuration enables the electrokinetic movement of nanoparticles from the central injection points toward the shoulder areas.

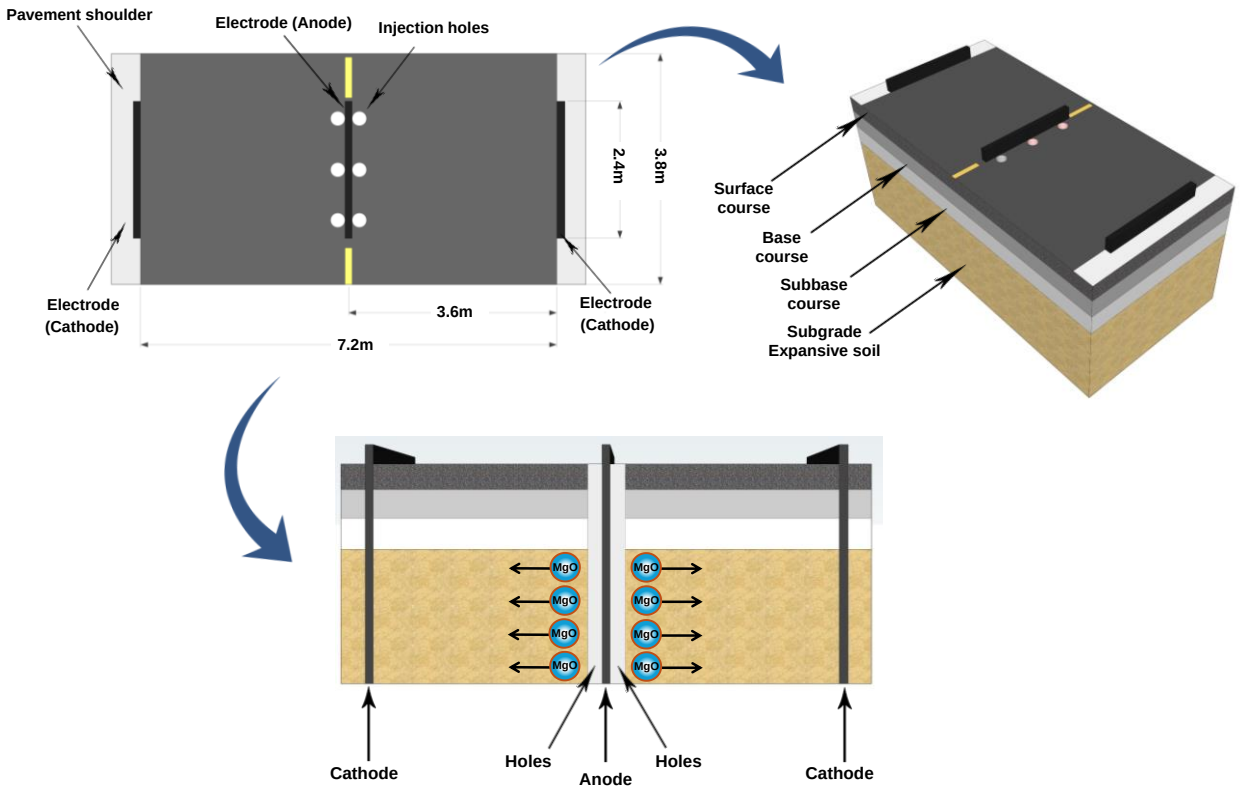

Figure 6.2: The schematic of the AL-5 highway section for electrokinetic nano-conditioning

We will conduct a detailed assessment of this segment, considering factors such as soil, depth of treatment required, equipment, and material needs for electrokinetic nano-conditioning. Once we have a comprehensive cost breakdown for this sample section, we will extrapolate these figures to cover the entire 0.5-mile stretch of the highway. In scaling up, we'll account for potential economies of scale, such as reduced equipment mobilization costs when spread over a larger area. By following this methodical approach, we aim to compile a detailed and accurate cost projection for implementing this electrokinetic nano-conditioning technique across the full 0.5-mile section of the highway. This estimation will balance the specifics of our sample section with the realities of a larger-scale implementation, providing a comprehensive view of the potential project costs. For this purpose, we have used 1% MgO nanoparticles based on the dry unit weight of the soil. To calculate the total cost of MgO needed for soil treatment, we first determine the weight of the soil by calculating the volume of the soil that needs to be treated. Next, we calculate the required amount of MgO nanoparticles based on the soil's dry weight, assuming a 1% MgO concentration. Finally, the total cost is determined using the cost per kilogram of MgO.

Calculation Steps:

1. Calculate the Volume of Soil (V):

$$V = L \times W \times h = 3.6\,m \times 2.4\,m \times 0.30\,m = 2.592\,m^3$$

Converting cubic meters to cubic centimeters:

$$V = 2.592 \times 10^6\,cm^3$$

2. **Calculate the Weight of the Soil (W):** Given the dry unit weight (γ) of the soil:

$$W = \gamma \times V = 1.27 \frac{g}{cm^3} \times 2.592 \times 10^6 cm^3 = 3291840 g = 3291.84 kg$$

3. **Calculate the Amount of MgO Required:** For 1% MgO:

$$1\% MgO = 0.01 \times 3291.84 kg = 32.91 kg \left(for\ one\ side\ of\ the\ road \right)$$

Since the treatment is for both sides of the road:

$$32.91 kg \times 2 = 65.82 kg$$

4. **Calculate the Total Cost of MgO:** The cost of MgO, a key component for this project's cost estimation, is currently estimated at $20 per kilogram. However, it's important to note that this price can fluctuate depending on the supplier and market conditions. For our calculations, we have used an average value to provide a baseline estimate.

$$total\ \cos t = 65.82 kg \times \frac{\$20}{kg} = \$1316.4$$

5. The other calculations are presented in Table 6.1 for that specific section of the highway. It should be noted that all other costs may also fluctuate, as most of the costs have been estimated as lump sums for this calculation. Now that we have obtained values for a known cross-section of the Al-5 proposed highway, we can extrapolate these results to estimate the costs for a 0.5-mile stretch. This allows us to evaluate the potential overall expense for the remainder of the highway. The detailed calculation steps are as follows

Table 6.1: Cost Estimation for the Highway Section Illustrated in Figure 2 (in US Dollars)

NO	Description	Unit	Amount	Unit Price	Quantity	Total Amount
1	Unclassified Excavation (depth of 1m by 2.4, 0.2m)	CUYD	0.63	55.23	3.00	104.02
2	Drill Holes (8-inch Diameter)	LF	1.00	26.94	6.00	161.64
3	Power supply (estimated for 7 days)	LS	1.00	2000.00	1.00	2000.00
4	Water Supply for mixing Nanoparticles (LS)	L	300.00	2.00	1.00	600.00
5	Amount of Nanoparticles needed based on soil	Kg	32.91	1.50	2.00	98.73
6	The graphite lectrode (2.4m, by 1.2, by 0.5)	LS	1.00	200.00	3.00	600.00
7	Mixing Remixing (digital cement mixer)	LS	1.00	200.00	1.00	200.00
8	Pumping equipment for injection (water pump is required)	LS	1.00	200.00	2.00	400.00
9	Sodium Hexametaphophate (chemical)	Lb	1.00	32.32	1.00	32.32
10	Safety Equipment	LS	1.00	300.00	2.00	600.00
11	Waste Disposal	LS	1.00	300.00	1.00	300.00
12	Miscellaneous Supplies	LS	1.00	1000.00	1.00	1000.00
13	Site prepration	LS	1.00	250.00	1.00	250.00
14	Transportaion	LS	1.00	2000.00	1.00	2000.00
15	Cones (36" High)	Each	1.00	30.00	10.00	300.00
16	Portable Changeable Message Sign	LS	1.00	300.00	2.00	600.00
Total						9142.69

Now that we have the cost for the given section, we can scale it up to the entire targeted area as follows:

1. **Identify Reusable and Non-Reusable Items:**

- **Reusable Items:** You only need to purchase these items once, and they can be reused across the entire project length. For example, the power supply, mixing equipment, and safety equipment. Since these items are not consumed or installed permanently, their costs do not scale with the project length.
- **Non-Reusable (Consumable) Items:** These items will be consumed or installed permanently in the project, so their costs scale directly with the length of the project. Examples include excavation costs, drilling, electrodes, and the amount of nanoparticles needed.

2. **Determine the Scaling Factor:**

    - The original cost estimate is based on a 2.4-meter section.
    - The project is being scaled up to an 800-meter section.

- The scaling factor is calculated as $Scaling\ Factor = \frac{800}{2.4} = 333.33$

3. Apply the Scaling Factor to Non-Reusable Items:

For each non-reusable item, multiply the original cost by the scaling factor (333.33) to get the cost for the 800-meter section.

- **unclassified Excavation**: $104.02 × 333.33 ≈ $34,673.33
- **Drill Holes (8-inch Diameter)**: $161.64 × 333.33 ≈ $53,878.67
- **Amount of Nanoparticles Needed:** $98.73 × 333.33 ≈ $32,907.97
- **Stainless steel Electrode**: $600.00 × 3 = $1,800.00 (this accounts for the reusability where electrodes are used three times for the entire 800m)

4. Sum the Scaled Total Costs:

Total Costs = 34,673.33+53,878.67+32,907.97+1,800.00 ≈ 123,260.00.

6.3 Cost Comparison

The various stabilization techniques for expansive soil discussed in section 2.9 have been implemented along the AL-5 highway to address highway distress. To provide a comprehensive cost comparison of these different stabilization approaches, Figure 6.3 illustrates a comparative cost analysis between previous remediation studies (Anderson et al., 2024) and our current findings. Figure 6.3 a focuses specifically on remediation costs across different methods, while Figure 6.3 (b) presents the combined costs of both remediation and resurfacing for each approach.

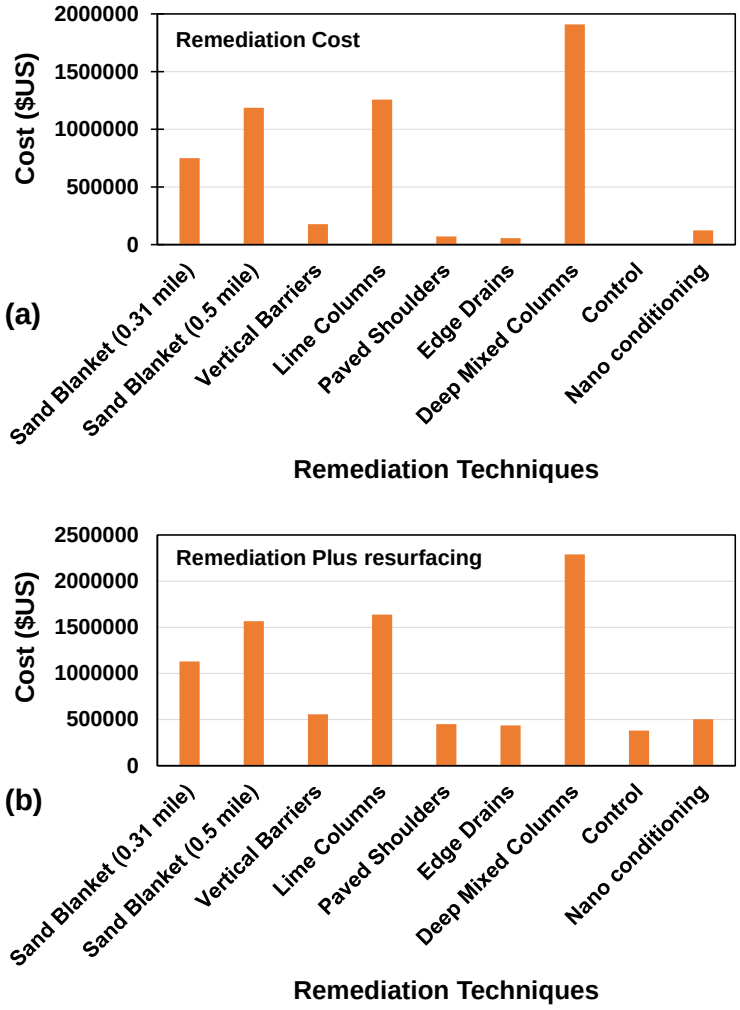

Figure 6.3: Cost comparison of various remediation techniques: (a) remediation costs and (b) remediation plus resurfacing costs

As evident from the cost analysis, nano-conditioning emerges as a highly cost-effective solution compared to traditional methods such as sand blanketing, deep mixing, and lime columns. When considering implementation over a 0.5-mile stretch, nano-conditioning demonstrates significantly lower costs across both remediation and total (remediation plus resurfacing) expenditures. The economic advantage of nano-conditioning is particularly striking comparing deep mixed columns or full-depth reclamation techniques.

The cost-effectiveness of nano-conditioning and its potential for enhanced soil stability position it as a promising alternative for expansive soil treatment along highways. This method offers substantial cost savings and potentially reduces construction time and environmental impact compared to more invasive techniques. However, it is important to note that the selection of a stabilization method should consider not only cost but also site-specific conditions, long-term performance, and maintenance requirements. The data presented in Figure 6.3 provides valuable insights for engineers and decision-makers when evaluating the most suitable and economically viable approach for expansive soil stabilization in highway construction and rehabilitation projects.

CHAPTER 7

Summary, Conclusion and Recommendation

7.1 Summary

This report presents a comprehensive study on stabilizing expansive soils using nanoparticles and electrokinetic methods. The research investigated the effects of MgO and SiO_2 nanoparticles on soil properties through physical mixing and electrokinetic injection. While both nanoparticles were used in physical mixing experiments, only 1% MgO nanoparticles were employed in the electrokinetic injection process to evaluate their efficacy for expansive soil improvement. To gain a deeper understanding of nanoparticle movement and tracking their movement, modeling was performed using COMSOL Multiphysics software. Additionally, a preliminary techno-economic assessment was conducted to evaluate the potential for real-world implementation.

Key findings of this study include:

1. Physical mixing of MgO or SiO_2 nanoparticles (1-3% by weight) significantly improved the soil's unconfined compressive strength (UCS) and water-holding capacity. The addition of MgO nanoparticles consistently decreased the soil's plasticity index (PI) and swell potential across all tested percentages. In contrast, SiO_2 nanoparticles exhibited a more complex behavior: at 1% concentration, they reduced PI and swell potential, but when added beyond 1%, both the swell potential and PI of the soil increased. This differential effect highlights the importance of carefully selecting nanoparticle type and concentration for optimal soil stabilization outcomes.
2. Electrokinetic treatment significantly altered soil properties along the anode-cathode axis, inducing notable variations in moisture content, pH, and strength. The non-uniform changes observed across the soil profile highlight the complex nature of electrokinetic

processes. This treatment method resulted in distinct modifications near the anode and cathode, demonstrating the intricate interplay of electrochemical reactions and ion migration.

3. The study investigated the electrokinetic injection of 1% MgO nanoparticles using three different MgO-to-water ratios (1:10, 1:15, and 1:20). In the presence of an electric field, MgO-treated soil exhibited significant improvements in plasticity index (PI), unconfined compressive strength (UCS), and swell potential compared to control samples. The effectiveness of this treatment varied based on several factors, including nanoparticle concentration, water content, and distance from electrodes. These findings demonstrate the potential of combining nanoparticle injection with electrokinetic methods for enhanced soil stabilization, while also highlighting the importance of optimizing treatment parameters for maximum efficacy.
4. X-ray fluorescence (XRF) analysis was conducted on samples collected from various locations within the soil profile to assess the distribution of nanoparticles. The results revealed consistently higher levels of MgO and Mg^{2+} in treated samples compared to control specimens. This finding provides strong evidence for the successful integration and distribution of MgO nanoparticles in to the treated soil matrix.

7.2 Future Research Directions and Recommendations

This comprehensive study has demonstrated the significant potential of electrokinetic nano-conditioning for treating expansive soils. Our research shows that even small quantities of nanoparticles can substantially alter soil properties, offering promising avenues for stabilization. As we look to the future, several key areas emerge as priorities for further investigation. These research directions aim to deepen our understanding of the complex processes involved and

optimize the electrokinetic soil conditioning process for real-world applications. The following areas have been identified as crucial for advancing this field:

1. **Electrokinetic Configuration:** During the electrokinetic process, water dissociation near the anode and cathode induces significant pH changes in the soil. These pH alterations can substantially impact the electrokinetic process and, consequently, the distribution of MgO nanoparticles within the system. In our experimental setup, a single outlet near the cathode was utilized, which may have been insufficient when injecting the nanoparticle solution, potentially limiting the efficiency of nanoparticle distribution.To optimize the electroosmotic flow and enhance MgO distribution, modifications to the experimental setup should be considered. One potential improvement is the incorporation of multiple outlet holes (e.g., two or three) strategically placed along the cathode side. While this modification may not directly address pH changes, it would provide additional pathways for water to exit the system, potentially reducing localized pressure buildup and promoting more uniform nanoparticle distribution through electroosmosis.
2. **Quantitative Analysis:** While X-ray Fluorescence (XRF) analysis was conducted on pre- and post-treated soil samples with MgO nanoparticles, more quantitative analytical techniques are needed for greater accuracy. Advanced methods such as Inductively Coupled Plasma Mass Spectrometry (ICP-MS) should be employed in future studies. ICP-MS offers superior sensitivity and precision, allowing for accurate detection and quantification of elements at trace levels. Additionally, increasing the sample size and analyzing soil from various positions would provide a more comprehensive understanding of nanoparticle distribution throughout the treated soil.

3. **Nanoparticle Aggregation:** Despite using Na-HMP as a dispersing agent, Nano MgO aggregation and settling during injection remain problematic. Alternative dispersion methods or increasing the water ratio and outlet ports should be investigated to mitigate this issue.
4. **Modeling Refinement:** While preliminary modeling results are promising, several assumptions have been made. To improve model accuracy, input variables should be carefully measured and imported. Integration with specialized software like PHREEQC could help measure reaction changes more precisely.
5. Future research should focus on enhancing model accuracy by integrating laboratory data and visual validation of MgO nanoparticle movement, potentially utilizing fluorescent-tagged MgO nanoparticles to capture their distribution under UV light, thereby providing direct visual evidence for comparison with model predictions and refinement of simulation results.
6. **Field Application and Monitoring:** Following laboratory-scale experiments optimization and modeling, it is recommended to apply the electrokinetic nanoparticle treatment in an actual field setting. This step is crucial for understanding how the process performs under real-world conditions, which often differ significantly from controlled laboratory environments. Field trials would enable assessment of factors such as natural soil heterogeneity's impact on nanoparticle distribution, effects of varying weather conditions and groundwater levels, long-term stability and effectiveness of the treatment, potential environmental impacts, and practical challenges in scaling up the technology. Implementing a comprehensive monitoring program during and after field application would provide valuable data on the treatment's performance, durability, and any unforeseen

effects. This real-world validation is essential for refining the technology and developing best practices for its widespread adoption in geotechnical engineering.

7.2 Conclusion

This study has demonstrated the potential of using nano MgO in electrokinetic soil conditioning to enhance the geotechnical properties of expansive soils. The results showed that electrokinetic nano-conditioning improved soil strength and stability and reduced swell strain; the outcomes were more pronounced when nano MgO was applied through physical mixing methods. The physical mixing yielded superior results compared to electrokinetic treatment, suggesting that directly incorporating nanoparticles into the soil matrix may be more effective for enhancing soil properties. Nonetheless, the successful migration of MgO nanoparticles under an electric field still underscores the promise of electrokinetic approaches, particularly for scenarios where direct mixing is impractical.

Future research should investigate optimizing the electrokinetic process to achieve results comparable to or better than physical mixing. Understanding the long-term durability of MgO-treated soils under various environmental conditions and minimizing challenges such as nanoparticle aggregation during electrokinetic treatment will be essential. Additionally, it will be important to explore the environmental impact of using MgO nanoparticles, particularly regarding potential leaching into groundwater. Overall, while this study highlights the benefits of both electrokinetic and physical mixing methods for soil stabilization, further refinement is needed to fully leverage the advantages of nano-based soil treatment techniques in geotechnical engineering.

REFERENCES:

Abdelhafez, M. A., Ellingwood, B., & Mahmoud, H. (2022). Hidden costs to building foundations due to sea level rise in a changing climate. Scientific reports, 12(1), 14020.

Abdelkader, H. A., Hussein, M. M., & Ye, H. (2021). Influence of waste marble dust on the improvement of expansive clay soils. Advances in Civil Engineering, 2021(1), 3192122.

Abdi, M. R., Parsapazhouh, A., & Arjmand, M. (2008). Effects of Random Fiber Inclusion on Consolicdation, Hydraulic Conductivity, Swelling, Shrinkage Limit and Desiccation Cracking of Clays.

Abdullah, W., & Al-Abadi, A. (2010). Cationic–electrokinetic improvement of an expansive soil. Applied clay science, 47(3-4), 343-350.

Abedi Koupai, J., Fatahizadeh, M., & Mosaddeghi, M. R. (2020). Effect of pore water pH on mechanical properties of clay soil. Bulletin of Engineering Geology and the Environment, 79, 1461-1469.

Abood, T. T., Kasa, A. B., & Chik, Z. B. (2007). Stabilisation of silty clay soil using chloride compounds. Journal of engineering science and technology, 2(1), 102-110.

Abu-Farsakh, M., Dhakal, S., & Chen, Q. (2015). Laboratory characterization of cementitiously treated/stabilized very weak subgrade soil under cyclic loading. Soils and Foundations, 55(3), 504-516.

Abu-Zreig, M. M., Al-Akhras, N. M., & Attom, M. F. (2001). Influence of heat treatment on the behavior of clayey soils. Applied clay science, 20(3), 129-135.

Acar, Y. B., & Alshawabkeh, A. N. (1993). Principles of electrokinetic remediation. Environmental science & technology, 27(13), 2638-2647.

Acar, Y. B., Alshawabkeh, A. N., & Gale, R. J. (1993). Fundamentals of extracting species from soils by electrokinetics. Waste Management, 13(2), 141-151.

Adamson, L. G., Chilingar, G. V., Beeson, C. M., & Armstrong, R. A. (1966). Electrokinetic dewatering, consolidation and stabilization of soils. Engineering geology, 1(4), 291-304.

Agarwal, B. K., & Sachan, A. (2024). Quantification of Desiccation Cracking and Strain Localization in Lime-Treated Compacted Expansive Soils Using DIA and DIC. Journal of Materials in Civil Engineering, 36(2), 04023541.

Anderson, J. B., Jackson, D. T., Young, E. S., Kennedy, L., & Jones, D. (2024). Evaluation of Remediation Strategies for Shrink-Swell Clays in Western Alabama (No. ALDOT 930-866R-1). Auburn University. Highway Research Center.

Ahmadi, H., & Shafiee, O. (2019). Experimental comparative study on the performance of nano-SiO_2 and microsilica in stabilization of clay. The European Physical Journal Plus, 134(9), 459.

Akram, S., Imran, M., Ashraf, S., Akram, A., Kamran, K., Ishaq, M., Hussain, A., Abbas, J., Ajaj, Y., & Habila, M. (2024). Effect of electroosmotic and hydraulic flow on the desalination of soils. Journal of Applied Electrochemistry, 1-14.

Alabama Department of Transportation Bureau of Materials and Tests Geotechnical Division. (2021). State of Alabama Geotechnical Manual. https://www.dot.state.al.us/publications/Materials/pdf/ALDOTGeotechManual.pdf

Alabama Department of Transportation (2015). "Research Project for Soil Stabilization on SR-5 from the Dallas County Line to 0.15 Miles North of E. Goley Road (MP 54.850)." Plans of Proposed Project Number 990305-535-005-401.

Al-Akhras, N., Attom, M., Al-Akhras, K., & Malkawi, A. (2008). Influence of fibers on swelling properties of clayey soil. Geosynthetics International, 15(4), 304-309.

Al-Atroush, M., & Sebaey, T. (2021). Stabilization of expansive soil using hydrophobic polyurethane foam: A review. Transportation Geotechnics, 27, 100494.

Al-Gharbawi, A. S., Najemalden, A. M., & Fattah, M. Y. (2022). Expansive soil stabilization with lime, cement, and silica fume. Applied Sciences, 13(1), 436.

Al-Mhaidib, A., & Al-Shamrani, M. (1996). Swelling characteristics of lime-treated expansive soils. Geotechnical engineering, 27, 37-54.

Almuaythir, S., & Abbas, M. F. (2023). Expansive soil remediation using cement kiln dust as stabilizer. Case Studies in Construction Materials, 18, e01983.

Al-Mukhtar, M., Khattab, S., & Alcover, J.-F. (2012). Microstructure and geotechnical properties of lime-treated expansive clayey soil. Engineering geology, 139, 17-27.

Al-Mukhtar, M., Lasledj, A., & Alcover, J.-F. (2010). Behaviour and mineralogy changes in lime-treated expansive soil at 20 C. Applied clay science, 50(2), 191-198.

Al-Rawas, A. A., & Goosen, M. F. (2006). Expansive soils: recent advances in characterization and treatment.

Alsabhan, A. H., Qadri, J., Sadique, M. R., Alam, S., Perveen, K., & Binyahya, A. S. (2023). Soil stabilization using Silicon Carbide (SiC) nanoparticles: confirmation using XRD, SEM, and FTIR. Journal of Civil Engineering and Management, 29(3), 194–201-194–201.

Alsharef, J., Taha, M. R., Firoozi, A. A., & Govindasamy, P. (2016). Potential of using nanocarbons to stabilize weak soils. Applied and Environmental Soil Science, 2016.

Alshawabkeh, A. N., & Sheahan, T. C. (2003). Soft soil stabilisation by ionic injection under electric fields. Proceedings of the Institution of Civil Engineers-Ground Improvement, 7(4), 177-185.

Arumugham, T., Kaleekkal, N. J., Rana, D., & Doraiswamy, M. (2016). Separation of oil/water emulsions using nano MgO anchored hybrid ultrafiltration membranes for environmental abatement. Journal of applied polymer science, 133(1).

Association, P. C. (2003). Reflective cracking in cement stabilized pavements. Portland Cement Association.

ASTM 2166. (2016). Standard Test Method for Unconfined Compressive Strength of Cohesive Soil. ASTM International: West Conshohocken, PA, USA.

ASTM D4318. (2017). Standard Test Methods for Liquid Limit, Plastic Limit, and Plasticity Index of Soils. ASTM International: West Conshohocken, PA, USA.

ASTM D4546. (2014). Standard Test Methods for One-Dimensional Swell or Collapse of Soils. ASTM International, West Conshohocken, PA. https://doi.org/10.1520/D4546-14E01

ASTM D4767. (2011). Standard Test Method for Consolidated Undrained Triaxial Compression Test for Cohesive Soils. ASTM International: West Conshohocken, PA, USA.

ASTM D6913 / D6913. (2017). Standard Test Methods for Particle-Size Distribution (Gradation) of Soils Using Sieve Analysis. ASTM International: West Conshohocken, PA, USA.

ASTM D698. (2012). Standard Test Methods for Laboratory Compaction Characteristics of Soil Using Standard Effort (12 400 ft-lbf/ft3 (600 kN-m/m3)). ASTM International: West Conshohocken, PA, USA.

Ayodele, A. L., Pamukcu, S., Shrestha, R. A., & Agbede, O. A. (2018). Electrochemical soil stabilization and verification. Geotechnical and Geological Engineering, 36, 1283-1293.

Aziz, M., Saleem, M., & Irfan, M. (2015). Engineering behaviour of expansive soils treated with rice husk ash [J]. Geomechanics and Engineering, 8(2), 173-186.

Azzam, W. (2012). Reduction of the shrinkage–swelling potential with polymer nanocomposite stabilization. Journal of applied polymer science, 123(1), 299-306.

Bahmani, S. H., Huat, B. B., Asadi, A., & Farzadnia, N. (2014). Stabilization of residual soil using SiO2 nanoparticles and cement. Construction and building materials, 64, 350-359.

Bakharev, T., Sanjayan, J. G., & Cheng, Y.-B. (1999). Effect of elevated temperature curing on properties of alkali-activated slag concrete. Cement and concrete research, 29(10), 1619-1625.

Barman, D., & Dash, S. K. (2022). Stabilization of expansive soils using chemical additives: A review. Journal of Rock Mechanics and Geotechnical Engineering, 14(4), 1319-1342.

Barman, D., & Mishra, A. (2022). Influence of salt and initial conditions on the shrinkage limit of bentonite. International Journal of Geotechnical Engineering, 16(1), 64-73.

Basma, A. A., & Tuncer, E. R. (1991). Effect of lime on volume change and compressibility of expansive clays. Transportation research record(1295).

Begum, A. S., Prasada Raju, G., Prasad, D., & Anjan Kumar, M. (2020). Influence of TerraZyme on compaction and consolidation properties of expansive soil. In Problematic Soils and Geoenvironmental Concerns: Proceedings of IGC 2018 (pp. 525-535). Springer.

Belchior, I. M. R. M., Casagrande, M. D. T., & Zornberg, J. G. (2017). Swelling behavior evaluation of a lime-treated expansive soil through centrifuge test. Journal of Materials in Civil Engineering, 29(12), 04017240.

Bell, F. (1988). Stabilisation and treatment of clay soils with lime. Part 1-basic principles. Ground engineering, 21(1).

Bell, F. (1993). Engineering treatment of soils. CRC Press.

Bell, F. (1995). Cement stabilization and clay soils, with examples. Environmental & Engineering Geoscience, 1(2), 139-151.

Bell, F. G. (1996). Lime stabilization of clay minerals and soils. Engineering geology, 42(4), 223-237.

Bhuvaneshwari, S., Robinson, R., & Gandhi, S. (2014). Behaviour of lime treated cured expansive soil composites. Indian Geotechnical Journal, 44, 278-293.

Bhuvaneshwari, S., Robinson, R., & Gandhi, S. (2019). Resilient modulus of lime treated expansive soil. Geotechnical and Geological Engineering, 37, 305-315.

Bin-Shafique, S., Rahman, K., & Azfar, I. (2011). The effect of freezing-thawing cycles on performance of fly ash stabilized expansive soil subbases. In Geo-Frontiers 2011: Advances in Geotechnical Engineering (pp. 697-706).

Biswas, N., Chakraborty, S., Puppala, A. J., & Banerjee, A. (2021). A novel method to improve the durability of lime-treated expansive soil. Proceedings of the Indian Geotechnical Conference 2019: IGC-2019 Volume III,

Bjerrum, L., Moum, J., & Eide, O. (1967). Application of electro-osmosis to a foundation problem in a Norwegian quick clay. Geotechnique, 17(3), 214-235.

Blanck, G., Cuisinier, O., & Masrouri, F. (2014). Soil treatment with organic non-traditional additives for the improvement of earthworks. Acta Geotechnica, 9, 1111-1122.

Blight, G. E., & De Wet, J. A. (1965). The acceleration of heave by flooding. A symposium in print. Moisture Equilibria Moisture Changes in Soils Beneath Covered Areas.

Bonaparte, R., Holtz, R. D., & Giroud, J. (1987). Soil reinforcement design using geotextiles and geogrids. In Geotextile testing and the design engineer. ASTM International.

Bouatia, M., Demagh, R., & Derriche, Z. (2020). Structural behavior of pipelines buried in expansive soils under rainfall infiltration (Part I: transverse behavior). Civil Engineering Journal, 6(9), 1822-1838.

Brough, A., & Atkinson, A. (2002). Sodium silicate-based, alkali-activated slag mortars: Part I. Strength, hydration and microstructure. Cement and concrete research, 32(6), 865-879.

Bukhary, A., & Azam, S. (2024). Flow through and Volume Change Behavior of a Compacted Expansive Soil Amended with Natural Biopolymers. Geotechnics, 4(1), 322-336.

Buhler, R. L., & Cerato, A. B. (2007). Stabilization of Oklahoma expansive soils using lime and class C fly ash. In Problematic soils and rocks and in situ characterization (pp. 1-10).

Carraro, J. A. H., Dunham-Friel, J., & Smidt, M. (2010). Beneficial use of scrap tire rubber in low-volume road and bridge construction with expansive soils.

Casagrande, A. (1952). Electro-osmotic stabilization of soils. Boston Society Civil Engineers Journal.

Changizi, F., & Haddad, A. (2016). Effect of nano-SiO 2 on the geotechnical properties of cohesive soil. Geotechnical and Geological Engineering, 34, 725-733.

Chavali, R. V. P., & Reshmarani, B. (2020). Characterization of expansive soils treated with lignosulfonate. International Journal of Geo-Engineering, 11(1), 17.

Chegenizadeh, A., & Nikraz, H. (2011). Investigation on strength of fiber reinforced clay. Advanced Materials Research, 261, 957-963.

Chen, F. H. (2012). Foundations on expansive soils (Vol. 12). Elsevier.

Chen, S., Ni, P., Sun, Z., & Yuan, K. (2023). Geotechnical properties and stabilization mechanism of nano-MgO stabilized loess. Sustainability, 15(5), 4344.

Chen, X., Duan, M., Zhou, B., & Cui, L. (2022). Effects of biochar nanoparticles as a soil amendment on the structure and hydraulic characteristics of a sandy loam soil. Soil Use and Management, 38(1), 836-849.

Chew, S., Kamruzzaman, A., & Lee, F. (2004). Physicochemical and engineering behavior of cement treated clays. Journal of Geotechnical and Geoenvironmental Engineering, 130(7), 696-706.

Chien, S.-C., Ou, C.-Y., & Wang, M.-K. (2009). Injection of saline solutions to improve the electro-osmotic pressure and consolidation of foundation soil. Applied Clay Science, 44(3-4), 218-224.

Chien, S.-C., Ou, C.-Y., & Wang, Y.-K. (2004). Soil Improvement Using Electroosmotic Method With the Injection of Saline Solution. ISOPE International Ocean and Polar Engineering Conference,

Ching, R., & Fredlund, D. (1984). A small Saskatchewan town copes with swelling clay problems. Proceedings of the 5th International Conference on Expansive Soils,

Chitragar, S. F., Shivayogimath, C. B., & Mulangi, R. H. (2019). Study on strength and volume change behavior of expansive soil using non-traditional (bio-enzyme) and traditional (lime and bagasse ash) stabilizers. Geotechnics for Transportation Infrastructure: Recent Developments, Upcoming Technologies and New Concepts, Volume 2,

Choobbasti, A. J., Samakoosh, M. A., & Kutanaei, S. S. (2019). Mechanical properties soil stabilized with nano calcium carbonate and reinforced with carpet waste fibers. Construction and Building Materials, 211, 1094-1104.

Chun, M.-S. (2002). Electrokinetic flow velocity in charged slit-like microfluidic channels with linearized poisson-boltzmann field. Korean Journal of Chemical Engineering, 19, 729-734.

Cokca, E. (2001). Use of class c fly ashes for the stabilizationof an expansive soil. Journal of Geotechnical and Geoenvironmental Engineering, 127(7), 568-573.

Coo, J. L., So, Z. P., & Ng, C. W. (2016). Effect of nanoparticles on the shrinkage properties of clay. Engineering geology, 213, 84-88.

Correia, A. G., Winter, M., & Puppala, A. (2016). A review of sustainable approaches in transport infrastructure geotechnics. Transportation Geotechnics, 7, 21-28.

Cristelo, N., Vieira, C. S., & de Lurdes Lopes, M. (2016). Geotechnical and geoenvironmental assessment of recycled construction and demolition waste for road embankments. Procedia Engineering, 143, 51-58.

Croft, J. (1967). The influence of soil mineralogical composition on cement stabilization. Géotechnique, 17(2), 119-135.

Dafalla, M., Mutaz, E., & Al-Shamrani, M. (2015). Compressive strength variations of lime-treated expansive soils. In IFCEE 2015 (pp. 1402-1409).

Dakshanamurthy, V., & Raman, V. (1973). A simple method of identifying an expansive soil. Soils and Foundations, 13(1), 97-104.

Das, B. M., & Sivakugan, N. (2017). Fundamentals of geotechnical engineering. Cengage Learning.

Dash, S. K., & Hussain, M. (2012). Lime stabilization of soils: reappraisal. Journal of Materials in Civil Engineering, 24(6), 707-714.

Deka, S., Dash, S., & Sreedeep, S. (2015). Strength of Lime-Treated fly ash using bentonite. Geotechnical engineering, 46(3SI), 73-81.

Di Maio, C. (1996). Exposure of bentonite to salt solution: osmotic and mechanical effects. Géotechnique, 46(4), 695-707.

Diamond, S., White, J. L., & Dolch, W. L. (1963). Transformation of clay minerals by calcium hydroxide attack. Clays and clay minerals, 12, 359-379.

Dunham-Friel, J., & Carraro, J. A. H. (2011). Shear strength and stiffness of expansive soil and rubber (ESR) mixtures in undrained axisymmetric compression. In Geo-Frontiers 2011: Advances in Geotechnical Engineering (pp. 1111-1120).

Durotoye, T. O., Akinmusuru, J., Ogbiye, A., & Bamigboye, G. (2016). Effect of common salt on the engineering properties of expansive soil. International Journal of Engineering and Technology, 6(7), 233-241.

Dye, H. B. (2008). Moisture movement through expansive soil and impact on performance of residential structures. Arizona State University.

Esrig, M. I. (1968). Pore pressures, consolidation, and electrokinetics. Journal of the Soil Mechanics and foundations Division, 94(4), 899-921.

Esrig, M. I., & Gemeinhardt Jr, J. P. (1967). Electrokinetic stabilization of an illitic clay. Journal of the Soil Mechanics and Foundations Division, 93(3), 109-128.

Estabragh, A., Rafatjo, H., & Javadi, A. (2014). Treatment of an expansive soil by mechanical and chemical techniques. Geosynthetics International, 21(3), 233-243.

Estabragh, A., Soltani, A., & Javadi, A. (2016). Models for predicting the seepage velocity and seepage force in a fiber reinforced silty soil. Computers and Geotechnics, 75, 174-181.

Eykholt, G. R., & Daniel, D. E. (1994). Impact of system chemistry on electroosmosis in contaminated soil. Journal of geotechnical engineering, 120(5), 797-815.

Eyo, E. U., Ng'ambi, S., & Abbey, S. J. (2022). An overview of soil–water characteristic curves of stabilised soils and their influential factors. Journal of King Saud University-Engineering Sciences, 34(1), 31-45.

Federico, A., Vitone, C., & Murianni, A. (2015). On the mechanical behaviour of dredged submarine clayey sediments stabilized with lime or cement. Canadian geotechnical journal, 52(12), 2030-2040.

Felt, E. (1953). Influence of vegetation on soil moisture contents and resulting soil volume changes.

Fetzer, C. A. (1967). Electro-osmotic stabilization of west branch dam. Journal of the Soil Mechanics and foundations Division, 93(4), 85-106.

Fondjo, A. A., Theron, E., & Ray, R. P. (2021). Stabilization of expansive soils using mechanical and chemical methods: a comprehensive review. Civ Eng Archit, 9(5), 1295-1308.

Frank, H. S., andW. Y.Wen. 1957. “Structural Aspects of Ion-Solvent Interaction in Aqueous Solutions: A Suggested Picture of Water Structures.” Faraday Society Discussions 24, 133–140.

Fredlund, D. G., & Rahardjo, H. (1993). Soil mechanics for unsaturated soils. John Wiley & Sons.

Fredlund, D. G., Sheng, D., & Zhao, J. (2011). Estimation of soil suction from the soil-water characteristic curve. Canadian geotechnical journal, 48(2), 186-198.

Fu, H., Yuan, L., Wang, J., Cai, Y., Hu, X., & Geng, X. (2019). Influence of high voltage gradients on electrokinetic dewatering for Wenzhou clay slurry improvement. Soil Mechanics and Foundation Engineering, 55, 400-407.

Gallage, C. P. K., Chan, D., & Kodikara, J. (2012). Response of a plastic pipe buried in expansive clay. Proceedings of the Institution of Civil Engineers-Geotechnical Engineering, 165(1), 45-57.

Gallo, A., Sprocati, R., Rolle, M., & Sethi, R. (2022). Electrokinetic delivery of permanganate in clay inclusions for targeted contaminant degradation. Journal of Contaminant Hydrology, 251, 104102.

Galvín, A. P., López-Uceda, A., Cabrera, M., Rosales, J., & Ayuso, J. (2021). Stabilization of expansive soils with biomass bottom ashes for an eco-efficient construction. Environmental Science and Pollution Research, 28, 24441-24454.

Gao, L., Ren, K.-y., Ren, Z., & Yu, X.-j. (2018). Study on the shear property of nano-MgO-modified soil. Marine Georesources & Geotechnology, 36(4), 465-470.

Ghasabkolaei, N., Janalizadeh, A., Jahanshahi, M., Roshan, N., & Ghasemi, S. E. (2016). Physical and geotechnical properties of cement-treated clayey soil using silica nanoparticles: An experimental study. The European Physical Journal Plus, 131, 1-11.

Ghasemipanah, A., Moayed, R. Z., & Niroumand, H. (2014). Effect of nanobentonite particles on geotechnical properties of Kerman clay. International Journal of Geotechnical and Geological Engineering, 14(1), 34-39.

Ghavami, S., Farahani, B., Jahanbakhsh, H., & Moghadas Nejad, F. (2018). Effects of silica fume and nano-silica on the engineering properties of kaolinite clay. AUT Journal of Civil Engineering, 2(2), 135-142.

Gleason, M. H., Daniel, D. E., & Eykholt, G. R. (1997). Calcium and sodium bentonite for hydraulic containment applications. Journal of Geotechnical and Geoenvironmental Engineering, 123(5), 438-445.

Goode, J. C. (1982). Heave prediction and moisture migration beneath slabs on expansive soils Colorado State University.

Ghorbani, Z., Khosravi, A., Maghsoudi, Y., & Voosoghi, B. (2024). InSAR Measurements for Landslide-Induced Damage Assessment on Part of North Alabama Highway, Morgan County. In Geo-Congress 2024 (pp. 523-532).

Gratchev, I. B., & Sassa, K. (2009). Cyclic behavior of fine-grained soils at different pH values. Journal of Geotechnical and Geoenvironmental Engineering, 135(2), 271-279.

Gray, D. H., & Mitchell, J. K. (1967). Fundamental aspects of electro-osmosis in soils. Journal of the Soil Mechanics and foundations Division, 93(6), 209-236.

Grim, R.E. (1968) Clay Mineralogy. McGraw-Hill, New York.

Gromko, G. J. (1974). Review of expansive soils. Journal of the Geotechnical Engineering Division, 100(6), 667-687.

Hamberg, D. J. (1985). A simplified method for predicting heave in expansive soils Colorado State University].

Hamid, W., Lemboye, K., & Dhowian, A. (2022). Characteristics and treatment of expansive soil using biopolymer. Arabian Journal of Geosciences, 15(5), 411.

Hamilton, J. (1965). Shallow foundations on swelling clays in Western Canada. National Research Council of Canada.

Han, D., Wu, X., Li, R., Tang, X., Xiao, S., & Scholz, M. (2021). Critical review of electro-kinetic remediation of contaminated soils and sediments: mechanisms, performances and technologies. Water, Air, & Soil Pollution, 232(8), 335.

Harris, M. C. (1997). Soil Survey of Perry County, Alabama.

Hart, S. S. (1974). Potentially swelling soil and rock in the front range urban corridor, Colorado. Colorado Geological Survey Publications.

Herzog, A., & Mitchell, J. K. (1963). Reactions accompanying stabilization of clay with cement. Highway Research Record(36).

Higgins, D. (2007). Briefing: GGBS and sustainability.

Holtz, W. G. (1959). Expansive clays--properties and problems. Commissioner's Office, Bureau of Reclamation, United States Department of the Interior.

Holtz, W. G., & Gibbs, H. J. (1956). Engineering properties of expansive clays. Transactions of the American Society of Civil Engineers, 121(1), 641-663.

Horpibulsuk, S., Phetchuay, C., & Chinkulkijniwat, A. (2012). Soil stabilization by calcium carbide residue and fly ash. Journal of Materials in Civil Engineering, 24(2), 184-193.

Horpibulsuk, S., Rachan, R., Chinkulkijniwat, A., Raksachon, Y., & Suddeepong, A. (2010). Analysis of strength development in cement-stabilized silty clay from microstructural considerations. Construction and building materials, 24(10), 2011-2021.

Hou, P., Wang, K., Qian, J., Kawashima, S., Kong, D., & Shah, S. P. (2012). Effects of colloidal nanoSiO2 on fly ash hydration. Cement and Concrete Composites, 34(10), 1095-1103.

Houston, S. L., Dye, H. B., Zapata, C. E., Walsh, K. D., & Houston, W. N. (2011). Study of expansive soils and residential foundations on expansive soils in Arizona. Journal of performance of constructed facilities, 25(1), 31-44.

Houston, S. L., Bharadwaj, A., Welfert, B., Houston, W. N., & Walsh, K. D. (2016). Unsaturated soil mechanics principles to remove and replace mitigation for expansive clays. Journal of Geotechnical and Geoenvironmental Engineering, 142(4), 04015102.

Hu, H., Qiu, Y., Lu, Z., Tang, C., Yao, H., & Cheng, M. (2022). Polyetheramine as swelling-inhibitor for expansive soil: Performance and mechanism. Journal of applied polymer science, 139(10), 51639.

Hussain, A. A., Kamran, K., Hina, M., Ishaq, M., Naz, M. Y., Bashir, S., Sarwar, N., & Quazi, M. M. (2023). Effect of electrokinetic treatment time on energy consumption and salt ions removal from clayey soils. Materials Research Express, 10(5), 055505.

Hussain, R., Ravi, K., & Garg, A. (2020). Influence of biochar on the soil water retention characteristics (SWRC): Potential application in geotechnical engineering structures. Soil and Tillage Research, 204, 104713.

Indraratna, B., Muttuvel, T., Khabbaz, H., & Armstrong, R. (2008). Predicting the erosion rate of chemically treated soil using a process simulation apparatus for internal crack erosion. Journal of Geotechnical and Geoenvironmental Engineering, 134(6), 837-844.

Ikeagwuani, C. C., & Nwonu, D. C. (2019). Emerging trends in expansive soil stabilisation: A review. Journal of rock mechanics and geotechnical engineering, 11(2), 423-440.

Iranpour, B. (2016). The influence of nanomaterials on collapsible soil treatment. Engineering geology, 205, 40-53.

Ito, M., & Azam, S. (2013). Engineering properties of a vertisolic expansive soil deposit. Engineering Geology, 152(1), 10-16.

Jackson, D. T. (2016). Insitu Measurement of Pavement Distress and Causal Mechanisms in Expansive Soil along Alabama Highway 5 Auburn University].

Jain, A. K., & Jha, A. K. (2020). Geotechnical behaviour and micro-analyses of expansive soil amended with marble dust. Soils and Foundations, 60(4), 737-751.

Jain, A., Choudhary, A. K., & Jha, J. (2020). Influence of rice husk ash on the swelling and strength characteristics of expansive soil. Geotechnical and Geological Engineering, 38(2), 2293-2302.

Jamsawang, P., Adulyamet, B., Voottipruex, P., Jongpradist, P., Likitlersuang, S., & Tantayopin, K. (2023). The free swell potential of expansive clays stabilized with the shallow bottom ash mixing method. Engineering geology, 315, 107027.

Jamshidi, R. J., Lake, C. B., Gunning, P., & Hills, C. D. (2016). Effect of freeze/thaw cycles on the performance and microstructure of cement-treated soils. Journal of Materials in Civil Engineering, 28(12), 04016162.

Jayasekera, S. (2015). Electrokinetics to modify strength characteristics of soft clayey soils: a laboratory based investigation. Electrochimica Acta, 181, 39-47.

Jeans, C. (1998). MOORE, DM & REYNOLDS, RC, Jr. 1997. X-Ray Diffraction and the Identification and Analysis of Clay Minerals, xviii+ 378 pp. Oxford, New York: Oxford University Press. Price£ 27.95 (spiral-bound paperback). ISBN 0 19 508713 5. Geological Magazine, 135(6), 819-842.

Ji-ru, Z., & Xing, C. (2002). Stabilization of expansive soil by lime and fly ash. Journal of Wuhan University of Technology-Mater. Sci. Ed., 17(4), 73-77.

Johnson, L. D. (1979). Overview for design of foundations on expansive soils.

Jones Jr, D. E., & Holtz, W. G. (1973). Expansive soils-the hidden disaster. Civil engineering, 43(8).

Jones Jr, D.E. and W.G. Holtz, Expansive soils-the hidden disaster. Civil engineering, 1973. 43(8).

Jones, D. T. (2017). Moisture Content Monitoring using a Nuclear Moisture Gauge and Preliminary Findings at Alabama Highway 5 Auburn University].

Jones, L. D., & Jefferson, I. (2012). Expansive soils.

Kalhor, A., Ghazavi, M., Roustaei, M., & Mirhosseini, S. (2019). Influence of nano-SiO2 on geotechnical properties of fine soils subjected to freeze-thaw cycles. Cold Regions Science and Technology, 161, 129-136.

Karumanchi, M., Avula, G., Pangi, R., & Sirigiri, S. (2020). Improvement of consistency limits, specific gravities, and permeability characteristics of soft soil with nanomaterial: Nanoclay. Materials Today: Proceedings, 33, 232-238.

Kennedy, L. P. (2019). Drained Residual Strength of Expansive Soils Causing Pavement Distress along Alabama Highway 5 Auburn University.

Khan, T. A., Taha, M. R., Khan, M. M., Shah, S. A. R., Aslam, M. A., Waqar, A., Khan, A. R., & Waseem, M. (2020). Strength and volume change characteristics of clayey soils: Performance evaluation of enzymes. Minerals, 10(1), 52.

Khattab, S., Al-Mukhtar, M., & Fleureau, J.-M. (2007). Long-term stability characteristics of a lime-treated plastic soil. Journal of Materials in Civil Engineering, 19(4), 358-366.

Khodaparast, M., Rajabi, A. M., & Mohammadi, M. (2021). Mechanical properties of silty clay soil treated with a mixture of lime and zinc oxide nanoparticles. Construction and Building Materials, 281, 122548.

Khosravi, A., & McCartney, J. S. (2012). Impact of hydraulic hysteresis on the small-strain shear modulus of low plasticity soils. Journal of Geotechnical and Geoenvironmental Engineering, 138(11), 1326-1333.

Khorshidi, M., & Lu, N. (2017). Intrinsic relation between soil water retention and cation exchange capacity. Journal of Geotechnical and Geoenvironmental Engineering, 143(4), 04016119.

Kim, S.-O., Moon, S.-H., & Kim, K.-W. (2001). Removal of heavy metals from soils using enhanced electrokinetic soil processing. Water, Air, and Soil Pollution, 125, 259-272.

King, D. J., Bouazza, A., Gniel, J. R., Rowe, R. K., & Bui, H. H. (2017). Serviceability design for geosynthetic reinforced column supported embankments. Geotextiles and Geomembranes, 45(4), 261-279.

Kolias, S., Kasselouri-Rigopoulou, V., & Karahalios, A. (2005). Stabilisation of clayey soils with high calcium fly ash and cement. Cement and Concrete Composites, 27(2), 301-313.

Kong, R., Zhang, F., Wang, G., & Peng, J. (2018). Stabilization of loess using nano-SiO2. Materials, 11(6), 1014.

RoKrishnan, J., & Shukla, S. (2019). The behaviour of soil stabilised with nanoparticles: an extensive review of the present status and its applications. Arabian Journal of Geosciences, 12(14), 436.

Krishnan, J., & Shukla, S. (2019). The behaviour of soil stabilised with nanoparticles: an extensive review of the present status and its applications. Arabian Journal of Geosciences, 12(14), 436.

Krohn, J. P., & JE, S. (1980). Assessment of Expansive Soils with the United States.

Kukko, H. (2000). Stabilization of clay with inorganic by-products. Journal of Materials in Civil Engineering, 12(4), 307-309.

Kulanthaivel, P., Soundara, B., Velmurugan, S., & Naveenraj, V. (2021). Experimental investigation on stabilization of clay soil using nano-materials and white cement. Materials Today: Proceedings, 45, 507-511.

Kumar Sharma, A., & Sivapullaiah, P. (2012). Improvement of strength of expansive soil with waste granulated blast furnace slag. In GeoCongress 2012: State of the Art and Practice in Geotechnical Engineering (pp. 3920-3928).

Kumar, A., & Gupta, D. (2016). Behavior of cement-stabilized fiber-reinforced pond ash, rice husk ash–soil mixtures. Geotextiles and Geomembranes, 44(3), 466-474.

Kumar, A., Walia, B. S., & Bajaj, A. (2007). Influence of fly ash, lime, and polyester fibers on compaction and strength properties of expansive soil. Journal of Materials in Civil Engineering, 19(3), 242-248.

Kumar, K., & Thyagaraj, T. (2020). Stabilization of Expansive Soil Using Lime Pile and Lime Precipitation Techniques—A Comparative Study. Geo-Congress 2020,

Kumar, K., & Thyagaraj, T. (2021). Comparison of lime treatment techniques for deep stabilization of expansive soils. International Journal of Geotechnical Engineering, 15(8), 1021-1039.

Kushwaha, S., Kishan, D., & Dindorkar, N. (2018). Stabilization of expansive soil using eko soil enzyme for highway embankment. Materials Today: Proceedings, 5(9), 19667-19679.

Kuttah, D., & Sato, K. (2015). Review on the effect of gypsum content on soil behavior. Transportation Geotechnics, 4, 28-37.

Lamb, D. R. (1973). Summary of Proceedings of Workshop on Expansive Clays and Shales in Highway Design and Construction. US Government Printing Office.

Lambe, T. W. (1960). character and identification of expansive soils.

Lambe, T.W. 1958. "The Structure of Compacted Clay." Journal of the Soil Mechanics and Foundations Division, ASCE 84(SM2): 1654-1–1654-34.

Lang, L., Chen, B., & Duan, H. (2021). Modification of nanoparticles for the strength enhancing of cement-stabilized dredged sludge. Journal of Rock Mechanics and Geotechnical Engineering, 13(3), 694-704.

Le, T. M., Dang, L. C., & Khabbaz, H. (2019). Strength characteristics of lime and bottom ash reinforced expansive soils. Eighth International Conference on Case Histories in Geotechnical Engineering,

Lear, G., Harbottle, M. J., Van Der Gast, C., Jackman, S., Knowles, C., Sills, G., & Thompson, I. (2004). The effect of electrokinetics on soil microbial communities. Soil Biology and Biochemistry, 36(11), 1751-1760.

Little, D. N. (1995). Stabilization of pavement subgrades and base courses with lime.

Little, D. N., & Nair, S. (2009). Recommended practice for stabilization of subgrade soils and base materials.

Little, D. N., Males, E. H., Prusinski, J. R., & Stewart, B. (2000). Cementitious stabilization. Transportation in the new millennium.

Liu, C., Zhang, Q., Zhao, C., Deng, L., & Fang, Q. (2023). Assessment of strength development of soil stabilized with cement and nano SiO2. Construction and building materials, 409, 133889.

Liu, J., Wang, Y., Lu, Y., Feng, Q., Zhang, F., Qi, C., Wei, J., & Kanungo, D. P. (2017). Effect of Polyvinyl Acetate Stabilization on the Swelling-Shrinkage Properties of Expansive Soil. International Journal of Polymer Science, 2017(1), 8128020.

Liu, Y., & Vanapalli, S. K. (2017). Influence of lateral swelling pressure on the geotechnical infrastructure in expansive soils. Journal of Geotechnical and Geoenvironmental Engineering, 143(6), 04017006.

Liu, Y., Chang, C.-W., Namdar, A., She, Y., Lin, C.-H., Yuan, X., & Yang, Q. (2019). Stabilization of expansive soil using cementing material from rice husk ash and calcium carbide residue. Construction and Building Materials, 221, 1-11.

Liu, Y., Bouazza, A., Gates, W., & Rowe, R. (2015). Hydraulic performance of geosynthetic clay liners to sulfuric acid solutions. Geotextiles and Geomembranes, 43(1), 14-23.

Lockhart, N. C., & Stickland, R. E. (1984). Dewatering coal washery tailings ponds by electroosmosis. Powder Technology, 40(1-3), 215-221.

López-Vizcaíno, R., Dos Santos, E. V., Yustres, A., Rodrigo, M., Navarro, V., & Martinez-Huitle, C. A. (2019). Calcite buffer effects in electrokinetic remediation of clopyralid-polluted soils. Separation and Purification Technology, 212, 376-387.

Luo, X., Kong, L., Bai, W., & Jian, T. (2022). Effect of superhydrophobic nano-SiO2 on the geotechnical characteristics of expansive soil. Journal of Testing and Evaluation, 50(6), 2932-2947.

Madhyannapu, R. S., & Puppala, A. J. (2014). Design and construction guidelines for deep soil mixing to stabilize expansive soils. Journal of Geotechnical and Geoenvironmental Engineering, 140(9), 04014051.

Ma, C., Chen, B., & Chen, L. (2018). Experimental feasibility research on a high-efficiency cement-based clay stabilizer. KSCE Journal of Civil Engineering, 22, 62-72.

Ma, S., Ma, M., Huang, Z., Hu, Y., & Shao, Y. (2023). Research on the improvement of rainfall infiltration behavior of expansive soil slope by the protection of polymer waterproof coating. Soils and Foundations, 63(3), 101299.

Malekzadeh, M., Lovisa, J., & Sivakugan, N. (2016). An overview of electrokinetic consolidation of soils. Geotechnical and Geological Engineering, 34, 759-776.

Mahedi, M., Cetin, B., & White, D. J. (2018). Performance evaluation of cement and slag stabilized expansive soils. Transportation research record, 2672(52), 164-173.

MANUAL, C. (2004). Lime-Treated Soil Construction Manual Lime Stabilization & Lime Modification. published by National Lime Association, USA, Bulletin, 326.

Mao, X., Shao, X., Zhang, Z., & Han, F. (2018). Mechanism and optimization of enhanced electro-kinetic remediation on 137Cs contaminated kaolin soils: a semi-pilot study based on experimental and modeling methodology. Electrochimica Acta, 284, 38-51.

Marasteanu, M. O., Hozalski, R. M., Clyne, T. R., & Velasquez, R. (2005). Preliminary laboratory investigation of enzyme solutions as a soil stabilizer.

Martin, L., Alizadeh, V., & Meegoda, J. (2019). Electro-osmosis treatment techniques and their effect on dewatering of soils, sediments, and sludge: A review. Soils and Foundations, 59(2), 407-418.

Masi, M., Ceccarini, A., & Iannelli, R. (2017a). Model-based optimization of field-scale electrokinetic treatment of dredged sediments. Chemical Engineering Journal, 328, 87-97.

Masi, M., Ceccarini, A., & Iannelli, R. (2017b). Multispecies reactive transport modelling of electrokinetic remediation of harbour sediments. Journal of hazardous materials, 326, 187-196.

McCarthy, M. J., Csetenyi, L. J., Sachdeva, A., & Dhir, R. K. (2012). Fly ash influences on sulfate-heave in lime-stabilised soils. Proceedings of the Institution of Civil Engineers-Ground Improvement, 165(3), 147-158.

McCarthy, M. J., Csetenyi, L. J., Sachdeva, A., & Dhir, R. K. (2014). Engineering and durability properties of fly ash treated lime-stabilised sulphate-bearing soils. Engineering geology, 174, 139-148.

McDowell, C. (1965). Remedial procedures used in the reduction of detrimental effects of swelling soils.

Mehmood, M., Guo, Y., Liu, Y., & Uge, B. U. (2023). Modification of Expansive Soil Characteristics by Employing Agro-waste Eggshell Powder: An Experimental Study. Iranian Journal of Science and Technology, Transactions of Civil Engineering, 1-16.

Melese, D. T. (2022). Utilization of waste incineration bottom ash to enhance engineering properties of expansive subgrade soils. Advances in Civil Engineering, 2022(1), 7716921.

Mir, B. A., & Sridharan, A. (2019). Mechanical behaviour of fly-ash-treated expansive soil. Proceedings of the Institution of Civil Engineers-Ground Improvement, 172(1), 12-24.

Misra, A. (1998). Stabilization characteristics of clays using class C fly ash. Transportation research record, 1611(1), 46-54.

Mitchell, J. K., & Soga, K. (2005). Fundamentals of soil behavior (Vol. 3). John Wiley & Sons New York.

Mitchell, T., & Raad, L. (1973). Control of volume changes in expansive earth materials. Publication of: Frost I Jord/Norway/, 2(Workshop Proceedings).

Miura, N., Horpibulsuk, S., & Nagaraj, T. (2001). Engineering behavior of cement stabilized clay at high water content. Soils and Foundations, 41(5), 33-45.

Moayed, R. Z., & Rahmani, H. (2017). Effect of Nano-SiO2 solution on the strength characteristics of Kaolinite. International Journal of Geotechnical and Geological Engineering, 11(1), 83-87.

Moore, D. M., and Reynolds, R. C. (1997). X-Ray diffraction and the identification and analysis of clay minerals, 2nd Ed., Oxford University Press, London.

Mujtaba, H., Aziz, T., Farooq, K., Sivakugan, N., & Das, B. M. (2018). Improvement in engineering properties of expansive soils using ground granulated blast furnace slag. Journal of the Geological Society of India, 92, 357-362.

Murgulet, D. (2009). Black Belt Irrigation Report [Map]. Geological Survey of Alabama. https://www.gsa.state.al.us/downloads/sgap/Blackbelt%20Irrigation/Black%20Belt%20Irrigation%20Report%20with%20Plates/Plate%204.pdf.

Nalbantoglu, Z. (2006). Lime stabilization of expansive clay. In Expansive Soils (pp. 353-360). CRC Press.

Nalbantoglu, Z., & Tuncer, E. R. (2001). Compressibility and hydraulic conductivity of a chemically treated expansive clay. Canadian geotechnical journal, 38(1), 154-160.

Nath, B. D., Molla, M. K. A., & Sarkar, G. (2017). Study on strength behavior of organic soil stabilized with fly ash. International scholarly research notices, 2017(1), 5786541.

National Lime Association (NLA). 2004. “Lime-Treated Soil Construction Manual: Lime Stabilization and Lime Modification.” Bulletin 326, National Lime Association

Naval, S., Chandan, K., & Sharma, D. (2017). Stabilization of expansive soil using nanomaterials. Proceedings of the International Interdisciplinary Conference on Science Technology Engineering Management Pharmacy and Humanities, Singapore,

Nelson, J. D., Chao, K. C., Overton, D. D., & Nelson, E. J. (2015). Foundation engineering for expansive soils. John Wiley & Sons.

Nelson, J., & Miller, D. J. (1997). Expansive soils: problems and practice in foundation and pavement engineering. John Wiley & Sons.

Nettleton, A. (1960). The electrical treatment of kaolinite. Proceedings of the 3rd Australia-New Zealand Conference on Soil Mechanics and Foundation Engineering,

Ng, C. W. W., & Coo, J. L. (2015). Hydraulic conductivity of clay mixed with nanomaterials. Canadian Geotechnical Journal, 52(6), 808-811.

Nicholson, P. G., & Kashyap, V. (1993). Flyash stabilization of tropical Hawaiian soils. Fly ash for soil improvement. ASCE Geotechnical special publication no. 36.

Nordin, N., Tajudin, S. A., & Kadir, A. A. (2013). Stabilisation of soft soil using electrokinetic stabilisation method. International Journal of Zero Waste Generation, 1(1), 5-12.

Norrish, K. 1954. "The Swelling of Montmorillonite." Discussions of the Faraday Society 18, 120–134.

Olive, W., Chleborad, A., Frahme, C., Schlocker, J., Schneider, R., & Schuster, R. (1989). Swelling clays map of the conterminous United States. https://ngmdb.usgs.gov/Prodesc/proddesc_10014.htm.

Onur, M. I., Tuncan, M., Evirgen, B., Ozdemir, B., & Tuncan, A. (2016). Behavior of soil reinforcements in slopes. Procedia Engineering, 143, 483-489.

Önal, O. (2015). Lime stabilization of soils underlying a salt evaporation pond: a laboratory study. *Marine Georesources & Geotechnology*, *33*(5), 391-402.

Ou, C.-Y., Chien, S.-C., Syue, Y.-T., & Chen, C.-T. (2018). A novel electroosmotic chemical treatment for improving the clay strength throughout the entire region. Applied clay science, 153, 161-171.

Palmeira, E. M. (2009). Soil–geosynthetic interaction: Modelling and analysis. Geotextiles and Geomembranes, 27(5), 368-390.

Pamukcu, S., & Kenneth Wittle, J. (1992). Electrokinetic removal of selected heavy metals from soil. Environmental Progress, 11(3), 241-250.

Pandey, P., Hossain, M. S., & Ahmed, A. (2021). Performance evaluation of modified moisture barrier in mitigating expansive soil associated pavement distresses. Transportation Geotechnics, 31, 100667.

Park, J., Vipulanandan, C., Kim, J. W., & Oh, M. H. (2006). Effects of surfactants and electrolyte solutions on the properties of soil. Environmental geology, 49, 977-989.

Parsons, R. L., & Milburn, J. P. (2003). Engineering behavior of stabilized soils. Transportation research record, 1837(1), 20-29.

Patrick, D. M., & Snethen, D. R. (1976). An occurrence and distribution survey of expansive materials in the United States by physiographic areas.

Peck, R. B., Hanson, W. E., & Thornburn, T. H. (1991). Foundation engineering. John Wiley & Sons.

Pedarla, A., Chittoori, S., & Puppala, A. J. (2011). Influence of mineralogy and plasticity index on the stabilization effectiveness of expansive clays. Transportation research record, 2212(1), 91-99.

Peethamparan, S., Olek, J., & Diamond, S. (2008). Physicochemical behavior of cement kiln dust–treated kaolinite clay. Transportation research record, 2059(1), 80-88.

Petry, T. M., & Little, D. N. (2002). Review of stabilization of clays and expansive soils in pavements and lightly loaded structures—history, practice, and future. Journal of Materials in Civil Engineering, 14(6), 447-460.

Phani Kumar, B., & Sharma, R. S. (2004). Effect of fly ash on engineering properties of expansive soils. Journal of Geotechnical and Geoenvironmental Engineering, 130(7), 764-767.

Phanikumar, B., & e, R. R. (2020). Silica fume stabilization of an expansive clay subgrade and the effect of silica fume-stabilised soil cushion on its CBR. Geomechanics and Geoengineering, 15(1), 64-77.

Phanikumar, B., & Singla, R. (2016). Swell-consolidation characteristics of fibre-reinforced expansive soils. Soils and Foundations, 56(1), 138-143.

Portland Cement Association, 2003. Reflective Cracking in Cement Stabilized Pavements. Portland Cement Association.

Pooni, J., Giustozzi, F., Robert, D., Setunge, S., & O'Donnell, B. (2019). Durability of enzyme stabilized expansive soil in road pavements subjected to moisture degradation. Transportation Geotechnics, 21, 100255.

Pooni, J., Robert, D., Gunasekara, C., Giustozzi, F., & Setunge, S. (2021). Mechanism of enzyme stabilization for expansive soils using mechanical and microstructural investigation. International Journal of Geomechanics, 21(10), 04021191.

Prusinski, J. R., & Bhattacharja, S. (1999). Effectiveness of Portland cement and lime in stabilizing clay soils. Transportation research record, 1652(1), 215-227.

Puppala, A. J., & Musenda, C. (2000). Effects of fiber reinforcement on strength and volume change in expansive soils. Transportation research record, 1736(1), 134-140.

Puppala, A. J., Punthutaecha, K., & D'Souza, N. (2002, January). Assessments of Fly Ash and Bottom Ash Stabilization Methods on Soft and Natural Expansive Soils. In *Proceedings of the International Conference on Advances in Civil Engineering, Indian Institute of Technology, Kharagpur, India* (pp. 3-5).

Puppala, A. J., Wattanasanticharoen, E., & Hoyos, L. R. (2003). Ranking of four chemical and mechanical stabilization methods to treat low-volume road subgrades in Texas. Transportation research record, 1819(1), 63-71.

Puppala, A. J., Punthutaecha, K., & Vanapalli, S. K. (2006). Soil-water characteristic curves of stabilized expansive soils. Journal of Geotechnical and Geoenvironmental Engineering, 132(6), 736-751.

Puppala, A. J., Wattanasanticharoen, E., & Hoyos, L. R. (2003). Ranking of four chemical and mechanical stabilization methods to treat low-volume road subgrades in Texas. Transportation research record, 1819(1), 63-71.

Puppala, A. J. (2021). Performance evaluation of infrastructure on problematic expansive soils: Characterization challenges, innovative stabilization designs, and monitoring methods. Journal of Geotechnical and Geoenvironmental Engineering, 147(8), 04021053.

Puppala, A. J. (2021). Case Studies of Problematic Expansive Soils: Characterization Challenges, Innovative Stabilization Designs, and Novel Monitoring Methods.

Raj Singh, P., Kanvinde, A., & Narasimhan, S. (2021). Assessing the fracture risk of corroded cast-iron pipes in expansive soils. Journal of Pipeline Systems Engineering and Practice, 12(4), 04021041.

Rajabi, A. M., Ardakani, S. B., & Abdollahi, A. H. (2021). The effect of nano-iron oxide on the strength and consolidation parameters of a clay soil: an experimental study. Iranian Journal of Science and Technology, Transactions of Civil Engineering, 45(3), 1759-1768.

Rajasekaran, G. (2005). Sulphate attack and ettringite formation in the lime and cement stabilized marine clays. Ocean engineering, 32(8-9), 1133-1159.

Rajasekaran, G., & Rao, S. N. (2002). Compressibility behaviour of lime-treated marine clay. Ocean engineering, 29(5), 545-559.

Rajoria, V., & Kaur, S. (2014). A review on stabilization of soil using bio-enzyme. International Journal of Research in Engineering and Technology, 3(1), 75-78.

Ramon, A., & Alonso, E. (2013). Analysis of ettringite attack to stabilized railway bases and embankments. Proceedings of the 18th international conference on soil mechanics and geotechnical engineering, Paris,

Rauch, A. F., Harmon, J. S., Katz, L. E., & Liljestrand, H. M. (2002). Measured effects of liquid soil stabilizers on engineering properties of clay. Transportation research record, 1787(1), 33-41.

Rauch, A. F., Katz, L. E., & Liljestrand, H. M. (2003). An analysis of the mechanisms and efficacy of three liquid chemical soil stabilizers. Center for Transportation Research, The University of Texas at Austin.

Reddy, K. R., & Cameselle, C. (2009). Electrochemical remediation technologies for polluted soils, sediments and groundwater. John Wiley & Sons.

Reddy, K. R., & Saichek, R. E. (2004). Enhanced electrokinetic removal of phenanthrene from clay soil by periodic electric potential application. Journal of Environmental Science and Health, Part A, 39(5), 1189-1212.

Reddy, K. R., Parupudi, U. S., Devulapalli, S. N., & Xu, C. Y. (1997). Effects of soil composition on the removal of chromium by electrokinetics. Journal of hazardous materials, 55(1-3), 135-158.

Rittirong, A. (2007). Soil stabilization using electrokinetics Faculty of Graduate Studies, University of Western Ontario].

Rosales, J., Agrela, F., Marcobal, J. R., Diaz-López, J. L., Cuenca-Moyano, G. M., Caballero, Á., & Cabrera, M. (2020). Use of nanomaterials in the stabilization of expansive soils into a road real-scale application. Materials, 13(14), 3058.

Saad, B. (2014). Analysis of excess water impact on the structural performance of flexible pavements. International Journal of Pavement Engineering, 15(5), 409-426.

Sadiq, A., Fattah, M. Y., & Aswad, M. F. (2023). Enhancement of the acid resistance of silty clay using nano-magnesium oxide. Materials, 16(14), 5035.

Sahoo, J. P., & Pradhan, P. K. (2010). Effect of lime stabilized soil cushion on strength behaviour of expansive soil. Geotechnical and Geological Engineering, 28, 889-897.

Sakr, M. A., Omar, A. E., Saad, A. M., & Moayedi, H. (2021). Geotechnical parameters modelling and the radiation safety of expansive clayey soil treated with waste marble powder: a case study at west Gulf of Suez, Egypt. Environmental Earth Sciences, 80, 1-18.

Salahudeen, A., Eberemu, A. O., & Osinubi, K. J. (2014). Assessment of cement kiln dust-treated expansive soil for the construction of flexible pavements. Geotechnical and Geological Engineering, 32, 923-931.

Samala, H. R., & Mir, B. (2020). Some studies on microstructural behaviour and unconfined compressive strength of soft soil treated with SiO 2 nanoparticles. Innovative Infrastructure Solutions, 5, 1-12.

Santoni, R. L., Tingle, J. S., & Nieves, M. (2005). Accelerated strength improvement of silty sand with nontraditional additives. Transportation research record, 1936(1), 34-42.

Santoni, R. L., Tingle, J. S., & Webster, S. L. (2002). Stabilization of silty sand with nontraditional additives. Transportation research record, 1787(1), 61-70.

Sapkota, A. (2019). Effect of Modified Moisture Barriers on Slopes Stabilized with Recycled Plastic Pins. The University of Texas at Arlington.

Sarker, D., Apu, O. S., Kumar, N., Wang, J. X., & Lynam, J. G. (2023). Sustainable lignin to enhance engineering properties of unsaturated expansive subgrade soils. Journal of Materials in Civil Engineering, 35(8), 04023259.

Saride, S., Puppala, A. J., & Chikyala, S. R. (2013). Swell-shrink and strength behaviors of lime and cement stabilized expansive organic clays. Applied Clay Science, 85, 39-45.

Sarker, D., Shahrear Apu, O., Kumar, N., Wang, J. X., & Lynam, J. G. (2021). Application of sustainable lignin stabilized expansive soils in highway subgrade. In IFCEE 2021 (pp. 336-348).

Scholen, D. E. (1992). Non-standard stabilizers.

Seco, A., Ramírez, F., Miqueleiz, L., & García, B. (2011). Stabilization of expansive soils for use in construction. Applied clay science, 51(3), 348-352.

Seed, H. B., Woodward Jr, R. J., & Lundgren, R. (1962). Prediction of swelling potential for compacted clays. Journal of the Soil Mechanics and Foundations Division, 88(3), 53-87.

Shang, J. Q. (1997). Electokinetic dewatering of clay slurries as engineered soil covers. Canadian Geotechnical Journal, 34(1), 78-86.

Shang, J., & Lo, K. (1997). Electrokinetic dewatering of a phosphate clay. Journal of Hazardous Materials, 55(1-3), 117-133.

Shang, J., & Lo, K. (1997). Electrokinetic dewatering of a phosphate clay. Journal of Hazardous Materials, 55(1-3), 117-133.

Shankar, A., Rai, H. K., & Mithanthaya, R. (2009). Bio-enzyme stabilized lateritic soil as a highway material. Indian Roads Congress Journal,

Sharma, A. K., & Sivapullaiah, P. V. (2016). Ground granulated blast furnace slag amended fly ash as an expansive soil stabilizer. Soils and Foundations, 56(2), 205-212.

She, J., Lu, Z., Duan, Y., Yao, H., & Liu, L. (2020). Experimental study on the engineering properties of expansive soil treated with Al13. Scientific Reports, 10(1), 13930.

Shon, C.-S., Saylak, D., & Mishra, S. K. (2010). Combined use of calcium chloride and fly ash in road base stabilization. Transportation research record, 2186(1), 120-129.

Show, K.-Y., Tay, J.-H., & Goh, A. T. (2003). Reuse of incinerator fly ash in soft soil stabilization. Journal of Materials in Civil Engineering, 15(4), 335-343.

Siddique, A., & Hossain, M. A. (2011). Effects of lime stabilisation on engineering properties of an expansive soil for use in road construction. J Soc Transp Traffic Stud, 1(4), 1-9.

Singh, P., Dash, H. K., & Samantaray, S. (2020). Effect of silica fume on engineering properties of expansive soil. Materials Today: Proceedings, 33, 5035-5040.

Singh, S. P., & Das, R. (2020). Geo-engineering properties of expansive soil treated with xanthan gum biopolymer. Geomechanics and Geoengineering, 15(2), 107-122.

Sivapullaiah, P., & Prakash, B. N. (2007). Electroosmotic flow behaviour of metal contaminated expansive soil. Journal of hazardous materials, 143(3), 682-689.

Skempton, A. (1953). The colloidal activity of clays. Selected papers on soil mechanics, 1, 57-61.

Slade, P. G., J. P. Quirk, and K. Norrish. 1991. "Crystalline Swelling of Smectite Samples in Concentrated NaCl Solutions in Relation to Layer Charge." Clays and Clay Minerals 39(3): 234–238.

Snethen, D. R. (1979). Technical guidelines for expansive soils in highway subgrades.

Snethen, D. R., Johnson, L. D., & Patrick, D. M. (1977). An evaluation of expedient methodology for identification of potentially expansive soils.

Snethen, D. R., Townsend, F. C., Johnson, L. D., Patrick, D. M., & Vedros, P. J. (1975). A review of engineering experiences with expansive soils in highway subgrades.

Soğancı, A. (2015). The effect of polypropylene fiber in the stabilization of expansive soils. International Journal of Geological and Environmental Engineering, 9(8), 994-997.

Solanki, P., Khoury, N., & Zaman, M. M. (2009). Engineering properties and moisture susceptibility of silty clay stabilized with lime, class C fly ash, and cement kiln dust. Journal of Materials in Civil Engineering, 21(12), 749-757.

Soltani, A., Azimi, M., Deng, A., & Taheri, A. (2019). A simplified method for determination of the soil–water characteristic curve variables. International Journal of Geotechnical Engineering, 13(4), 316-325.

Soltani, A., Deng, A., & Taheri, A. (2018). Swell–compression characteristics of a fiber–reinforced expansive soil. Geotextiles and Geomembranes, 46(2), 183-189.

Soltani, A., Deng, A., Taheri, A., & Mirzababaei, M. (2019). A sulphonated oil for stabilisation of expansive soils. International Journal of Pavement Engineering, 20(11), 1285-1298.

Soltani, A., Deng, A., Taheri, A., & O'Kelly, B. C. (2022). Intermittent swelling and shrinkage of a highly expansive soil treated with polyacrylamide. Journal of Rock Mechanics and Geotechnical Engineering, 14(1), 252-261.

Soltani, A., Raeesi, R., & O'Kelly, B. C. (2022). Cyclic swell–shrink behaviour of an expansive soil treated with a sulfonated oil. Proceedings of the Institution of Civil Engineers-Ground Improvement, 175(3), 166-179.

Sprocati, R., & Rolle, M. (2022). On the interplay between electromigration and electroosmosis during electrokinetic transport in heterogeneous porous media. Water Research, 213, 118161.

Sprocati, R., Flyvbjerg, J., Tuxen, N., & Rolle, M. (2020). Process-based modeling of electrokinetic-enhanced bioremediation of chlorinated ethenes. Journal of hazardous materials, 397, 122787.

Sprocati, R., Gallo, A., Caspersen, M. B., & Rolle, M. (2023). Impact of variable density on electrokinetic transport and mixing in porous media. Advances in water resources, 174, 104422.

Sprocati, R., Masi, M., Muniruzzaman, M., & Rolle, M. (2019). Modeling electrokinetic transport and biogeochemical reactions in porous media: A multidimensional Nernst–Planck–Poisson approach with PHREEQC coupling. Advances in water resources, 127, 134-147.

Stallings, E. G. (2016). Investigation of pavement and subgrade distress at Alabama Highway 5 Auburn University].

Steinberg, M. (1998). Geomembranes and the control of expansive soils in construction.

Steinberg, M. (2000). Expansive soils and the geomembrane remedy. In Advances in unsaturated geotechnics (pp. 456-466).

Steinberg, M. L. (1981). Deep-vertical-fabric moisture barriers in swelling soils. Transportation research record, 790.

Stoltz, G., Cuisinier, O., & Masrouri, F. (2012). Multi-scale analysis of the swelling and shrinkage of a lime-treated expansive clayey soil. Applied clay science, 61, 44-51.

Sudheer Kumar, J., & Janewoo, U. (2016). Stabilization of expansive soil with cement kiln dust and RBI grade 81 at subgrade level. Geotechnical and Geological Engineering, 34, 1037-1046.

Sukmak, P., De Silva, P., Horpibulsuk, S., & Chindaprasirt, P. (2015). Sulfate resistance of clay-portland cement and clay high-calcium fly ash geopolymer. Journal of Materials in Civil Engineering, 27(5), 04014158.

Sutar, A. A., & Rotte, V. M. (2022). A Study on Electrokinetic Dewatering of Saturated Soil. Advances in Transportation Geotechnics IV: Proceedings of the 4th International Conference on Transportation Geotechnics Volume 1,

Tabarsa, A., Latifi, N., Meehan, C. L., & Manahiloh, K. N. (2018). Laboratory investigation and field evaluation of loess improvement using nanoclay–A sustainable material for construction. Construction and Building Materials, 158, 454-463.

Taha, M. R., Jawad, I. T., & Majeed, Z. H. (2015). Treatment of soft soil with nano-magnesium oxide. Proceedings of the 5th International Symposium on Nanotechnology in Construction, Chicago, IL, USA,

MaTaher, Z. J., Scalia IV, J., & Bareither, C. A. (2020). Comparative assessment of expansive soil stabilization by commercially available polymers. Transportation Geotechnics, 24, 100387.

Tang, C., Shi, B., Gao, W., Chen, F., & Cai, Y. (2007). Strength and mechanical behavior of short polypropylene fiber reinforced and cement stabilized clayey soil. Geotextiles and Geomembranes, 25(3), 194-202.

Tanyıldızı, M., Uz, V. E., & Gökalp, İ. (2023). Utilization of waste materials in the stabilization of expansive pavement subgrade: An extensive review. Construction and Building Materials, 398, 132435.

Telysheva, G., & Shulga, G. (1995). Silicon-containing polycomplexes for protection against wind erosion of sandy soil. Journal of agricultural engineering research, 62(4), 221-227.

Thomas, A. G., & Rangaswamy, B. K. (2019). Strength behavior of enzymatic cement treated clay. International Journal of Geotechnical Engineering.

Thomas, G., & Rangaswamy, K. (2020). Strengthening of cement blended soft clay with nano-silica particles. Geomech. Eng, 20(6), 505-516.

Thompson, M. R. (1966). Lime reactivity of Illinois soils. Journal of the Soil Mechanics and Foundations Division, 92(5), 67-92.

Thyagaraj, T., Rao, S. M., Sai Suresh, P., & Salini, U. (2012). Laboratory studies on stabilization of an expansive soil by lime precipitation technique. Journal of Materials in Civil Engineering, 24(8), 1067-1075.

Tingle, J. S., & Santoni, R. L. (2003). Stabilization of clay soils with nontraditional additives. Transportation research record, 1819(1), 72-84.

Tingle, J. S., Newman, J. K., Larson, S. L., Weiss, C. A., & Rushing, J. F. (2007). Stabilization mechanisms of nontraditional additives. Transportation research record, 1989(1), 59-67.

Tiwari, N., Satyam, N., & Puppala, A. J. (2021). Strength and durability assessment of expansive soil stabilized with recycled ash and natural fibers. Transportation Geotechnics, 29, 100556.

Tiwari, N., Satyam, N., & Puppala, A. J. (2021a). Effect of synthetic geotextile on stabilization of expansive subgrades: experimental study. Journal of Materials in Civil Engineering, 33(10), 04021273.

Tiwari, N., Satyam, N., & Puppala, A. J. (2021b). Strength and durability assessment of expansive soil stabilized with recycled ash and natural fibers. Transportation Geotechnics, 29, 100556.

Tiwari, N., Satyam, N., & Shukla, S. K. (2020). An experimental study on micro-structural and geotechnical characteristics of expansive clay mixed with EPS granules. Soils and Foundations, 60(3), 705-713.

RaTremblay, H., Leroueil, S., & Locat, J. (2001). Mechanical improvement and vertical yield stress prediction of clayey soils from eastern Canada treated with lime or cement. Canadian geotechnical journal, 38(3), 567-579.

Turkoz, M., Savas, H., Acaz, A., & Tosun, H. (2014). The effect of magnesium chloride solution on the engineering properties of clay soil with expansive and dispersive characteristics. Applied clay science, 101, 1-9.

U.S. Department of Transport. Federal Highway administration: chapter 3.0 Geotechnical aspects of pavements reference manual [online]. Available at: http s://www.fhwa.dot.gov/engineering/geotech/pubs/05037/03a.cfm. (Accessed 13 April 2020).

Van der Merwe, D., Steyn, A., & Hugo, F. (1980). The pretreatment of clay soils for road construction. Expansive Soils,

Van Genuchten, M. T. (1980). A closed-form equation for predicting the hydraulic conductivity of unsaturated soils. Soil science society of America journal, 44(5), 892-898.

Van Olphen, H. (1964). An introduction to clay colloid chemistry. Soil Science, 97(4), 290.

Vane, L. M., & Zang, G. M. (1997). Effect of aqueous phase properties on clay particle zeta potential and electro-osmotic permeability: Implications for electro-kinetic soil remediation processes. Journal of hazardous materials, 55(1-3), 1-22.

Venkatasubramanian, C., & Dhinakaran, G. (2011). Effect of bio-enzymatic soil stabilisation on unconfined compressive strength and California Bearing Ratio.

Virkutyte, J., Sillanpää, M., & Latostenmaa, P. (2002). Electrokinetic soil remediation—critical overview. Science of the total environment, 289(1-3), 97-121.

Viswanadham, B., Phanikumar, B., & Mukherjee, R. V. (2009). Swelling behaviour of a geofiber-reinforced expansive soil. Geotextiles and Geomembranes, 27(1), 73-76.

Voottipruex, P., & Jamsawang, P. (2014). Characteristics of expansive soils improved with cement and fly ash in Northern Thailand. Geomechanics & engineering, 6(5), 437-453.

Walsh, K. D., Colby, C. A., Houston, W. N., & Houston, S. L. (2009). Method for evaluation of depth of wetting in residential areas. Journal of geotechnical and geoenvironmental engineering, 135(2), 169-176.

Wang, M., Benway, J. M., & Arayssi, A. M. (1990). The effect of heating on engineering properties of clays. In Physico-chemical aspects of soil and related materials. ASTM International.

Wang, W., Kang, H., Li, N., Guo, J., Girma, D. Y., & Liu, Y. (2022). Experimental investigations on the mechanical and microscopic behavior of cement-treated clay modified by nano-MgO and fibers. International Journal of Geomechanics, 22(6), 04022059.

Wang, Y., Li, A., & Cui, C. (2021). Remediation of heavy metal-contaminated soils by electrokinetic technology: Mechanisms and applicability. Chemosphere, 265, 129071.

Wang, Y.-X., Guo, P.-P., Ren, W.-X., Yuan, B.-X., Yuan, H.-P., Zhao, Y.-L., Shan, S.-B., & Cao, P. (2017). Laboratory investigation on strength characteristics of expansive soil treated with jute fiber reinforcement. International Journal of Geomechanics, 17(11), 04017101.

Wild, S., Kinuthia, J., Jones, G., & Higgins, D. (1999). Suppression of swelling associated with ettringite formation in lime stabilized sulphate bearing clay soils by partial substitution of lime with ground granulated blastfurnace slag (GGBS). Engineering geology, 51(4), 257-277.

Wohlbier, H., & Henning, D. (1969). Effect of preliminary heat treatment on the shear strength of kaolinite clay. Highway Research Board Special Report(103).

Wu, H., Hu, L., & Zhang, G. (2016). Effects of electro-osmosis on the physical and chemical properties of bentonite. Journal of Materials in Civil Engineering, 28(8), 06016010.

Xeidakis, G. (1996a). Stabilization of swelling clays by Mg (OH) 2. Changes in clay properties after addition of Mg-hydroxide. Engineering geology, 44(1-4), 107-120.

Xeidakis, G. (1996b). Stabilization of swelling clays by Mg (OH) 2. Factors affecting hydroxy-Mg-interlayering in swelling clays. Engineering geology, 44(1-4), 93-106.

Xeidakis, G., Koudoumakis, P., & Tsirambides, A. (2004). Road construction on swelling soils: the case of Strymi Soils, Rhodope, Thrace, Northern Greece. Bulletin of engineering geology and the environment, 63, 93-101.

Xie, Y., Costa, S., Zhou, L., & Kandra, H. (2020). Mitigation of desiccation cracks in clay using fibre and enzyme. Bulletin of Engineering Geology and the Environment, 79, 4429-4440.

Xu, B., & Zhang, Q. (2021). Preparation and properties of hydrophobically modified nano-SiO2 with hexadecyltrimethoxysilane. ACS omega, 6(14), 9764-9770.

Yang, P., Ye, S., Wu, J., & Wu, J. (2022). Process-based pore-scale simulation of electrokinetic remediation of organic pollutant in porous media. Journal of Hydrology, 613, 128436.

Yang, X., Shi, G., Wu, C., Yuan, Y., Sun, H., & Cang, L. (2024). Nonlinearly coupled electro-osmotic flow in variable charge soils. Chemosphere, 363, 142873.

Yarbaşı, N., Kalkan, E., & Akbulut, S. (2007). Modification of the geotechnical properties, as influenced by freeze–thaw, of granular soils with waste additives. Cold regions science and technology, 48(1), 44-54.

Yazdandoust, F., & Yasrobi, S. S. (2010). Effect of cyclic wetting and drying on swelling behavior of polymer-stabilized expansive clays. Applied clay science, 50(4), 461-468.

Yeung, A. T., Hsu, C.-n., & Menon, R. M. (1997). Physicochemical soil-contaminant interactions during electrokinetic extraction. Journal of hazardous materials, 55(1-3), 221-237.

Yi, Y., Liska, M., Jin, F., & Al-Tabbaa, A. (2016). Mechanism of reactive magnesia–ground granulated blastfurnace slag (GGBS) soil stabilization. Canadian geotechnical journal, 53(5), 773-782.

Yilmaz, I., & Civelekoglu, B. (2009). Gypsum: an additive for stabilization of swelling clay soils. Applied clay science, 44(1-2), 166-172.

Yong, L. L., Namal Jayasanka Perera, S., Syamsir, A., Emmanuel, E., Paul, S. C., & Anggraini, V. (2019). Stabilization of a residual soil using calcium and magnesium hydroxide nanoparticles: A quick precipitation method. Applied Sciences, 9(20), 4325.

Yu-Feng, C., Hui, C., Ju-Zhi, D., Sui-Ming, L., Wen-Wu, T., & Shuo, W. (2022). Three-dimensional forward modeling and response characteristics analysis of foundation pit leakage electric-field considering electrokinetic effect. Applied Geophysics, 19(1), 117-131.

Zada, U., Jamal, A., Iqbal, M., Eldin, S. M., Almoshaogeh, M., Bekkouche, S. R., & Almuaythir, S. (2023). Recent advances in expansive soil stabilization using admixtures: current challenges and opportunities. Case Studies in Construction Materials, 18, e01985.

Zapata, C., Houston, S., Houston, W., & Dye, H. (2006). Expansion index and its relationship with other index properties. In Unsaturated Soils 2006 (pp. 2133-2137).

Zha, F., Qiao, B., Kang, B., Xu, L., Chu, C., & Yang, C. (2021). Engineering properties of expansive soil stabilized by physically amended titanium gypsum. Construction and building materials, 303, 124456.

Zhang, H., Zhou, G., Zhong, J., Shen, Z., & Shi, X. (2017). Effect of nanomaterials and electrode configuration on soil consolidation by electroosmosis: experimental and modeling studies. RSC advances, 7(20), 12103-12112.

Zhang, R., Lu, Y., Tan, T., Phoon, K., & Santoso, A. (2014). Long-term effect of curing temperature on the strength behavior of cement-stabilized clay. Journal of Geotechnical and Geoenvironmental Engineering, 140(8), 04014045.

Zhang, X., Yu, X., Guo, Y., & Fan, X. (2019). Behaviors of expansive soils mixed with polymeric stabilizing foams. Eighth International Conference on Case Histories in Geotechnical Engineering,

Zhao, H., Chun-Ji, Z., Xiao, Z., & Chan, L. (2013). Physicochemical characterization of cement stabilized highly expansive soil. Geo-congress 2013: stability and performance of slopes and embankments III,

Zhao, H., Liu, J., Guo, J., Zhao, C., & Gong, B.-w. (2015). Reexamination of lime stabilization mechanisms of expansive clay. Journal of Materials in Civil Engineering, 27(1), 04014108.

Zheng, F., Yue, W., & Yuanzheng, Z. (2024). A coupling numerical model for simulating groundwater uranium removal in coupling device of electric field and PRB. Journal of Hydrology, 131837.

Zheng, F., Zhai, Y., Yue, W., & Teng, Y. (2023). Coupling flow and electric fields to simulate migration and remediation of uranium in groundwater remediated by electroosmosis and a permeable reactive bio-barrier. Journal of Environmental Management, 346, 118947.

Zhou, B., & Chen, X. (2017). Effect of Nano-carbon on water holding capacity in a Sandy soil of the loess plateau. Earth Sciences Research Journal, 21(4), 189-195.

Zhou, H., Liu, Z., Li, X., & Xu, J. (2021). Remediation of lead (II)-contaminated soil using electrokinetics assisted by permeable reactive barrier with different filling materials. Journal of Hazardous Materials, 408, 124885.

Zomorodian, S. A., Shabnam, M., Armina, S., & O'Kelly, B. C. (2017). Strength enhancement of clean and kerosene-contaminated sandy lean clay using nanoclay and nanosilica as additives. Applied Clay Science, 140, 140-147.

Zornberg, J. G. (2017). Functions and applications of geosynthetics in roadways. Procedia Engineering, 189, 298-306.

Zornberg, J. G., & Gupta, R. (2009). Reinforcement of pavements over expansive clay subgrades. In Proceedings of the 17th International Conference on Soil Mechanics and Geotechnical Engineering (Volumes 1, 2, 3 and 4) (pp. 765-768). IOS Press.

Zornberg, J. G., Azevedo, M., Sikkema, M., & Odgers, B. (2017). Geosynthetics with enhanced lateral drainage capabilities in roadway systems. Transportation Geotechnics, 12, 85-100.

Zulfeqar, N., Khosravi, A., & Zou, S. Soil Conditioning Using Nanoparticles and Stability Enhancement: A Review of the Impacts on Hydro-Physico-Mechanical Characteristics. Geo-Congress 2024,

Zumrawi, M. M., & Eltayeb, K. A. (2016). Laboratory investigation of expansive soil stabilized with calcium chloride. Int Sch Sci Res Innov, 10, 223-227.

Zumrawi, M. M., Mahjoub, A. M., & Alnour, I. M. (2016). Effect of some chloride salts on swelling properties of expansive soil. University Of Khartoum Engineering Journal, 6(2).